



UNIL | Université de Lausanne

Unicentre

CH-1015 Lausanne

<http://serval.unil.ch>

Year : 2023

Biological characterization and targeted delivery of NAMPT inhibitors in hematological malignancies

Biniecka Paulina

Biniecka Paulina, 2023, Biological characterization and targeted delivery of NAMPT inhibitors in hematological malignancies

Originally published at : Thesis, University of Lausanne

Posted at the University of Lausanne Open Archive <http://serval.unil.ch>

Document URN : urn:nbn:ch:serval-BIB_821A9D529FDC0

Droits d'auteur

L'Université de Lausanne attire expressément l'attention des utilisateurs sur le fait que tous les documents publiés dans l'Archive SERVAL sont protégés par le droit d'auteur, conformément à la loi fédérale sur le droit d'auteur et les droits voisins (LDA). A ce titre, il est indispensable d'obtenir le consentement préalable de l'auteur et/ou de l'éditeur avant toute utilisation d'une oeuvre ou d'une partie d'une oeuvre ne relevant pas d'une utilisation à des fins personnelles au sens de la LDA (art. 19, al. 1 lettre a). A défaut, tout contrevenant s'expose aux sanctions prévues par cette loi. Nous déclinons toute responsabilité en la matière.

Copyright

The University of Lausanne expressly draws the attention of users to the fact that all documents published in the SERVAL Archive are protected by copyright in accordance with federal law on copyright and similar rights (LDA). Accordingly it is indispensable to obtain prior consent from the author and/or publisher before any use of a work or part of a work for purposes other than personal use within the meaning of LDA (art. 19, para. 1 letter a). Failure to do so will expose offenders to the sanctions laid down by this law. We accept no liability in this respect.



UNIL | Université de Lausanne

Faculté de biologie
et de médecine

**Central Laboratory of Hematology, Department of Medical Laboratory and Pathology,
Lausanne University Hospital**

Biological characterization and targeted delivery of NAMPT inhibitors in hematological malignancies

Thèse de doctorat ès sciences de la vie (PhD)

Présentée à la

Faculté de biologie et de médecine
de l'Université de Lausanne

par

Paulina Biniecka

Master of Science from the University of Copenhagen

Jury

Prof. Jean Bourhis, Président
Prof. Michel Duchosal, Directeur de thèse
Dr. Aimable Nahimana, Co-directeur de thèse
Prof. Ivan Stamenkovic, Expert
Prof. Alessio Nencioni, Expert

Lausanne 2023



UNIL | Université de Lausanne

Faculté de biologie
et de médecine

**Central Laboratory of Hematology, Department of Medical Laboratory and Pathology,
Lausanne University Hospital**

Biological characterization and targeted delivery of NAMPT inhibitors in hematological malignancies

Thèse de doctorat ès sciences de la vie (PhD)

Présentée à la

Faculté de biologie et de médecine
de l'Université de Lausanne

par

Paulina Biniecka

Master of Science from the University of Copenhagen

Jury

Prof. Jean Bourhis, Président
Prof. Michel Duchosal, Directeur de thèse
Dr. Aimable Nahimana, Co-directeur de thèse
Prof. Ivan Stamenkovic, Expert
Prof. Alessio Nencioni, Expert

Lausanne 2023

Imprimatur

Vu le rapport présenté par le jury d'examen, composé de

Président·e	Monsieur	Prof.	Jean	Bourhis
Directeur·trice de thèse	Monsieur	Prof.	Michel	Duchosal
Co-directeur·trice	Monsieur	Dr	Aimable	Nahimana
Expert·e·s	Monsieur	Prof.	Ivan	Stamenkovic
	Monsieur	Prof.	Alessio	Nencioni

le Conseil de Faculté autorise l'impression de la thèse de

Paulina Bozena Biniecka

Masters in Pharmaceutical sciences, University of Copenhagen, Danemark

intitulée

**Biological characterization and targeted delivery of
NAMPT inhibitors in hematological malignancies**

Lausanne, le 26 juin 2023

pour le Doyen
de la Faculté de biologie et de médecine

CHUV
Prof. Jean BOURHIS
Chef de Service
Radio-Oncologie
Rue du Bugnon 46
CH-1011 Lausanne
GLN:7601003330328

Prof. Jean Bourhis



Acknowledgements

I would like to express my gratitude towards all the people that supported me in diverse ways during my journey towards obtaining a PhD degree.

Foremost, I would like to thank my supervisors for the guidance, support and for sharing their precious knowledge and scientific experience with me. Prof Michel Duchosal for his invaluable advice, feedback and discussions and Dr Aimable Nahimana for the daily exchange of inspiring ideas and creating multiple learning opportunities for me.

Secondly, I would like to distinguish my labmates, former post-doc Oussama El Mokh for the initial guidance and help with lab experiments. Saki Matsumoto for her support, fun events and sharing all the struggles of doing a PhD together. Axel Belotti for all the help and conversations in the lab.

I would like to also thank my thesis committee members (President Prof Jean Bourhis and experts Prof Ivan Stamenkovic and Prof Alessio Nencioni) for their availability, taking the time to evaluate my PhD project and for precious advice and comments on how to improve my work.

I would like to give special thanks to the whole Integrata Network, I appreciate all the scientific discussions and fun we had together during our meetings.

I want to give special thanks to Simone Fratta, who shared with me all his knowledge on chemistry, discussed many times our scientific ideas and helped in my project. Simone synthesized the compounds in Table 3 and prepared all the payload-linkers for the antibody attachments.

Another special thanks go to Dr Torsten Hechler, Anikó Pálfi and Pablo Ruedas-Batuecas, who hosted me in Heidelberg Pharma. Torsten and Anikó advised me scientifically and organized my project. Pablo has helped me daily with all the doubts and encouraged me to be not only a better scientist, but also a better person.

I would like to acknowledge Prof Vogel and his former students for synthesizing the compounds (JJ08, FEI191 and FEI199), described in this work. And Prof Laurent A. Decosterd's lab members for performing pharmacokinetic analysis.

Further, my gratitude goes to all the people who made my personal life in Lausanne an amazing experience. Especially, my first neighbors (Jessica, Rita, Samantha and Daniel), who quickly became my friends, for all the experiences we shared during travels and gatherings. Sofia and Ana for the trips and fun times together. Xisca, besides the trips and laughs, for always listening to me and for all the support.

I would like to give my special thanks to Parras, who was always there through good and tough times, who continuously told me to *be patient* and gave me invaluable advice for my work and life.

Special thanks also go to Tullio, who always helped me scientifically and who was available (despite being in a different time zone) to discuss any problem with me.

Finally, I would like to thank my parents and family, who always encouraged me to pursue my dreams. I also have to mention my dogs (Bali and Fiji, who passed away and a new puppy Timor), who never forgot about me, although they did not see me too often in the past years.

Abstract

Cancer cells must reprogram their metabolism to sustain their continuous growth and proliferation. They rely on fast nicotinamide adenine dinucleotide (NAD⁺) turnover for their energy supply, which is crucial for their survival. Nicotinamide phosphoribosyltransferase (NAMPT) is the rate limiting enzyme involved in the production of NAD⁺. The inhibition of NAMPT induces NAD⁺ depletion and is a therapeutic strategy to selectively eliminate malignant cells highly dependent on NAD⁺. Until now, several NAMPT inhibitors have been developed and, despite their high efficacy in preclinical studies, their clinical activity was limited. Therefore, there is still a need to synthesize novel more potent NAMPT inhibitors and/or to specifically target them to cancer cells.

In this work, new NAMPT inhibitors were characterized for their biological activities *in vitro* and *in vivo* on haematological malignancies. Moreover, few selected NAMPT inhibitors were conjugated to an anti-CD138 antibody, targeting inhibitors to multiple myeloma cells.

All tested compounds exhibited low nanomolar cytotoxicity against various haematological cancer cell lines. They depleted NAD⁺ after 24 hours of drug treatment, followed by ATP depletion and mitochondrial membrane depolarization, what finally led to various types of cell death (apoptosis and necrosis). Treatments with NAMPT inhibitors caused time-dependent reactive oxygen species (ROS) production that was rescued by catalase (CAT).

Unfortunately, the most potent compounds *in vitro* (i.e., FEI199) did not translate their efficacy *in vivo*. Indeed, among all compounds (JJ08, FEI191, FEI199) administered into mouse xenograft model of human Burkitt lymphoma only JJ08 completely eradicated tumour growth. Moreover, the pharmacokinetics (PK) profile of JJ08 was like that of APO866.

Some of the synthesized analogues were further modified to be attached to an anti-CD138 antibody to create antibody-drug-conjugates (ADCs). CD138 is an antigen selectively overexpressed on MM cells and its responsible for its malignant growth. The cytotoxicity of the NAMPT inhibitors ADCs (NAMPTi_ADCs) was assessed on target-positive and negative cells. Additionally, a positive control ADC was synthesized with amanitin as a payload (ADC-ama) instead of the inhibitor. The native NAMPT inhibitors used as payloads had IC₅₀ on target-positive (RPMI8226) cells between 2.3-118 nM, and the anti-CD138 antibody itself was not toxic to the cells. The ADC-ama resulted in very potent activity against RPMI8226 cells (IC₅₀ 0.1 nM). However, the NAMPTi_ADCs did not exhibit cytotoxicity on RPMI8226 cells up to 500 nM, except for SF316 and SF319, sharing the same payload. The compounds induced 60-70% cell death at 500 nM concentrations, which was considered unspecific.

Taken together, these findings demonstrate the mode of action and the very potent cytotoxicity of different NAMPT inhibitors *in vitro*, and the high efficacy of JJ08 *in vivo*. Despite the successful conjugation of the selected compounds to the anti-CD138 antibody, they were not effective *in vitro*. Therefore, further optimization of the NAMPTi_ADCs is needed.

Résumé

Les cellules cancéreuses reprogramment leur métabolisme pour maintenir leur prolifération et leur croissance continues. Elles se reposent sur un renouvellement rapide du nicotinamide adénine dinucléotide (NAD⁺) pour leur apport en énergie, ce qui est crucial pour les cellules cancéreuses. La nicotinamide phosphoribosyltransferase (NAMPT) est l'enzyme limitante impliquée dans la production de NAD⁺. L'inhibition de l'enzyme NAMPT et donc la déplétion du NAD⁺ est une stratégie thérapeutique pour éliminer de manière sélective les cellules malignes qui sont fortement dépendantes du NAD⁺. Jusqu'à maintenant, beaucoup d'inhibiteurs de NAMPT ont été développés et malgré leur forte efficacité dans les études précliniques, leur activité clinique était limitée. Il reste donc un besoin de synthétiser de nouveaux inhibiteurs du NAMPT plus performants et/ou spécialement ciblés contre les cellules cancéreuses.

Dans ce travail, de nouveaux inhibiteurs du NAMPT ont été caractérisés pour leur activité biologique *in vitro* et *in vivo* sur des cellules hématologiques malignes. De plus, certains inhibiteurs de NAMPT sélectionnés ont été conjugués à un anticorps anti-CD138 ciblant les myélomes multiples (MM).

Tous les composés ont montré à basses concentrations molaires une cytotoxicité contre diverses lignées cellulaires cancéreuses hématologiques. Le NAD⁺ était dépleted après 24 heures de traitement, suivi par une déplétion de l'ATP et une dépolarisation de la membrane mitochondriale, qui ont finalement amené à différents types de morts cellulaires (apoptose et nécrose). Le traitement avec les inhibiteurs de NAMPT a causé la production d'espèces réactives de l'oxygène (ERO) dépendant du temps, production qui a pu être prévenue par la catalase (CAT).

Finalement, le composé le plus efficace *in vitro* était le 35a (un IC₅₀ de 18pM sur des cellules ML2), malgré ça, l'efficacité *in vitro* des inhibiteurs les plus efficaces ne s'est pas retranscrite dans les expériences *in vivo*. Tous les composés ont été administrés dans des modèles de souris xénotransplantés soit de lymphomes Burkitt (JJ08, FEI191, FEI199) ou de leucémie myéloïde aigüe (35a, 47), Seul JJ08 a complètement éradiqué la croissance de la tumeur. De plus, le profil pharmacocinétique de JJ08 était similaire à celui d'APO866.

Certains des analogues synthétisés ont été modifiés pour permettre leur attachement à l'anticorps anti-CD138 dans le but de créer des conjugués anticorps-médicaments. Le CD138 est un antigène surexprimé chez les myélomes multiples qui est responsable de leur croissance maligne. La cytotoxicité des inhibiteurs de NAMPT conjugués anticorps-médicaments a été testée sur des cellules cibles positives et négatives. De plus, un contrôle positif du conjugué anticorps-médicament a été synthétisé avec l'amanitine comme payload. Les inhibiteurs de NAMPT utilisés comme payloads avaient un IC₅₀ sur les cellules cibles positives (RPMI8226) entre 2.3 et 118 nM. L'anticorps anti-CD138 n'était pas toxique lui-même pour les cellules. Le conjugué anticorps-médicament amanitine a montré des résultats extrêmement efficaces sur les cellules RPMI8226 (IC₅₀ 0.1nM). Malgré cela, les conjugués anticorps-médicaments inhibiteurs de NAMPT n'ont pas montré de cytotoxicité sur les RPMI8226 jusqu'à 500nM, à l'exception de SF316 et SF 319 qui partagent le même payload. Ces composés ont induit une mort cellulaire autour de 60 à 70% avec une concentration de 500nM qui a été considérée comme non spécifique.

En conclusion, ces observations démontrent le mode d'action et la forte cytotoxicité de différents inhibiteurs de NAMPT *in vitro*, ainsi que la grande efficacité de JJ08 *in vivo*. Bien que la conjugaison des composés choisis à l'anticorps anti-CD138 ait été un succès, ils n'ont pas montré d'efficacité *in vitro*. Par conséquent, une meilleure optimisation des inhibiteurs de NAMPT conjugués anticorps-médicaments est nécessaire.

List of Abbreviations

ADC_ama - the anti-CD138-amanitin ADC
ADCC - antibody-dependent cell cytotoxicity
ADCP - antibody-dependent cellular phagocytosis
ADCs - antibody drug conjugates
ADME - absorption, distribution, metabolism and excretion
CAR - chimeric antigen receptor
CAR-Ts - chimeric antigen receptor-transduced T cells
CDC - complement-dependent cytotoxicity
CLL1 - C-type lectin domain family 12 member A
ClogP - calculated partition coefficient
DAR - Drug to antibody ratio
DLTs - dose limiting toxicities
DM1 – maytansanoids
FLT3 - Fms like tyrosine kinase 3
GI – gastrointestinal
GLUT1 - glucose transporter 1
HC - heavy chain
HDAC - histone deacetylase
HDP - Heidelber Pharma
i.v. – intravenous
LC - light chain
mAb - monoclonal antibodies
MM - Multiple Myeloma
MMAE, MMAF - monomethyl auristatin E and F
MTD - maximum tolerated dose
NA/NAR - nicotinic acid/nicotinic acid riboside
NAD⁺ - nicotinamide adenine dinucleotide
NAM/NR - nicotinamide/nicotinamide riboside
NAMPT- Nicotinamide phosphoribosyltransferase
NAMPTi_ADCs – the anti-CD138-NAMPT inhibitors ADCs
NMN - nicotinamide mononucleotide
NRH - reduced nicotinamide riboside
OXPHOS - oxidative phosphorylation
PARPs - Poly(ADP-Ribose) polymerases
PK – pharmacokinetics
PPP - pentose phosphate pathway
Redox - reduction-oxidation
SIRT1-7 – Sirtuins
TCA - tricarboxylic acid
TME - tumour microenvironment
TOPO1 - inhibitors of topoisomerase I

Table of Contents

Acknowledgements	1
Abstract	2
Résumé	3
List of Abbreviations	5
List of Figures	8
List of Tables	9
Chapter 1: General Introduction	10
1 Cancer hallmark – Reprogramming of energy metabolism	10
<i>Nicotinamide Adenine Dinucleotide (NAD⁺)</i>	11
1.1 Biosynthesis of NAD	11
1.2 Roles of NAD	11
<i>NAMPT inhibitors as promising anticancer agents</i>	12
1.3 Overview	12
1.4 Clinical Trials	13
2 Targeted therapies for cancer treatment	14
<i>Antibody-Drug Conjugates</i>	15
1.1 Overview	15
1.2 Antibody	17
1.3 Linker chemistry	17
1.4 Payload – cytotoxic molecule	18
1.5 Mechanism of action	18
General aims of the thesis	21
Chapter 2: Biological characterization of novel NAMPT inhibitors	22
1 Articles contributions	22
2 Summary of the results	23
Chapter 3: Targeted delivery of NAMPT inhibitors	25
1 Introduction	25
1.1 Antibody Drug Conjugates for multiple myeloma Treatment	25
1.2 CD138 as molecular target for multiple myeloma	26
1.3 The CD138-amanitin ADCs	27
1.4 The CD138-NAMPT inhibitors ADCs	28
2 Materials and Methods	31
2.1 Production of anti-CD138 antibodies	31
2.2 Production of payload and payload-linker modifications	33
2.3 Bioconjugation of payload-linker to the anti-CD138 antibody	33
2.4 Biological evaluation of NAMPT inhibitors, anti-CD138 antibodies, and ADCs <i>in vitro</i>	33
3 Results	35
3.1 Evaluation of NAMPT inhibitors as payloads for ADCs <i>in vitro</i>	35

3.2	Preparation of anti-CD138-NAMPT inhibitors ADCs	36
3.3	Evaluation of anti-CD138-NAMPT inhibitors ADCs <i>in vitro</i>	41
4	Conclusions	45
	Chapter 4: General discussion and perspectives	46
1	Biological characterization of novel NAMPT inhibitors.....	46
2	Targeted delivery of NAMPT inhibitors – Antibody Drug Conjugates	48
3	Conclusions	51
	References.....	52
	Articles.....	60
	Anticancer Activities of Novel Nicotinamide Phosphoribosyltransferase Inhibitors in Haematological Malignancies.....	61
	Synthesis and structure-activity relationship of new Nicotinamide Phosphoribosyltransferase inhibitors with antitumor activity on solid and haematological cancer.	84

List of Figures

Figure 1 NAD⁺ production and functions overview. NAD⁺ biosynthesis and NAD⁺ metabolism. TRP – Tryptophan, NA – Nicotinic Acid, NAR – Nicotinic Acid Riboside, NRH – reduced nicotinamide riboside, NAM – Nicotinamide, NR – Nicotinic acid riboside, NAPRT – Nicotinic Acid Phosphoribosyltransferase, AK – NRH kinase, NMNH – reduced nicotinamide riboside, NADH – reduced NAD, NADP(H) – Nicotinamide adenine dinucleotide phosphate, NQO1 – NAD(P)H:quinone oxidoreductase, NRK – nicotinamide riboside kinase, IDO/TDO – Indoleamine-2,3-dioxygenase/Tryptophan-2,3-dioxygenase, NAMN – Nicotinic Acid mononucleotide, NMN – Nicotinamide mononucleotide, NMNAT – NMN adenytransferase, QAPRT – Quinolinic Acid Phosphoribosyltransferase, QA – Quinolinic acid, NAAD – Nicotinic Acid adenine dinucleotide, NADS – NAD synthetase, PARPs – Poly(ADP-ribose)polymerases, ARTs – mono(ADP-ribose)transferases.	12
Figure 2 Antibody-Drug Conjugate components and functions. Adapted from (64).	15
Figure 3 Mechanism of action of ADCs. Adapted from (64).	19
Figure 4 Mechanisms of action of therapeutic antibodies. i. complement-dependent cytotoxicity (CDC). ii. antibody-dependent cell cytotoxicity (ADCC). iii. antibody-dependent cellular phagocytosis (ADCP). Adapted from (64).	20
Figure 5 Scheme of the mode of action of NAMPT inhibitors	24
Figure 6 Example structures of existing NAMPT inhibitors ADCs. Figure adapted from (106, 108). Figure prepared by Simone Fratta.	30
Figure 7 Structures of NAMPT inhibitors. Original, very potent molecule 47a (SF183) (A). An improved molecule 74 (SF223), an ADC payload.	31
Figure 8 Possible chemical modifications. Figure prepared by Simone Fratta	31
Figure 9 SEC-HPLC analysis of aggregates of anti-CD138 antibody. The results showed 90.8 % of monomers.	37
Figure 10 CD138 marker expression on RPMI8226 and Namalwa cells.	37
Figure 11 anti-CD138 antibody binding assay. (A) RPMI8226 cell line and (B) Namalwa cell line. Results are shown of the representative experiment.	38
Figure 12 Structures of the used linkers for ADCs. Figure prepared by Simone Fratta.	38
Figure 13 Synthesis of five payload-linkers. DIPEA – N,N-Diisopropylethylamine; DMF – Dimethylformamide. Figure prepared by Simone Fratta.	39
Figure 14 Synthesis of the specific payload-linker for SF223 compound. Fmoc-Ala-Val-PAB-OH – commercially available linker. Pbr ₃ – Phosphorus tribromide; DMF – Dimethylformamide; Et ₂ NH – Diethylamine. Figure prepared by Simone Fratta.	40
Figure 15 Synthesis of 6 NAMPT inhibitors ADCs. Figure prepared by Simone Fratta	41
Figure 16 NAMPT inhibitors as payloads and anti-CD138 antibody induce cell death in RPMI8226 cell line in concentration dependent manner. Dose-dependent analysis of cell death induced by SF223, SF270, SF271 and anti-CD138 antibody on RPMI8226 cell line (A-D). Cell death was assessed with flow cytometry by double staining with annexin V (ANXN) and 7AAD after 96 hours of treatment. The percentage of early apoptotic cells (ANXN+ 7AAD-) is shown in white and the percentage of late apoptotic and dead cells (7AAD+) is shown in black. Data are n=3 ± SD.	42
Figure 17 Anti-CD138 antibody conjugated with amanitin via Val-Ala-PABC linker and its aggregates assessment. (A) ADC_ama is used as positive control, DAR = 7. Scheme prepared by Simone Fratta. (B) SEC-HPLC analysis of ADC_ama, showing 93 % of monomers.	43
Figure 18 Cytotoxicity of amanitin and ADC_ama. On RPMI8226 (A, B) and Namalwa (C, D) cell lines. The cell death was assessed as described in Figure 14. Data are n=3 ± SD. The IC ₅₀ of 0.11 ± 0.03 nM was calculated for ADC_ama on RPMI8226 cell line.	43
Figure 19 Cytotoxicity of NAMPT inhibitors ADCs on RPMI8226 cell line. The cell death was assessed as described in Figure 14. Data are n=3 ± SD.	44
Figure 20 SEC-HPLC analysis of aggregates. A – SF306, B – SF315, C – SF316, D – SF318, E – SF319, F – SF322-T1.	45
Figure 21 NAMPT inhibitors tested in this work. (A) APO9866, (B) JJ08, (C) FE1191, (D) FE1199, (E) SF103, (F) SF164, (G) SF183.	46

List of Tables

Table 1 Overview of FDA approved ADCs.....	15
Table 2 ADCs in clinical trials for MM.....	25
Table 3 Evaluation of new payloads for ADCs on ML2 and RPMI8226 cell lines. NA – not available. Data are n=3 ±SD.	35
Table 4 Summary of synthesized NAMPT inhibitors ADCs.....	40

Chapter 1: General Introduction

1 Cancer hallmark – Reprogramming of energy metabolism

Based on WHO estimations from 112 countries, cancer has ranked as first or second leading cause of death before the age of 70. There were 19.3 million new cases diagnosed worldwide and 10.0 million cancer deaths in 2020 (1). Biologically, cancer is characterized as a group of cells that grow and expand uncontrollably. As initially described by Hanahan and Weinberg, the first hallmarks of cancer cells include property of infinite replicative potential, evading apoptosis and growth suppressors, sustaining their proliferation, inducing angiogenesis, invasion and metastasis (2). Recently, additional cancer hallmarks such as, (i) avoiding immune destruction, (ii) deregulating cellular metabolism, (iii) unlocking phenotypic plasticity and (iv) senescent cells have emerged and are considered to characterize the malignant nature of cancer cells (3, 4). Whereas genome instability, mutation, tumor-promoting inflammation, non-mutational epigenetic reprogramming and polymorphic microbiomes are considered enabling characteristics that drive tumor development (3, 4).

To fuel the continuous cancer cell growth and division, malignant cells reprogram their energy metabolism. To ensure their survival, rapidly dividing cancer cells need continuous and fast ATP production, they increase the biosynthesis of various intermediates, used as building blocks, and also carefully maintain the redox balance, to counteract the oxidative stress (5). Generally, this metabolic reprogramming involves increased uptake of nutrients, such as glucose or amino acids. Even in the presence of oxygen, cancer cells preferentially use glycolytic pathway to provide their building blocks (6). Glycolysis is redirected to pentose phosphate pathway (PPP), from which cancer cells gain upregulated NADPH production to counteract ROS and ribose-5-phosphate intermediate for nucleic acid synthesis (7). Since many tumors still rely on oxidative phosphorylation (OXPHOS) to produce their energy, the fatty acid oxidation is promoted for acetyl-CoA production to sustain the TCA cycle, hence the support of mitochondrial ATP production (6).

One of the central molecules responsible for cellular homeostasis and regulation of cancer cell metabolism is nicotinamide adenine dinucleotide (NAD⁺) (8, 9). It functions as a cofactor for reduction-oxidation (redox) enzymes involved in metabolic pathways, such as glycolysis, tricarboxylic acid (TCA) cycle and OXPHOS and as a substrate for several enzymes involved in cell signalling pathways (7, 8). Therefore, regardless of cancer cells reprogramming their energy production towards glycolysis or OXPHOS, NAD⁺ is implicated in both processes.

Nicotinamide Adenine Dinucleotide (NAD⁺)

1.1 Biosynthesis of NAD

In mammalian cells, NAD⁺ is produced from different precursors originating mainly from our diet or gut microbiota (10). It is synthesized through different molecular pathways: *de novo* pathway from tryptophan, Preiss-Handler pathway from nicotinic acid/nicotinic acid riboside (NA/NAR) and salvage pathways from nicotinamide/nicotinamide riboside (NAM/NR) and reduced nicotinamide riboside (NRH) (11, 12). In mammalian cells, NAM is the most used precursor to synthesize NAD⁺. Nicotinamide phosphoribosyltransferase (NAMPT) is the rate-limiting enzyme that catalyzes the phosphoribosylation of NAM to produce nicotinamide mononucleotide (NMN) (13, 14). The latter is then converted to NAD⁺ by NMN adenylyltransferases (Figure 1).

1.2 Roles of NAD

Besides playing an important role as a cofactor for redox enzymes and maintaining cellular bioenergetics, NAD⁺ is also a substrate for various types of enzymes involved in cell signalling and transcriptional regulation (15). As a substrate for Sirtuins (SIRT1-7), NAD⁺ is involved in cellular stress responses, cell cycle control, longevity and aging (16). Poly(ADP-Ribose) polymerases (PARPs), other NAD⁺ consuming enzymes, play a role in DNA repair, cellular proliferation and transcriptional regulation (17). Whereas mono(ADP-Ribose) transferases are using co-enzyme function of NAD⁺ to sustain cell signalling, cellular apoptosis or oncogene regulation. Last but not least, ectoenzymes CD38 and CD157, that consume NAD⁺, are involved in cellular adhesion, calcium signalling and cell cycle control (18).

The most used way to produce NAD⁺ in mammalian cells is catalysed through NAMPT, which is overexpressed in many haematological and solid tumors, and it is associated with poorer outcome in patients with various cancer types (19-25).

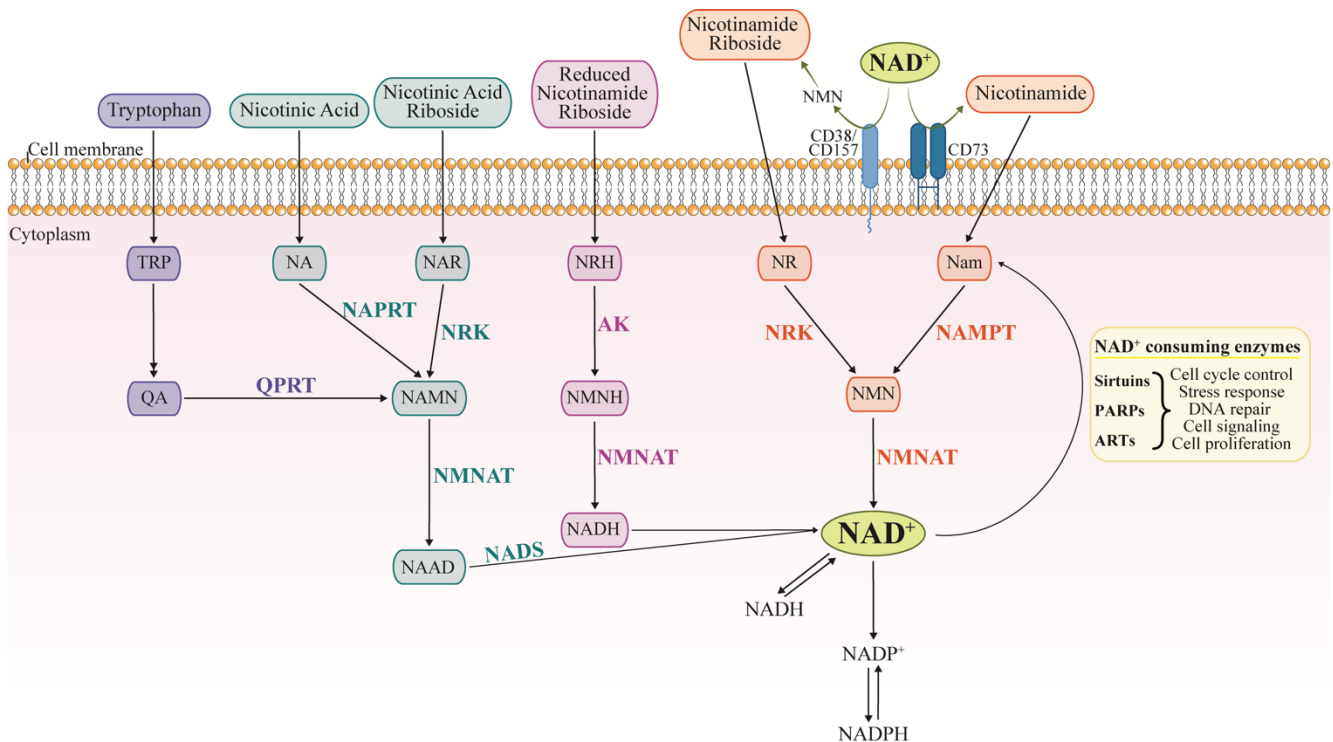


Figure 1 NAD⁺ production and functions overview. NAD⁺ biosynthesis and NAD⁺ metabolism. TRP – Tryptophan, NA – Nicotinic Acid, NAR – Nicotinic Acid Riboside, NRH – reduced nicotinamide riboside, NAM – Nicotinamide, NR – Nicotinic acid riboside, NAPRT – Nicotinic Acid Phosphoribosyltransferase, AK – NRH kinase, NMNH – reduced nicotinamide riboside, NADH – reduced NAD, NADP(H) – Nicotinamide adenine dinucleotide phosphate, NQO1 – NAD(P)H:quinone oxidoreductase, NRK – nicotinamide riboside kinase, IDO/TDO – Indoleamine-2,3-dioxygenase/Tryptophan-2,3-dioxygenase, NAMN – Nicotinic Acid mononucleotide, NMN – Nicotinamide mononucleotide, NMNAT – NMN adenylyltransferase, QPRT – Quinolinic Acid Phosphoribosyltransferase, QA – Quinolinic acid, NAAD – Nicotinic Acid adenine dinucleotide, NADS – NAD synthetase, PARPs - Poly(ADP-ribose)polymerases, ARTs - mono(ADP-ribose)transferases.

NAMPT inhibitors as promising anticancer agents

1.3 Overview

NAMPT is a crucial enzyme involved in NAD⁺ production, and its targeting has emerged as an anticancer strategy to selectively eliminate malignant cells (9, 26-29). In recent years, many small molecule inhibitors were developed against NAMPT, they are discussed below.

FK866 (known as APO866 or Daporinad) is the first and most broadly described NAMPT inhibitor, identified by Hasmann *et al.* and characterized to be a very potent anticancer agent, with the activity around 1 nM in various malignancies (30). Lately, it was defined as competitive NAMPT inhibitor (31). FK866 has broad anticancer activity among different types of cancer cells, specifically at a very low nanomolar range on haematological malignancies (IC₅₀ from 0.1 nM), without being cytotoxic to normal hematopoietic progenitor cells (32). APO866 causes NAD depletion in the first 24 hours after treatment and subsequent ATP depletion. The APO866-mediated cell death involves caspase-independent apoptosis, mitochondrial depolarization, autophagy and high ROS accumulation (32-34).

CHS-828 was first characterized as an anticancer agent in 1997 and 1999, with an anti tumor activity *in vivo* on mice xenografts of breast and lung cancer models (35, 36). Ten years after its first description, CHS-828 was identified as NAMPT inhibitor (37). Further studies, aiming to improve the pharmacokinetic properties resulted in identification of a more soluble pro-drug GMX1777, that is faster released when given intravenously (38).

OT-82, the most recently described NAMPT inhibitor, is optimized to be administered orally and it exhibits a very strong activity against haematological malignancies, causing apoptotic cell death by NAD and ATP depletions (39).

Other specific single agent NAMPT inhibitors have been described, such as GEN617/618 (40, 41), LSN3154567 (42), A1293201 (43), STF-118804 (44) and MV87 (45). Their development is less advanced and not described here.

Dual inhibitors have been developed as well. KPT-9274 (ATG-019) has a combined activity against p21-activated kinase 4 (PAK4) and NAMPT. It induced apoptosis in *in vitro* and *in vivo* models of lymphoma (46). Another discovered inhibitor was originally reported to be active against glucose transporter 1 (GLUT1) as well (47). As described previously, cancer cells rely on high glucose uptake and anaerobic glycolysis, in which NAD⁺ is a co-enzyme. The dual inhibitor, STF-31 inhibited glucose uptake and was cytotoxic to cells, by the activity against GLUT1 and NAMPT (48), however the results were drug concentration and cancer cell type dependent (49).

Recently, based on pharmacophore analysis and biological assays, NAMPT was identified as additional target for one of the histone deacetylase (HDAC) inhibitors (50).

These promising pre-clinical results have advanced some of the NAMPT inhibitors to clinical trials.

1.4 Clinical Trials

Clinical studies on NAMPT inhibitors are scarce. The first and only one completed is with FK866. The results of phase I and II clinical trials were posted back in 2007 (51) and 2016 (52). The Phase I study was done to determine the safety of 96 hours continuous infusion of APO866, maximum tolerated dose (MTD), dose limiting toxicities (DLTs) and recommended phase II dose. However, the results reported no objective response and the most significant dose-limiting toxicity was thrombocytopenia (51). Next phase I/II clinical study assessed safety and tolerability of APO866 in 10 patients with leukemia [NCT00435084]. Consecutive phase II study assessed the efficacy and safety of APO866 on 25 participants with advanced melanoma [NCT00432107]. The last phase II clinical trial was done on 25 patients with refractory or relapsed cutaneous T-cell lymphoma [NCT00431912].

This latter study was stopped early, as no drug efficacy was observed, and the treatment resulted in severe lymphocytopenia and thrombocytopenia (52).

The first phase I study with CHS-828 was performed on sixteen patients with solid tumors. No partial or complete response was observed and the main DLTs were from gastrointestinal (GI) origin (53). Another phase I clinical study was conducted on seven patients with solid tumors. The main toxicity was thrombocytopenia and GI symptoms (54). A further phase I study with CHS-828 given orally to patients with solid tumors resulted in no objective response with DLTs such as vomiting, thrombocytopenia or leucopenia (55). The GMX1777, a prodrug, also entered phase I clinical trials, the DLTs were thrombocytopenia and diverse GI issues (56). The last two clinical studies with GMX1777 were withdrawn or terminated due to financial constraints [NCT00457574, NCT00724841].

The newest inhibitors that entered clinical trials are dual inhibitor of PAK4 and NAMPT (KPT-9274/ATG-019) and OT-82. The latter was administered to patients with relapsed or refractory lymphoma. The dose escalation and expansion were assessed, however there are no results posted [NCT03921879]. The KPT-9274 (ATG-019) is in a recruiting phase of clinical studies. The drug will be evaluated on patients with advanced solid tumors, non-Hodgkin's lymphoma and relapsed/refractory myeloid leukemia. The administration will be oral at different doses to estimate the MTD [NCT04281420, NCT04914845].

In summary, so far there is no effective NAMPT inhibitor, which would give a satisfactory response in patients without DLTs. Therefore, there is still a strong need to develop new inhibitors and more specifically targeted NAD-depleting therapies.

2 Targeted therapies for cancer treatment

The conventional approach to treat solid cancers involves surgery, which can be the most effective at early stages and is very often followed by radiotherapy and chemotherapy (57). Radiotherapy is a high energy radiation that induces DNA damage and/or promotes the formation of reactive oxygen species, that consequently damage DNA (58, 59). Chemotherapy treatment is administered as a medicine that inhibits cancer cells growth and/or proliferation and kills tumoral cells (60). It is a preferred treatment if cancer has spread around the body as the drugs can reach various body sites via bloodstream, in opposition to surgery and radiotherapy, that are used for locally formed tumors (60).

Targeted therapies are drugs or other substances that target specific proteins, or receptors, which are usually overexpressed on cancer cell. These treatments include small molecules, monoclonal

antibodies (mAb), immunotherapeutic cancer vaccines, cell and gene therapies (61). Their mode of action is to interfere with molecular pathways by binding to cell surface antigens and receptors, that are responsible for cancer growth or metastasis (61). One of the main advantages of targeted therapies is an effective delivery to malignant cells that would spare most of the healthy cells and avoid systemic toxicities. Of note, the targeted therapy only works if the specific biomarker is expressed on the cancer cell surface (61). The most used molecular targets revolve around initial cancer hallmarks widely described by Hanahan *et al.* (2). Namely, evading apoptosis, uncontrollable proliferation, increased angiogenesis or escaping immune cells are the cancer features that are targeted (62).

Antibody-Drug Conjugates

1.1 Overview

Antibody drug conjugates (ADCs) are therapeutics that are design to deliver the cytotoxic drug linked to a monoclonal antibody targeting specific antigen (63). They consist of an antibody, a chemically designed linker and a cytotoxic compound (also known as payload) (Figure 2) (63). These three components must be specifically designed to achieve the best pharmacological properties and clinical outcomes (63). The specifications of each component are discussed below.

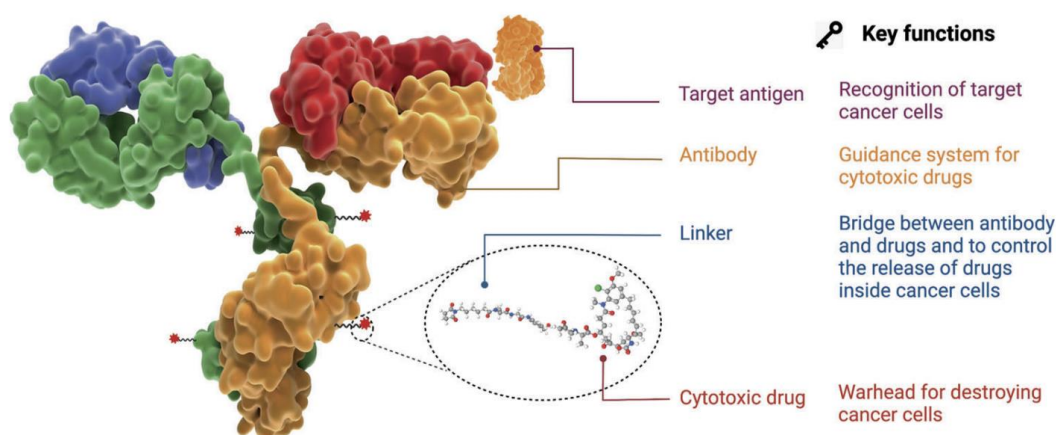


Figure 2 Antibody-Drug Conjugate components and functions. Adapted from (64).

Currently, there are 13 ADCs approved by FDA as drugs (Table 1).

Table 1 Overview of FDA approved ADCs.

Drug	Target antigen	Linkers	Payload	Payload action	Average DAR	Disease indication (Year)
Gemtuzumab ozogamicin	CD33	hydrazone	N-acetyl- γ -calicheamicin	DNA cleavage	2-3	AML (2000, 2017)

Targeted therapies for cancer treatment

Brentuximab vedotin	CD30	mc-VC-PABC	MMAE (auristatin)	Microtubule inhibitor	4	R/R sALCL or cHL (2011) R/R pcALCL or CD30+ MF (2017) cHL, sALCL or CD30+ PTCL (2018) ^a
Ado-trastuzumab emtansine	HER2	SMCC	DM1 (maytansinoid)	Microtubule inhibitor	3.5	Advanced-stage HER2+ breast cancer previously treated with trastuzumab and a taxane (2013); early stage HER2+ breast cancer in patients with residual disease after neoadjuvant trastuzumab–taxanebased treatment (2019)
Inotuzumab ozogamicin	CD22	hydrazone	N-acetyl- γ -calicheamicin	DNA cleavage	5-7	R/R B-ALL (2017)
Moxetumomab pasudotox	CD22	mc-VC-PABC	PE38 (Pseudomonas exotoxin-A fragment)	Protein translation inhibitor	NA	R/R HCL (2018)
Fam-trastuzumab deruxtecan	HER2	tetrapeptide	DXd (Camptothecin)	TOPO1 inhibitor	8	Advanced-stage HER2+ breast cancer after two or more anti-HER2-based regimens (2019)
Polatuzumab vedotin	CD79b	mc-VC-PABC	MMAE (auristatin)	Microtubule inhibitor	3.5	R/R DLBCL (2019) ^b
Sacituzumab govitecan	TROP2	CL2A	SN38 (active metabolite of irinotecan)	TOPO1 inhibitor	8	Advanced-stage, triple-negative breast cancer in the third line setting or beyond (2020)
Enfortumab vedotin	Nectin 4	mc-VC-PABC	MMAE (auristatin)	Microtubule inhibitor	4	Advanced-stage urothelial carcinoma, following progression on a PD-1 or PD-L1 inhibitor and platinum-containing chemotherapy (2020)
Belantamab mafodotin	BCMA	mc	MMAF (auristatin)	Microtubule inhibitor	4	R/R multiple myeloma in the fifth line setting or beyond (2020)
Loncastuximab tesirine	CD19	dipeptide	PBD dimer (SG3199)	DNA crosslinking agent	2.3	R/R large B-cell lymphoma (2021)

Tisotumab vedotin	TF	mc-VC-PABC	MMAE (auristatin)	Microtubule inhibitor	4	Recurrent or metastatic cervical cancer (2021)
Mirvetuximab soravtansine	FR α	sulfo-SPDB	DM4 (maytansinoid)	Microtubule inhibitor	2	Platinum-Resistant ovarian cancer (2022)

AML - acute myeloid leukaemia; B-ALL - B cell acute lymphoblastic leukaemia; BCMA - B cell maturation antigen; cHL - classical Hodgkin lymphoma; DAR - drug-to-antibody ratio; mc-VC-PABC - maleimidocaproyl-valine-citrulline-p-aminobenzoyloxycarbonyl; DLBCL - diffuse large B cell lymphoma; mAb - monoclonal antibody; MF - mycosis fungoides; MMAE - monomethyl auristatin E; MMAF - monomethyl auristatin F; SMCC - succinimidyl-4-(N-maleimidomethyl)cyclohexane-1-carboxylate; pcALCL - primary cutaneous anaplastic large cell lymphoma; PTCL - peripheral T cell lymphoma; R/R - relapsed and/or refractory; sALCL - systemic anaplastic large cell lymphoma; TOPO1 - topoisomerase I; TROP2 - tumour-associated calcium signal transducer 2. CL2A a cleavable complicated PEG8- and triazole-containing PABC-peptide-mc linker; mc - maleimidocaproyl; TF - tissue factor; HER2 - human epidermal growth factor; DM1 - derivative of maytansine 1; PD-L1 - programmed cell death-ligand 1; PD-1 - programmed cell death protein-1; DXd - Exatecan derivative for ADC; HCL – hairy cell leukemia; PBD – pyrrolobenzodiazepine; DM4 - derivative of maytansine 4; FR α – folate receptor 1.

a. In combination with cyclophosphamide, doxorubicin and prednisone for newly diagnosed sALCL or CD30+ PTCL and in combination with doxorubicin, vinblastine and dacarbazine for newly diagnosed cHL.

b. In combination with bendamustine and rituximab. Table adapted from (63, 64).

1.2 Antibody

Monoclonal antibodies used in ADCs are mostly of the IgG1 subclass. Moreover, novel ADCs are made with humanized antibody backbone to avoid immunogenicity (63). To circumvent most of the systemic toxicities, the mAb must be specific to a target preferentially expressed on cancer cells surface when compared to healthy cells (63).

1.3 Linker chemistry

The linker connecting the antibody with the cytotoxic molecule is a very crucial component of the ADC (65). Specifically modified linkers can be divided into cleavable and non-cleavable ones. The cleavable linkers can be cleaved by cathepsins, glutathione, Fe(II), photo-responsive, bioorthogonal or acid (65). The linker has two main roles, first it is responsible for the stability of the whole ADC in the blood circulation and secondly, it influences the release of the payload after the delivery to the specific target (65). These competing features pose a great challenge in the area of linker development. The unstable linkers can release the cytotoxic payload before they reach cancer cells resulting in systemic toxicities (63). Therefore, the specific linkers have to be designed with an attention to chemical triggers, additional attachments and optimized with improved absorption, distribution, metabolism and excretion (ADME) properties (65). Besides the linker itself, there are also different linker-antibody and linker-payload attachments (65). The most common linker-antibody attachment is through maleimide, which reacts with thiol groups of the antibody (65). That coupling is however vulnerable to retro-Michael reaction, in which the reactive maleimide can be freed in the blood circulation,

resulting in instability of the ADC (65). In terms of linker-payload attachment, either payload or linker can be modified. The modifications of the payloads carry the risk of reduced cytotoxicity (65).

1.4 Payload – cytotoxic molecule

When it comes to molecules that are commonly attached to the antibodies, in the initial developments of ADCs the known anticancer chemotherapeutics were used, such as methotrexate (66), vinca alkaloids (67) or doxorubicin (68). However, after testing in clinical trials, some limitations occurred, such as lack of potency, immunogenicity or even poor selectivity (69). These early observations have led to development of improved class of ADCs, with humanized antibodies, conjugated to 1,000-fold more toxic compounds and with more carefully selected targets (63, 69). Consequently, highly potent ADCs were developed with different chemotherapeutics and 13 of them are currently FDA-approved. Among them are calicheamicins (ozogamicin) and camptothecins (inhibitors of topoisomerase I; TOPO1) that induces DNA breaks and auristatins (monomethyl auristatin E and F; MMAE, MMAF) and maytansanoids (DM1), which are microtubule inhibitors (63).

Drug to antibody ratio (DAR) is an average number of molecules attached to the antibody. In fact, the approved ADCs are mixtures of different DAR numbers, ranging between 2-8 (63, 65). There are two strategies to control the number of payload moieties, site-specific conjugation and chemical modifications of the linker-antibody attachment (70). Many conjugations rely on native cysteines or lysines present on the mAb, then the obtained DAR can be considerably heterogenous (63).

1.5 Mechanism of action

ADCs are a type of a complex delivery system, that is recently more commonly used for cancer treatment (63, 64). It is combining the modes of action and pharmacokinetic properties of small molecule drugs with antibodies. Briefly, the main mechanism of action of ADC involves binding the target antigen by the mAb part of ADC, then the whole ADC is internalized into lysosomes, where the payload is released and acts on its intracellular target (Figure 3) (64).

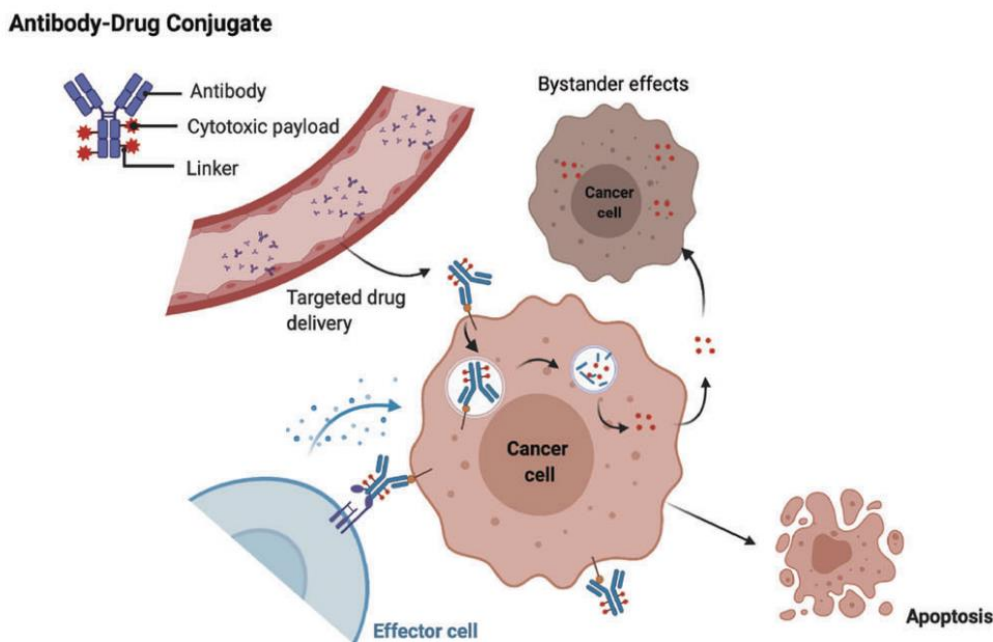


Figure 3 Mechanism of action of ADCs. Adapted from (64).

The first challenge in the mode of the action of ADCs *in vivo* is its circulation in the blood. Administered ADCs must be preserved in the circulation, without disintegration, which is prevented by the adequate linkers and attachments. Overall, the antibodies and therefore ADCs have much longer half-life (days), compared to small molecules alone (minutes - hours) (71). Moreover, ADCs are much bigger molecules than other chemotherapeutics, and this can limit their distribution and the penetration into tumours: However, once they reach the tumour side, ADC have higher tumour accumulation than small molecule drugs alone (71). After they penetrate the tissue and reach the tumour microenvironment (TME), they must bind their target. The antigen recognition part of the mAb that is used in ADCs remains unaffected, therefore the affinity of the ADCs is typically the same as of the naked antibody (63). It is also known that ADCs preserve the same functionality on the mechanisms of cell killing as naked antibodies (63, 64). Therefore, they can also exert the complement-dependent cytotoxicity (CDC), antibody-dependent cell cytotoxicity (ADCC) or antibody-dependent cellular phagocytosis (ADCP), the typical mechanisms of action of antibodies cell killing (Figure 4) (72). The example is the T-DM1 ADC, which consists of Trastuzumab (anti-HER2 antibody) and DM1 (microtubule inhibitor). The study comparing Trastuzumab alone with T-DM1 showed that both inhibit cancer cell growth using the same mechanisms, namely by blocking the HER2 dimerization, what in turn inhibits further cell signalling induced cell death (73). After the ADC binds its target, the internalization process occurs, that can happen in two ways, during antigen-dependent endocytosis or antigen-independent pinocytosis (64). Then, depending on the type of the linker, the payload can be

released in early endosomes (acid-cleavable linkers) or late endosomes (enzymatic or proteolytic cleavage) (63). Some of the ADCs can cause a bystander effect, that is a diffusion of the payload to neighbouring cancer cells, that do not express the target antigen. This can be beneficial, especially in cancers with high heterogeneity, however it requires the conjugated molecules to be lipophilic in order to cross the cell membranes (63).

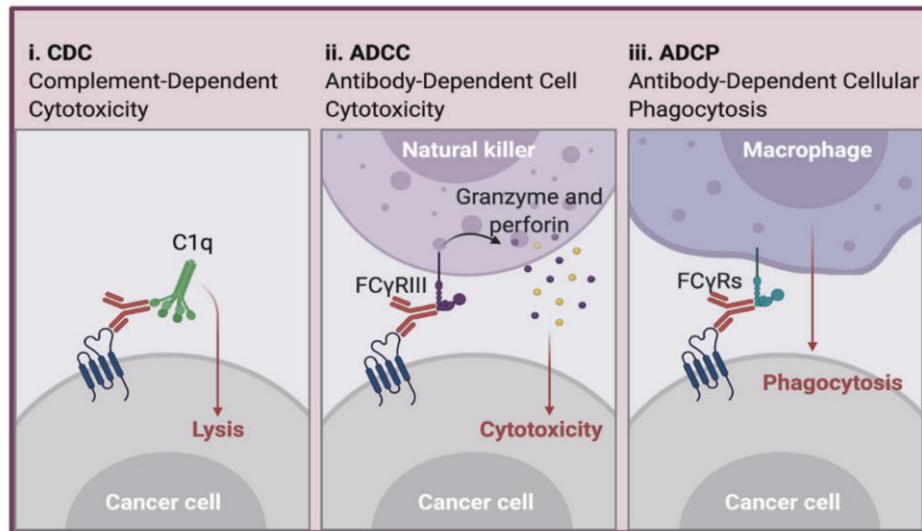


Figure 4 Mechanisms of action of therapeutic antibodies. i. complement-dependent cytotoxicity (CDC). ii. antibody-dependent cell cytotoxicity (ADCC). iii. antibody-dependent cellular phagocytosis (ADCP). Adapted from (64).

General aims of the thesis

I Biological characterization of novel NAMPT inhibitors

Evaluation of anti-cancer activities of novel NAMPT inhibitors *in vitro* and *in vivo* in various blood cancer models in comparison to APO866.

II Targeted delivery of NAMPT inhibitors

Development of Antibody Drug Conjugates by conjugation of novel NAMPT inhibitors to anti-CD138 antibody, targeting multiple myeloma cells.

Chapter 2: Biological characterization of novel NAMPT inhibitors

1 Articles contributions

During my PhD studentship I evaluated and characterized the mechanism of action of different classes of NAMPT inhibitors.

The first group of NAMPT inhibitors was synthesized within 7th framework project PANACREAS (74). Three promising compounds (JJ08, FEI191 and FEI199) were chosen for further characterization *in vitro* and *in vivo* in several hematopoietic malignant cells. These results are published in:

Anticancer Activities of Novel Nicotinamide Phosphoribosyltransferase Inhibitors in Hematological Malignancies

Paulina Binniecka, Saki Matsumoto, Axel Belotti, Jessie Jousset, Jian-Fei Bai, Somi Reddy Majjigapu, Paul Thoueille, Dany Spaggiari, Vincent Desfontaine, Francesco Piacente, Santina Bruzzone, Michele Cea, Laurent A. Decosterd, Pierre Vogel, Alessio Nencioni, Michel A. Duchosal, Aimable Nahimana.

Molecules **2023**, 28(4), 1897; <https://doi.org/10.3390/molecules28041897>

In this study, I designed, performed, and analyzed all the *in vitro* experiments. Moreover, I also analyzed and discussed the results of *in vivo* efficacy and pharmacokinetics.

The second group of NAMPT inhibitors was synthesized at the University of Sevilla within a collaborative project funded by the European Union's Horizon 2020 research and innovation program. This study is published in:

Synthesis and structure-activity relationship of new Nicotinamide Phosphoribosyltransferase inhibitors with antitumor activity on solid and haematological cancer.

Simone Fratta, **Paulina Binniecka**, Antonio J. Moreno-Vargas, Ana T. Carmona, Aimable Nahimana, Michel A. Duchosal, Francesco Piacente, Santina Bruzzone, Irene Caffa, Alessio Nencioni, Inmaculada Robina.

Eur J Med Chem. 2023 Jan 31;250:115170. doi: 10.1016/j.ejmech.2023.115170

In the second manuscript, I planned, performed the experiments, and analyzed the data on the characterization of chosen NAMPT inhibitors in hematological malignancies that include: (i) cytotoxicity on ML2, JRKT, NMLW, RPMI8226 and NB4 cell lines (Table 2); (ii) intracellular NAD and ATP depletion (Figure 4) and IC₅₀ of NAD depletion on ML2, Jurkat and RPMI8226 cells (Table 3); (iii) characterization of production of different ROS (Figure 5); (iv) time dependent MMP depolarization and (v) cell death analysis (Figure 6). Further confirmation that evaluated compounds are NAMPT inhibitors (Figure 7) and the abrogation of NAMPT-inhibitors induced cell death by catalase (Figure 8).

2 Summary of the results

Article: Anticancer Activities of Novel Nicotinamide Phosphoribosyltransferase Inhibitors in Hematological Malignancies.

Biniecka *et al. Molecules* **2023**, 28(4), 1897.

JJ08, FEI191 and FEI199 were first assessed for their ability to inhibit the enzymatic activity of NAMPT, confirming that they are indeed NAMPT inhibitors. Then their *in vitro* cytotoxicities and mode of action was characterized on different haematological malignant cell lines (myeloid and lymphoblastic leukemias, Burkitt lymphoma and multiple myeloma). Subsequently, the *in vivo* efficacy of JJ08, FEI191 and FEI199 was assessed on Burkitt lymphoma human xenograft mouse model and additionally their pharmacokinetics (PK) study was carried out.

All the inhibitors caused dose-dependent cell death *in vitro*, with the most potent inhibitor being FEI199, as its IC₅₀ was almost half lower than that of APO866.

The proposed mode of action of JJ08, FEI191 and FEI199 is depicted in Figure 5. Briefly, the first direct consequence of treatment with NAMPT inhibitors is the depletion of NAD⁺. We observed a very fast drop in intracellular NAD⁺ levels, already after 8 hours of treatment and almost no NAD⁺ detected at 24 hours. The depletion of NADP(H) happened in the similar time as that of NAD⁺. As NADPH is a powerful antioxidant, its depletion caused the increase in oxidative stress and elevated ROS production. The high levels of mitochondrial and cytosolic ROS and H₂O₂ were produced at 72 hours after cell treatment with JJ08, FEI191 and FEI199. The NAD⁺ depletion was subsequently followed by a drop of ATP, with no detectable levels at 48 hours, when the mitochondrial membrane started to get depolarized. Full depolarization was observed at 72 hours. The complete cell death occurred at 96 hours. Additionally, to characterize different types of cell death, the involvement of caspases-induced apoptosis and necrosis was assessed. Caspases -3, -8 and -9 were activated at 72 hours after treatment with NAMPT inhibitors, and cytosolic enzyme LDH was released extracellularly at 72 hours indicating the involvement of necrotic cell death. The final assessment of the cause of cell death was done with catalase (ROS scavenger), that did not protect the cells from NAD⁺ depletion, however it was able to fully abrogate the cell death caused by NAMPT inhibitors, indicating the crucial role of oxidative stress in the cell death induced by NAMPT inhibitors.

The *in vivo* efficacy of JJ08, FEI191 and FEI199 was done in a mouse xenograft model of Burkitt lymphoma. Only JJ08 was able to fully eradicate the tumor growth and significantly prolong the mice survival, like APO866. The FEI compounds were able to significantly delay the mouse death. The PK parameters of JJ08 were like that of APO866, whereas both FEI inhibitors had overall worse detected plasma concentrations and drug exposure.

The findings describe the new small molecules as potent NAMPT inhibitors *in vitro* and the potential of JJ08 as an effective compound *in vitro* and *in vivo* for further anti-cancer evaluations.

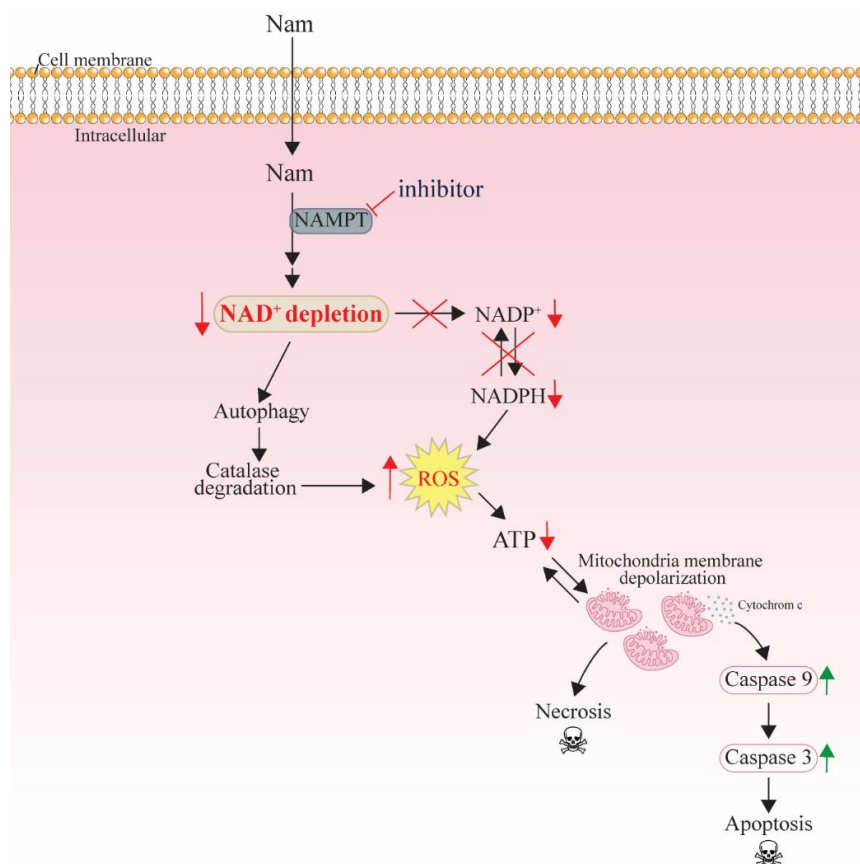


Figure 5 Scheme of the mode of action of NAMPT inhibitors

Article: Synthesis and structure-activity relationship of new Nicotinamide Phosphoribosyltransferase inhibitors with antitumor activity on solid and haematological cancer.

Fratta S., *et al.* *Eur J Med Chem.* 2023 Jan 31;250:115170.

In this work, the cytotoxicities of different NAMPT inhibitors were assessed on pancreatic and hematological cancer cell lines. The most potent compounds were 35a, 39a and 47 with IC₅₀ in picomolar range, especially on ML2 cell line (18, 46 and 49 pM, respectively). The mechanisms of cell death of compounds 35a, 39a and 47 were the same as of mentioned above NAMPT inhibitors. They depleted intracellular NAD⁺ levels after 24 hours of treatment, followed by ATP depletion at 48 hours. The mitochondrial membrane depolarization started at 48 hours, correlating with 80% of cell death in ML2 cell line. Whereas in Jurkat and RPMI8226 cells, the MMP completely decreased at 72 hours, all events leading to cell death at 96 hours. Moreover, the quantification of ROS levels, resulted in a profound production of mitochondrial and cytosolic ROS and H₂O₂ at 72 hours after treatment with 35a, 39a and 47. Of note, the addition of catalase was able to fully abrogate the cell death caused by those inhibitors.

Chapter 3: Targeted delivery of NAMPT inhibitors

1 Introduction

1.1 Antibody Drug Conjugates for multiple myeloma Treatment

To achieve the second aim of this thesis the model cancer cell line of multiple myeloma (MM) was used. MM is currently an incurable disease, and is estimated to account for about 2 % of newly diagnosed cancer cases in United States in 2021 and has a five-year survival at 54 % (76, 77). As summarized below, there are many promising ADCs for MM in clinical trials, however only one is so far accepted as a drug. MM is an example of blood cancer, for which the development of specifically targeting antibodies is particularly relevant giving the complex contribution of bone marrow microenvironment.

Multiple myeloma is a B-cell malignancy developed in bone marrow, where plasma cells accumulate and form tumors (75). Current standard of care involves chemotherapy consisting of alkylating agents, corticosteroids, immunomodulatory drugs, and/or proteasome inhibitors. Although MM survival has improved in recent years, most of the patients relapse after 3-4 years of treatment and develop resistance (78). MM cells produce different surface adhesion molecules to keep a tight connection between them and bone marrow microenvironment, which plays a crucial role in their growth and survival (79). Cell surface markers, such as CD38, CD47, CD138, FcRH5, GPRC5D, SLAMF7 or BCMA are highly expressed on MM cells and are used as targets for different therapeutic treatments (80). The most common target for immunotherapeutic approaches is BCMA, a target for chimeric antigen receptor (CAR) T cells, and bispecific antibodies (81). Considering antibody-based therapies, among FDA approved treatments for MM, there are two mAb against CD38 (isatuximab and daratumumab), mAb against SLAMF7 (elotuzumab) and one ADC (belantamab mafodotin). This latter ADC consists of anti-BCMA antibody conjugated to auristatin F via a non-cleavable linker (80, 82). In clinical trials, there are some more ADCs targeting MM evaluated (Table 2) (83).

Table 2 ADCs in clinical trials for MM.

ADC name	Target	Linker	Payload	Status
Lorvotuzumab mertansine	CD56	Disulfide bond (SPP)	DM1	Phase I

Milatumzumab doxorubicin	CD74	Acid-labile (hydrazine)	Doxorubicin	Phase I
Indatuximab ravtansine	CD138	Disulfide bond (SPP)	DM4	Phase I/II
GSK2857916	CD269	Non-cleavable (MC)	MMAF	Phase I
AMG 224	BCMA	Non-cleavable	mertansine (DM1)	Phase I
MEDI 2228	BCMA	valine–alanine dipeptide	PBD	Phase I
CC 99712	BCMA	undisclosed	undisclosed	Phase I
TAK-573	CD38	fused to the Fc part of the antibody	Attenuated form of IFN α	Phase I/II
TAK-169	CD38	fused to the Fc part of the antibody	Ribosome inactivating SLTA	Phase I
STRO-001	CD74	A non-cleavable dibenzocyclooctyne	Maytansoid	Phase I
FOR46-002	CD46	undisclosed	undisclosed	Phase I
HDP 101	BCMA	cleavable	amanitin	Phase I

PBD – pyrrolobenzodiazepine; BCMA - B cell maturation antigen; MMAF - monomethyl auristatin IFN α - interferon alpha; SLTA - Shiga-like toxin A-subunit. Table adapted from: (83, 84).

1.2 CD138 as molecular target for multiple myeloma

CD138 (Syndecan-1) is a type I transmembrane protein and important cell surface marker responsible for cell adhesion, migration and cell-cell interactions (85). CD138 plays a role in cancer cell progression, as it is promoting malignant cells proliferation and its expression is correlated with poor cancer prognosis (86). It is a prognostic marker for MM and Hodgkin’s lymphoma, that can be released from the cell surface and its increased levels can be found in the plasma of cancer patients (86). It is also a relevant molecule for solid tumors where it is often overexpressed in breast, bladder,

cervical, colorectal, pancreatic, prostate, and liver cancers. However, in some cases, for example in carcinomas, CD138 is downregulated, leading to the decreased adhesion of the cells to extracellular matrix, what increases their motility and triggers cancer metastasis (86).

CD138 plays an important role in molecular signaling and it is a coreceptor for various growth factors, for example epidermal growth factor, which increases MM cell proliferation (87). Moreover, it participates in immunomodulation by binding various inflammatory cytokines, chemokines and integrins (88, 89). It is of high therapeutical interest, as CD138 antibody drug conjugates (ADCs) along with chimeric antigen receptor-transduced T cells (CAR-Ts) are currently in clinical trials (90-92). Indatuximab ravtansine (BT062) is an anti-CD138 antibody conjugated to microtubule inhibitor (DM4). Firstly described by Ikeda *et al.* (93), it was tested *in vitro* on cell lines and primary cells and *in vivo* in mouse xenograft models of human MM. The results showed a significant cytotoxicity towards malignant cells, but not healthy ones. Moreover, an inhibition of tumors growth *in vivo* and prolonged mouse survival, strongly triggered further evaluation of this ADC in clinical trials (93). The first clinical trial was initiated with indatuximab ravtansine as monotherapy in patients with relapsed and/or refractory MM. Safety, efficacy and pharmacokinetics were assessed in 2 studies (phase I and phase I/IIa) (94). There were only mild adverse effects, such as fatigue or diarrhea, and stable disease or better results were achieved in over 75 % of heavily pretreated patients (94). Other phase I/IIa studies were initiated with indatuximab ravtansine in combination with dexamethasone, lenalidomide or pomalidomide in patients with relapsed and/or refractory MM and all tested combinations appeared to be well tolerated (91, 95). More recently also a multicentre, phase I/IIa study was carried out with indatuximab ravtansine in combination with dexamethasone, lenalidomide or pomalidomide on activity, safety and pharmacokinetics in patients with relapsed and/or refractory MM (96). An objective response was observed in 71.7 % of patients treated with indatuximab ravtansine plus lenalidomide and in 70.6 % of patients treated with indatuximab ravtansine and pomalidomide. The most common, serious (grade 3-4) adverse effects were thrombocytopenia and neutropenia (96).

Currently, there is no treatment using CD138 as a target that has been accepted by FDA. Considering the promising results with recent clinical trials using BT062, there is indeed a high interest in this target.

1.3 The CD138-amanitin ADCs

Alpha-amanitin

Amanitins belong to the group of toxins derived from the poisonous mushrooms, *A. phalloides* (97). One of them, α -amanitin, is the most studied bicyclic peptide, that causes severe toxicity to

humans, causing extreme liver and kidney injuries (97, 98). It is a very potent eukaryotic RNA polymerase II inhibitor, causing transcription and protein synthesis inhibition (98). Alpha-amanitin is hydrophilic in nature, thus it cannot passively cross the cell membrane, however, it is taken up by a specific transporter into hepatocytes, leading to complete cytolysis (98-100). Additionally, α -amanitin causes nephrotoxicity, as it is accumulated and excreted via kidneys, although the kidney injury could be also caused by GI issues, which appear first after mushroom ingestion (101, 102).

The potent cytotoxic properties of α -amanitin, resulting in complete stop of cell proliferation, which can affect dividing, as well as resting cells are desirable features in cancer treatment. Moreover, its inability to passively cross cell membranes and its physicochemical properties, make it a perfect candidate to be used as payload in ADCs, which allow for its specific delivery into cancer cells (103).

Alpha-amanitin as ADCs payload

The α -amanitin used as a payload was chemically synthesized at Heidelberg Pharma (HDP), the anti-CD138 antibody was expressed in mammalian expression system using Expi293F cells and the further bioconjugation of the toxin to the antibody was done at HDP as a part of my PhD secondment.

As the α -amanitin is already well characterized as a payload for ADCs (103-105), therefore the anti-CD138-amanitin ADC (ADC_ama) was used as a positive control. The cytotoxicity of ADC_ama was assessed in MM cells (RPMI8226) expressing CD138 and in Burkitt's lymphoma cells (Namalwa) not expressing CD138. If the cell death is induced in MM cells, but not lymphoma ones, after the treatment with ADC_ama, then the specificity and proper internalization of anti-CD138 antibodies used in these ADCs is confirmed. This validates MM cells as target positive and Burkitt's lymphoma as target negative cells for further cytotoxicity assessments with NAMPT inhibitors ADCs.

1.4 The CD138-NAMPT inhibitors ADCs

The NAMPT inhibitors and all the modifications needed for them to be used as payloads were synthesized and adapted at the University of Sevilla and at HDP. The anti-CD138 antibody was expressed in mammalian expression system using Expi293F cells and the further bioconjugation of the inhibitors to the antibody was done at HDP.

NAMPT inhibitors as ADCs payloads

Currently there are three independently published approaches for ADCs with NAMPT inhibitors (106-108) (Figure 6). First, Novartis has developed novel NAMPT inhibitors synthesized with different linkers and assessed *in vitro* and *in vivo* (106). Then, some of them were conjugated to anti-c-Kit (receptor tyrosine kinase) mAbs and one candidate to anti-HER2 trastuzumab mAb and they were tested on different cell lines and in gastrointestinal stromal tumour xenograft models in mice. The ADCs that were chosen for further evaluation had non-cleavable linkers, their aggregation was below 10 % and DAR of 2-4. The ADC tested with cathepsin-cleavable linker resulted in high aggregation of 29 %. The cytotoxicity of trastuzumab ADC was in a picomolar range on HER2⁺ cells, and anti-c-Kit ADC had very low picomolar activity on their target cells. However, also the non-binding IgG isotype control ADCs showed some activity against all tested targets. Two anti-c-Kit ADCs with different linkers were assessed *in vivo*, by single-dose intravenous (i.v.) injection and they were able to fully eradicate the tumour growth. Moreover, the ADCs were well tolerated, without any sign of body weight loss in mice (106).

Secondly developed ADCs, by Seattle Genetics, were synthesized with APO866 (FK866) and a few new compounds (107). Cell viability of 5 different payloads was assessed and based on the best cytotoxic profile on different cell lines (L540cy – Hodgkin lymphoma; A549 – lung adenocarcinoma; HepG2 – hepatocellular carcinoma). Three compounds were chosen to be attached to β -glucuronidase cleavable linkers and anti-CD30 antibody, with DAR = 8. Then these ADCs were tested *in vitro* for NAD and ATP depletions. The results showed a profound NAD depletion on target positive cell lines, moreover the kinetics of NAD/ATP depletion was monitored in L540cy cell line over 5 days. The doses of anti-CD30 ADCs of previously established EC₅₀ were tested over time. The dose below EC₅₀ was able to deplete the NAD levels only at 24h and 48h. However, over 72h time point the NAD levels went back to its baseline, whereas ATP levels were almost not affected. The dose above the EC₅₀ fully depleted the NAD levels after 24h and ATP levels dropped after 48-72h. Its noteworthy that these observations are consistent with the effects caused by NAMPT inhibitors alone (109, 110). Besides anti-CD30 ADCs, additional ADCs with NAMPT inhibitors were developed with anti-CD19 and anti-CD123 antibodies and they were all tested *in vivo* on respective tumour xenograft mouse models. Only with the anti-CD123 ADCs administered 3x per week in mice with established AML xenografts the results showed complete and sustained tumour response. Moreover, the single-dose rat toxicology studies were carried out with different doses of one ADC. The results showed no retinal or cardiac toxicity, which were previously observed with other NAMPT inhibitors alone (111, 112) and only

mild, dose-dependent cytopenias. These results underline the potential of targeted delivery and improvement of therapeutic window for NAMPT inhibitors administration (107).

The most recently developed ADCs with NAMPT inhibitors were by Bayer (108). They have synthesized a new class of NAMPT inhibitors conjugated to three different antibodies (anti-C4.4a - colorectal cancer; anti-HER2 - breast cancer; anti-B7H3 - non-small-cell lung cancer and prostate) with non- and cleavable linkers. The average DAR of the ADCs was between 2.2-7.8 and aggregation lower than 2 %. Initially synthesized isotypic controls for each linker, showed high off-target cytotoxicities on one of the cell lines. This prompted the authors to measure intracellular generation of metabolites of one of the ADCs. They observed deconjugation of the payload from the mAb, possibly explaining the off-target activity. To prevent this deconjugation, two new linkers with succinic amide were synthesized and attached to inhibitors, one with extra polyethylene glycol (PEG) chain. The latter ADCs with new linkers have achieved better selectivity, while at the same time preserving their cytotoxicity. Then, three ADCs were tested *in vivo* on antigen expressing tumour xenografts in mice. The best selectivity and anti-tumour effect was observed in mice xenografted with breast cancer cells, treated with ADC conjugated with anti-C4.4a antibody with improved linker (DAR 6.9). Overall, the treatment was well tolerated, without significant weight loss in mice.

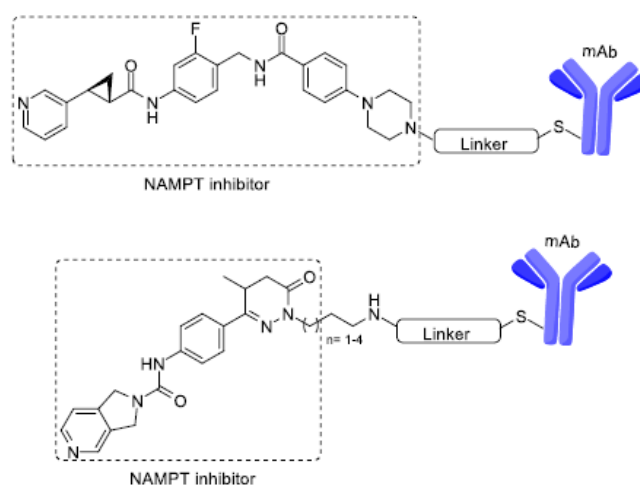


Figure 6 Example structures of existing NAMPT inhibitors ADCs. Figure adapted from (106, 108). Figure prepared by Simone Fratta.

Taken together, these findings open new avenues for testing and optimizing NAMPT inhibitors as payloads for ADCs.

In the present work, the NAMPT inhibitors used as payloads were synthesized at the University of Sevilla. Following previous *in vitro* assessment of NAMPT inhibitors, we chose compound 47a (SF183) (Figure 7A) as a base structure for our payload synthesis, as this inhibitor was the most

cytotoxic one on both Mia-Paca2 and different haematological cell lines (113). First, different approaches were investigated to prepare the suitable payload, namely the influence of conformational flexibility was explored and compound 74 (SF223) was synthesized, resulting in more rigid molecule. Moreover, the synthetic route of preparation of compound 74 (SF223) (Figure 7B) was considerably shorter than of compound 47a (SF183) (Figure 7B).

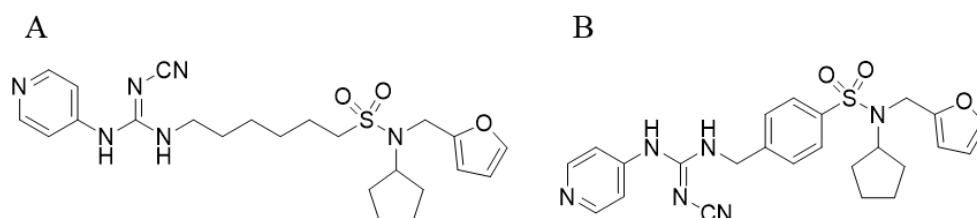


Figure 7 Structures of NAMPT inhibitors. Original, very potent molecule 47a (SF183) (A). An improved molecule 74 (SF223), an ADC payload.

Different chemical modifications can be done to obtain the payload, that would be suitable for conjugation to mAb (Figure 8). Therefore, to analyze the Structure-Activity Relationship (SAR), a small library of thirteen compounds (containing cyanoguanidine, triazole/tetrazole, acrylamide or thiourea as different connecting units) was synthesized at the University of Sevilla.

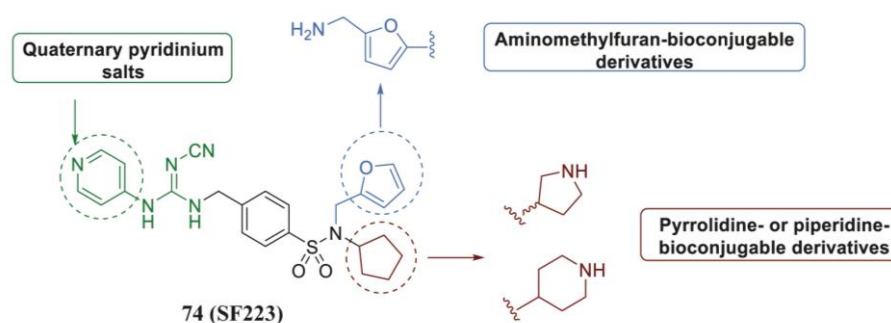


Figure 8 Possible chemical modifications. Figure prepared by Simone Fratta

2 Materials and Methods

2.1 Production of anti-CD138 antibodies

Construction of heavy and light chain expression vectors

The heavy chain (HC) and light chain (LC) variable regions of anti-CD138 antibody were based on the humanized antibody nBT062, that is used in indatuximab ravtansine (93) and they were chosen from the patent (Daelken *et al.* US 2009/0169570 A1, Jul. 2, 2009). All further experiments were performed at HDP during my secondment.

The plasmids containing the anti-human HC and LC variable regions of anti-CD138 antibody were ordered from GeneArt (LifeTechnologies). Then the variable regions were amplified by PCR, using specific primers (designed at HDP) and Phusion® High-Fidelity PCR Master Mix with HF Buffer (NEB), subsequently purified (QIAquick PCR purification Kit, following the instructions) and cut by restriction enzymes (*PmeI* and *ApaI* for HC and *NotI* and *BspEI* for LC). Meanwhile the Trastuzumab backbone vectors for HC and LC were digested with corresponding restriction enzymes and purified on 1 % agarose gel. Cut inserts were ligated into Trastuzumab backbones for HC and LC respectively. Briefly, 50 ng of vector (HC and LC) was mixed with 3-fold molar excess of corresponding insert. Then 2 µL of Ligase Reaction Buffer (NEB) and 1 µL of T4-DNA ligase (NEB) was added to the mixture of vector and insert of HC and LC. Ligation reaction was incubated for 2 hours at RT and chilled on ice after. After, the NEB5α chemical competent cells (NEB), were thawed and aliquoted, 5 µL of each HC and LC ligase reactions were added to the cells and mixed by finger-flicking. The tubes were incubated on ice for 30 min, then 30 sec at 42°C and finally 5 min on ice. Then, 950 µL of recovery media (SOC medium, Fluka) was added, and cells were incubated in cell culture tube for 1 hour at 37°C with shaking. After, the bacteria were spread into antibiotic selection plates (LB agar plates with ampicillin, prepared before as described by Invivogen) and incubated overnight at 37°C. The next day, 4 colonies were picked, and each put in 3 mL of TB medium (Gibco) with added ampicillin and incubated overnight at 37°C with shaking. The following day the mini prep was performed according to the manufacturer's instructions of QIAprep Spin Miniprep Kit (Qiagen). The plasmid DNA from selected clones was sent for sequencing, to confirm the correct HC and LC structures. After the structures were confirmed, the NEB5α were transformed again, but this time in a bigger volume, in total 500 mL of TB medium was used for each chain and incubated overnight. The next day the mega prep was performed according to the manufacturer's instructions of EndoFree Plasmid Mega Kit (Qiagen). The collected plasmid DNA was again sent for sequencing to confirm the correct HC and LC structures.

Transient expression of anti-CD138 antibodies in Expi293 cells

The plasmid DNA of anti-CD138 antibody HC and LC was transfected in Expi293F cells (Expression System Kit). Two 2 L shake flasks were prepared with 425 mL of medium with 1.25×10^9 cells in each flask and incubated at 37°C in humidified atmosphere of 8 % CO₂ in orbital shaker at 125 rpm for 2-3 hours. Meanwhile the lipid-DNA complex solution was prepared, for that 200 µg of HC and 300 µg of LC plasmid DNA was diluted in Opti-MEM medium (Invitrogen) to a total volume of 25 mL. Also, 2.5 mL of PEI reagent (HDP) was diluted in Opti-MEM medium to a total volume of 25

mL and incubated for 5 min at RT. After, the transfection reagents were added immediately and all at once to the DNA solutions, obtaining the total volume of 50 mL for each, then, they were vortexed briefly and incubated for 15 min at RT. The ready mixture of DNA-transfection reagents (50 mL) was added to shaker flasks with Expi293F cells. The cells were incubated at 37°C in humidified atmosphere of 8 % CO₂ in orbital shaker at 125 rpm. After 16-18 hours post-transfection, the cells were resuspended in a fresh Expression Medium without antibiotics (Expression System Kit).

At day 6 the medium with the cells was collected and filtered using Sartolab® RF unit and vacuum. The Antibodies were purified using IgG Protein A chromatography, following HDP's protocol. Next, aggregates and toxins were removed by gel filtration (preparative FPLC – ÄKTA), using hiLoad 26/600 Superdex 200 pg, prepacked XK26 column. The antibodies were also analysed by SEC-HPLC, for presence of monomers and by EndoZyme® II Recombinant Factor C (rFC) Assay for endotoxin detection.

2.2 Production of payload and payload-linker modifications

All the chemistry was done at the University of Sevilla and at HDP. Detailed materials and methods can be found in his PhD thesis – “Synthesis of new NAMPT inhibitors as potential anti-cancer drugs. An approach to antibody-drug-conjugates.” – Simone Fratta, Sevilla 2022.

2.3 Bioconjugation of payload-linker to the anti-CD138 antibody

The bioconjugation of the prepared payload-linkers to the produced anti-CD138 antibodies was performed HDP. Briefly, the reaction was carried out in a buffer solution (pH 7.4) with DMSO as co-solvent (10-20%) Firstly, the anti-CD138 antibodies were treated with tris(2-carboxyethyl) phosphine) (TCEP) to reduce the disulfide bonds, while the non-reacted thiols were capped with an excess of N-ethylmaleimide, which was quenched with N-acetyl-L-cysteine before purification on PD-10 column. Then the eluted protein-containing fractions from the column were pooled, dialysed overnight in PBS (pH 7.4) in Slide-A-Lyzer Dialysis Cassettes 20'000 MWCO. The protein concentration was then adjusted to 5 mg/mL and sterile-filtered. Next, the analytical department of HDP verified the formation of protein aggregates by size exclusion chromatography (SEC-HPLC) and performed DAR analysis by Time-of-flight mass spectrometry (TOF-MS).

2.4 Biological evaluation of NAMPT inhibitors, anti-CD138 antibodies, and ADCs *in vitro*

The final evaluation of synthesized payloads, anti-CD138 antibodies and finally ADCs was performed back at CHUV. All the cell lines were cultured in RPMI medium in 5 % CO₂ at 37°C.

Cell surface expression of CD138 and antibody binding assay – flow cytometry

To assess the cell surface expression of CD138 antigen on RPMI8226 and Namalwa cell lines, an anti-CD138 antibody (Beckman Coulter) labelled with PE was used. The cells were collected and stained with 3 μL of the antibody, incubated at 4 °C for 30 min and washed with cold PBS before analysis by flow cytometry.

The antibody binding assay was carried out with anti-CD138 antibody (5mg/mL), human IgG1 isotype control (Invitrogen) and anti-human IgG (Fc specific) – FITC antibody produced in goat (2nd antibody). Firstly, the equal number of cells was collected (300,000) for RPMI8226 and Namalwa. Then the cells were resuspended in 50 μL of medium and 50 μL of pre-diluted anti-CD138 antibody and IgG control solutions (each of final concentration of 2 $\mu\text{g}/\text{mL}$). Fifty μL of medium were added to the untreated sample and 2nd antibody control. Samples were incubated for 30 min on ice and then washed 2 times with ice cold PBS. After, 100 μL of the 2nd antibody solution was added in the dilution 1:10 000, and 100 μL of medium for untreated sample. Samples were incubated on ice and protected from light for 30 min and then washed 2 times with ice cold PBS. After the last wash, the cells were resuspended in 300 μL of PBS and analysed by flow cytometry.

Cytotoxicity of payloads and ADCs on different cell lines – Flow cytometry

The cytotoxicity of synthesized payloads and all anti-CD138 ADCs was assessed on flow cytometry. The cells (ML2, RPMI8226 or Namalwa) were plated (200'000 cells/well) and the compounds were added in a range of concentrations. After 96 hours of incubation the cells were collected and double-stained with Annexin V (ANXN) and 7AAD fluorescent probes in annexin V binding buffer (BD Biosciences). After 15 min incubation in the dark the samples were analysed with flow cytometry.

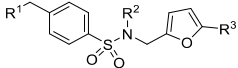
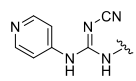
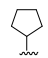
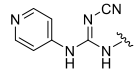
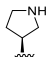
3 Results

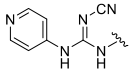

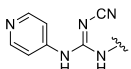
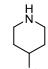
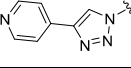
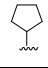
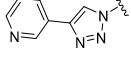
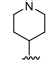
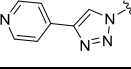

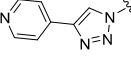
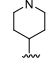
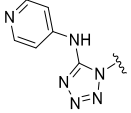

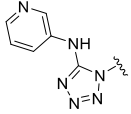
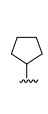
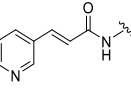
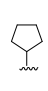
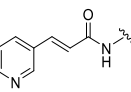
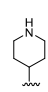
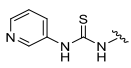
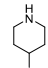
3.1 Evaluation of NAMPT inhibitors as payloads for ADCs *in vitro*

The library of 14 conjugable NAMPT inhibitors was prepared at the University of Sevilla (Table 3). The compounds were first evaluated on ML2 cell line (acute myeloid leukemia) and then, the most potent compounds were additionally assessed on RPMI8226 (MM) cell line, expressing CD138, the target for our ADCs.

Among the furfurylamine derivatives, the compound SF271 (with the tetrazole connecting group) had the highest cytotoxicity against both cell lines (entry 11), with IC_{50} of 0.9 and 34 nM on ML2 and RPMI8226, respectively. Another furfurylamine derivative, SF270 (entry 12), had the second highest IC_{50} (11 nM on ML2 and 118 nM on RPMI8226) in this group of compounds. The direct analogues of SF223, compounds containing cyanoguanidines groups, were also very potent, with IC_{50} between 9 and 18 nM on ML2 cell line. However, the modification of cyclopentyl group (R^2), lowered their cytotoxicity (entry 3,4,5 vs 2). Noteworthy, the position of N in the pyridine has influenced the cytotoxicity of the compounds, the compounds with 3-pyridine (entry 7 and 11) were significantly more potent than the same compounds with 4-pyridine (entry 6 and 10) (Table 3). Therefore, considering the cytotoxicity *in vitro* and variability of the structures of the molecules, SF223 (74), SF270 (89) and SF271 (93) were chosen as payloads for ADCs synthesis. Additionally, their calculated partition coefficient (ClogP) values were determined at the University of Sevilla, resulting in ClogP of: SF223 – 3.12, SF270 – 2.64, SF271 – 3.2.

Table 3 Evaluation of new payloads for ADCs on ML2 and RPMI8226 cell lines. NA – not available. Data are $n=3 \pm SD$.

						
Entry	ID	R ¹	R ²	R ³	ML2 IC_{50} [nM] \pm SD	RPMI8226 IC_{50} [nM] \pm SD
1	APO866	-	-	-	0.2 ± 0.5	6 ± 0.4
Cyanoguanidines						
2	74 (SF223)			H	0.53 ± 0.02	2.8 ± 0.11
3	102a			H	18 ± 0.4	NA

4	102b			H	11.5 ± 2.4	NA
5	102c			H	9 ± 1	NA
Triazoles						
6	82			CH ₂ NH ₂	> 2000	NA
7	96c			H	131 ± 18	NA
8	97a			H	> 2000	NA
9	97c			H	> 2000	NA
Tetrazoles						
10	92			CH ₂ NH ₂	169 ± 19	NA
11	93 (SF271)			CH ₂ NH ₂	0.89 ± 0.02	34.13 ± 1
Acrylamides						
12	89 (SF270)			CH ₂ NH ₂	10.67 ± 3	118 ± 10.7
13	104c			H	164 ± 15	NA
Thiourea						
14	103c			H	> 2000	NA

3.2 Preparation of anti-CD138-NAMPT inhibitors ADCs

Synthesis and characterization of anti-CD138 antibodies

Anti-CD138 antibody was synthesized during my secondment at HDP. Briefly, the sequences of heavy chain (HC) and light chain (LC) variable regions (inserts) were ligated into HC and LC backbones (based on Trastuzumab, provided by HDP) and transformed into chemical competent *E. coli* cells. After successful cloning, the plasmid DNA of both HC and LC was transiently expressed in Expi293F cells (derived from human HEK293 cell line). The antibodies were recovered from the Expi293F cell culture supernatant after 6 days using protein A chromatography and purified by gel filtration.

Subsequently, they were analyzed for aggregates formation (Figure 9), resulting in 90.8 % purity of monomers.

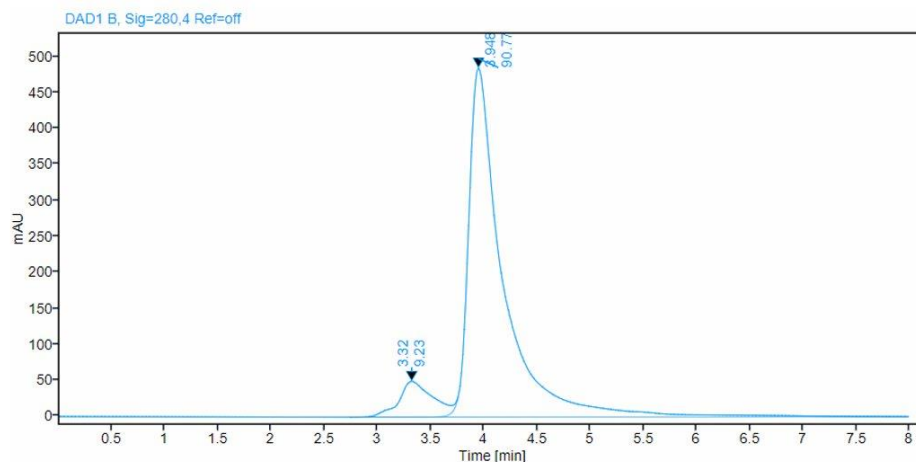


Figure 9 SEC-HPLC analysis of aggregates of anti-CD138 antibody. The results showed 90.8 % of monomers.

Next, the produced anti-CD138 antibody was assessed for its ability to bind the target (CD138 antigen). Therefore, target-positive (RPMI8226) and target-negative (Namalwa) cell lines were used (Figure 10).

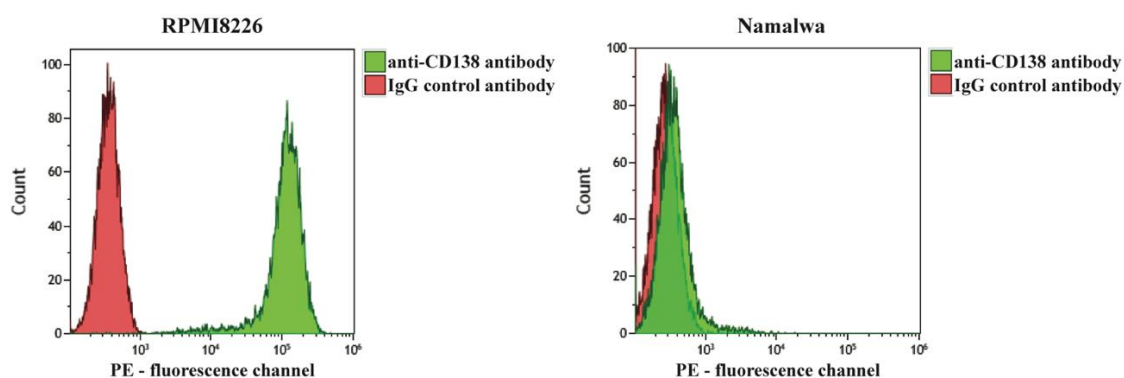


Figure 10 CD138 marker expression on RPMI8226 and Namalwa cells.

Antibody binding assay was subsequently carried out on both cell lines (Figure 11). The cells were first incubated with anti-CD138 antibody or IgG control and then stained with the 2nd anti-human IgG (Fc) antibody, which is labelled with FITC. Therefore, when the primary antibody is binding its target, the 2nd antibody subsequently binds the primary one, giving the fluorescence signal, that is finally detected by flow cytometry.

The results showed that the produced anti-CD138 antibody binds to RPMI8226 cells, but not to Namalwa cells in the same tested concentrations (Figure 11). This observation supported indirectly, the target specificity of this antibody.

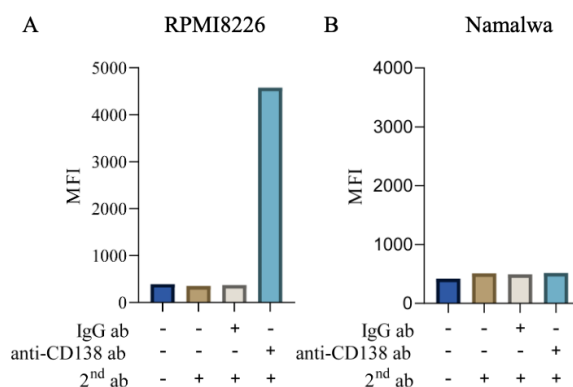


Figure 11 anti-CD138 antibody binding assay. (A) RPMI8226 cell line and (B) Namalwa cell line. Results are shown of the representative experiment.

Collectively, the generated anti-CD138 antibodies can be used for further bioconjugation to the payloads.

Payload-Linker preparation

Two types of linkers were selected for conjugations; i) a classic dipeptide cathepsin-B sensitive linker (MC-Val-Ala-PAB-PNP, Figure 12A) and ii) cathepsin-B sensitive linker, modified with PEG chain, to increase the hydrophilicity of the linker-drug complex (Figure 12B). The latter linker has two variants, one with Ala-Val fragment (106a) and the other with Ala-Cit fragment (106b) (Figure 12B).

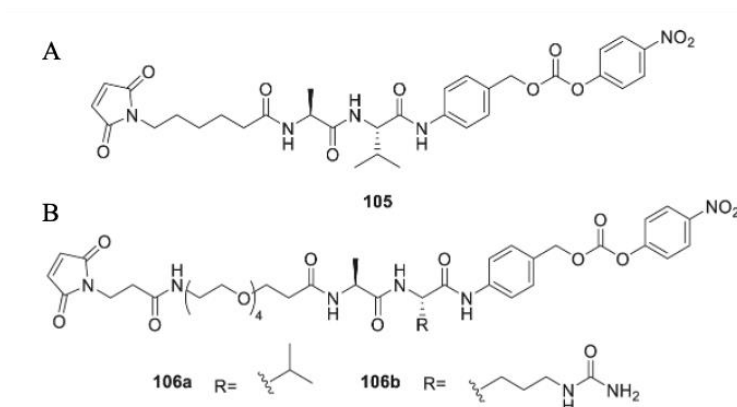


Figure 12 Structures of the used linkers for ADCs. Figure prepared by Simone Fratta.

The presented linkers are suitable for amino-functionalized payloads, that is for compounds SF270 and SF271. Therefore, the synthesis of those payloads with chosen linkers was done as described in Figure 13. The five payload-linkers were synthesized, 107, 108a-b and 109a-b.

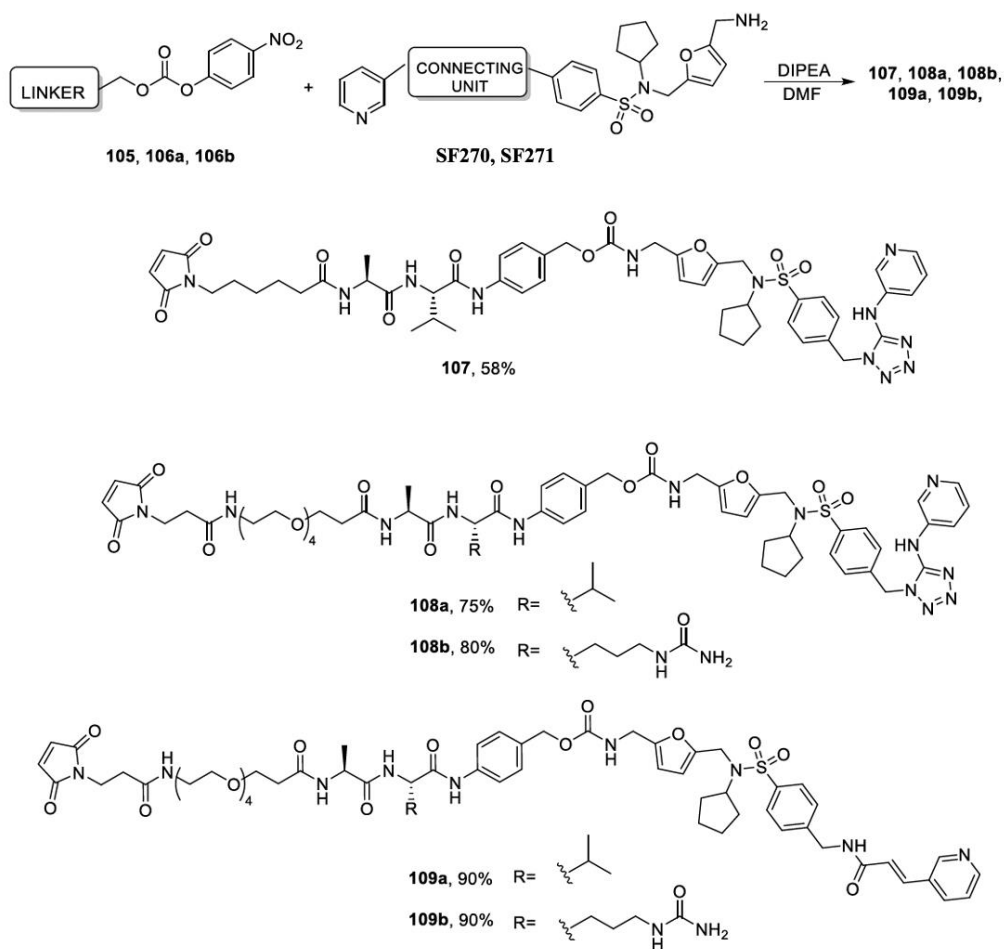


Figure 13 Synthesis of five payload-linkers. DIPEA – N,N-Diisopropylethylamine; DMF – Dimethylformamide. Figure prepared by Simone Fratta.

The compound SF223 does not bear an amino group, therefore the initial modification of linker (106a) was conducted. After the chemical synthesis, which is shown in Figure 14 the quaternary pyridinium salt of Val-Ala (PEG4) linker was synthesized (112), that was finally conjugable to SF223 compound.

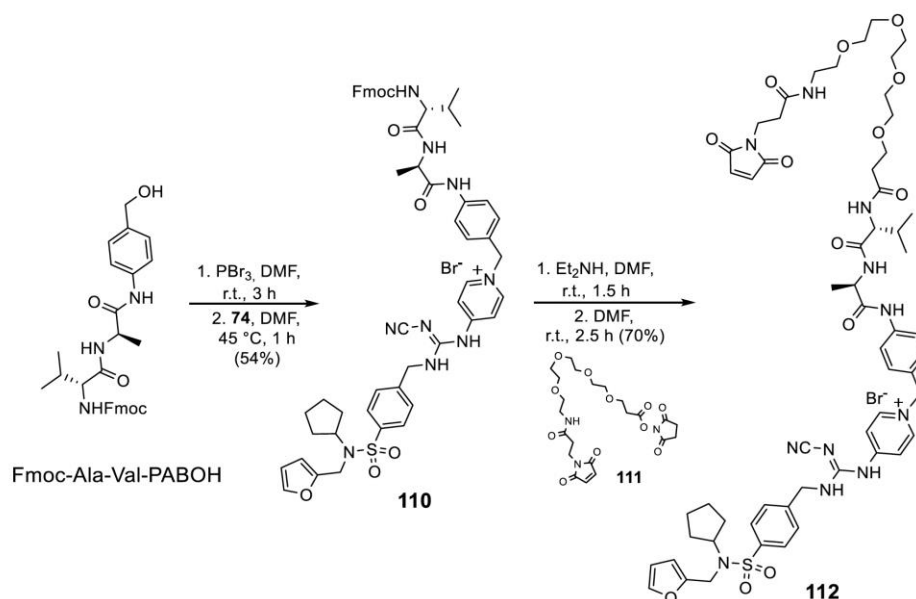


Figure 14 Synthesis of the specific payload-linker for SF223 compound. Fmoc-Ala-Val-PAB-OH – commercially available linker. PBr_3 – Phosphorus tribromide; DMF – Dimethylformamide; Et_2NH – Diethylamine. Figure prepared by Simone Fratta.

Bioconjugation of payload-linker to the antibody

The bioconjugation of payload-linkers 107, 108a-b, 109a-b and 112 to anti-CD138 antibody was carried out at HDP. The summary of synthesized ADCs is shown in Table 4 and Figure 15.

Table 4 Summary of synthesized NAMPT inhibitors ADCs.

Name	Compound	Antibody	Linker	DAR (drug to antibody ratio)
SF306	SF271	CD138	Val-Ala-PABC	7.83
SF315	SF270	CD138	Val-Ala-PABC (PEG 4)	7.72
SF316	SF271	CD138	Val-Ala-PABC (PEG 4)	7.55
SF318	SF270	CD138	Val-Cit-PABC (PEG 4)	8.42
SF319	SF271	CD138	Val-Cit-PABC (PEG 4)	8.33
SF322- T1	SF223	CD138	Val-Ala-PAB (PEG 4)	7.69

PABC= *p*-aminobenzylcarbamate, PAB= *p*-aminobenzyl.

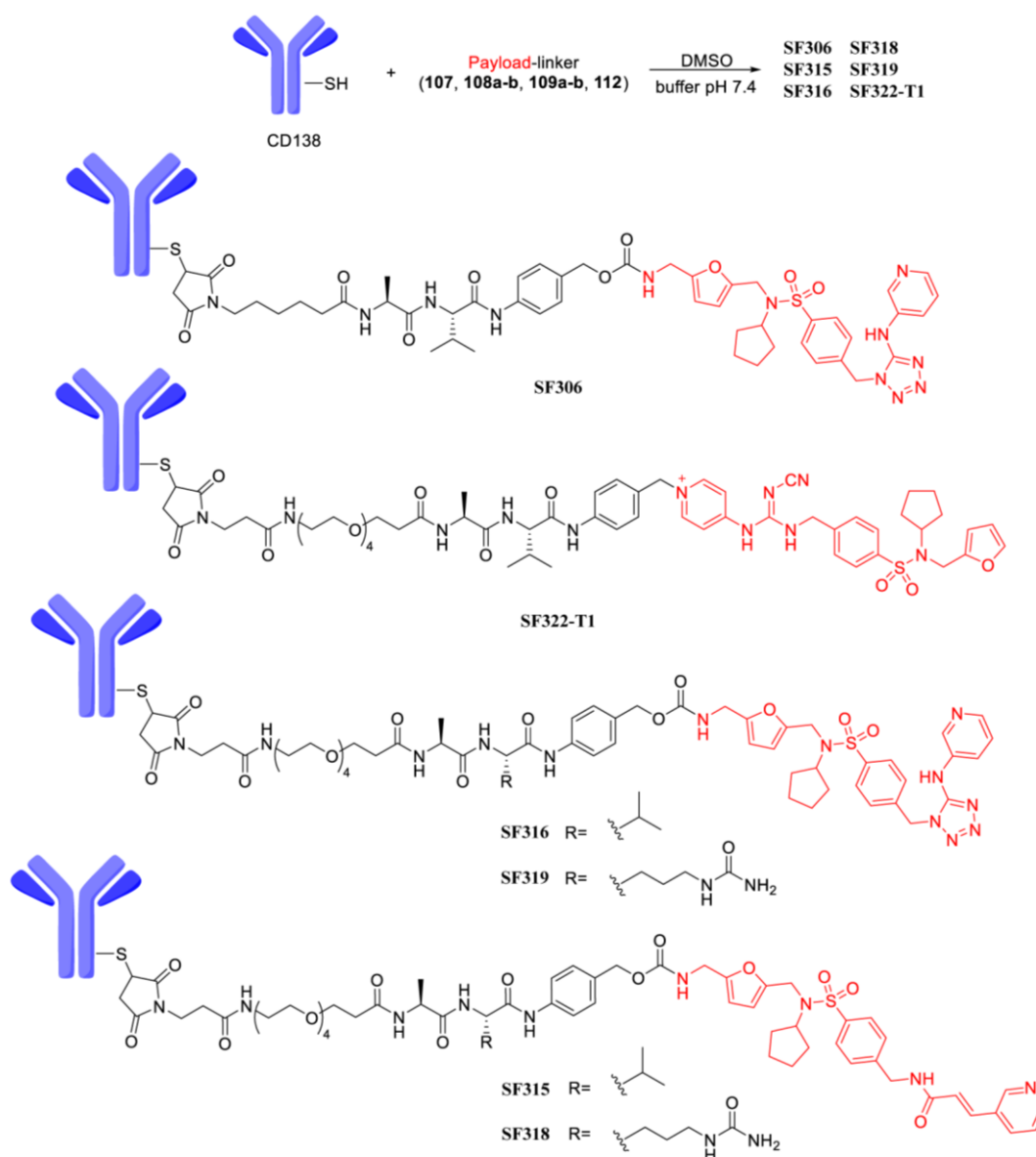


Figure 15 Synthesis of 6 NAMPT inhibitors ADCs. Figure prepared by Simone Fratta

3.3 Evaluation of anti-CD138-NAMPT inhibitors ADCs *in vitro*

Firstly, as shown in Table 3, the inhibitors alone were evaluated for their cytotoxicity against RPMI8226 cell line. They were able to cause a concentration-dependent cell death after 96 hours of treatment, resulting in an IC_{50} in low nanomolar range, 2.8, 34 and 118 nM, for SF223, SF271 and SF270 respectively (Figure 16A-C). The cytotoxicity of the anti-CD138 antibody alone was also assessed, the RPMI8226 cells were treated with a range of concentrations of anti-CD138 antibody and the cell death was measured at 96 hours (Figure 16D).

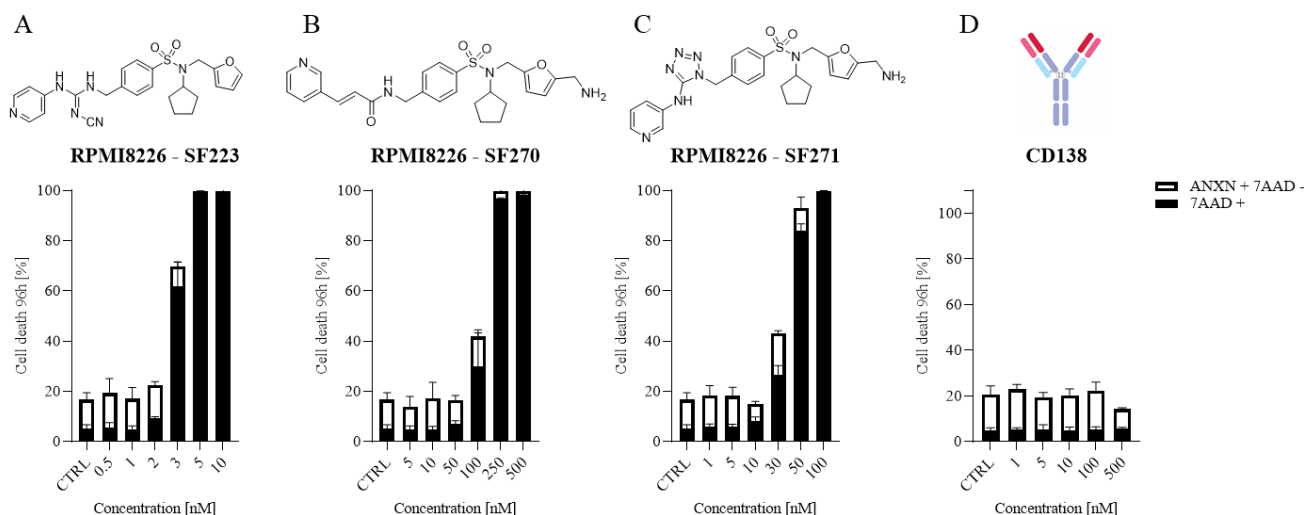


Figure 16 NAMPT inhibitors as payloads and anti-CD138 antibody induce cell death in RPMI8226 cell line in concentration dependent manner. Dose-dependent analysis of cell death induced by SF223, SF270, SF271 and anti-CD138 antibody on RPMI8226 cell line (A-D). Cell death was assessed with flow cytometry by double staining with annexin V (ANXN) and 7AAD after 96 hours of treatment. The percentage of early apoptotic cells (ANXN+ 7AAD-) is shown in white and the percentage of late apoptotic and dead cells (7AAD+) is shown in black. Data are $n=3 \pm SD$.

The ADC_ama structure and aggregates assessment is depicted in Figure 17. The cytotoxicity of ADC_ama towards RPMI8226 cells but not towards Namalwa also confirmed the specificity and the proper internalization of anti-CD138 antibody. Amanitin alone causes cytotoxicity only in hepatocytes, as it gets inside these cells via specific transporter. However, while conjugated in the ADC, it is targeted, internalized, and released only in antigen expressing cells, causing specific cell death. The treatment of RPMI8226 cells with the concentrations range of ADC_ama resulted in high cytotoxicity, the 0.5 nM concentration of ADC_ama causing 80 % of cell death (Figure 18B). It was also tested on target negative cells (Figure 18C-D). The results showed, that amanitin alone is toxic towards Namalwa cells only in very high (3.5 μM) concentration, and in ADC it does not cause the cell death up to 100 nM. However, in 500 nM concentration of ADC_ama, the cytotoxicity is also caused in target negative cells. The 500 nM of tested ADC_ama corresponds to 3.5 μM of amanitin alone. A similar concentration of amanitin alone was tested on the cells and caused cytotoxicity (Figure 18C).

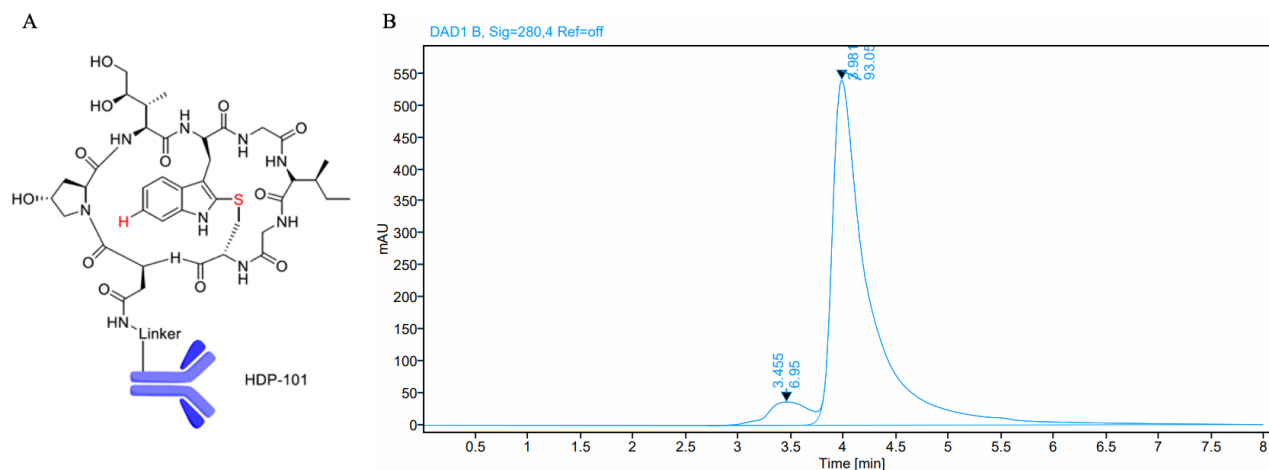


Figure 17 Anti-CD138 antibody conjugated with amanitin via Val-Ala-PABC linker and its aggregates assessment. (A) ADC_ama is used as positive control, DAR = 7. Scheme prepared by Simone Fratta. **(B)** SEC-HPLC analysis of ADC_ama, showing 93 % of monomers.

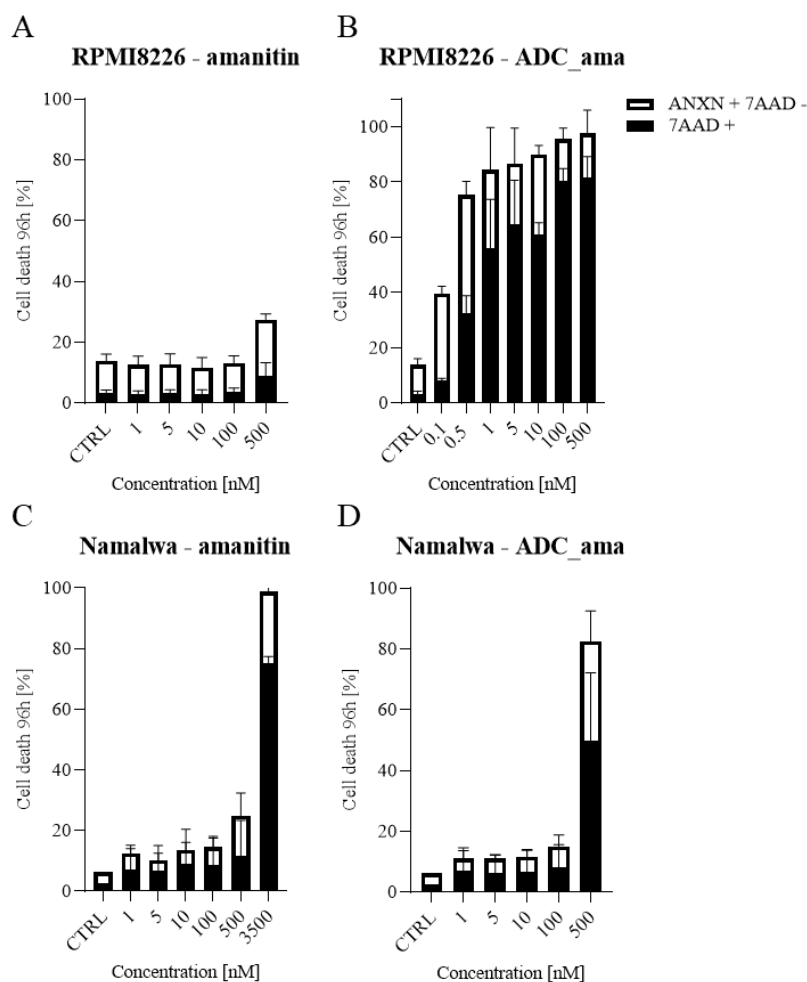


Figure 18 Cytotoxicity of amanitin and ADC_ama. On RPMI8226 (A, B) and Namalwa (C, D) cell lines. The cell death was assessed as described in Figure 14. Data are $n=3 \pm SD$. The IC_{50} of 0.11 ± 0.03 nM was calculated for ADC_ama on RPMI8226 cell line.

Finally, newly synthesized NAMPT inhibitors ADCs (NAMPTi_ADCs) were evaluated for their cytotoxicity *in vitro* on RPMI8226 cell line. The results showed no cytotoxicity up to 500 nM for SF306, SF315, SF318 and SF322-T1. SF316 and SF319 caused between 60 and 70 % of cell death at 500 nM (Figure 19A-F). Of note, this cell line is overall less sensitive to APO866 (IC₅₀ of 6 nM; Table 3), compared to other haematological malignancies (32). Additionally, each of NAMPTi_ADCs was also assessed for the presence of monomers. As depicted on figure 20, all the NAMPTi_ADCs have formed aggregates, with no monomers present in the sample.

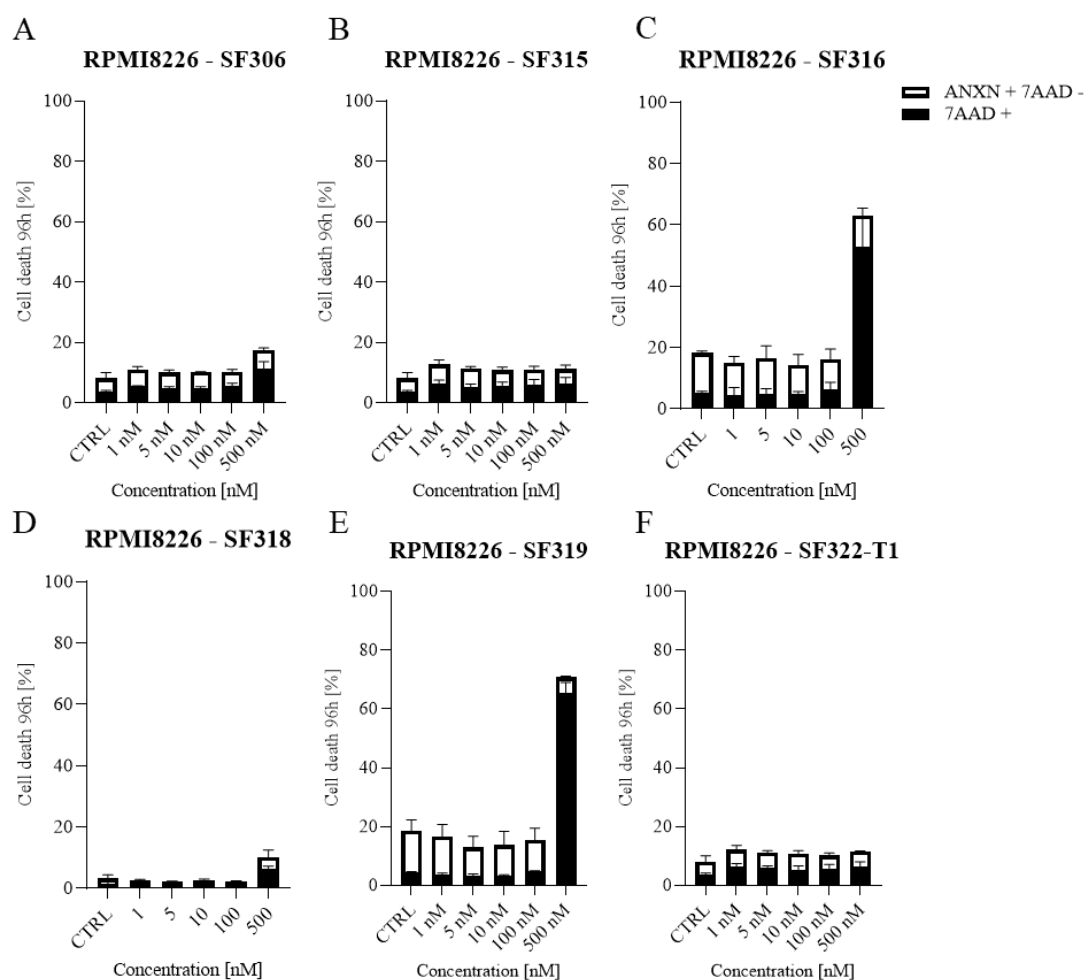


Figure 19 Cytotoxicity of NAMPT inhibitors ADCs on RPMI8226 cell line. The cell death was assessed as described in Figure 14. Data are $n=3 \pm$ SD.

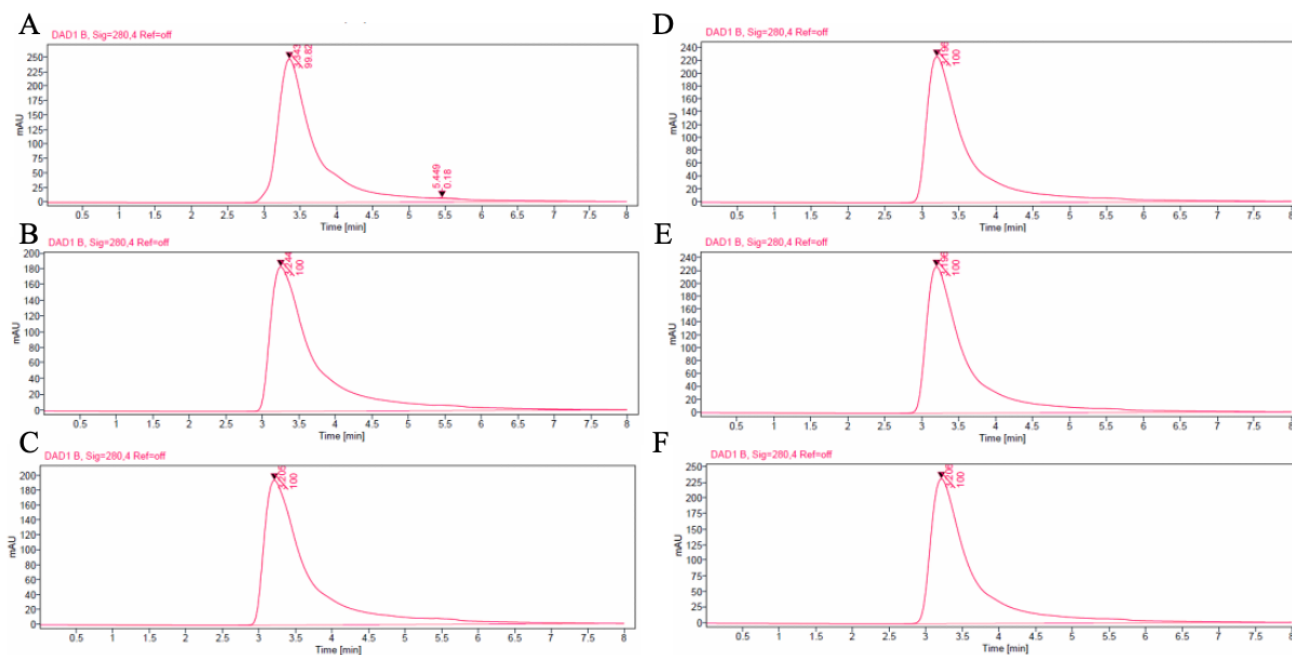


Figure 20 SEC-HPLC analysis of aggregates. A – SF306, B – SF315, C – SF316, D – SF318, E – SF319, F – SF322-T1.

4 Conclusions

In conclusion, six NAMPTi_ADCs were synthesized. Further analysis showed that they all formed aggregates. The anti-CD138 antibody successfully targeted CD138 antigen and delivered amanitin intracellularly, causing high cytotoxicity, not caused by amanitin alone. NAMPTi_ADCs however did not exhibit high on-target cytotoxicity, compared to their positive control.

Chapter 4: General discussion and perspectives

1 Biological characterization of novel NAMPT inhibitors

APO866 was discovered 20 years ago, but there is still an ongoing challenge to produce effective NAMPT inhibitors. Indeed, cancer cells upregulate NAMPT, to intensively produce NAD^+ to sustain their fast metabolism.

In this project, I have characterized different classes of APO866 analogues. All the compounds were functionalized with furan ring in their tail group (Figure 21). Furan moiety in the structure of NAMPT inhibitors can increase their polarity (114). The modification done in connecting unit of most of the molecules was with cyanoguanidine group. The NAMPT inhibitors with cyanoguanidine moiety have been previously reported having good potency *in vitro* and *in vivo* in ovarian mouse xenograft tumor model (115). However, in our hands, the introduction of cyanoguanidine group suppressed the *in vivo* efficacy of otherwise very potent *in vitro* molecules. Only JJ08 (Figure 21B), having the same connecting unit as APO866 (Figure 21A), had good efficacies both *in vitro* and *in vivo*. Overall, the most potent inhibitor *in vitro* was SF183 with sulfonyl and cyclopentyl groups (Figure 21G). This was exquisitely observed on acute myeloid leukemia cells.

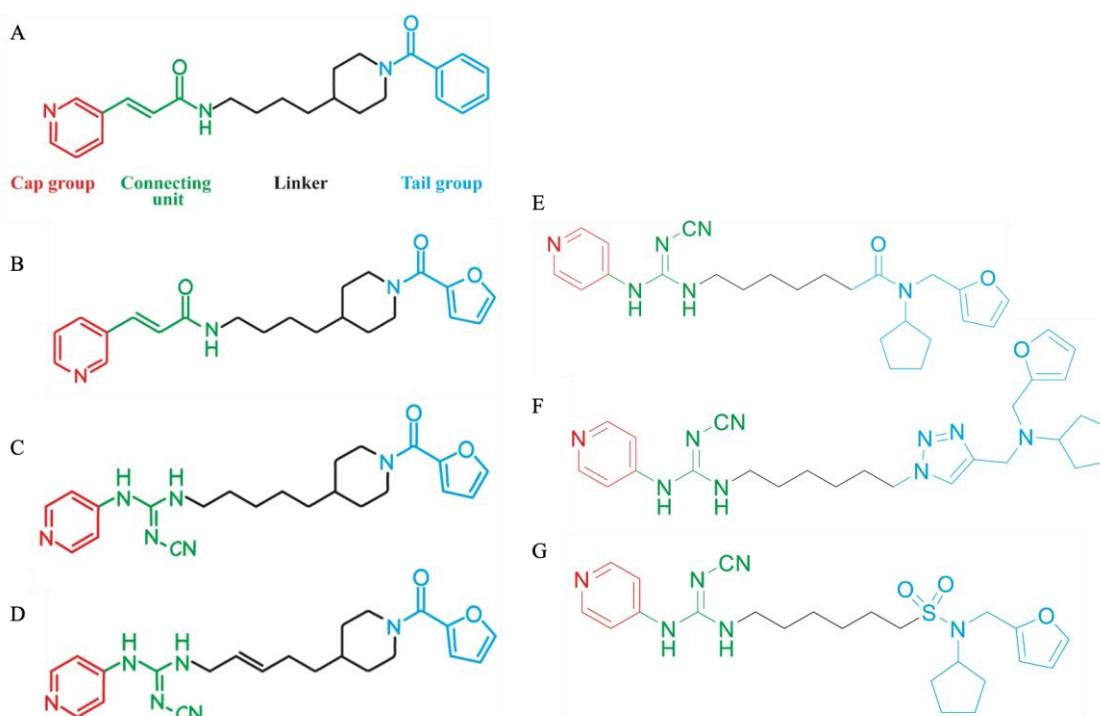


Figure 21 NAMPT inhibitors tested in this work. (A) APO9866, (B) JJ08, (C) FEI191, (D) FEI199, (E) SF103, (F) SF164, (G) SF183.

The mode of action of the new inhibitors followed the same known mechanism as that observed with APO866 (32-34, 116). They induce diverse types of cell death, caspase-dependent apoptosis or

necrosis as described here. However, it can be hypothesized, as it is known for APO866 (32, 34), that they may also induce caspase independent apoptosis and autophagy. As caspase dependent apoptosis requires ATP and in later stages of incubation with NAMPT inhibitors there is no ATP available anymore, the initial caspase-dependent apoptosis may turn into caspase-independent one, which is finally followed by necrosis. The fast drop in ATP, even before the mitochondrial membrane depolarization, can be explained by a great decrease of NAD^+ (in first 8 hours after inhibiting NAMPT), a glycolysis substrate, which also contributes to ATP production. Nonetheless, as an ultimate step, when the MMP decreases, ATP is completely depleted and that directly correlates with cell death.

The interesting observation is the abrogation of NAMPTi caused cell death by CAT, the potent ROS scavenger. After treatment of the cells with CAT together with NAMPTi, an NAD^+ depletion was still observed as well as a small decrease in ATP levels. However, no cell death occurred, indicating that ROS production is an ultimate step of cell death caused by NAMPTi.

Finally, the *in vivo* evaluation of new NAMPTi shows the discrepancy between the *in vitro* and *in vivo* results, which is an important consideration in the development of drugs implicated in cancer cells metabolism. As NAD^+ is the most important molecule for cellular energetics, there are many pathways through which it can be produced. It is also known, that different types of cancers have different predominant pathways, dependent on NAMPT and/or NAPRT, to produce NAD^+ (28). For tumors that rely on salvage pathway, NAMPTi will be effective, however for those with overexpression of NAPRT, the inhibition of the latter enzyme can bring more effective results. Indeed, there has been a recent attempt to develop potent NAPRT inhibitors (117, 118). Moreover, the inhibition of NAPRT in breast cancer models *in vitro* and *in vivo*, has sensitized the cells to NAMPT inhibitors (119). Therefore, the dual inhibition strategies can be explored also in hematological malignancies. The study of gene expressions of both NAMPT and NAPRT, done by Olesen *et al.* on different lymphomas, suggests that however most of the tested lymphomas have high expression of NAMPT, resulting in sensitivity to NAMPTi, there are some, such as follicular lymphoma, that has higher expression of NAPRT (23). Noteworthy is another aspect, as the authors argue, the low expression of NAPRT gene in some tumors allows the co-administration of NA, that can be used by healthy cells to counteract some cytotoxicity caused by NAMPTi (23). That underlines the importance of assessing the differences in enzyme expression levels in various cancer types and patients.

Moreover, in *in vitro* settings the main source of NAD⁺ is NAM originating from the cell culture medium. However *in vivo*, in mice or humans, many other precursors are present from which NAD⁺ can be synthesized. We and the others have previously reported the contribution of gut microbiota to resistance to NAMPTi in mice (120, 121). It was reported that the nicotinamidase, the enzyme present in bacteria, can convert the NAM to NA, therefore circumventing the salvage pathway and using the alternate one, through NAPRT (121).

Therefore, targeting more than one route of NAD⁺ synthesis and the control of NAD⁺ precursors, i.e., through a specific diet, should be taken into consideration in future therapeutic approaches with NAMPTi.

2 Targeted delivery of NAMPT inhibitors – Antibody Drug Conjugates

Before the ADCs described in this thesis were developed, there were two publications available with NAMPTi_ADCs targeting different antigens on several cancer models (106, 107). The third, most recent one was published after our ADCs were produced and provided detailed information on the mode of action of NAMPTi_ADCs, analysing their metabolites formation both *in vitro* and *in vivo* (108). The NAMPTi_ADCs designed by Karpov *et al.* were targeting biomarkers expressed on gastrointestinal and breast cancer cells (106). Whereas, from the NAMPTi_ADCs proposed by Neumann *et al.* the most effective *in vivo* were ADCs targeting Hodgkin lymphoma and acute myeloid leukemia (107). Moreover, the most potent payload was APO866, modified with the additional amine group used for payload-linker attachment (107). The NAMPTi_ADCs published by Böhnke *et al.* have the most optimized payload and they were tested *in vivo* in breast cancer and leukemia models. Collectively, these studies show the potential for development of improved NAMPTi_ADCs, with different payloads and most importantly targeting other malignancies.

In this work six NAMPTi_ADCs were successfully synthesized, each of them with cathepsin-cleavable linker, and with PEG4 side chain (except SF306). PEG chains are commonly used to increase the hydrophilicity of the molecules (122, 123). The ADCs synthesized here are targeting the CD138 antigen, a marker for MM which is involved in cancer cells aggressiveness (86). Currently, there are no FDA approved ADCs against CD138. However, indatuximab ravtansine is in advanced clinical trials, carrying a microtubule inhibitor as a payload (94, 96). The anti-CD138 antibody, that was used in indatuximab ravtansine had very good target selectivity and exhibited no cytotoxicity alone (93). Therefore, the same structures of binding regions were used here for the preparation of anti-CD138 antibody for NAMPTi_ADCs. In line with previous results (93), the produced anti-CD138 antibody is also selective towards MM cells, highly expressing CD138 antigen, with no binding to antigen-negative cells and with no cytotoxicity up to 500 nM (Figure 11 and 18D).

The payloads selected for the conjugation were designed based on our previous results (113, 124) and then functionalized with amine group which is one of the most common handles used in payload-linker attachments (125). Most FDA approved ADCs have the cleavable linkers (64, 126). Therefore, also here the common cathepsin cleavable linkers were used. The cytotoxicity results with positive control (ADC_ama) on target expressing (RPMI8226) cells, confirmed that anti-CD138 antibody is well internalized into the cells and amanitin is released causing very potent cell death at low concentrations (Figure 18B). However, some unspecific cytotoxicity of ADC_ama was observed on target-negative cells (Namalwa) (Figure 18D). It can be hypothesized that, when the cells are treated with 500 nM of ADC_ama, there is some free amanitin released, which in very high concentrations can be also toxic alone (Figure 18C). The payload deconjugation was observed in recent studies by Böhnke *et al.* who measured the stability of the payload-antibody connection of NAMPTi_ADC with incorporated Val-Ala linker (108). The metabolites *in vitro* were measured after 24 hours exposure to NAMPTi_ADC and isotype control ADC. Interestingly, the presence of payload with intact linker was observed inside the target expressing and mock cells, as well as in the medium after addition of specific and isotype control ADCs (108). Although, we have not performed the stability studies, based on the published data and the unspecific cytotoxicity of our NAMPTi_ADC, the payload-linker deconjugation could be hypothesized.

The aggregation of NAMPTi_ADC was observed in first developed ADCs by Karpov *et al.* The highest aggregation of 29 % was detected with the ADC with cleavable linker (106). Here, All the synthesized NAMPTi_ADC resulted in almost 100 % of aggregates. Overall, NAMPT inhibitors are rather hydrophobic, and the compounds used as payloads have ClogP around 3. The correlation between the logP and aggregation, showed that the higher the hydrophobicity of the payload the lower the stability of ADCs (127).

Finally, the NAMPTi_ADC did not show the cytotoxicity up to 500 nM on target-positive RPMI8226 cell line, in exception of SF316 and SF319 that showed up to 60 % of cytotoxicity at 500 nM concentration (Figure 19). Both ADCs have the same payload and contain PEG4. However, the exhibited cytotoxicity at 500 nM could be unspecific as discussed above, and possibly occurred due to deconjugation of the payload.

It is known that the number of loaded molecules onto ADCs influence their efficacy (128). The study conducted by Hamblett *et al.* have tested how different DARs influence the efficacy of ADCs *in vitro* and *in vivo*. They have synthesized ADCs with anti-CD30 antibody and MMAE payload and Val-Cit linker, that had a DAR between 2 and 8 and tested them *in vitro* and *in vivo* in mouse xenograft model. The most effective ADCs *in vitro* were with DAR 8 (the lowest IC₅₀ on target positive cells), the lower the DAR, the worse the efficacy of ADCs. However, *in vivo*, the lower DAR numbers had

equivalent or better efficacy. The tested ADC with DAR 4 resulted in more effective tumour eradication, than DAR 8 when treated with the same single-dose and in the same efficacy as DAR 8 in multi-dose treatment (128). Usually, higher DAR number results in higher aggregation, due to hydrophobic nature of small molecules (129). However, in the *in vivo* experiment, comparing low and high DAR done by Böhnke *et al.*, we can see that less payload molecules on NAMPTi_ADC results in less efficacy in inhibiting the tumour growth (DAR 4 vs DAR 8) (108). Therefore, when it comes to NAMPT inhibitors as payloads, the balance between an effective DAR number and no molecule aggregation must be achieved. For that, the inhibitors could be further functionalized with longer PEG chains, what would also make them less permeable, and the potential bystander effect could be avoided. The bystander effect is when the ADC metabolites cross the cell membrane and cause cytotoxicity to the surrounding cells. This effect was avoided by creating more polar compounds with no activity alone, but with high efficacy when conjugated to the antibody and delivered to its target (108).

Taking into consideration the most recent results with NAMPTi_ADC by Böhnke *et al.* the best selectivity and efficacy *in vivo* was achieved with ADCs with non-cleavable linkers of DAR between 6 and 7 (108). The NAMPTi_ADC from this work could be conjugated with non-cleavable linkers and different ratios of payload to antibody could be explored. Moreover, the optimization of payload itself or of the conjugation conditions can be done to improve the overall hydrophilicity of the ADC to avoid aggregates formation.

It is worth mentioning, that compounds SF270 and SF271, that were developed as payloads, were very potent on ML2 cell line (Table 3), with IC_{50} of 11 and 0.9 nM respectively, despite the presence of amine handle used for the antibody attachment. Therefore, it could be worth to explore those inhibitors as payloads for antibodies targeting AML. There is one FDA approved ADC against CD33 (Table 1) and a few in pre-clinical studies against other targets, such as CD123 (130-133), CXCR4 (134), C-type lectin domain family 12 member A (CLL1) (135) or Fms like tyrosine kinase 3 (FLT3) (136). Hence, the above-mentioned compounds could be used as payloads for proposed AML targets.

3 Conclusions

In summary, this work describes the *in vitro* and *in vivo* biological characterizations of a new class of APO866 analogues. The newly developed inhibitors induce very high cytotoxicity on a panel of hematological cell lines. They also follow the same mode of action as that of APO866. The JJ08 compound resulted in the same *in vivo* efficacy as that of APO866 and both FEI molecules prolonged significantly mouse survivals.

The results also highlight the importance of *in vivo* studies over *in vitro* assessments of small molecule inhibitors. As very potent compounds *in vitro*, lose their activity *in vivo*.

Moreover, in case of NAMPTi being ineffective in clinical studies, the additional targeting is crucial, as described here by creating an optimized delivery system. However, the NAMPTi_ADCs presented here need to be further optimized with different linkers and improved conjugation conditions.

Overall, the future treatments with NAMPTi, specifically delivered or not, need to be carefully managed in terms of the given diet, as the availability of different NAD⁺ synthesis precursors is a crucial aspect in developing effective NAD⁺ depleting agents. Additionally, the NAMPTi can be combined with other NAD⁺ synthesis inhibitors, possibly based on expression patterns of different enzymes in cancer patients, to obtain the most effective treatments.

References

1. Sung H, Ferlay J, Siegel RL, Laversanne M, Soerjomataram I, Jemal A, et al. Global Cancer Statistics 2020: GLOBOCAN Estimates of Incidence and Mortality Worldwide for 36 Cancers in 185 Countries. *CA Cancer J Clin.* 2021;71(3):209-49.
2. Hanahan D, Weinberg RA. The hallmarks of cancer. *Cell.* 2000;100(1):57-70.
3. Hanahan D, Weinberg RA. Hallmarks of cancer: the next generation. *Cell.* 2011;144(5):646-74.
4. Hanahan D. Hallmarks of Cancer: New Dimensions. *Cancer Discov.* 2022;12(1):31-46.
5. Cairns RA, Harris IS, Mak TW. Regulation of cancer cell metabolism. *Nature Reviews Cancer.* 2011;11(2):85-95.
6. Li J, Eu JQ, Kong LR, Wang L, Lim YC, Goh BC, et al. Targeting Metabolism in Cancer Cells and the Tumour Microenvironment for Cancer Therapy. *Molecules.* 2020;25(20).
7. Zhu Y, Liu J, Park J, Rai P, Zhai RG. Subcellular compartmentalization of NAD(+) and its role in cancer: A sereneNAde of metabolic melodies. *Pharmacology & therapeutics.* 2019;200:27-41.
8. Yaku K, Okabe K, Hikosaka K, Nakagawa T. NAD Metabolism in Cancer Therapeutics. 2018;8(622).
9. Garten A, Petzold S, Körner A, Imai S, Kiess W. Nampt: linking NAD biology, metabolism and cancer. *Trends in endocrinology and metabolism: TEM.* 2009;20(3):130-8.
10. Ghanem MS, Monacelli F, Nencioni A. Advances in NAD-Lowering Agents for Cancer Treatment. 2021;13(5):1665.
11. Nikiforov A, Kulikova V, Ziegler M. The human NAD metabolome: Functions, metabolism and compartmentalization. *Critical reviews in biochemistry and molecular biology.* 2015;50(4):284-97.
12. Reiten OK, Wilvang MA, Mitchell SJ, Hu Z, Fang EF. Preclinical and clinical evidence of NAD(+) precursors in health, disease, and ageing. *Mech Ageing Dev.* 2021;199:111567.
13. Revollo JR, Grimm AA, Imai S. The NAD biosynthesis pathway mediated by nicotinamide phosphoribosyltransferase regulates Sir2 activity in mammalian cells. *J Biol Chem.* 2004;279(49):50754-63.
14. Rongvaux A, Shea RJ, Mulks MH, Gigot D, Urbain J, Leo O, et al. Pre-B-cell colony-enhancing factor, whose expression is up-regulated in activated lymphocytes, is a nicotinamide phosphoribosyltransferase, a cytosolic enzyme involved in NAD biosynthesis. *European journal of immunology.* 2002;32(11):3225-34.
15. Navas LE, Carnero A. NAD(+) metabolism, stemness, the immune response, and cancer. *Signal Transduct Target Ther.* 2021;6(1):2.
16. Covarrubias AJ, Perrone R, Grozio A, Verdin E. NAD+ metabolism and its roles in cellular processes during ageing. *Nature Reviews Molecular Cell Biology.* 2021;22(2):119-41.
17. Kincaid JW, Berger NA. NAD metabolism in aging and cancer. *Exp Biol Med (Maywood).* 2020;245(17):1594-614.
18. Kincaid JWR, Berger NA. NAD metabolism in aging and cancer. *Experimental Biology and Medicine.* 2020;1535370220929287.
19. Zhou SJ, Bi TQ, Qin CX, Yang XQ, Pang K. Expression of NAMPT is associated with breast invasive ductal carcinoma development and prognosis. *Oncol Lett.* 2018;15(5):6648-54.
20. Li X-q, Lei J, Mao L-h, Wang Q-l, Xu F, Ran T, et al. NAMPT and NAPRT, Key Enzymes in NAD Salvage Synthesis Pathway, Are of Negative Prognostic Value in Colorectal Cancer. *Front Oncol.* 2019;9.

21. Ye C, Qi L, Li X, Wang J, Yu J, Zhou B, et al. Targeting the NAD(+) salvage pathway suppresses APC mutation-driven colorectal cancer growth and Wnt/ β -catenin signaling via increasing Axin level. *Cell Commun Signal*. 2020;18(1):16.
22. Lucena-Cacace A, Otero-Albiol D, Jiménez-García MP, Peinado-Serrano J, Carnero A. NAMPT overexpression induces cancer stemness and defines a novel tumor signature for glioma prognosis. *Oncotarget*. 2017;8(59):99514-30.
23. Olesen UH, Hastrup N, Sehested M. Expression patterns of nicotinamide phosphoribosyltransferase and nicotinic acid phosphoribosyltransferase in human malignant lymphomas. *Apmis*. 2011;119(4-5):296-303.
24. Audrito V, Messana VG, Moiso E, Vitale N, Arruga F, Brandimarte L, et al. NAMPT Over-Expression Recapitulates the BRAF Inhibitor Resistant Phenotype Plasticity in Melanoma. *Cancers (Basel)*. 2020;12(12):3855.
25. Lucena-Cacace A, Otero-Albiol D, Jiménez-García MP, Muñoz-Galvan S, Carnero A. NAMPT Is a Potent Oncogene in Colon Cancer Progression that Modulates Cancer Stem Cell Properties and Resistance to Therapy through Sirt1 and PARP. 2018;24(5):1202-15.
26. Garten A, Schuster S, Penke M, Gorski T, de Giorgis T, Kiess W. Physiological and pathophysiological roles of NAMPT and NAD metabolism. *Nature reviews Endocrinology*. 2015;11(9):535-46.
27. Sampath D, Zabka TS, Misner DL, O'Brien T, Dragovich PS. Inhibition of nicotinamide phosphoribosyltransferase (NAMPT) as a therapeutic strategy in cancer. *Pharmacology & therapeutics*. 2015;151:16-31.
28. Galli U, Colombo G, Travelli C, Tron GC, Genazzani AA, Grolla AA. Recent Advances in NAMPT Inhibitors: A Novel Immunotherapeutic Strategy. 2020;11(656).
29. Galli U, Travelli C, Massarotti A, Fakhfour G, Rahimian R, Tron GC, et al. Medicinal chemistry of nicotinamide phosphoribosyltransferase (NAMPT) inhibitors. *Journal of medicinal chemistry*. 2013;56(16):6279-96.
30. Hasmann M, Schemainda I. FK866, a highly specific noncompetitive inhibitor of nicotinamide phosphoribosyltransferase, represents a novel mechanism for induction of tumor cell apoptosis. *Cancer research*. 2003;63(21):7436-42.
31. Khan JA, Tao X, Tong L. Molecular basis for the inhibition of human NMPRTase, a novel target for anticancer agents. *Nat Struct Mol Biol*. 2006;13(7):582-8.
32. Nahimana A, Attinger A, Aubry D, Greaney P, Ireson C, Thougard AV, et al. The NAD biosynthesis inhibitor APO866 has potent antitumor activity against hematologic malignancies. *Blood*. 2009;113(14):3276-86.
33. Cloux AJ, Aubry D, Heulot M, Widmann C, ElMokh O, Piacente F, et al. Reactive oxygen/nitrogen species contribute substantially to the antileukemia effect of APO866, a NAD lowering agent. *Oncotarget*. 2019;10(62):6723-38.
34. Ginet V, Puyal J, Rummel C, Aubry D, Breton C, Cloux AJ, et al. A critical role of autophagy in antileukemia/lymphoma effects of APO866, an inhibitor of NAD biosynthesis. *Autophagy*. 2014;10(4):603-17.
35. Schou C, Ottosen ER, Petersen HJ, Björkling F, Latini S, Hjarnaa PV, et al. Novel cyanoguanidines with potent oral antitumour activity. *Bioorganic & Medicinal Chemistry Letters*. 1997;7(24):3095-100.
36. Hjarnaa PJ, Jonsson E, Latini S, Dhar S, Larsson R, Bramm E, et al. CHS 828, a novel pyridyl cyanoguanidine with potent antitumor activity in vitro and in vivo. *Cancer research*. 1999;59(22):5751-7.

37. Olesen UH, Christensen MK, Björkling F, Jäätelä M, Jensen PB, Sehested M, et al. Anticancer agent CHS-828 inhibits cellular synthesis of NAD. *Biochemical and biophysical research communications*. 2008;367(4):799-804.
38. Binderup E, Björkling F, Hjarnaa PV, Latini S, Baltzer B, Carlsen M, et al. EB1627: a soluble prodrug of the potent anticancer cyanoguanidine CHS828. *Bioorganic & Medicinal Chemistry Letters*. 2005;15(10):2491-4.
39. Korotchkina L, Kazyulkin D, Komarov PG, Polinsky A, Andrianova EL, Joshi S, et al. OT-82, a novel anticancer drug candidate that targets the strong dependence of hematological malignancies on NAD biosynthesis. *Leukemia*. 2020;34(7):1828-39.
40. Zheng X, Bair KW, Bauer P, Baumeister T, Bowman KK, Buckmelter AJ, et al. Identification of amides derived from 1H-pyrazolo[3,4-b]pyridine-5-carboxylic acid as potent inhibitors of human nicotinamide phosphoribosyltransferase (NAMPT). *Bioorganic & Medicinal Chemistry Letters*. 2013;23(20):5488-97.
41. Zheng X, Bauer P, Baumeister T, Buckmelter AJ, Caligiuri M, Clodfelter KH, et al. Structure-Based Discovery of Novel Amide-Containing Nicotinamide Phosphoribosyltransferase (Nampt) Inhibitors. *Journal of medicinal chemistry*. 2013;56(16):6413-33.
42. Zhao G, Green CF, Hui Y-H, Prieto L, Shepard R, Dong S, et al. Discovery of a Highly Selective NAMPT Inhibitor That Demonstrates Robust Efficacy and Improved Retinal Toxicity with Nicotinic Acid Coadministration. *Molecular cancer therapeutics*. 2017;16(12):2677-88.
43. Wilsbacher JL, Cheng M, Cheng D, Trammell SAJ, Shi Y, Guo J, et al. Discovery and Characterization of Novel Nonsubstrate and Substrate NAMPT Inhibitors. *Molecular cancer therapeutics*. 2017;16(7):1236-45.
44. Matheny CJ, Wei MC, Bassik MC, Donnelly AJ, Kampmann M, Iwasaki M, et al. Next-generation NAMPT inhibitors identified by sequential high-throughput phenotypic chemical and functional genomic screens. *Chem Biol*. 2013;20(11):1352-63.
45. Travelli C, Aprile S, Rahimian R, Grolla AA, Rogati F, Bertolotti M, et al. Identification of Novel Triazole-Based Nicotinamide Phosphoribosyltransferase (NAMPT) Inhibitors Endowed with Antiproliferative and Antiinflammatory Activity. *Journal of medicinal chemistry*. 2017;60(5):1768-92.
46. Abu Aboud O, Chen CH, Senapedis W, Baloglu E, Argueta C, Weiss RH. Dual and Specific Inhibition of NAMPT and PAK4 By KPT-9274 Decreases Kidney Cancer Growth. *Molecular cancer therapeutics*. 2016;15(9):2119-29.
47. Chan DA, Sutphin PD, Nguyen P, Turcotte S, Lai EW, Banh A, et al. Targeting GLUT1 and the Warburg effect in renal cell carcinoma by chemical synthetic lethality. *Sci Transl Med*. 2011;3(94):94ra70.
48. Adams DJ, Ito D, Rees MG, Seashore-Ludlow B, Puyang X, Ramos AH, et al. NAMPT is the cellular target of STF-31-like small-molecule probes. *ACS Chem Biol*. 2014;9(10):2247-54.
49. Kraus D, Reckenbeil J, Veit N, Kuerpig S, Meisenheimer M, Beier I, et al. Targeting glucose transport and the NAD pathway in tumor cells with STF-31: a re-evaluation. *Cell Oncol (Dordr)*. 2018;41(5):485-94.
50. Wu Y, Wang L, Huang Y, Chen S, Wu S, Dong G, et al. Nicotinamide Phosphoribosyltransferase (NAMPT) Is a New Target of Antitumor Agent Chidamide. *ACS medicinal chemistry letters*. 2020;11(1):40-4.
51. Holen K, Saltz LB, Hollywood E, Burk K, Hanauske A-R. The pharmacokinetics, toxicities, and biologic effects of FK866, a nicotinamide adenine dinucleotide biosynthesis inhibitor. *Investigational New Drugs*. 2008;26(1):45-51.

52. Goldinger SM, Gobbi Bischof S, Fink-Puches R, Klemke C-D, Dréno B, Bagot M, et al. Efficacy and Safety of APO866 in Patients With Refractory or Relapsed Cutaneous T-Cell Lymphoma: A Phase 2 Clinical Trial. *JAMA dermatology*. 2016;152(7):837-9.
53. Hovstadius P, Larsson R, Jonsson E, Skov T, Kissmeyer AM, Krasilnikoff K, et al. A Phase I study of CHS 828 in patients with solid tumor malignancy. *Clinical cancer research : an official journal of the American Association for Cancer Research*. 2002;8(9):2843-50.
54. von Heideman A, Berglund Å, Larsson R, Nygren P. Safety and efficacy of NAD depleting cancer drugs: results of a phase I clinical trial of CHS 828 and overview of published data. *Cancer Chemotherapy and Pharmacology*. 2010;65(6):1165-72.
55. Ravaud A, Cerny T, Terret C, Wanders J, Bui BN, Hess D, et al. Phase I study and pharmacokinetic of CHS-828, a guanidino-containing compound, administered orally as a single dose every 3 weeks in solid tumours: an ECSI/EORTC study. *European journal of cancer (Oxford, England : 1990)*. 2005;41(5):702-7.
56. Pishvaian MJ, Marshall JL, Hwang JJ, Malik S, He AR, Deeken JF, et al. A phase I trial of GMX1777, an inhibitor of nicotinamide phosphoribosyl transferase (NAMPT), given as a 24-hour infusion. *Journal of Clinical Oncology*. 2009;27(15_suppl):3581-.
57. Arruebo M, Vilaboa N, Sáez-Gutierrez B, Lambea J, Tres A, Valladares M, et al. Assessment of the evolution of cancer treatment therapies. *Cancers (Basel)*. 2011;3(3):3279-330.
58. Azzam EI, Jay-Gerin JP, Pain D. Ionizing radiation-induced metabolic oxidative stress and prolonged cell injury. *Cancer Lett*. 2012;327(1-2):48-60.
59. Liu YP, Zheng CC, Huang YN, He ML, Xu WW, Li B. Molecular mechanisms of chemo- and radiotherapy resistance and the potential implications for cancer treatment. *MedComm (2020)*. 2021;2(3):315-40.
60. Chabner BA, Roberts TG. Chemotherapy and the war on cancer. *Nature Reviews Cancer*. 2005;5(1):65-72.
61. Lee YT, Tan YJ, Oon CE. Molecular targeted therapy: Treating cancer with specificity. *European journal of pharmacology*. 2018;834:188-96.
62. Hou J, He Z, Liu T, Chen D, Wang B, Wen Q, et al. Evolution of Molecular Targeted Cancer Therapy: Mechanisms of Drug Resistance and Novel Opportunities Identified by CRISPR-Cas9 Screening. *Front Oncol*. 2022;12:755053.
63. Drago JZ, Modi S, Chandarlapaty S. Unlocking the potential of antibody-drug conjugates for cancer therapy. *Nat Rev Clin Oncol*. 2021;18(6):327-44.
64. Fu Z, Li S, Han S, Shi C, Zhang Y. Antibody drug conjugate: the “biological missile” for targeted cancer therapy. *Signal Transduction and Targeted Therapy*. 2022;7(1):93.
65. Su Z, Xiao D, Xie F, Liu L, Wang Y, Fan S, et al. Antibody–drug conjugates: Recent advances in linker chemistry. *Acta Pharmaceutica Sinica B*. 2021.
66. Kanellos J, Pietersz GA, McKenzie IFC. Studies of Methotrexate-Monoclonal Antibody Conjugates for Immunotherapy. *JNCI: Journal of the National Cancer Institute*. 1985;75(2):319-32.
67. Starling JJ, Maciak RS, Law KL, Hinson NA, Briggs SL, Laguzza BC, et al. In vivo antitumor activity of a monoclonal antibody-Vinca alkaloid immunoconjugate directed against a solid tumor membrane antigen characterized by heterogeneous expression and noninternalization of antibody-antigen complexes. *Cancer research*. 1991;51(11):2965-72.
68. Saleh MN, Sugarman S, Murray J, Ostroff JB, Healey D, Jones D, et al. Phase I trial of the anti-Lewis Y drug immunoconjugate BR96-doxorubicin in patients with lewis Y-expressing epithelial tumors. *J Clin Oncol*. 2000;18(11):2282-92.

69. Teicher BA, Chari RV. Antibody conjugate therapeutics: challenges and potential. *Clinical cancer research : an official journal of the American Association for Cancer Research*. 2011;17(20):6389-97.
70. Tsuchikama K, An Z. Antibody-drug conjugates: recent advances in conjugation and linker chemistries. *Protein Cell*. 2018;9(1):33-46.
71. Pretto F, FitzGerald RE. In vivo safety testing of Antibody Drug Conjugates. *Regulatory Toxicology and Pharmacology*. 2021;122:104890.
72. Redman JM, Hill EM, AlDeghaither D, Weiner LM. Mechanisms of action of therapeutic antibodies for cancer. *Mol Immunol*. 2015;67(2 Pt A):28-45.
73. Junttila TT, Li G, Parsons K, Phillips GL, Sliwkowski MX. Trastuzumab-DM1 (T-DM1) retains all the mechanisms of action of trastuzumab and efficiently inhibits growth of lapatinib insensitive breast cancer. *Breast Cancer Res Treat*. 2011;128(2):347-56.
74. Bai J-F, Majjigapu SR, Sordat B, Poty S, Vogel P, Elías-Rodríguez P, et al. Identification of new FK866 analogues with potent anticancer activity against pancreatic cancer. *European Journal of Medicinal Chemistry*. 2022;239:114504.
75. Bird SA, Boyd K. Multiple myeloma: an overview of management. *Palliat Care Soc Pract*. 2019;13:1178224219868235-.
76. Siegel RL, Miller KD, Fuchs HE, Jemal A. Cancer Statistics, 2021. *CA Cancer J Clin*. 2021;71(1):7-33.
77. Cancer Facts & Figures 2021. . American Cancer Society. 2021.
78. Rajkumar SV, Kumar S. Multiple myeloma current treatment algorithms. *Blood Cancer Journal*. 2020;10(9):94.
79. Costa F, Dalla Palma B, Giuliani N. CD38 Expression by Myeloma Cells and Its Role in the Context of Bone Marrow Microenvironment: Modulation by Therapeutic Agents. *Cells*. 2019;8(12).
80. Leow CC, Low MSY. Targeted Therapies for Multiple Myeloma. *J Pers Med*. 2021;11(5).
81. Shah UA, Mailankody S. Emerging immunotherapies in multiple myeloma. *BMJ*. 2020;370:m3176.
82. Vaxman I, Abeykoon J, Dispenzieri A, Kumar SK, Buadi F, Lacy MQ, et al. “Real-life” data of the efficacy and safety of belantamab mafodotin in relapsed multiple myeloma—the Mayo Clinic experience. *Blood Cancer Journal*. 2021;11(12):196.
83. Yu B, Liu D. Antibody-drug conjugates in clinical trials for lymphoid malignancies and multiple myeloma. *Journal of hematology & oncology*. 2019;12(1):94.
84. McMillan A, Warcel D, Popat R. Antibody-drug conjugates for multiple myeloma. *Expert Opinion on Biological Therapy*. 2021;21(7):889-901.
85. Gharbaran R. Advances in the molecular functions of syndecan-1 (SDC1/CD138) in the pathogenesis of malignancies. *Critical Reviews in Oncology/Hematology*. 2015;94(1):1-17.
86. Akl MR, Nagpal P, Ayoub NM, Prabhu SA, Gliksman M, Tai B, et al. Molecular and clinical profiles of syndecan-1 in solid and hematological cancer for prognosis and precision medicine. *Oncotarget*. 2015;6(30):28693-715.
87. Mahtouk K, Cremer FW, Rème T, Jourdan M, Baudard M, Moreaux J, et al. Heparan sulphate proteoglycans are essential for the myeloma cell growth activity of EGF-family ligands in multiple myeloma. *Oncogene*. 2006;25(54):7180-91.
88. Saleh ME, Gadalla R, Hassan H, Afifi A, Götte M, El-Shinawi M, et al. The immunomodulatory role of tumor Syndecan-1 (CD138) on ex vivo tumor microenvironmental CD4+ T cell polarization in inflammatory and non-inflammatory breast cancer patients. *PloS one*. 2019;14(5):e0217550.
89. McCarron MJ, Park PW, Fooksman DR. CD138 mediates selection of mature plasma cells by regulating their survival. *Blood*. 2017;129(20):2749-59.

90. Jagannath S, Chanan-Khan A, Heffner LT, Avigan D, Zimmerman TM, Lonial S, et al. BT062, An Antibody-Drug Conjugate Directed Against CD138, Shows Clinical Activity in Patients with Relapsed or Relapsed/Refractory Multiple Myeloma. *Blood*. 2011;118(21):305-.
91. Kelly KR, Siegel DS, Chanan-Khan AA, Somlo G, Heffner LT, Jagannath S, et al. Indatuximab Ravtansine (BT062) in Combination with Low-Dose Dexamethasone and Lenalidomide or Pomalidomide: Clinical Activity in Patients with Relapsed / Refractory Multiple Myeloma. *Blood*. 2016;128(22):4486-.
92. Sun C, Mahendravada A, Ballard B, Kale B, Ramos C, West J, et al. Safety and efficacy of targeting CD138 with a chimeric antigen receptor for the treatment of multiple myeloma. *Oncotarget*. 2019;10(24):2369-83.
93. Ikeda H, Hideshima T, Fulciniti M, Lutz RJ, Yasui H, Okawa Y, et al. The Monoclonal Antibody nBT062 Conjugated to Cytotoxic Maytansinoids Has Selective Cytotoxicity Against CD138-Positive Multiple Myeloma Cells *In vitro* and *In vivo*. *Clinical Cancer Research*. 2009;15(12):4028-37.
94. Jagannath S, Heffner LT, Ailawadhi S, Munshi NC, Zimmerman TM, Rosenblatt J, et al. Indatuximab Ravtansine (BT062) Monotherapy in Patients With Relapsed and/or Refractory Multiple Myeloma. *Clinical Lymphoma Myeloma and Leukemia*. 2019;19(6):372-80.
95. Kelly KR, Chanan-Khan A, Heffner LT, Somlo G, Siegel DS, Zimmerman T, et al. Indatuximab Ravtansine (BT062) in Combination with Lenalidomide and Low-Dose Dexamethasone in Patients with Relapsed and/or Refractory Multiple Myeloma: Clinical Activity in Patients Already Exposed to Lenalidomide and Bortezomib. *Blood*. 2014;124(21):4736-.
96. Kelly KR, Ailawadhi S, Siegel DS, Heffner LT, Somlo G, Jagannath S, et al. Indatuximab ravtansine plus dexamethasone with lenalidomide or pomalidomide in relapsed or refractory multiple myeloma: a multicentre, phase 1/2a study. *The Lancet Haematology*. 2021;8(11):e794-e807.
97. Vetter J. Toxins of *Amanita phalloides*. *Toxicon*. 1998;36(1):13-24.
98. Lindell TJ, Weinberg F, Morris PW, Roeder RG, Rutter WJ. Specific inhibition of nuclear RNA polymerase II by α -amanitin. *Science (New York, NY)*. 1970;170(3956):447-9.
99. Kaplan CD, Larsson K-M, Kornberg RD. The RNA polymerase II trigger loop functions in substrate selection and is directly targeted by α -amanitin. *Molecular cell*. 2008;30(5):547-56.
100. Letschert K, Faulstich H, Keller D, Keppler D. Molecular characterization and inhibition of amanitin uptake into human hepatocytes. *Toxicological sciences*. 2006;91(1):140-9.
101. Jaeger A, Jehl F, Flesch F, Sauder P, Kopferschmitt J. Kinetics of amatoxins in human poisoning: Therapeutic implications. *Journal of Toxicology: Clinical Toxicology*. 1993;31(1):63-80.
102. Rodrigues DF, Pires das Neves R, Carvalho ATP, Lourdes Bastos M, Costa VM, Carvalho F. *In vitro* mechanistic studies on α -amanitin and its putative antidotes. *Archives of Toxicology*. 2020;94(6):2061-78.
103. Pahl A, Lutz C, Hechler T. Amanitins and their development as a payload for antibody-drug conjugates. *Drug Discovery Today: Technologies*. 2018;30:85-9.
104. Lanieri L, Lamothe TL, Miske O, McDonough SM, Sarma GN, Bhattarai P, et al. A Single Dose of a Novel Anti-Human CD117-Amanitin Antibody Drug Conjugate (ADC) Engineered for a Short Half-Life Provides Dual Conditioning and Anti-Leukemic Activity and Extends Survival Compared to Standard of Care in Multiple Preclinical Models of Acute Myeloid Leukemia (AML). *Blood*. 2020;136(Supplement 1):47-8.
105. Figueroa-Vazquez V, Ko J, Breunig C, Baumann A, Giesen N, Pálfi A, et al. HDP-101, an Anti-BCMA Antibody–Drug Conjugate, Safely Delivers Amanitin to Induce Cell Death in Proliferating and Resting Multiple Myeloma Cells. *Molecular cancer therapeutics*. 2021;20(2):367-78.

106. Karpov AS, Abrams T, Clark S, Raikar A, D'Alessio JA, Dillon MP, et al. Nicotinamide Phosphoribosyltransferase Inhibitor as a Novel Payload for Antibody-Drug Conjugates. *ACS medicinal chemistry letters*. 2018;9(8):838-42.
107. Neumann CS, Olivas KC, Anderson ME, Cochran JH, Jin S, Li F, et al. Targeted Delivery of Cytotoxic NAMPT Inhibitors Using Antibody-Drug Conjugates. *Molecular cancer therapeutics*. 2018;17(12):2633-42.
108. Böhnke N, Berger M, Griebenow N, Rottmann A, Erkelenz M, Hammer S, et al. A Novel NAMPT Inhibitor-Based Antibody-Drug Conjugate Payload Class for Cancer Therapy. *Bioconjugate Chemistry*. 2022;33(6):1210-21.
109. Tan B, Young DA, Lu ZH, Wang T, Meier TI, Shepard RL, et al. Pharmacological inhibition of nicotinamide phosphoribosyltransferase (NAMPT), an enzyme essential for NAD⁺ biosynthesis, in human cancer cells: metabolic basis and potential clinical implications. *J Biol Chem*. 2013;288(5):3500-11.
110. Watson M, Roulston A, Bélec L, Billot X, Marcellus R, Bédard D, et al. The small molecule GMX1778 is a potent inhibitor of NAD⁺ biosynthesis: strategy for enhanced therapy in nicotinic acid phosphoribosyltransferase 1-deficient tumors. *Mol Cell Biol*. 2009;29(21):5872-88.
111. Misner DL, Kauss MA, Singh J, Uppal H, Bruening-Wright A, Liederer BM, et al. Cardiotoxicity Associated with Nicotinamide Phosphoribosyltransferase Inhibitors in Rodents and in Rat and Human-Derived Cells Lines. *Cardiovasc Toxicol*. 2017;17(3):307-18.
112. Zabka TS, Singh J, Dhawan P, Liederer BM, Oeh J, Kauss MA, et al. Retinal toxicity, in vivo and in vitro, associated with inhibition of nicotinamide phosphoribosyltransferase. *Toxicol Sci*. 2015;144(1):163-72.
113. Fratta S, Binięcka P, Moreno-Vargas AJ, Carmona AT, Nahimana A, Duchosal MA, et al. Synthesis and structure-activity relationship of new nicotinamide phosphoribosyltransferase inhibitors with antitumor activity on solid and haematological cancer. *European Journal of Medicinal Chemistry*. 2023;250:115170.
114. Sun L, Wang J, Mahmud S, Jiang Y, Zhu J, Liu X. New insight into the mechanism for the excellent gas properties of poly(ethylene 2,5-furandicarboxylate) (PEF): Role of furan ring's polarity. *European Polymer Journal*. 2019;118:642-50.
115. Zheng X, Baumeister T, Buckmelter AJ, Caligiuri M, Clodfelter KH, Han B, et al. Discovery of potent and efficacious cyanoguanidine-containing nicotinamide phosphoribosyltransferase (Nampt) inhibitors. *Bioorganic & Medicinal Chemistry Letters*. 2014;24(1):337-43.
116. Kozako T, Yoshimitsu M, Arima N, Sato K, Toyoshima M, Honda S-i, et al. Induction of Apoptosis and Autophagy By Nampt Inhibition in Adult T-Cell Leukemia/Lymphoma and Leukemic Cell Lines. *Blood*. 2016;128(22):2327-.
117. Franco J, Piacente F, Walter M, Fratta S, Ghanem M, Benzi A, et al. Structure-Based Identification and Biological Characterization of New NAPRT Inhibitors. *Pharmaceuticals (Basel)*. 2022;15(7).
118. Ghanem MS, Caffa I, Del Rio A, Franco J, Parenti MD, Monacelli F, et al. Identification of NAPRT Inhibitors with Anti-Cancer Properties by In Silico Drug Discovery. *Pharmaceuticals (Basel)*. 2022;15(7).
119. Piacente F, Caffa I, Ravera S, Sociali G, Passalacqua M, Vellone VG, et al. Nicotinic Acid Phosphoribosyltransferase Regulates Cancer Cell Metabolism, Susceptibility to NAMPT Inhibitors, and DNA Repair. *Cancer research*. 2017;77(14):3857-69.
120. Shats I, Williams JG, Liu J, Makarov MV, Wu X, Lih FB, et al. Bacteria Boost Mammalian Host NAD Metabolism by Engaging the Deamidated Biosynthesis Pathway. *Cell metabolism*. 2020;31(3):564-79.e7.


121. ELMokh O, Matsumoto S, Binięcka P, Bellotti A, Schaeuble K, Piacente F, et al. Gut microbiota severely hampers the efficacy of NAD-lowering therapy in leukemia. *Cell Death Dis.* 2022;13(4):320.
122. Zhao RY, Wilhelm SD, Audette C, Jones G, Leece BA, Lazar AC, et al. Synthesis and Evaluation of Hydrophilic Linkers for Antibody–Maytansinoid Conjugates. *Journal of medicinal chemistry.* 2011;54(10):3606-23.
123. Lyon RP, Bovee TD, Doronina SO, Burke PJ, Hunter JH, Neff-LaFord HD, et al. Reducing hydrophobicity of homogeneous antibody-drug conjugates improves pharmacokinetics and therapeutic index. *Nature biotechnology.* 2015;33(7):733-5.
124. Binięcka P, Matsumoto S, Belotti A, Jousot J, Bai JF, Majjigapu SR, et al. Anticancer Activities of Novel Nicotinamide Phosphoribosyltransferase Inhibitors in Hematological Malignancies. *Molecules.* 2023;28(4):1897.
125. Kostova V, Désos P, Starck JB, Kotschy A. The Chemistry Behind ADCs. *Pharmaceuticals (Basel).* 2021;14(5).
126. Bargh JD, Isidro-Llobet A, Parker JS, Spring DR. Cleavable linkers in antibody-drug conjugates. *Chem Soc Rev.* 2019;48(16):4361-74.
127. Buecheler JW, Winzer M, Tonillo J, Weber C, Gieseler H. Impact of Payload Hydrophobicity on the Stability of Antibody–Drug Conjugates. *Molecular Pharmaceutics.* 2018;15(7):2656-64.
128. Hamblett KJ, Senter PD, Chace DF, Sun MM, Lenox J, Cerveny CG, et al. Effects of drug loading on the antitumor activity of a monoclonal antibody drug conjugate. *Clinical cancer research : an official journal of the American Association for Cancer Research.* 2004;10(20):7063-70.
129. Li W, Prabakaran P, Chen W, Zhu Z, Feng Y, Dimitrov DS. Antibody Aggregation: Insights from Sequence and Structure. *Antibodies (Basel, Switzerland).* 2016;5(3).
130. Han Y-C, Kahler J, Piché-Nicholas N, Hu W, Thibault S, Jiang F, et al. Development of Highly Optimized Antibody–Drug Conjugates against CD33 and CD123 for Acute Myeloid Leukemia. *Clinical Cancer Research.* 2021;27(2):622-31.
131. Kirchhoff D, Stelte-Ludwig B, Lerchen HG, Wengner AM, Ahsen OV, Buchmann P, et al. IL3RA-Targeting Antibody-Drug Conjugate BAY-943 with a Kinesin Spindle Protein Inhibitor Payload Shows Efficacy in Preclinical Models of Hematologic Malignancies. *Cancers (Basel).* 2020;12(11).
132. Kovtun Y, Jones GE, Adams S, Harvey L, Audette CA, Wilhelm A, et al. A CD123-targeting antibody-drug conjugate, IMGN632, designed to eradicate AML while sparing normal bone marrow cells. *Blood Adv.* 2018;2(8):848-58.
133. Li F, Sutherland MK, Yu C, Walter RB, Westendorf L, Valliere-Douglass J, et al. Characterization of SGN-CD123A, A Potent CD123-Directed Antibody-Drug Conjugate for Acute Myeloid Leukemia. *Molecular cancer therapeutics.* 2018;17(2):554-64.
134. Costa MJ, Kudravalli J, Ma JT, Ho WH, Delaria K, Holz C, et al. Optimal design, anti-tumour efficacy and tolerability of anti-CXCR4 antibody drug conjugates. *Sci Rep.* 2019;9(1):2443.
135. Jiang YP, Liu BY, Zheng Q, Panuganti S, Chen R, Zhu J, et al. CLT030, a leukemic stem cell-targeting CLL1 antibody-drug conjugate for treatment of acute myeloid leukemia. *Blood Adv.* 2018;2(14):1738-49.
136. Roas M, Vick B, Kasper M-A, Able M, Polzer H, Gerlach M, et al. TARGETING FLT3 BY NEW-GENERATION ANTIBODY-DRUG-CONJUGATE IN COMBINATION WITH KINASE INHIBITORS FOR TREATMENT OF AML. *Blood.* 2022.

Articles

Anticancer Activities of Novel Nicotinamide Phosphoribosyltransferase Inhibitors in Haematological Malignancies

Article

Anticancer Activities of Novel Nicotinamide Phosphoribosyltransferase Inhibitors in Hematological Malignancies

Paulina Binięcka ¹, Saki Matsumoto ¹, Axel Belotti ¹, Jessie Jousot ², Jian Fei Bai ²,
Somi Reddy Majjigapu ², Paul Thoueille ³, Dany Spaggiari ³, Vincent Desfontaine ³, Francesco Piacente ⁴,
Santina Bruzzone ⁴, Michele Cea ^{5,6}, Laurent A. Decosterd ³, Pierre Vogel ², Alessio Nencioni ^{5,6},
Michel A. Duchosal ^{1,7,*} and Aimable Nahimana ^{1,*}

- ¹ Central Laboratory of Hematology, Department of Medical Laboratory and Pathology, Lausanne University Hospital and University of Lausanne, 1011 Lausanne, Switzerland
 - ² Laboratory of Glycochemistry and Asymmetric Synthesis, Swiss Federal Institute of Technology (EPFL), 1015 Lausanne, Switzerland
 - ³ Service and Laboratory of Clinical Pharmacology, Department of Laboratory Medicine and Pathology, Lausanne University Hospital and University of Lausanne, 1011 Lausanne, Switzerland
 - ⁴ Department of Experimental Medicine, Section of Biochemistry, University of Genoa, 16132 Genoa, Italy
 - ⁵ Department of Internal Medicine and Medical Specialties, University of Genoa, 16132 Genoa, Italy
 - ⁶ Ospedale Policlinico San Martino IRCCS, Department of Internal Medicine, University of Genoa, 16132 Genoa, Italy
 - ⁷ Service of Hematology, Department of Oncology, Lausanne University Hospital and University of Lausanne, 1011 Lausanne, Switzerland
- * Correspondence: michel.duchosal@chuv.ch (M.A.D.); aimable.nahimana@chuv.ch (A.N.)



Citation: Binięcka, P.; Matsumoto, S.; Belotti, A.; Jousot, J.; Bai, J.F.; Majjigapu, S.R.; Thoueille, P.; Spaggiari, D.; Desfontaine, V.; Piacente, F.; et al. Anticancer Activities of Novel Nicotinamide Phosphoribosyltransferase Inhibitors in Hematological Malignancies. *Molecules* **2023**, *28*, 1897. <https://doi.org/10.3390/molecules28041897>

Academic Editor: Giulia Bononi

Received: 12 December 2022

Revised: 20 January 2023

Accepted: 2 February 2023

Published: 16 February 2023



Copyright: © 2023 by the authors. Licensee MDPI, Basel, Switzerland. This article is an open access article distributed under the terms and conditions of the Creative Commons Attribution (CC BY) license (<https://creativecommons.org/licenses/by/4.0/>).

Abstract: Targeting cancer cells that are highly dependent on the nicotinamide adenine dinucleotide (NAD⁺) metabolite is a promising therapeutic strategy. Nicotinamide phosphoribosyltransferase (NAMPT) is the rate-limiting enzyme catalyzing NAD⁺ production. Despite the high efficacy of several developed NAMPT inhibitors (i.e., **FK866** (APO866)) in preclinical studies, their clinical activity was proven to be limited. Here, we report the synthesis of new NAMPT Inhibitors, **JJ08**, **FEI191** and **FEI199**, which exhibit a broad anticancer activity in vitro. Results show that these compounds are potent NAMPT inhibitors that deplete NAD⁺ and NADP(H) after 24 h of drug treatment, followed by an increase in reactive oxygen species (ROS) accumulation. The latter event leads to ATP loss and mitochondrial depolarization with induction of apoptosis and necrosis. Supplementation with exogenous NAD⁺ precursors or catalase (ROS scavenger) abrogates the cell death induced by the new compounds. Finally, in vivo administration of the new NAMPT inhibitors in a mouse xenograft model of human Burkitt lymphoma delays tumor growth and significantly prolongs mouse survival. The most promising results are collected with **JJ08**, which completely eradicates tumor growth. Collectively, our findings demonstrate the efficient anticancer activity of the new NAMPT inhibitor **JJ08** and highlight a strong interest for further evaluation of this compound in hematological malignancies.

Keywords: NAMPT inhibitor; NAD; anticancer; leukemia; lymphoma; multiple myeloma; ATP; apoptosis; oxidative stress; vitamin B3; PK studies

1. Introduction

Cancer cells have very high nutrient and energy demands in order to sustain their constant growth and rapid cell proliferation. Their metabolic reprogramming has recently emerged as an important cancer hallmark [1,2]. First described by Otto Warburg, a particular characteristic of cancerous cells resides in their preference towards aerobic glycolysis over oxidative phosphorylation [3]. However, this preference does not exclude the involvement of oxidative metabolism. Malignant cells rely on ATP and oncometabolite production

from the mitochondrial tricarboxylic acid (TCA) cycle as much as they rely on glycolysis for their survival and proliferation [4].

Nicotinamide adenine dinucleotide (NAD⁺) is the main co-factor associated with cellular energetics and mediates redox reactions in crucial metabolic pathways, such as glycolysis, the TCA cycle and oxidative phosphorylation [5]. Additionally, it serves as a substrate for several NAD-degrading enzymes, including poly ADP-ribose polymerases (PARPs), mono (ADP-ribose) transferases (ARTs), NAD-ases/ADP-ribose cyclases/cyclic ADP-ribose hydrolases (CD38/CD157) and sirtuins (SIRT). Subsequently, through these enzymes, NAD⁺ is involved in numerous biological processes, such as cellular proliferation, signaling and adhesion, calcium mobilization, cell cycle control, stress response, DNA damage, genomic integrity and transcriptional regulation [6]. NAD⁺ results from different molecular pathways, de novo from tryptophan, from nicotinic acid/nicotinic acid riboside (NA/NAR) through the Preiss–Handler pathway or through salvage pathways from nicotinamide/nicotinamide riboside (NAM/NR) and reduced nicotinamide riboside (NRH) [7,8]. In mammalian cells, NAM/NA are the most commonly used precursors to synthesize NAD⁺. Nicotinamide phosphoribosyltransferase (NAMPT) is the rate-limiting enzyme that catalyzes the phosphoribosylation of NAM to produce nicotinamide mononucleotide (NMN) [9,10]. Then, the latter is converted to NAD⁺, a process catalyzed by NMN adenylyltransferase. Furthermore, NAMPT expression is upregulated in most cancer cells [11–13] and is associated with tumor progression [14,15]. Thus, targeting NAMPT has emerged as a promising strategy to eliminate malignant cells selectively, as they highly rely on NAD⁺ synthesis [16,17]. The first NAMPT inhibitor, **FK866**, also known as APO866 (Figure 1), was described by Hasmann et al. [18]. Its high killing ability on multiple cancer cell lines was observed in several preclinical studies [19–23]. This observation has provided a rationale for testing **FK866** (APO866) and another NAMPT inhibitor **CHS-828** (also known as GMX-1778, Figure 1) in clinical trials on hematological and solid malignancies (NCT00435084, NCT00432107, NCT00431912, NCT00457574 and NCT00724841). Despite their high anticancer activity observed in several preclinical studies, these inhibitors did not achieve the same efficacy in clinical trials. The clinical results showed a few dose-limiting toxicities and no significant tumor response [24–26]. The orally available NAMPT inhibitors **KPT-9274** and **OT-82** (Figure 1) have been tested as potential drugs in patients with solid tumors or with relapsed/refractory lymphoma [27,28]. Up to now, none of the published NAMPT inhibitors have become an anticancer agent. Thus, there is still a strong need for developing new potent and highly efficient NAMPT inhibitors.

We report here the synthesis of the three new NAMPT inhibitors: **JJ08**, **FEI191** and **FEI199**. We test them for their potential antitumor activities toward hematological malignancies. We show that these compounds are potent NAMPT inhibitors that profoundly deplete NAD(H) and NADP(H) after 24 h of incubation, which is followed by a strong, time-dependent increase in ROS production including cytosolic/mitochondrial superoxide anions and hydrogen peroxide. That increase correlates with ATP depletion and mitochondrial depolarization. We provide evidence that **JJ08**, **FEI191** and **FEI199** exhibit cell death at low nanomolar concentrations towards several hematopoietic malignant cells. Treatment of mouse xenografts with the three new NAMPT inhibitors significantly prolonged mouse survival. **JJ08** presented the most promising results as it abolished tumor growth completely.

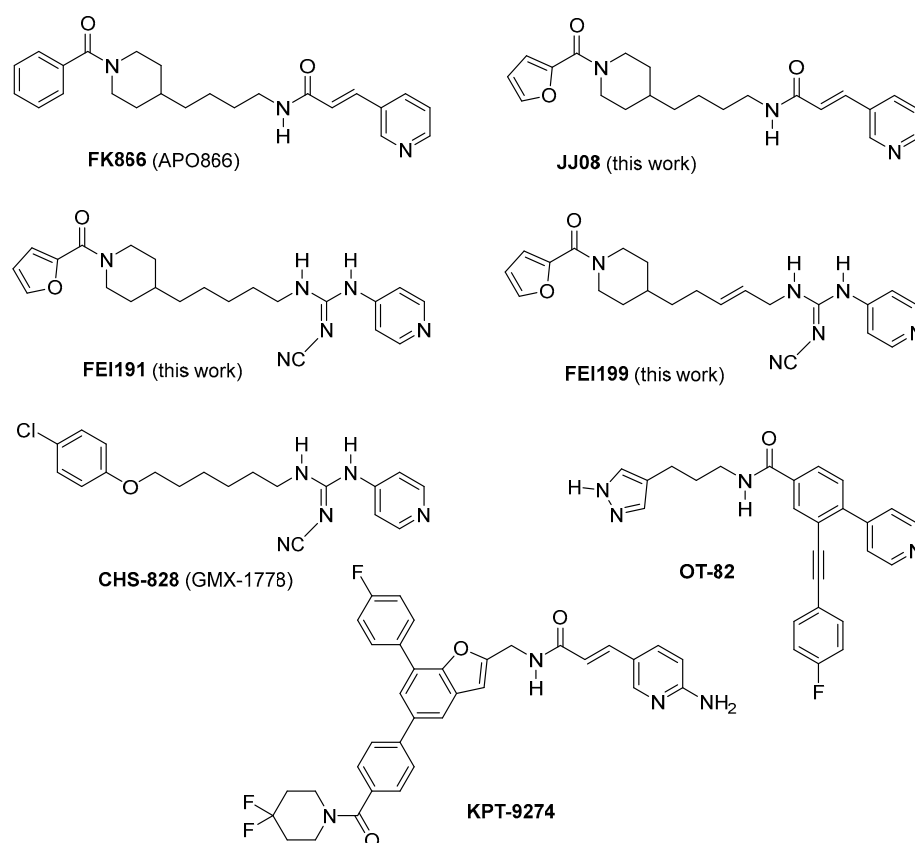
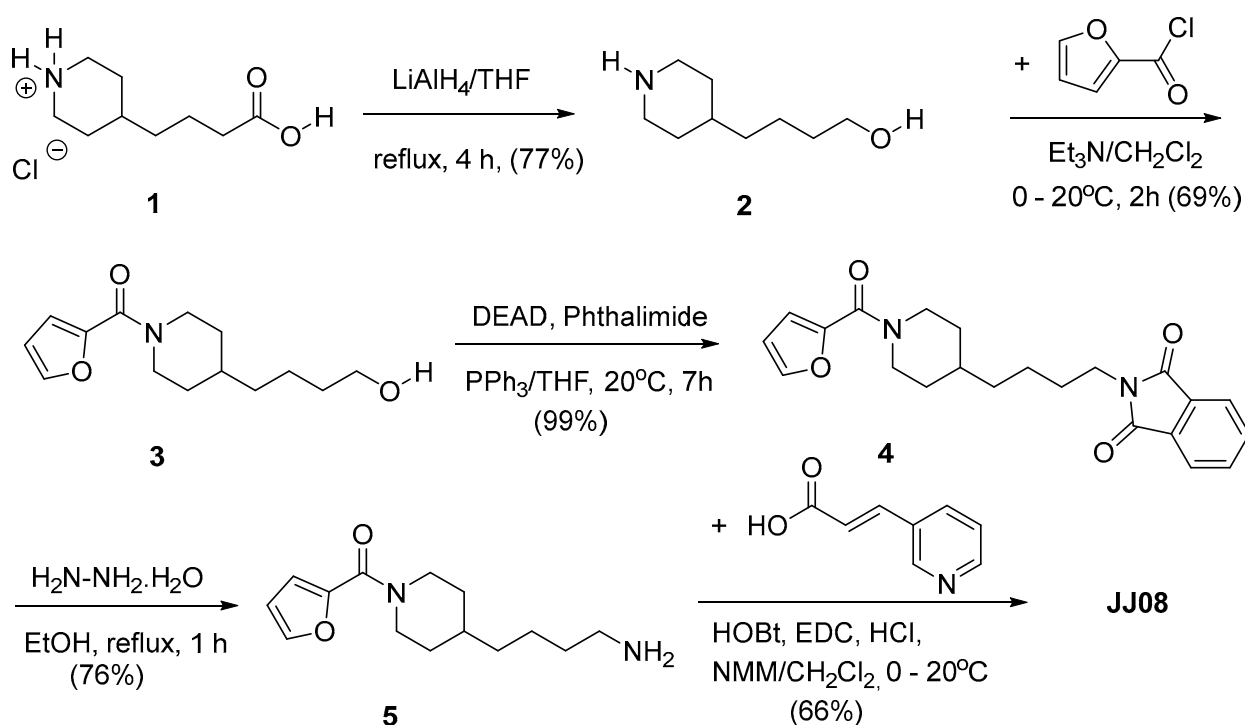


Figure 1. Chemical structures of NAMPT inhibitors. **JJ08** is an **FK866** (APO866) analogue with a furan-2-carboxamide group instead of a benzamide group (tail group). With their cyanoguanidine moieties, **FEI191** and **FEI199** can be seen as analogues of **CHS-828** and they also contain a furan-2-carboxamide tail group.

2. Results

2.1. Synthesis of New Potent NAMPT Inhibitors

Within the European Health 7th framework project PANACREAS (grant agreement ID: 256986) we have synthesized a series of novel **FK866** (APO866) analogues and shown that some of them are very toxic toward pancreatic cell lines [29]. Applying an analogous synthetic route to that reported for the synthesis of **FK866** [29], we have prepared ((*E*)-*N*-(4-(1-(furan-2-carbonyl)piperidin-4-yl)butyl)-3-(pyridin-3-yl)acrylamide) (**JJ08**) which exchanges the benzamide moiety of **FK866** for a furan-2-carboxamide group. The synthesis starts with the reduction of the HCl salt of 4-(piperidin-4-yl)butyric acid (**1**) into alcohol **2**. The latter reacted with 2-furanoyl chloride and triethylamine, giving the corresponding carboxamide **3**. A Mitsunobu displacement of the alcoholic moiety of **3** with phthalimide gave **4**. Selective liberation of the primary amine **5** was realized by treatment with hydrazine chlorhydrate in ethanol. Amide coupling of **5** with (*E*)-3-(pyridin-3-yl) provided **JJ08** (Scheme 1).

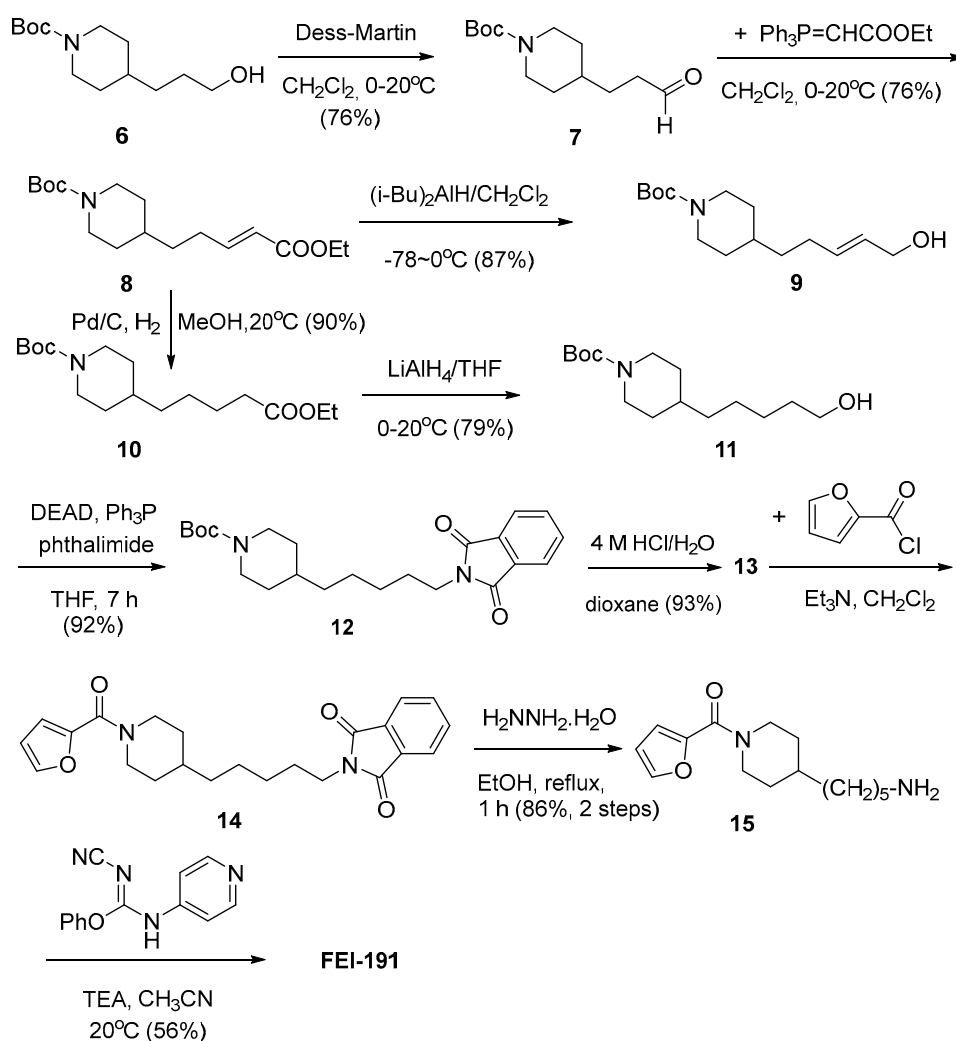


Scheme 1. Synthesis of JJ08.

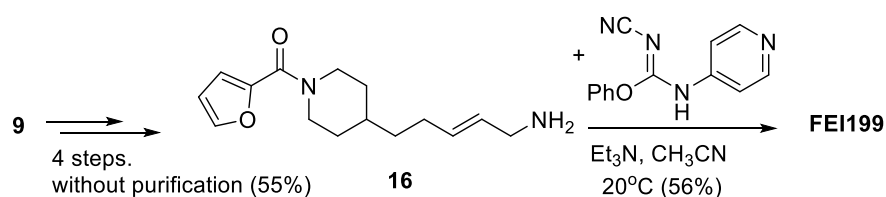
FEI191 ((*Z*)-2-cyano-1-(5-(1-(furan-2-carbonyl)piperidin-4-yl)pentyl)-3-phenylguanidine) and **FEI199** ((*Z*)-2-cyano-1-((*E*)-5-(1-(furan-2-carbonyl)piperidin-4-yl)pent-2-en-1-yl)-3-phenylguanidine) are compounds in which the (pyridine-3-yl)acrylamide moiety of **JJ08** has been exchanged for a (pyridin-4-yl)cyanoguanidine moiety and the C4-tether for C5-tethers. These compounds can be seen as chimeric derivatives of **CHS-828**. The synthesis of **FEI191** (Scheme 2) starts with the commercially available tert-butyl 4-(3-hydroxypropyl)piperidine-1-carboxylate (**6**), a primary alcohol that undergoes Dess–Martin oxidation into the corresponding aldehyde **7**. Wittig–Horner–Emmons olefination of **7** furnished the (*E*)-ene-ester **8** that was reduced into the corresponding (*E*)-allylic alcohol **9** by di(isobutyl)aluminum hydride in CH_2Cl_2 . Catalytic hydrogenation of **8** provided ester **10**, which was reduced into the corresponding alcohol **11**. Mitsunobu displacement of the primary alcohol **11** with phthalimide gave **12**. The piperidine moiety of **12** was deprotected selectively on treatment with aqueous HCl in dioxane furnishing chlorhydrate **13**, which was converted into carboxamide **14** with 2-furoic chloride and trimethylamine. Selective liberation of the primary amine with hydrazine gave **15**, which was treated with phenyl (*Z*)-*N'*-cyano-*N*-(pyridin-4-yl)carbamimidate to provide **FEI191**.

The synthesis of **FEI199** starts with allylic alcohol **9** obtained above (Scheme 2). Over four steps, and without purification of the intermediate products, crude **16** was obtained in 55% yield. The preparations followed the same procedures as those for the conversion of **11** into **15**. Treatment of **16** with phenyl (*Z*)-*N'*-cyano-*N*-(pyridin-4-yl)carbamimidate provided **FEI199** (Scheme 3).

The detailed synthesis and characterization of **JJ08**, **FEI191** and **FEI199** can be found in Supplementary Materials, p. 3–13.



Scheme 2. Synthesis of FEI191.



Scheme 3. Synthesis of FEI199.

2.2. JJ08, FEI191 and FEI199 Are Potent NAMPT Inhibitors That Efficiently Deplete Intracellular NAD⁺ Content

First, we assessed whether the novel compounds are indeed NAMPT inhibitors by examining their capacity to inhibit *in vitro* NAMPT activity. Using **FK866** (APO866), a prototype of NAMPT inhibitors, as a positive control, **JJ08**, **FEI191** and **FEI199** were tested in a NAMPT enzymatic inhibition assay. Figure 2 indicates that they were all potent NAMPT inhibitors, showing full inhibition of NAMPT. The direct consequence of NAMPT inhibition is the decrease in intracellular NAD⁺ content. Hence, we investigated whether treatment of hematopoietic malignant cells with the selected NAMPT inhibitors led to NAD⁺ depletion. To this end, we performed a time course analysis of intracellular NAD⁺ levels on four hematological cancer cell lines, including ML2, Jurkat, Namalwa and RPMI8226, which were treated with the selected compounds. As reported in Figure 3A–D,

all tested NAMPT inhibitors fully depleted the NAD⁺ cell content within the first 24 h after treatment. Notably, in ML2 cells, an additional 8 h time point was recorded, indicating a fast drop in NAD⁺ levels (Figure 3A).

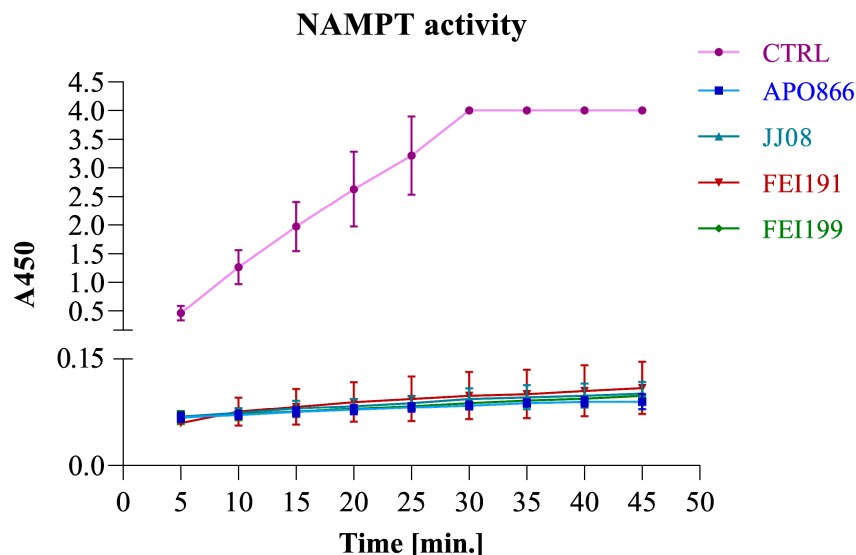


Figure 2. New compounds with a potent NAMPT inhibitory activity. Compounds were added in 1 μ M final concentration to purified NAMPT and incubated with co-substrates, resulting in a reduction of tetrazolium salt (WST-1) to colorful formazan. The amount of formed dye is directly proportional to the enzyme activity. The absorbance of the dye was detected at OD 450 nm.

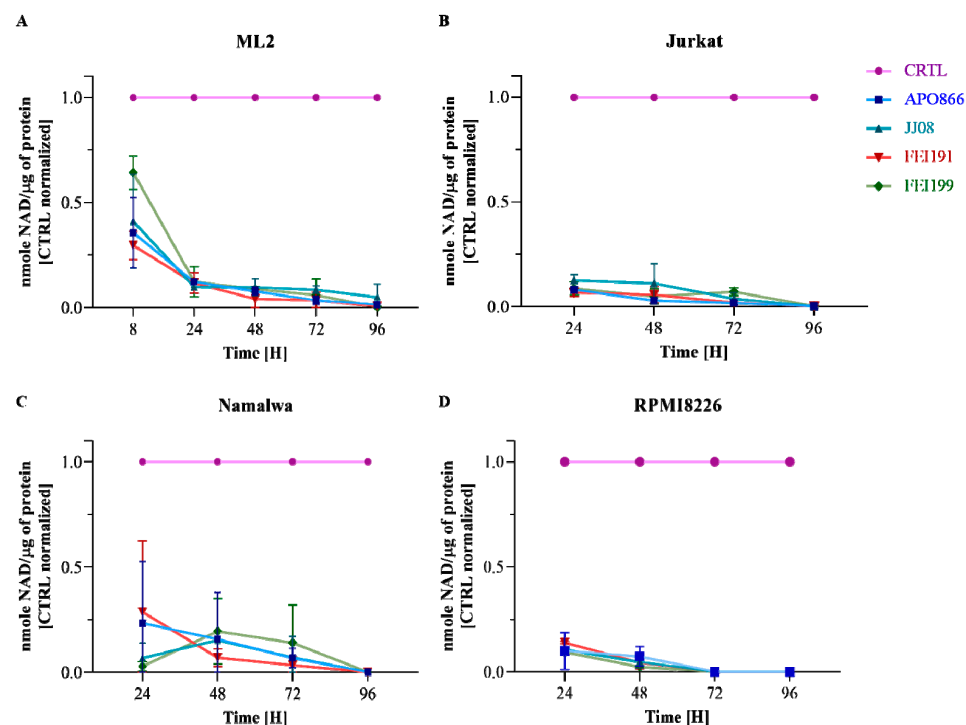


Figure 3. New NAMPT inhibitors induce profound depletion of intracellular NAD⁺. ML2 (A), Jurkat (B), Namalwa (C) and RPMI8226 (D) cells were incubated with NAMPT inhibitors for 96 h. Intracellular NAD⁺ content was measured in a time-dependent manner as indicated on the x-axis. NAD⁺ levels were first normalized to the total protein and then to the control at each time point.

Taken together, these results indicate that all tested compounds are potent NAMPT inhibitors.

2.3. JJ08, FEI191 and FEI199 Induce Different Types of Cell Death in Several Hematological Malignancies in NAD⁺ Dependent Manner

NAD⁺ depletion has been proposed as a promising strategy to eliminate hematological malignancies [19,23,28,30,31]. We measured the cytotoxic activities of JJ08, FEI191 and FEI199 in the four aforementioned hematological cancer cell lines. The cell growth inhibitory effects were compared to that of FK866 (APO866). As summarized in Table 1, the half-maximal inhibitory concentration (IC₅₀) values of the tested inhibitors were in the low nanomolar range. Among them, FEI199 was the most potent, with a measured IC₅₀ that was lower than 0.3 nM in all malignancies.

Table 1. NAMPT inhibitors induce cell death in various cell lines of hematological malignancies. IC₅₀ (nM) after 96 h of treatment with NAMPT inhibitors.

	APO866	JJ08	FEI191	FEI199
ML2	0.41	0.51	0.31	0.21
JURKAT	0.47	0.85	0.45	0.25
NAMALWA	0.58	0.58	0.45	0.29
RPMI8226	0.23	0.30	0.25	0.12

ML2: acute myeloid leukemia; Jurkat: acute lymphoblastic leukemia; NMLW: Burkitt lymphoma; RPMI8226: multiple myeloma.

To assess whether apoptosis is involved in the NAMPT inhibitor-induced cytotoxicity, malignant cells were first treated with the compounds for 96 h and subsequently double stained with ANXN/7AAD and analyzed by flow cytometry. As shown for ML2 cells and additional different malignant hematopoietic cell lines, all the inhibitors induced early (ANXN+/7AAD-) and late apoptotic (7AAD+) cell death at drug concentrations ranging between 0.1 and 10 nM. FEI199 induced maximal cell killings at very low concentrations (≤ 0.5 nM) on all tested cell lines, whereas at similar concentrations, FK866 (APO866) and JJ08 induced cell death at only between 20 and 75%, depending on the cell line (Figure 4A–D). Moreover, FEI191 and FEI199 induced more late apoptotic/necrotic (7AAD+) than early apoptotic cell death (ANXN+/7AAD-) compared with APO866. To provide additional evidence of the involvement of apoptosis in the cell death induced by the new NAMPT inhibitors, we assessed the activation of various caspases, including CASP-3, CASP-8 and CASP-9. Hematopoietic malignant cells were treated for 72 h with the compounds and caspase activation was assessed using the specific CaspGLOW™ Red Active probes specific for each caspase and flow cytometry. The results show a strong increase in CASP-3, CASP-8 and CASP-9 activities in treated versus untreated cells (Figure 5), suggesting that caspase-dependent apoptosis contributes to the antitumor activity of the tested compounds.

Another possible type of cell death is necrosis, which correlates with the release of the cytosolic enzymes, especially lactate dehydrogenase (LDH), into the extracellular space. Therefore, the detection of LDH in the medium is used as a marker of necrotic cell death [32]. Accordingly, we monitored necrotic cell death in time-dependent analyses, as well as the drug effect on cell proliferation in ML2 and Jurkat cells cultured with or without the new NAMPT inhibitors. As shown in Figure 6A,B, LDH release in the medium significantly increased over time in leukemic cells treated with the NAMPT inhibitors compared to untreated ones, whereas cell proliferation decreased over time and only approximately 40% of proliferating cells remained at 48 h after treatment (Figure 6C,D). These findings show the involvement of necrotic cell death in treatment with NAMPT inhibitors.

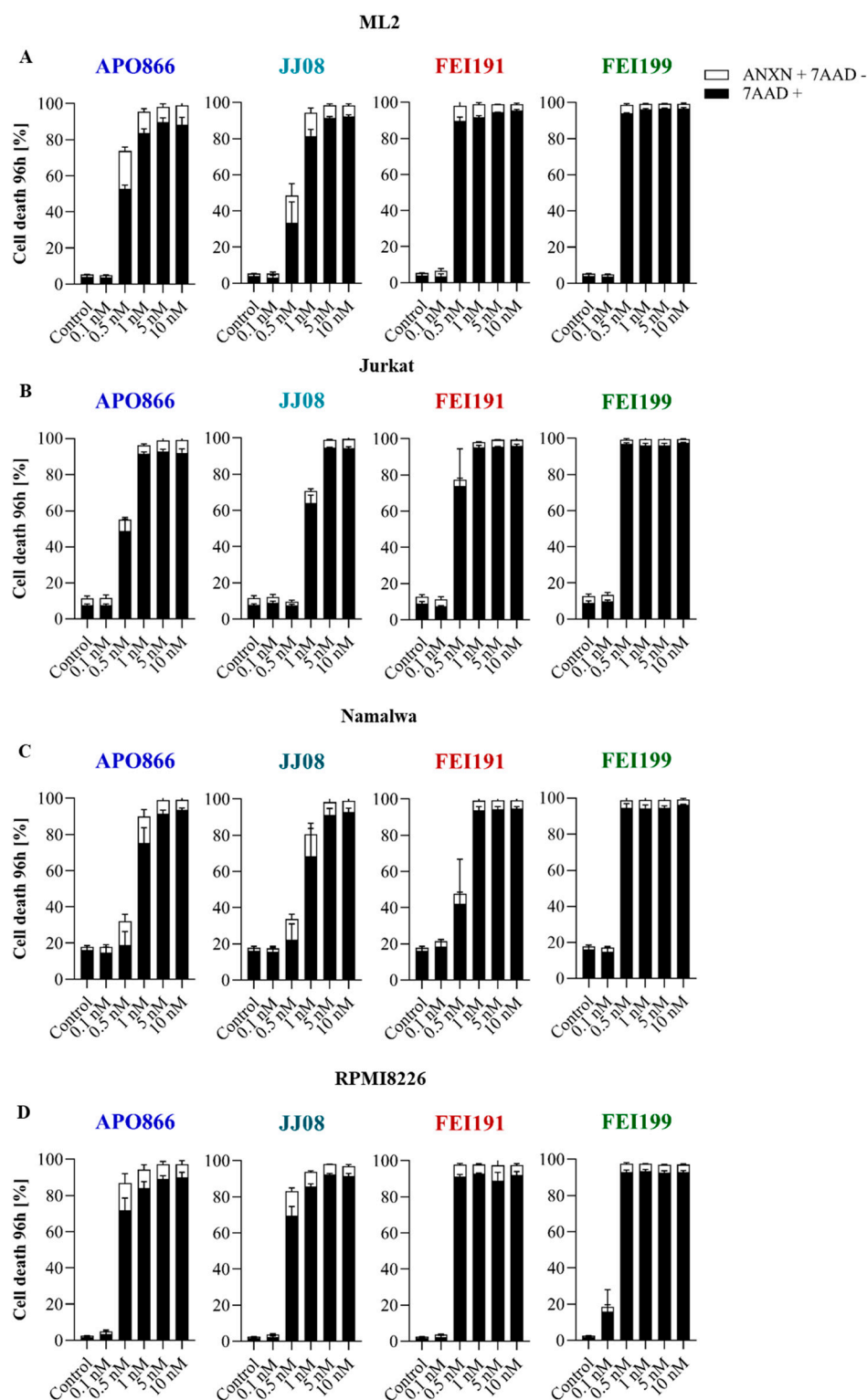


Figure 4. NAMPT inhibitors induce cell death in hematological malignancies in a dose-dependent manner, with **FEI199** being the most potent. A dose-dependent analysis of cell death induced by NAMPT inhibitors on ML2 (**A**), Jurkat (**B**), Namalwa (**C**) and RPMI8226 (**D**) cell lines. The cells were treated with various concentrations of NAMPT inhibitors for 96 h and cell death was assessed by flow cytometry using ANXN and 7AAD staining. The percentages of early apoptotic cells (ANXN⁺ 7AAD⁻) are shown as white columns and those of late apoptotic cells (7AAD⁺) are shown as solid black columns. Data are means \pm SD, $n \geq 3$.

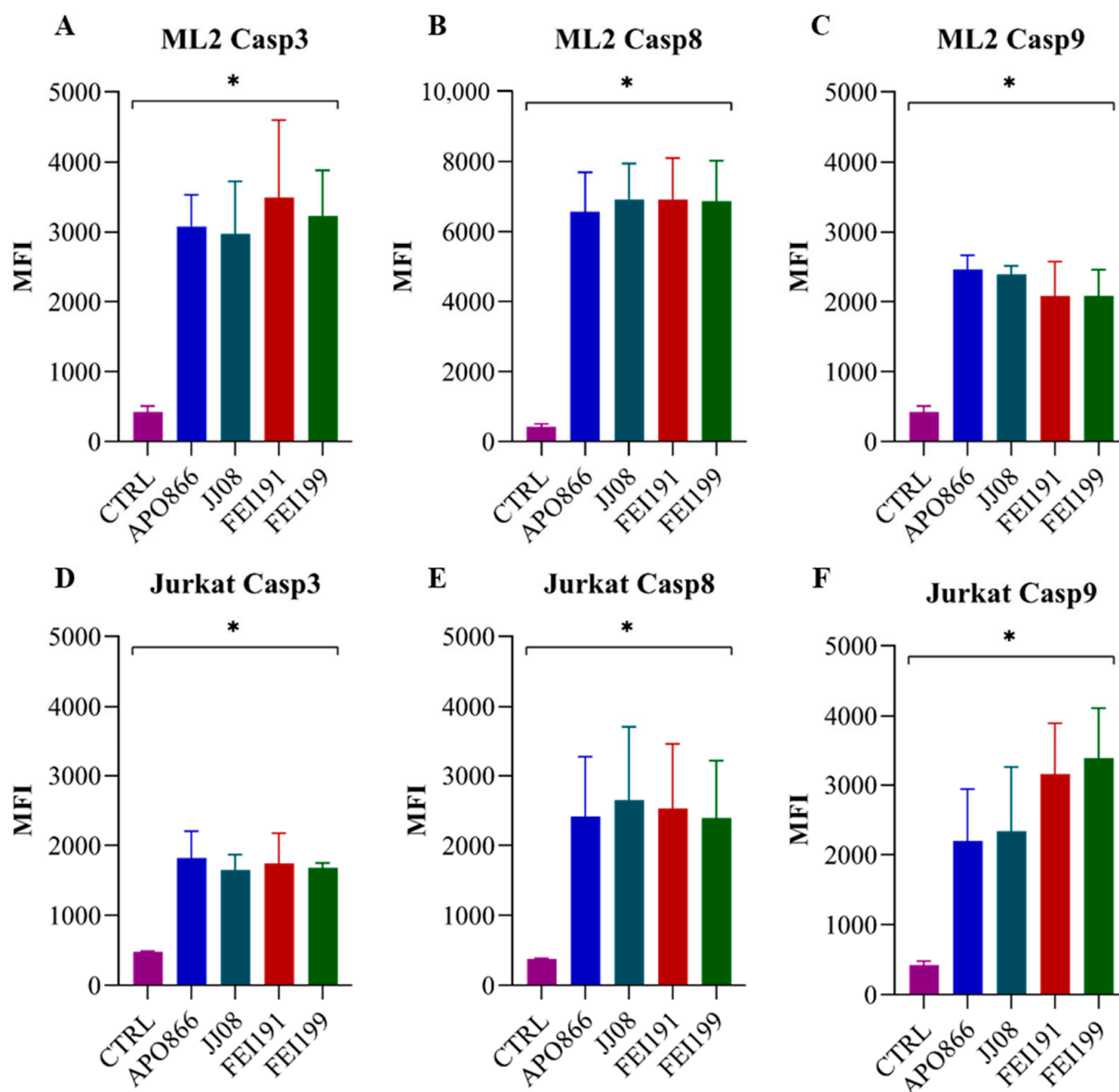


Figure 5. Treatment with NAMPT inhibitors induces strong activation of caspase –3, –8 and –9. ML2 (A–C) and Jurkat (D–F) cells were treated with 10 nM of NAMPT inhibitors for 72 h and activated forms of CASP-3, CASP-8 and CASP-9 were detected using a fluorescent-specific probe for each caspase and flow cytometry. Data are representative of at least three independent experiments and the graphs show mean fluorescence intensity (MFI). * $p < 0.005$.

To demonstrate that the antitumor activity of the new NAMPT inhibitors was due to NAD^+ depletion, we evaluated the ability of NAM and NA (precursors involved in the NAD^+ biosynthesis), as well as NAD^+ , to abrogate the cell death caused by our compounds. Extracellular supplementation in excess with NAD^+ or its precursors fully restored the viability of the cells despite the presence of the inhibitors (Figure 7). Interestingly, the supplementation with NA (but not with NAM or NAD^+) did not protect Namalwa cells from cell death in response to treatment with the NAMPT inhibitors (Figure 7C). This can be explained by the fact that Namalwa cells have a naturally very low expression of the nicotinic acid phosphoribosyltransferase (NAPRT) gene [33], which is required to utilize NA in NAD^+ biosynthesis.

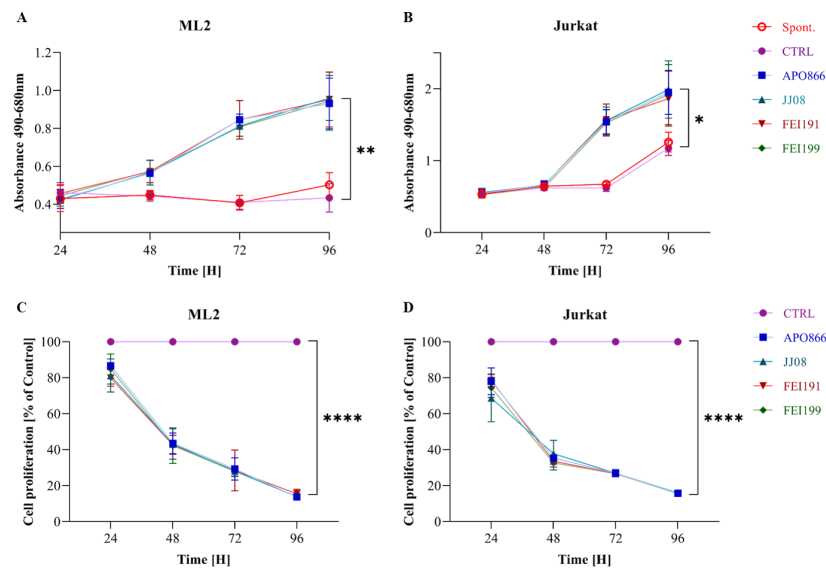


Figure 6. NAMPT inhibitors induce necrotic cell death and decrease cell proliferation in hematological malignancies. A time-dependent analysis of LDH release on ML2 (A) and Jurkat (B) cells treated with NAMPT inhibitors (10 nM) was assessed according to the manufacturer’s instructions. Cell proliferation was assessed on ML2 (C) and Jurkat (D) cells based on the ability of metabolically active cells to reduce resazurin sodium salt to a highly fluorescence product using AlamarBlue reagent. The absorbance of both products was measured with a spectrophotometer at the appropriate wavelength. Data are \pm SD, $n = 3$, * $p < 0.05$, ** $p < 0.01$, **** $p < 0.0001$ (CTRL vs. inhibitors treated groups).

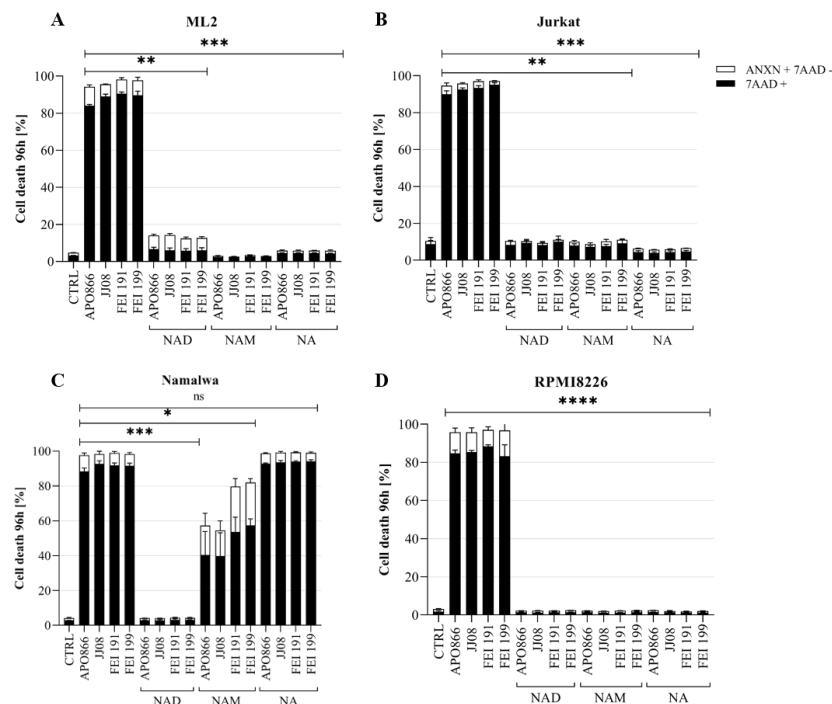


Figure 7. Supplementation with NAD, NAM and NA abrogates the killing effect of NAMPT inhibitors. ML2 (A), Jurkat (B), Namalwa (C) and RPMI8226 (D) cells were incubated for 96 h with NAMPT inhibitors in the presence or absence of NAD (0.5 mM), NAM (1 mM) or NA (10 μ M). Cell death was assessed as mentioned in Figure 4. Data are \pm SD, $n = 3$, * $p < 0.05$, ** $p < 0.01$, *** $p < 0.001$, **** $p < 0.0001$ (inhibitors treated vs. NAD, NAM and NA groups).

Collectively, these results indicate that the new NAMPT inhibitors induce both apoptotic and necrotic cell death in an NAD⁺-dependent manner in several human hematopoietic malignant cells.

2.4. Treatment with JJ08, FEI191 and FEI199 Induces High Levels of ROS Production and ATP Depletion in Hematological Malignant Cells

The first consequence of NAMPT inhibition is NAD⁺ depletion, which occurs within 24 h and will subsequently result in a profound decrease in NADP(H). To verify this hypothesis, we evaluated the intracellular NADP(H) content in myeloid leukemia cells upon treatment with NAMPT inhibitors. As shown in Figure 8, treatment with the compounds significantly depleted NADP(H) cell content compared to untreated cells. Since NADPH, a powerful cell antioxidant, is directly involved in redox reactions and is essential to maintain cellular homeostasis, its depletion is expected to generate high levels of oxidative stress. Therefore, cytosolic and mitochondrial superoxide anions, as well as intracellular hydrogen peroxide, were measured in hematopoietic malignant cells treated with the new compounds, using DHE, MitoSOX and carboxy-H2DCFDA probes, respectively. In accordance with our hypothesis, Figure 9 shows that the new NAMPT inhibitors increased the levels of various ROS in all treated cell types. High ROS production is known to be detrimental for the cells, since it oxidizes proteins, lipids and cell organelles, including mitochondria, resulting in ATP depletion [19,34] and ultimately leading to cell death [35]. As expected, the treatment of hematopoietic malignant cells with the new NAMPT inhibitors led to an ATP loss in a time-dependent manner (Figure 10A), which was followed by mitochondrial membrane depolarization (Figure 10B), that ultimately resulted in cell death at 96 h (Figure 10C). To provide strong evidence that high levels of ROS production are the main driver of these events that led to cell death, we monitored cell death in hematopoietic malignant cells treated with these compounds in the presence or absence of catalase, a potent H₂O₂ scavenger [36,37]. As shown in Figure 11, the supplementation with catalase did not prevent NAD⁺ depletion in ML2 cells (Figure 11A), but it fully abrogated the loss in ATP (Figure 11B) and MMP (Figure 11C), as well as the ultimate cell death (Figure 11D), in response to all of the tested NAMPT inhibitors. Moreover, the supplementation with catalase also prevented the cell death caused by NAMPT inhibitors at 72 h in Jurkat and RPMI8226 cell lines (Figure 11E–G).

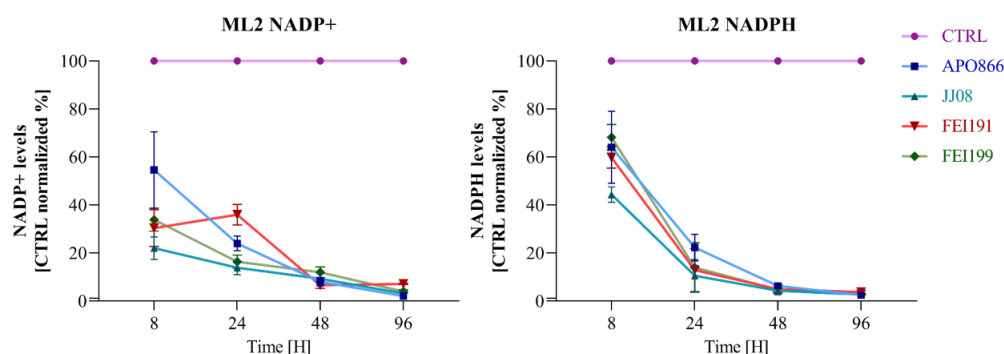


Figure 8. New NAMPT inhibitors severely deplete NADP(H) cell content in hematopoietic malignant cells. ML2 cells were incubated with NAMPT inhibitors for 96 h. A time-dependent analysis of intracellular NADP⁺/NADPH content was performed according to the manufacturer's instructions. NADP⁺/NADPH levels were first normalized to the total protein and then to control at each time point.

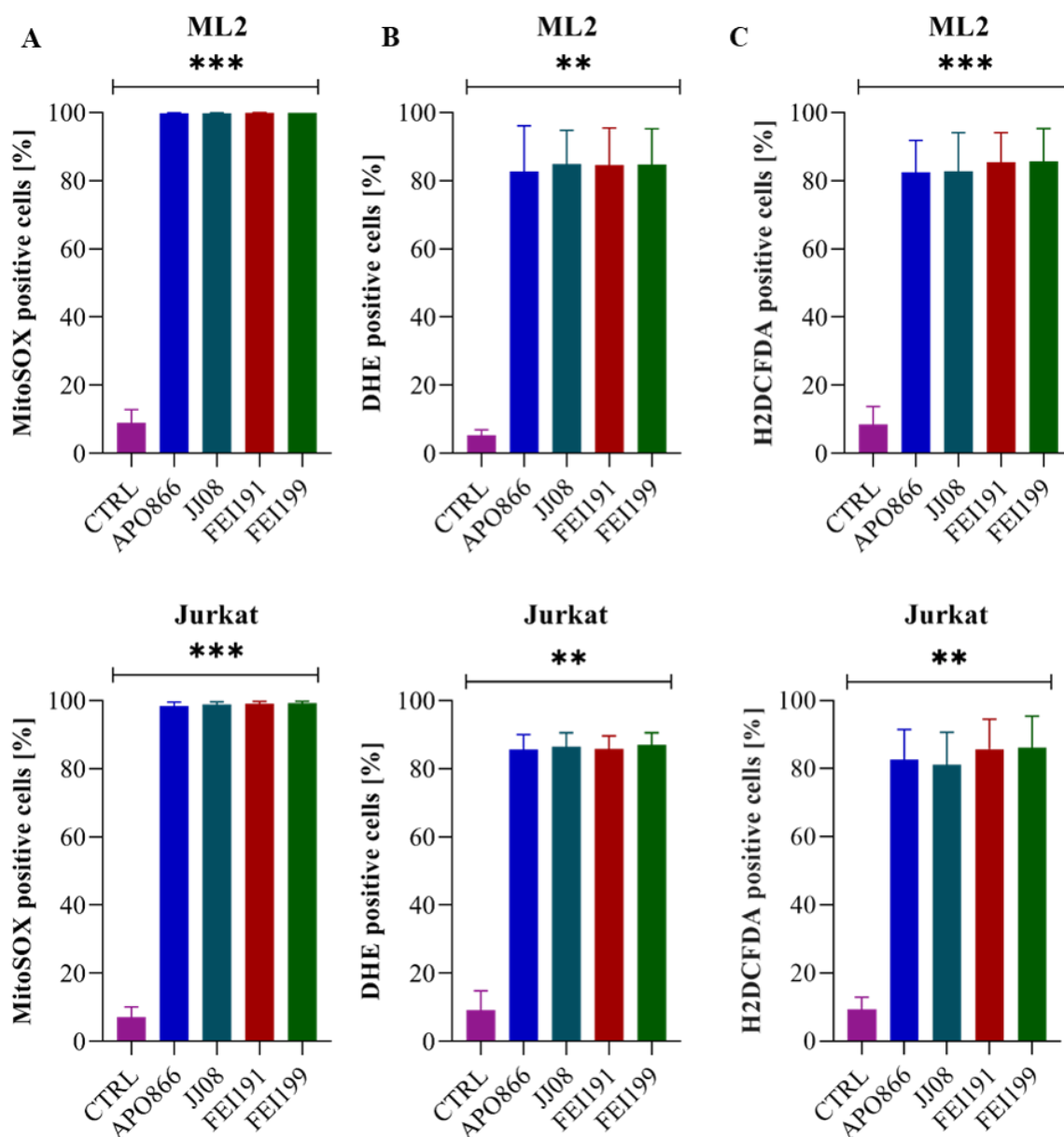


Figure 9. NAMPT inhibitors induce high levels of ROS production upon cell death in malignant cells. ML2 and Jurkat cells were treated with APO866, JJ08, FEI191 and FEI199 for 72 h. Mitochondrial (A) and cytosolic (B) superoxide anions and hydrogen peroxide (C) were detected by flow cytometry using MitoSOX, DHE and H2DCFDA fluorescent probes, respectively. The percentage of positive cells is proportional to the amount of produced superoxide anions. Data are \pm SD, $n = 3$, ** $p < 0.01$, *** $p < 0.001$ (CTRL vs. inhibitors treated groups).

Collectively, these results indicate that all of the tested NAMPT inhibitors significantly depleted cellular NADP(H) content, resulting in a burst of ROS production. In turn, this induces the loss of ATP, which is followed by mitochondrial membrane depolarization and ultimately leads to cell death. Importantly, oxidative stress appears to be the main cause of cancer cell death after NAMPT inhibitor treatment.

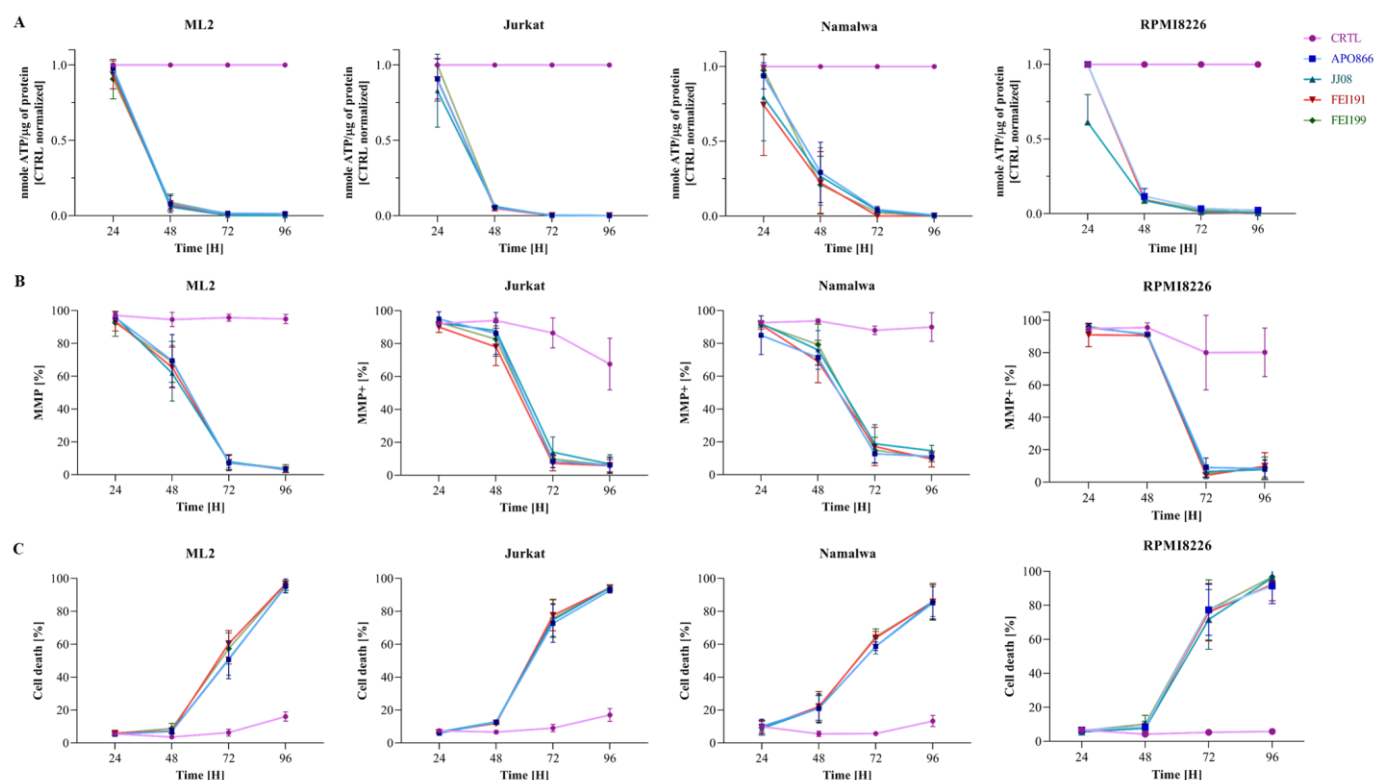


Figure 10. JJ08, FEI191 and FEI199 deplete intracellular ATP content (A), induce the loss of MMP (B) and ultimately cause cell death (C). ML2, Jurkat, Namalwa and RPMI8226 cells were treated with NAMPT inhibitors for 96 h. Intracellular ATP content, MMP and cell death were measured in a time-dependent fashion. ATP levels were first normalized to protein content and then to control at each time point. MMP was detected by flow cytometry using TMRM staining, and cell death was analyzed as described in Figure 4. Data are \pm SD, $n = 3$.

2.5. The Therapeutic Activity of JJ088 in SCID Mice Bearing Burkitt Lymphoma Is Superior to That of FEI191 and FEI199

The promising results presented above led us to explore the potential therapeutic efficacy of the new NAMPT inhibitors in a mouse xenograft model of Burkitt lymphoma. To this end, NAMPT inhibitors (10 mg/kg) were administered intraperitoneally (I.P.) to mice with established Namalwa tumors (human Burkitt lymphoma cell line) and tumor growth was monitored over time. As shown in Figure 12, treatment with the new NAMPT inhibitors exerted a significant therapeutic effect (Figure 12A) and significantly prolonged overall mice survival compared to untreated control animals (Figure 12B, log-rank test, $P < 0.05$). Interestingly, treatment with JJ08 completely eradicated tumor growth 5 days after administration. Instead, FEI191 and FEI199 did not stop tumor progression, but significantly delayed it compared to the vehicle-injected group (Figure 12A), suggesting that the *in vitro* efficiencies of FEI191 and FEI199 do not translate into equally potent *in vivo* activities. To understand why FEI191 and FEI199 were less efficient in abrogating tumor growth than JJ08, pharmacokinetics (PK) studies were carried out. Plasma concentrations of the compounds were monitored in mice ($n=3$) after I.P. administration for up to 24 h (Supplementary Materials, Figure S1). Then, PK parameters were derived and are presented in Table 2. The PK values of FK866 (APO866), which is known to effectively abrogate tumor growth *in vivo*, are shown as a reference [19]. The measured compound concentrations used for the PK data analysis are given in Supplementary Materials, Table S1. Notably, the concentrations of FEI199 measured after 8 h and 24 h were excluded, as the analytical responses were below the lower limit of quantification of the method. For FEI191, concentrations measured at 8 h and 24 h were also excluded from the PK data analysis due to carryover issues.

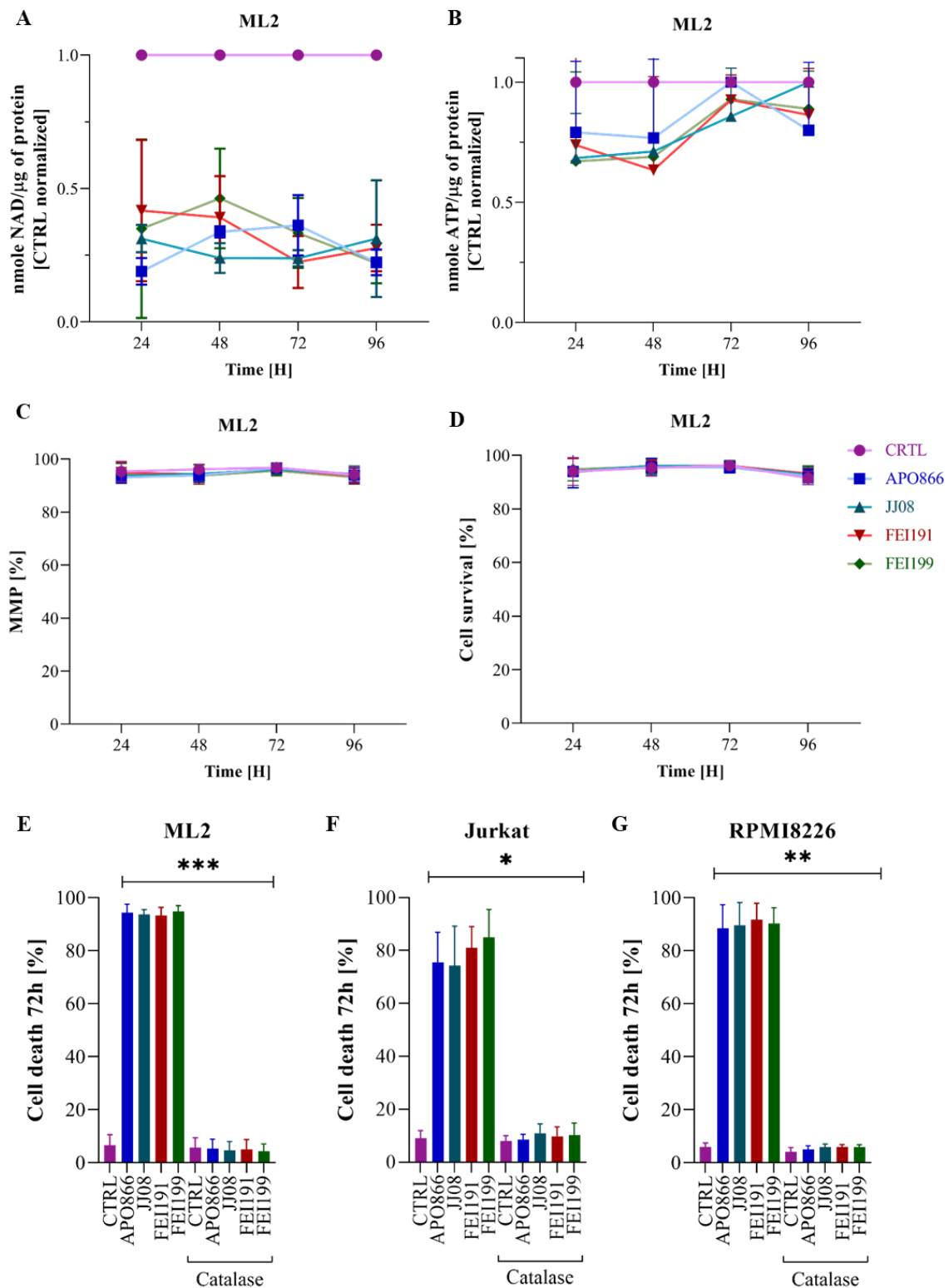


Figure 11. Catalase supplementation abrogates the killing effect of NAMPT inhibitors but not NAD^+ depletion in tested cell lines, except for Namalwa cells. Catalase (1000 U / ml) was added 1 h before the inhibitors. Kinetic analyses of intracellular NAD^+ , ATP, MMP and cell death were assessed on the ML2 cell line (A–D). Cell death was assessed as described in Figure 4, at 72 h on ML2 (E), Jurkat (F) and RPMI8226 (G). Data are \pm SD, $n = 3$, * $p < 0.05$, ** $p < 0.01$, *** $p < 0.001$ (inhibitors treated vs. catalase treated groups).

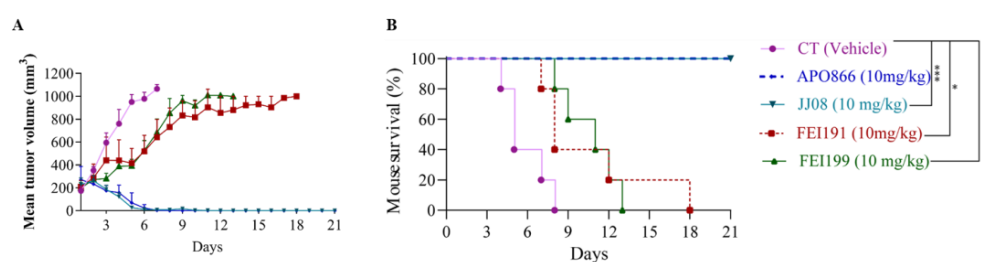


Figure 12. JJ08 eradicates tumor growth and significantly prolongs the survival in a xenograft mouse model of human Burkitt lymphoma. Tumor size (A) and survival rate (B) of mice xenografted with Namalwa cells treated or untreated with NAMPT inhibitors were monitored for 21 days. Twenty-five 6-to-8-week-old C.B.-17 SCID mice were transplanted subcutaneously with Namalwa cells (10^7). Once tumors reached a volume of approximately 100–150 mm³, at day 14, mice were randomized into five groups of animals ($n = 5$) with similar body weight. Control groups received vehicle (pink line) and JJ08 (10 mg/kg; light blue line), FEI191 (10 mg/kg; red line), FEI199 (10 mg/kg; green line) or APO866 (10 mg/kg; blue line) were administered as described in the Materials and Methods section. Day 1 on the graphs corresponds to the beginning of the treatment (when the tumor volume reached >100 mm³). Error bars = SD. * $p < 0.05$, ** $p < 0.01$, *** $p < 0.001$. Data were analyzed by the Kaplan–Meier survival analysis with log-rank test.

Table 2. Pharmacokinetic parameters of JJ08, FEI191 and FEI199 in female SCID mice following intraperitoneal administration.

	APO866	JJ08	FEI191	FEI199
C_{max} (ng/mL)	28,028	24,302	2683	12,031
T_{max} (h)	0.17	0.17	0.17	0.17
$T_{1/2}$ (h)	3.74	6.58	-	-
AUC_{0-24} (ng*h/mL)	16,426	7563	1820 *	3718 *
CL/F (mL/h)	24	53	220	108
V_z/F (mL)	131	502	-	-

C_{max} : maximum concentration; T_{max} : time to reach maximum concentration; $T_{1/2}$: half-life of the compounds; AUC_{0-24} : area under the plasma concentration–time curve over the last 24 h dosing interval; CL/F: apparent drug clearance; V_z/F : apparent terminal volume of distribution. * AUC was calculated from PK measurements up to 8 h. However, given the low concentrations, terminal exposure is not expected to induce significant changes in calculated exposure.

The four compounds showed broadly similar PK profiles, but FK866 (APO866) distinctively appeared to provide the best systemic exposure (i.e., AUC_{0-24}). In addition, the plasma concentrations of APO866 were less variable between the mice samples (Table S1). The maximum plasma concentrations (C_{max}) of JJ08 and APO866 were comparable, while the AUC_{0-24} of JJ08 appeared to be approximately 2-fold lower than that of APO866. This difference is mainly due to the early time points, which contribute significantly to the calculated AUC_{0-24} values. Similarly, the calculated apparent drug clearance (CL/F) for JJ08 was found to be 2-fold higher, whereas its half-life ($T_{1/2}$) appeared to be two times shorter as compared to APO866, indicating that JJ08 was cleared faster from circulation. Finally, based on the calculated apparent terminal volume of distribution (V_z/F), both JJ08 and APO866 compounds seemed to be well absorbed into tissues and/or highly metabolized.

Regarding FEI191 and FEI199, the terminal rate constant, λ_z , value (and therefore, $T_{1/2}$ and V_z/F) could not be assessed because their terminal phases were insufficiently characterized due to analytical issues, as discussed above. However, the maximal concentrations (C_{max}) were lower than those of APO866 or JJ08 and the clearance of FEI191 and FEI199 proved to be more than 4-fold higher, suggesting faster drug elimination.

Taken together, our in vivo data indicate that the new NAMPT inhibitors delayed and/or prevented tumor growth in a mouse Burkitt lymphoma model, with JJ08 being the most potent anticancer agent. Furthermore, JJ08 had very similar PK parameters to

APO866, whereas both **FEI** compounds exhibited lower concentrations in the blood after administration, which could explain their lower anticancer activities *in vivo*.

3. Discussion

In this study, we report the synthesis and evaluation of the therapeutic efficacies of three novel NAMPT inhibitors, **JJ08**, **FEI191** and **FEI199**, in hematological malignancies. We show that the new compounds have a broad antitumor activity against various hematological malignancies. In agreement with our previous studies on APO866, a prototype NAMPT inhibitor [19,36,38,39], we found that the new NAMPT inhibitors are highly toxic towards leukemia (AML and ALL), lymphoma (Burkitt) and multiple myeloma (MM) cells. Mechanistically, these compounds caused a strong NAD⁺ depletion that led to exhaustion of NADPH, which in turn resulted in a burst of oxidative stress. The high levels of ROS induced by these compounds disrupted the mitochondrial membrane integrity, causing ATP depletion and cell death. Scavenging ROS production with catalase abrogated cell death induced by NAMPT inhibitors, despite NAD⁺ depletion, pointing out the major contribution of oxidative stress to the antitumor activity of APO866 and of the new NAMPT inhibitors. In addition, we demonstrated that the new NAMPT inhibitors induced different types of cell death, including both caspase-dependent and caspase-independent apoptosis, but also necrotic cell death. Therefore, their mode of action described in this study is similar to that reported previously for NAMPT inhibitors [19,30,36,38–41], indicating that although these compounds have different chemical structures, they have common mechanisms involved with cell death.

Importantly, *in vivo* administration of the new NAMPT inhibitors as a single agent prevented and/or delayed tumor growth in an animal model of human Burkitt lymphoma and significantly prolonged median survival, thereby underlining the therapeutic potential of these molecules. It is noteworthy to mention that **JJ08** fully eradicated tumor growth and allowed mouse disease-free survival. In line with the *in vivo* data, **JJ08**, as well as APO866, exhibited the best PK properties when compared to those of both **FEI** compounds.

The search for new NAMPT inhibitors is motivated by the need to identify novel drugs that counter cancer progression and thereby increase patient life expectancy and quality of life, a goal of a high priority. In this endeavor, the development of anticancer therapies targeting the NAMPT-mediated NAD⁺ biosynthetic pathway represents a promising strategy and should have broad clinical implications. We and others have demonstrated that NAMPT inhibitors exhibit high efficacy against a wide range of human solid tumors and blood cancers, without significant toxicity to laboratory animal models [19,29,36,42–49]. In an effort to discover new anticancer agents, we here have identified three novel NAMPT inhibitors with broad and strong anti-leukemic/lymphoma activity. Among them, **JJ08** exhibited a promising profile as an overall potent antitumor agent both *in vitro* and *in vivo*, despite the fact that *in vitro*, **FEI191** and **FEI199** had higher antitumor activity than **JJ08**. This discrepancy between *in vitro* and *in vivo* studies is most probably related to the worse PK profiles of **FEI** compounds. Indeed, PK analyses showed that **FEI** compounds were rapidly cleared out of body circulation compared to **JJ08** (or APO866). Moreover, the calculated clearance of **FEI** compounds was at least 4-fold higher, the C_{max} was lower and their AUCs were approximately 2-to-9-fold smaller than those of **JJ08** (or APO866). The apparent volume of distribution calculated for all molecules indicated that they are highly absorbed into the tissues and/or highly metabolized. The calculated clearance for all compounds indirectly suggested that these novel NAMPT inhibitors are molecules with high hepatic excretion. Further studies aiming at improving the PK properties of novel NAMPT inhibitors are needed.

To put our results in a global context, one should keep in mind that the striking antitumor activity of NAMPT inhibitors reported in several studies is closely correlated with their *in vitro* experimental conditions. For instance, RPMI medium widely used for cell culture contains only nicotinamide as an NAD⁺ precursor. In our study, and in many preclinical studies, the major (if not the only) source of NAD⁺ synthesis was

also nicotinamide, indicating that only one route of NAD⁺ synthesis, namely, the salvage pathway, is activated within these experimental settings. In a real life situation, where many NAD⁺ precursors could be present in a tumor environment, blocking only one pathway of NAD⁺ synthesis would not be sufficient and this could greatly contribute to the loss of the therapeutic efficacy of NAMPT inhibitors. In agreement with this scenario, we and others have demonstrated that the levels and/or presence of NAD⁺ precursors (other than nicotinamide) considerably affect the antitumor efficiency of NAMPT inhibitors [39,50]. The loss of the efficacy of NAMPT inhibitors in the latter circumstance was mainly due to the activation of the alternative NAD⁺ production pathways. We also showed that gut microbiota played a crucial role in host NAD⁺ metabolism, as they contribute to resistance to NAMPT inhibitors [39]. These observations should be taken into consideration in future clinical trials, for instance, the nature and level of NAD⁺ precursors or alternatively targeting more than one route of NAD⁺ synthesis should be investigated.

In this study, we showed that the novel NAMPT inhibitors delayed or eradicated the tumor growth and thus significantly prolonged xenografted mouse survival, without evident signs of toxicity including loss of body weight, lethargy, rough coat or premature death. However, in clinical trials, the common dose-limiting toxicities were thrombocytopenia and a variety of gastrointestinal symptoms [24–26,51]. Therefore, the strategies to limit off-target toxicities need to be refined. FEI191 and FEI199 had high activities *in vitro*. Therapeutic modalities to significantly boost their *in vivo* activities and reduce their systemic associated toxicities should be explored. In this line, the next generation of NAMPT inhibitors can be conjugated to antibodies (creating antibody–drug conjugates, or ADCs). In this drug delivery system, the inhibitor is conjugated to the antibody that targets the antigens/proteins specifically expressed in cancer cells, thus allowing specific inhibitor delivery. Using such a strategy, several investigators [52–54] have demonstrated the antitumor efficacy of ADCs with NAMPT inhibitors in different mouse xenograft models. Only mild, reversible hematologic side effects were observed with ADCs in toxicological *in vivo* studies, with no signs of retinal or cardiac toxicities, as reported for NAMPT inhibitors alone in preclinical studies [52]. These findings open a new era in clinical trials to specifically target and improve the therapeutic window of NAMPT inhibition.

4. Conclusions

In summary, we have synthesized three novel NAMPT inhibitors: JJ08, FEI191 and FEI199. They are strong growth inhibitors of cancer cells from numerous hematological malignancies. Our *in vitro* and *in vivo* data demonstrate that these compounds are potent anticancer agents. JJ08 shows the best efficacy and is well tolerated in the mouse xenograft model of Burkitt lymphoma. We propose that JJ08 should undergo further clinical development for the treatment of hematologic malignancies.

5. Materials and Methods

5.1. Cell Lines and Culture Conditions

Four hematological cell lines (ML2—acute myeloid leukemia; Jurkat—acute lymphoblastic leukemia; Namalwa—Burkitt lymphoma; and RPMI8226—multiple myeloma) were purchased from DSMZ (German Collection of Microorganisms and Cell Cultures, Braunschweig, Germany) or ATCC.

All cells were cultured in RPMI medium (Invitrogen AG, 61870-01) supplemented with 10% heat inactivated fetal calf serum (Amimed, 2-01F30-I) and 1% penicillin/streptomycin at 37 °C (Amimed, 4-01F00-H) in a humidified atmosphere of 95% air and 5% CO₂.

5.2. NAMPT Enzymatic Activity Assay

The ability of FK866 (APO866) analogues to inhibit NAMPT activity was assessed with an NAMPT Activity Assay Kit (Colorimetric) (Abcam, ab221819, Cambridge, UK) according to the manufacturer's instructions. Briefly, NAMPT inhibitors were dissolved in DMSO to a final concentration of 1 μM and distributed in a 96-well plate in duplicate. Then,

a reaction mix containing assay buffer, ATP, NMNAT1, NAM, PRPP and ddH₂O was added and the plate was incubated at 30 °C for 60 min. After, to measure the generated NAD⁺, a mix of WST-1, ADH, diaphorase and ethanol was added to the wells. The absorbance was measured in kinetic mode at 450 nm on a microplate reader for 45 min at 30 °C.

5.3. Flow Cytometry Analyses

The cellular effects of **FK866** (APO866) and the new NAMPT inhibitors, **JJ08**, **FEI191** and **FEI199**, on hematopoietic malignant cells were evaluated using a Beckman Coulter Cytomics Gallios flow cytometer (Beckman Coulter International S.A., Nyon, Switzerland). The measured parameters included cell death, mitochondrial membrane potential (MMP), reactive oxygen species (ROS) production and caspase activation.

5.4. Characterization of Cell Death

To determine the cell death induced by NAMPT inhibitors, malignant cells were stained with ANNEXIN-V (ANXN, eBioscience, BMS306FI/300) and 7-aminoactinomycin D (7AAD, Immunotech, A07704) as described by the manufacturer and analyzed using flow cytometry. Dead cells were identified as ANXN+7AAD+ /7AAD+ and early apoptotic cells as ANXN+ 7AAD-. Specific cell death induced by inhibitors was calculated using the following formula: percent of cell death induced by compound = [(S – C) / (100 – C)] × 100; where S = treated sample cell death and C = untreated sample cell death.

5.5. Analysis of Mitochondrial Membrane Potential

Mitochondrial membrane depolarization was determined using tetramethylrhodamine methyl ester (TMRM, ThermoFisher Scientific, T668) according to the manufacturer's protocol. TMRM is a cationic, cell-permeant, red-orange fluorescent dye that accumulates in polarized mitochondria, but it is released after their depolarization. Untreated or treated cells were harvested, centrifuged and resuspended in culture medium containing 50 nM TMRM, and then incubated at 37 °C for 30 min in the dark. Cells were washed twice with PBS and immediately analyzed using flow cytometry.

5.6. Detection of Cellular and Mitochondrial Reactive Oxygen Species (ROS)

Various types of ROS were determined in untreated and drug-treated hematopoietic malignant cells by flow cytometry using live-cell permeant specific fluorogenic probes. Dihydroethidium (DHE, Marker Gene Technologies, M1241) was used as probe for detection of the cytosolic superoxide anion (cO₂•-), MitoSox (Molecular Probes, M36008) was used as probe for detection of the mitochondrial superoxide anion (mO₂•-) and 6-carboxy-2,7-dichlorodihydrofluorescein diacetate (carboxy-H₂DCFDA; Molecular Probes, C-400) was used as probe for detection of H₂O₂. DHE was oxidized to red fluorescent ethidium by cytosolic superoxide and MitoSOX was selectively targeted to mitochondria, where it was oxidized by superoxide and exhibited red fluorescence. Carboxy-H₂DCFDA was cleaved by esterase to yield DCFH, a polar nonfluorescent product, but in the presence of hydrogen peroxide, the latter is oxidized to a green fluorescent product, dichlorofluorescent (DCF). For cell staining, cells were centrifuged and the pellets were resuspended in PBS with a final concentration of 5 μM for each probe. The mixture was incubated in the dark at 37 °C for 15 min. Then, the cell suspension was analyzed using flow cytometry within 20 min.

5.7. Detection of Caspases Activation

Activation of various caspases was assessed using flow cytometry and specific CaspGLOW™ Red Active (BioVision, K190, Cambridge, UK) for following caspases: CASP3 (BioVision Inc., BV-K193-100), CASPASE 8 (CASP8; BioVision Inc., BV-K198-100) and CASPASE 9 (CASP9; BioVision Inc., BV-K199-25). The CaspGLOW assays offer a convenient way for measuring activated caspases in living cells. The assay uses a specific inhibitor for each caspase conjugated to sulforhodamine as a fluorescent marker, which is cell permeable, nontoxic and irreversibly binds in specific manner to activated caspase in apoptotic cells.

The red fluorescence label allows for direct detection of activated caspase in apoptotic cells by flow cytometry. Cell staining was performed according to the manufacturer's information and analyzed.

5.8. Quantification of Intracellular NAD⁺, NADP(H) and ATP Contents

Cells (1×10^6 /mL) in the log growth phase were seeded in a 6-well plate in the presence or absence of the NAMPT inhibitors. At each time point, 800 μ L of cells was centrifuged at 900 g (2000 rpm) for 5 min and washed with cold PBS. Then, the supernatant was discarded and cells were resuspended in 300 μ L of lysis buffer (20 mM NaHCO₃, 100 mM Na₂CO₃) and kept at -80 °C for at least 4 h before analysis.

Total NAD⁺ content was measured in cell lysates using a biochemical assay described previously [18]. Briefly, cell lysates (20 μ L) were plated in a 96-well flat bottom plate. A standard curve was generated using a 1:3 serial dilution in lysis buffer of a β -NAD⁺ stock solution. Cycling buffer (160 μ L) was added into each well and the plate was incubated for 5 min at 37 °C. Afterwards, ethanol (20 μ L), pre-warmed to 37 °C, was added into each well and the plate was incubated for an additional 5 min at 37 °C. The absorbance was measured in kinetic mode at 570 nm after 5, 10, 15, 20 and 30 min at 37 °C on a spectrophotometer. The amount of NAD⁺ in each sample was normalized to the protein content for each test sample at each time point.

The NADP⁺ and NADPH contents in the cells were determined separately using an NADP/NADPH-GloTM kit (Promega, G9081, Madison, WI, USA) and according to the manufacturer's protocol.

The total ATP cell content was quantified using an ATP determination Kit (Life Technologies, A22066, Carlsbad, CA, USA) according to the manufacturer's instructions.

5.9. Detection of Necrotic Cell Death with LDH Assay

The LDH release quantification was performed using a colorimetric CyQUANT LDH Cytotoxicity Assay (Invitrogen, C20300, Carlsbad, CA, USA). Lactate dehydrogenase (LDH) is a cytosolic enzyme that is released into the cell culture medium upon the disruption of the plasma membrane, indicating the necrotic type of death. LDH is quantified in the media in enzymatic reactions. Firstly, LDH catalyzes the conversion of lactate to pyruvate with the accompanying reduction of NAD⁺ to NADH. Then, the added diaphorase oxidizes NADH, which leads to the reduction of a tetrazolium salt to a red formazan. The amount of formulated formazan is directly proportional to the total LDH released into the media. Here, cells (1×10^5 /mL) in the log growth phase were seeded in a 24-well plate in the presence or absence of NAMPT inhibitors. At each time point, 100 μ L of cells was transferred to a 96-well plate and the reaction mixture from the kit was added. The plate was then incubated at RT for 30 min and protected from light. Afterwards, the stop solution was added and the absorbance was measured at 490 nm with a spectrophotometer. The higher the absorbance intensity in the sample, the more LDH is released to the culture medium.

5.10. Cell Proliferation Determination

The cell proliferation was assessed with alamarBlue® reagent (Bio-Rad, BUF012B, Hercules, CA, USA), which is based on REDOX reaction by viable cells. Specifically, resazurin sodium salt is reduced by the reducing environment of metabolically active cells to the highly fluorescence resorufin sodium salt. Cells were seeded in a 24-well plate (1×10^5 /mL) and treated with NAMPT inhibitors. After incubation, at each time point, 200 μ L of cells was transferred to a 96-well plate and alamarBlue® dye (20 μ L) was added, then the plate was incubated for 4 h in 37 °C in the dark. At the end, the absorbance at 570 and 600 nm was measured. Proliferation is depicted as a percentage of the control.

5.11. Therapeutic Efficacy Evaluation of Novel NAMPT Inhibitors Using a Mouse Xenograft Model of Human Burkitt Lymphoma

The new NAMPT inhibitors (**JJ08**, **FEI191** and **FEI199** (in comparison with lead compound, **FK866** (APO866))) were evaluated *in vivo* in a mouse xenograft model of human Burkitt lymphoma. Twenty non-leaky C.B.-17 SCID mice (8 to 10 weeks old; Iffa Credo, L'Arbresle, France) were housed in micro-isolator cages in a specific pathogen-free room in the animal facility at the University Hospital of Lausanne. Firstly, the mice spent one week alone to acclimatize to their new environment. All animals were handled according to the institutional regulations and with the prior approval of the animal ethic committee of the University of Lausanne. Manipulations were performed in sterile conditions under a laminar flow hood. Firstly, Namalwa cells (1×10^7) were injected subcutaneously into the mouse flank side. Once the tumors became palpable and reached a size between 100 and 150 mm³, mice ($n = \text{five}/\text{group}$) were randomized into control and treated groups. The drugs were administered intraperitoneally (10 mg/kg body weight) in 200 μL 0.9% saline twice a day for 4 days, repeated weekly over 3 weeks. The control group was treated only with 200 μL 0.9% saline. Every day, the animals were monitored for any signs of illness, and in cases where the tumor size reached a diameter of 15 mm, they were sacrificed immediately.

5.12. Analytical Method of Pharmacokinetic Studies *In Vivo*

Concentration measurements in mice EDTA plasma samples were performed using a Vanquish Flex ultra-high-performance liquid chromatography (UHPLC) system attached to a TSQ QuantisTM triple quadrupole mass spectrometer (MS) (ThermoFisher Scientific, Waltham, MA, USA). The chromatographic column was a Luna Omega Polar C18 3 μm , 50 \times 2.1 mm from Phenomenex (Torrance, CA, USA), kept at 40 °C in a UHPLC oven. The mobile phase was made of water and acetonitrile (ACN) with 0.1% formic acid in each. The gradient program ranged from 20 to 95% ACN in 1.5 min and the total method duration (including equilibration for the next injection) was 3 min. The flow rate and injection volume were 0.5 mL/min and 5 μL , respectively.

For the sample preparation, 90 μL of ACN was added to an aliquot of 30 μL of mouse plasma for protein precipitation. The mixture was then centrifuged at 14,000 rpm and the supernatant was directly injected in the UHPLC–MS.

5.13. Pharmacokinetic Analyses

Drug plasma concentrations were measured at selected time points after intraperitoneal administration in mice (sacrificed mice in triplicates for each time point). Samples were analyzed on two separate occasions for each sampling. Then, pharmacokinetic (PK) parameters were computed using standard non-compartmental calculations for geometric means of the measured concentrations using the “PKNCA R Package” (R version 4.0.2, R Development Core Team, <http://www.r-project.org/> access date: 4 February 2023).

The area under the curve (AUC₀₋₂₄) was calculated for the four drugs using the trapezoidal and log-trapezoidal rule when appropriate. The terminal rate constant (λ_z) was approximated using the slope of the terminal phase, while the half-life ($T_{1/2}$) was calculated as $\ln(2)/\lambda_z$, the apparent clearance (CL/F) as the dose divided by AUC₀₋₂₄ and the apparent volume of distribution (V_z/F) as $(\text{CL}/F)/\lambda_z$.

5.14. Statistical Analysis

All experiments were performed in triplicate and data are expressed as means with the standard error of the mean (SEM), unless otherwise noted. Unpaired t-tests were performed to test differences in pre- and post-treatment malignant cells. The Kaplan–Meier survival method using a long rank test was applied for the analyses of animal survival studies. GraphPad Prism version 9.1.0 (GraphPad Software, San Diego, CA, USA) was used for statistical analysis. p values less than 0.05 were considered statistically significant.

Supplementary Materials: The following supporting information can be downloaded at: <https://www.mdpi.com/article/10.3390/molecules28041897/s1>, Information on chemical synthesis of JJ08 and its characterization, p. 3; Information on chemical synthesis of FEI191, FEI199 and their characterizations, p.7; Figure S1: Geometric means of plasma concentrations of NAMPT inhibitors after intraperitoneal administration of drugs at 20 mg/kg; Table S1: Measured concentrations of JJ08, APO866, FEI-191 and FEI-199.

Author Contributions: P.B. designed and executed the biological experiments, analyzed the data and wrote the paper. S.M. and A.B. performed the experiments, analyzed the data and drafted the manuscript. J.F.B., S.R.M. and P.V. synthesized and characterized the new NAMPT inhibitors and wrote the paper. J.J. participated in the synthesis of the JJ08 compound. P.T., D.S., V.D. and L.A.D. performed the P.K. studies and wrote the paper. F.P., S.B., M.C. and A.N. (Alessio Nencioni) analyzed the results and wrote the paper. M.A.D. designed and analyzed experiments, coordinated the project and wrote the paper. A.N. (Aimable Nahimana) designed, executed and analyzed experiments, coordinated the project and wrote the paper. All authors have read and agreed to the published version of the manuscript.

Funding: This work was supported by a grant from Fondation Dubois-Ferrière Dinu Lipatti (A.N. (Aimable Nahimana)), by the Fondation Emma Muschamp (A.N.) (Aimable Nahimana, by the Seventh Framework Program PANACREAS (GA #256986 to S.B., P.V., A.N. (Alessio Nencioni), A.N. (Aimable Nahimana) and M.A.D.) and by the European FP7 project INTEGRATA (#813284-1 to SB, PV, A.N. (Aimable Nahimana), A.N. (Alessio Nencioni) and M.A.D.).

Institutional Review Board Statement: The animal study protocol was approved by the Ethics Committee of the University of Lausanne (Cantonal number VD3039x1a and National number 31354).

Informed Consent Statement: Not applicable.

Data Availability Statement: The data presented in this study are available on request from the corresponding author.

Conflicts of Interest: The authors declare no conflict of interest.

References

1. Pavlova, N.N.; Thompson, C.B. The Emerging Hallmarks of Cancer Metabolism. *Cell Metab.* **2016**, *23*, 27–47. [[CrossRef](#)]
2. Hanahan, D.; Weinberg, R.A. Hallmarks of cancer: The next generation. *Cell* **2011**, *144*, 646–674. [[CrossRef](#)]
3. Warburg, O. On the origin of cancer cells. *Science* **1956**, *123*, 309–314. [[CrossRef](#)] [[PubMed](#)]
4. DeBerardinis, R.J.; Chandel, N.S. We need to talk about the Warburg effect. *Nat. Metab.* **2020**, *2*, 127–129. [[CrossRef](#)] [[PubMed](#)]
5. Yaku, K.; Okabe, K.; Hikosaka, K.; Nakagawa, T. NAD Metabolism in Cancer Therapeutics. *Front. Oncol.* **2018**, *8*, 622. [[CrossRef](#)] [[PubMed](#)]
6. Kincaid, J.W.; Berger, N.A. NAD metabolism in aging and cancer. *Exp. Biol. Med.* **2020**, *245*, 1594–1614. [[CrossRef](#)]
7. Nikiforov, A.; Kulikova, V.; Ziegler, M. The human NAD metabolome: Functions, metabolism and compartmentalization. *Crit. Rev. Biochem. Mol. Biol.* **2015**, *50*, 284–297. [[CrossRef](#)]
8. Reiten, O.K.; Wilvang, M.A.; Mitchell, S.J.; Hu, Z.; Fang, E.F. Preclinical and clinical evidence of NAD(+) precursors in health, disease, and ageing. *Mech. Ageing Dev.* **2021**, *199*, 111567. [[CrossRef](#)]
9. Revollo, J.R.; Grimm, A.A.; Imai, S. The NAD biosynthesis pathway mediated by nicotinamide phosphoribosyltransferase regulates Sir2 activity in mammalian cells. *J. Biol. Chem.* **2004**, *279*, 50754–50763. [[CrossRef](#)]
10. Rongvaux, A.; Shea, R.J.; Mulks, M.H.; Gigot, D.; Urbain, J.; Leo, O.; Andris, F. Pre-B-cell colony-enhancing factor, whose expression is up-regulated in activated lymphocytes, is a nicotinamide phosphoribosyltransferase, a cytosolic enzyme involved in NAD biosynthesis. *Eur. J. Immunol.* **2002**, *32*, 3225–3234. [[CrossRef](#)]
11. Gallí, M.; Van Gool, F.; Rongvaux, A.; Andris, F.; Leo, O. The Nicotinamide Phosphoribosyltransferase: A Molecular Link between Metabolism, Inflammation, and Cancer. *Cancer Res.* **2010**, *70*, 8. [[CrossRef](#)] [[PubMed](#)]
12. Garten, A.; Schuster, S.; Penke, M.; Gorski, T.; de Giorgis, T.; Kiess, W. Physiological and pathophysiological roles of NAMPT and NAD metabolism. *Nat. Rev. Endocrinol.* **2015**, *11*, 535–546. [[CrossRef](#)] [[PubMed](#)]
13. Lucena-Cacace, A.; Otero-Albiol, D.; Jiménez-García, M.P.; Muñoz-Galvan, S.; Carnero, A. NAMPT Is a Potent Oncogene in Colon Cancer Progression that Modulates Cancer Stem Cell Properties and Resistance to Therapy through Sirt1 and PARP. *J Clin. Cancer Res.* **2018**, *24*, 1202–1215. [[CrossRef](#)]
14. Sawicka-Gutaj, N.; Waligórska-Stachura, J.; Andrusiewicz, M.; Biczysko, M.; Sowiński, J.; Skrobisz, J.; Ruchala, M. Nicotinamide phosphoribosyltransferase overexpression in thyroid malignancies and its correlation with tumor stage and with survivin/survivin DEx3 expression. *Tumour Biol.* **2015**, *36*, 7859–7863. [[CrossRef](#)]

15. Nakajima, T.E.; Yamada, Y.; Hamano, T.; Furuta, K.; Gotoda, T.; Katai, H.; Kato, K.; Hamaguchi, T.; Shimada, Y. Adipocytokine levels in gastric cancer patients: Resistin and visfatin as biomarkers of gastric cancer. *J. Gastroenterol.* **2009**, *44*, 685–690. [[CrossRef](#)] [[PubMed](#)]
16. Galli, U.; Colombo, G.; Travelli, C.; Tron, G.C.; Genazzani, A.A.; Grolla, A.A. Recent Advances in NAMPT Inhibitors: A Novel Immunotherapeutic Strategy. *Front. Pharmacol.* **2020**, *11*, 656. [[CrossRef](#)]
17. Heske, C.M. Beyond Energy Metabolism: Exploiting the Additional Roles of NAMPT for Cancer Therapy. *Front. Oncol.* **2020**, *9*, 1514. [[CrossRef](#)]
18. Hasmann, M.; Schemainda, I. FK866, a highly specific noncompetitive inhibitor of nicotinamide phosphoribosyltransferase, represents a novel mechanism for induction of tumor cell apoptosis. *Cancer Res.* **2003**, *63*, 7436–7442.
19. Nahimana, A.; Attinger, A.; Aubry, D.; Greaney, P.; Ireson, C.; Thougard, A.V.; Tjornelund, J.; Dawson, K.M.; Dupuis, M.; Duchosal, M.A. The NAD biosynthesis inhibitor APO866 has potent antitumor activity against hematologic malignancies. *Blood* **2009**, *113*, 3276–3286. [[CrossRef](#)]
20. Cagnetta, A.; Caffa, I.; Acharya, C.; Soncini, D.; Acharya, P.; Adamia, S.; Pierri, I.; Bergamaschi, M.; Garuti, A.; Fraternali, G.; et al. APO866 Increases Antitumor Activity of Cyclosporin-A by Inducing Mitochondrial and Endoplasmic Reticulum Stress in Leukemia Cells. *Clin. Cancer Res.* **2015**, *21*, 3934–3945. [[CrossRef](#)]
21. Yang, P.; Zhang, L.; Shi, Q.J.; Lu, Y.B.; Wu, M.; Wei, E.Q.; Zhang, W.P. Nicotinamide phosphoribosyltransferase inhibitor APO866 induces C6 glioblastoma cell death via autophagy. *Die Pharmazie* **2015**, *70*, 650–655. [[PubMed](#)]
22. Barraud, M.; Garnier, J.; Loncle, C.; Gayet, O.; Lequeue, C.; Vasseur, S.; Bian, B.; Duconseil, P.; Gilibert, M.; Bigonnet, M.; et al. A pancreatic ductal adenocarcinoma subpopulation is sensitive to FK866, an inhibitor of NAMPT. *Oncotarget* **2016**, *7*, 53783–53796. [[CrossRef](#)] [[PubMed](#)]
23. Cea, M.; Zoppoli, G.; Bruzzzone, S.; Fruscione, F.; Moran, E.; Garuti, A.; Rocco, I.; Cirmena, G.; Casciaro, S.; Olcese, F.; et al. APO866 activity in hematologic malignancies: A preclinical in vitro study. *Blood* **2009**, *113*, 6035–6037, author reply 6037–6038. [[CrossRef](#)] [[PubMed](#)]
24. Hovstadius, P.; Larsson, R.; Jonsson, E.; Skov, T.; Kissmeyer, A.M.; Krasilnikoff, K.; Bergh, J.; Karlsson, M.O.; Lönnebo, A.; Ahlgren, J. A Phase I study of CHS 828 in patients with solid tumor malignancy. *Clin. Cancer Res.* **2002**, *8*, 2843–2850.
25. Ravaud, A.; Cerny, T.; Terret, C.; Wanders, J.; Bui, B.N.; Hess, D.; Droz, J.P.; Fumoleau, P.; Twelves, C. Phase I study and pharmacokinetic of CHS-828, a guanidino-containing compound, administered orally as a single dose every 3 weeks in solid tumours: An ECGS/EOBTC study. *Eur. J. Cancer* **2005**, *41*, 702–707. [[CrossRef](#)]
26. Holen, K.; Saltz, L.B.; Hollywood, E.; Burk, K.; Hanauske, A.-R. The pharmacokinetics, toxicities, and biologic effects of FK866, a nicotinamide adenine dinucleotide biosynthesis inhibitor. *Investig. New Drugs* **2008**, *26*, 45–51. [[CrossRef](#)]
27. Naing, A.; Leong, S.; Pishvaian, M.J.; Razak, A.R.A.; Mahipal, A.; Berlin, J.; Cho, D.; Senapedis, W.; Shacham, S.; Kauffman, M.; et al. A first in human phase 1 study of KPT-9274, a first in class dual inhibitor of PAK4 and NAMPT, in patients with advanced solid malignancies or NHL. *Ann. Oncol.* **2017**, *28*, v125. [[CrossRef](#)]
28. Korotchikina, L.; Kazyulkin, D.; Komarov, P.G.; Polinsky, A.; Andrianova, E.L.; Joshi, S.; Gupta, M.; Vujcic, S.; Kononov, E.; Toshkov, I.; et al. OT-82, a novel anticancer drug candidate that targets the strong dependence of hematological malignancies on NAD biosynthesis. *Leukemia* **2020**, *34*, 1828–1839. [[CrossRef](#)]
29. Bai, J.-F.; Majjigapu, S.R.; Sordat, B.; Poty, S.; Vogel, P.; Elías-Rodríguez, P.; Moreno-Vargas, A.J.; Carmona, A.T.; Caffa, I.; Ghanem, M.; et al. Identification of new FK866 analogues with potent anticancer activity against pancreatic cancer. *Eur. J. Med. Chem.* **2022**, *239*, 114504. [[CrossRef](#)]
30. Kozako, T.; Aikawa, A.; Ohsugi, T.; Uchida, Y.-i.; Kato, N.; Sato, K.; Ishitsuka, K.; Yoshimitsu, M.; Honda, S.-i. High expression of NAMPT in adult T-cell leukemia/lymphoma and anti-tumor activity of a NAMPT inhibitor. *Eur. J. Pharmacol.* **2019**, *865*, 172738. [[CrossRef](#)]
31. Mitchell, S.R.; Larkin, K.; Grieselhuber, N.R.; Lai, T.-H.; Cannon, M.; Orwick, S.; Sharma, P.; Asemelash, Y.; Zhang, P.; Goettl, V.M.; et al. Selective targeting of NAMPT by KPT-9274 in acute myeloid leukemia. *Blood Adv.* **2019**, *3*, 242–255. [[CrossRef](#)] [[PubMed](#)]
32. Chan, F.K.-M.; Moriwaki, K.; De Rosa, M.J. Detection of necrosis by release of lactate dehydrogenase activity. *Methods Mol. Biol.* **2013**, *979*, 65–70. [[CrossRef](#)] [[PubMed](#)]
33. Klijn, C.; Durinck, S.; Stawiski, E.W.; Haverty, P.M.; Jiang, Z.; Liu, H.; Degenhardt, J.; Mayba, O.; Gnad, F.; Liu, J.; et al. A comprehensive transcriptional portrait of human cancer cell lines. *Nat. Biotechnol.* **2015**, *33*, 306–312. [[CrossRef](#)] [[PubMed](#)]
34. Stein, L.R.; Imai, S. The dynamic regulation of NAD metabolism in mitochondria. *Trends Endocrinol. Metab.* **2012**, *23*, 420–428. [[CrossRef](#)]
35. Redza-Dutordoir, M.; Averill-Bates, D.A. Activation of apoptosis signalling pathways by reactive oxygen species. *BBA* **2016**, *1863*, 2977–2992. [[CrossRef](#)]
36. Ginet, V.; Puyal, J.; Rummel, C.; Aubry, D.; Breton, C.; Cloux, A.J.; Majjigapu, S.R.; Sordat, B.; Vogel, P.; Bruzzzone, S.; et al. A critical role of autophagy in antileukemia/lymphoma effects of APO866, an inhibitor of NAD biosynthesis. *Autophagy* **2014**, *10*, 603–617. [[CrossRef](#)]
37. Liou, G.-Y.; Storz, P. Reactive oxygen species in cancer. *Free Radic Res.* **2010**, *44*, 479–496. [[CrossRef](#)]
38. Cloux, A.J.; Aubry, D.; Heulot, M.; Widmann, C.; ElMokh, O.; Piacente, F.; Cea, M.; Nencioni, A.; Bellotti, A.; Bouzourène, K.; et al. Reactive oxygen/nitrogen species contribute substantially to the antileukemia effect of APO866, a NAD lowering agent. *Oncotarget* **2019**, *10*, 6723–6738. [[CrossRef](#)]

39. ElMokh, O.; Matsumoto, S.; Binięcka, P.; Bellotti, A.; Schaeuble, K.; Piacente, F.; Gallart-Ayala, H.; Ivanisevic, J.; Stamenkovic, I.; Nencioni, A.; et al. Gut microbiota severely hampers the efficacy of NAD-lowering therapy in leukemia. *Cell Death Dis.* **2022**, *13*, 320. [[CrossRef](#)]
40. Cea, M.; Cagnetta, A.; Fulciniti, M.; Tai, Y.T.; Hideshima, T.; Chauhan, D.; Roccaro, A.; Sacco, A.; Calimeri, T.; Cottini, F.; et al. Targeting NAD⁺ salvage pathway induces autophagy in multiple myeloma cells via mTORC1 and extracellular signal-regulated kinase (ERK1/2) inhibition. *Blood* **2012**, *120*, 3519–3529. [[CrossRef](#)]
41. Cagnetta, A.; Cea, M.; Calimeri, T.; Acharya, C.; Fulciniti, M.; Tai, Y.T.; Hideshima, T.; Chauhan, D.; Zhong, M.Y.; Patrone, F.; et al. Intracellular NAD⁺ depletion enhances bortezomib-induced anti-myeloma activity. *Blood* **2013**, *122*, 1243–1255. [[CrossRef](#)] [[PubMed](#)]
42. Ghanem, M.S.; Monacelli, F.; Nencioni, A. Advances in NAD-Lowering Agents for Cancer Treatment. *Nutrients* **2021**, *13*, 1665. [[CrossRef](#)] [[PubMed](#)]
43. Olesen, U.H.; Christensen, M.K.; Björkling, F.; Jäättelä, M.; Jensen, P.B.; Sehested, M.; Nielsen, S.J. Anticancer agent CHS-828 inhibits cellular synthesis of NAD. *Biochem. Biophys. Res. Commun.* **2008**, *367*, 799–804. [[CrossRef](#)]
44. Zhao, G.; Green, C.F.; Hui, Y.-H.; Prieto, L.; Shepard, R.; Dong, S.; Wang, T.; Tan, B.; Gong, X.; Kays, L.; et al. Discovery of a Highly Selective NAMPT Inhibitor That Demonstrates Robust Efficacy and Improved Retinal Toxicity with Nicotinic Acid Coadministration. *Mol. Cancer Ther.* **2017**, *16*, 2677–2688. [[CrossRef](#)] [[PubMed](#)]
45. Del Nagro, C.; Xiao, Y.; Rangell, L.; Reichelt, M.; O'Brien, T. Depletion of the central metabolite NAD leads to oncosis-mediated cell death. *J. Biol. Chem.* **2014**, *289*, 35182–35192. [[CrossRef](#)]
46. Beauparlant, P.; Bédard, D.; Bernier, C.; Chan, H.; Gilbert, K.; Goulet, D.; Gratton, M.O.; Lavoie, M.; Roulston, A.; Turcotte, E.; et al. Preclinical development of the nicotinamide phosphoribosyl transferase inhibitor prodrug GMX1777. *Anticancer Drugs* **2009**, *20*, 346–354. [[CrossRef](#)]
47. Okumura, S.; Sasaki, T.; Minami, Y.; Ohsaki, Y. Nicotinamide phosphoribosyltransferase: A potent therapeutic target in non-small cell lung cancer with epidermal growth factor receptor-gene mutation. *J. Thorac. Oncol.* **2012**, *7*, 49–56. [[CrossRef](#)] [[PubMed](#)]
48. Drevs, J.; Löser, R.; Rattel, B.; Esser, N. Antiangiogenic potency of FK866/K22.175, a new inhibitor of intracellular NAD biosynthesis, in murine renal cell carcinoma. *Anticancer Res.* **2003**, *23*, 4853–4858.
49. Johanson, V.; Arvidsson, Y.; Kölby, L.; Bernhardt, P.; Swärd, C.; Nilsson, O.; Ahlman, H. Antitumoural effects of the pyridyl cyanoguanidine CHS 828 on three different types of neuroendocrine tumours xenografted to nude mice. *Neuroendocrinology* **2005**, *82*, 171–176. [[CrossRef](#)]
50. Shats, I.; Williams, J.G.; Liu, J.; Makarov, M.V.; Wu, X.; Lih, F.B.; Deterding, L.J.; Lim, C.; Xu, X.; Randall, T.A.; et al. Bacteria Boost Mammalian Host NAD Metabolism by Engaging the Deamidated Biosynthesis Pathway. *Cell Metab.* **2020**, *31*, 564–579.e7. [[CrossRef](#)] [[PubMed](#)]
51. von Heideman, A.; Berglund, Å.; Larsson, R.; Nygren, P. Safety and efficacy of NAD depleting cancer drugs: Results of a phase I clinical trial of CHS 828 and overview of published data. *Cancer Chemother. Pharmacol.* **2010**, *65*, 1165–1172. [[CrossRef](#)] [[PubMed](#)]
52. Neumann, C.S.; Olivas, K.C.; Anderson, M.E.; Cochran, J.H.; Jin, S.; Li, F.; Loftus, L.V.; Meyer, D.W.; Neale, J.; Nix, J.C.; et al. Targeted Delivery of Cytotoxic NAMPT Inhibitors Using Antibody-Drug Conjugates. *Mol. Cancer Ther.* **2018**, *17*, 2633–2642. [[CrossRef](#)] [[PubMed](#)]
53. Böhnke, N.; Berger, M.; Griebenow, N.; Rottmann, A.; Erkelenz, M.; Hammer, S.; Berndt, S.; Günther, J.; Wengner, A.M.; Stelte-Ludwig, B.; et al. A Novel NAMPT Inhibitor-Based Antibody-Drug Conjugate Payload Class for Cancer Therapy. *Bioconjug. Chem.* **2022**, *33*, 1210–1221. [[CrossRef](#)] [[PubMed](#)]
54. Karpov, A.S.; Abrams, T.; Clark, S.; Raikar, A.; D'Alessio, J.A.; Dillon, M.P.; Gesner, T.G.; Jones, D.; Lacaud, M.; Mallet, W.; et al. Nicotinamide Phosphoribosyltransferase Inhibitor as a Novel Payload for Antibody-Drug Conjugates. *ACS Med. Chem. Lett.* **2018**, *9*, 838–842. [[CrossRef](#)]

Disclaimer/Publisher's Note: The statements, opinions and data contained in all publications are solely those of the individual author(s) and contributor(s) and not of MDPI and/or the editor(s). MDPI and/or the editor(s) disclaim responsibility for any injury to people or property resulting from any ideas, methods, instructions or products referred to in the content.

Synthesis and structure-activity relationship of new Nicotinamide Phosphoribosyltransferase inhibitors with antitumor activity on solid and haematological cancer.

Synthesis and structure-activity relationship of new Nicotinamide Phosphoribosyltransferase inhibitors with antitumor activity on solid and haematological cancer.



Research paper



Synthesis and structure-activity relationship of new nicotinamide phosphoribosyltransferase inhibitors with antitumor activity on solid and haematological cancer

Simone Fratta^a, Paulina Binięcka^b, Antonio J. Moreno-Vargas^a, Ana T. Carmona^{a,**}, Aimable Nahimana^b, Michel A. Duchosal^{b,c}, Francesco Piacente^d, Santina Bruzzone^d, Irene Caffa^{e,f}, Alessio Nencioni^{e,f}, Inmaculada Robina^{a,*}

^a Departamento de Química Orgánica, Facultad de Química, Universidad de Sevilla, Sevilla, 41012, Spain

^b Central Laboratory of Hematology, Medical Laboratory and Pathology Department, Lausanne University Hospital, 1011, Lausanne, Switzerland

^c Service of Hematology, Oncology Department, Lausanne University Hospital, 1011, Lausanne, Switzerland

^d Department of Experimental Medicine, Section of Biochemistry, University of Genoa, 16132, Genoa, Italy

^e Department of Internal Medicine and Medical Specialties, University of Genoa, 16132, Genoa, Italy

^f IRCCS Ospedale Policlinico San Martino, 16132, Genoa, Italy

ARTICLE INFO

Keywords:

NAMPT inhibitors
Cytotoxic agents
Cancer
NAD⁺
Cyanoguanidines
Furan

ABSTRACT

Cancer cells are highly dependent on Nicotinamide phosphoribosyltransferase (NAMPT) activity for proliferation, therefore NAMPT represents an interesting target for the development of anti-cancer drugs. Several compounds, such as FK866 and CHS828, were identified as potent NAMPT inhibitors with strong anti-cancer activity, although none of them reached the late stages of clinical trials. We present herein the preparation of three libraries of new inhibitors containing (pyridin-3-yl)triazole, (pyridin-3-yl)thiourea and (pyridin-3/4-yl)cyanoguanidine as cap/connecting unit and a furyl group at the tail position of the compound. Antiproliferative activity *in vitro* was evaluated on a panel of solid and haematological cancer cell lines and most of the synthesized compounds showed nanomolar or sub-nanomolar cytotoxic activity in MiaPaCa-2 (pancreatic cancer), ML2 (acute myeloid leukemia), JRKT (acute lymphoblastic leukemia), NMLW (Burkitt lymphoma), RPMI8226 (multiple myeloma) and NB4 (acute myeloid leukemia), with lower IC₅₀ values than those reported for FK866. Notably, compounds **35a**, **39a** and **47** showed cytotoxic activity against ML2 with IC₅₀ = 18, 46 and 49 pM, and IC₅₀ towards MiaPaCa-2 of 0.005, 0.455 and 2.81 nM, respectively. Moreover, their role on the NAD⁺ synthetic pathway was demonstrated by the NAMPT inhibition assay. Finally, the intracellular NAD⁺ depletion was confirmed *in vitro* to induced ROS accumulation that cause a time-dependent mitochondrial membrane depolarization, leading to ATP loss and cell death.

1. Introduction

Nicotinamide phosphoribosyltransferase (NAMPT) is a key enzyme for the biosynthesis of nicotinamide adenine dinucleotide (NAD⁺) in cells. NAD⁺ is a cofactor in multiple redox reactions related to cell energy production and is used as a substrate by enzymes involved in protein chemical modifications (post-translational modifications) and modulation of intracellular Ca²⁺ homeostasis, thus regulating important functions, including metabolic pathways, DNA repair, and inflammatory

responses. Due to these relevant redox and non-redox functions of NAD⁺, NAMPT constitutes an attractive target in drug research [1]. Mammalian cells utilize three biosynthetic pathways to generate NAD⁺. NAMPT controls the rate-limiting step of one of these pathways, the so-called salvage pathway, where nicotinamide (NAM) generates NAD⁺, this being the preferred NAD⁺ production route of many types of cancer (salvage-dependent tumors) [2]. In this type of cancer cells, NAMPT is typically over-expressed compared to normal tissues and helps enhancing NAD⁺ synthesis. Overall, since many cancer cells are highly

* Corresponding author.

** Corresponding author.

E-mail addresses: anater@us.es (A.T. Carmona), robina@us.es (I. Robina).

<https://doi.org/10.1016/j.ejmech.2023.115170>

Received 10 January 2023; Accepted 29 January 2023

Available online 31 January 2023

0223-5234/© 2023 The Authors. Published by Elsevier Masson SAS. This is an open access article under the CC BY license (<http://creativecommons.org/licenses/by/4.0/>).

dependent on NAMPT activity for proliferation, NAMPT represents an interesting target for the development of anti-cancer drugs [3]. Over the last years, several compounds were identified as potent NAMPT inhibitors with strong anti-cancer activity [4]. FK866 (compound 1, also known as APO866, Fig. 1) was the first compound that was co-crystallized in 2006 with NAMPT [5], therefore representing the most relevant reference for this class of anti-cancer drugs. Although this molecule entered phase II clinical trials in patients with advanced solid tumors, it failed due to limited antitumor activity and off-target toxicity (i.e., thrombocytopenia) [6]. Similar results in patients were obtained with Teglirad, a prodrug of the known NAMPT inhibitor CHS828 (compound 2, Fig. 1), that was found to induce thrombocytopenia and gastrointestinal symptoms while not achieving significant antitumor activity [7]. Besides, most NAMPT inhibitors are known to be associated with on-target hematological and retinal toxicities [8] which have limited their clinical development. Nevertheless, the inhibition of NAMPT still remains as a promising strategy for cancer therapy as it was demonstrated with compound 3 (KPT-9274), a dual inhibitor of NAMPT and of the serine/threonine-protein kinase PAK4 [9], that was successfully transited in phase I from advanced solid malignancies to acute myeloid leukemia [10]. OT-82 (compound 4) was also identified as a new NAMPT inhibitor with marked efficacy against hematopoietic malignancies such as leukemia, lymphoma and myeloma and it is being currently evaluated in clinical studies [11].

Recently triazole-, cyanoguanidine- and urea derivatives 5–7 were identified as potent NAMPT inhibitors showing similar or improved anticancer activity with respect to FK866 and CHS828 [12–14].

As part of a program for the development of new NAMPT inhibitors with improved anticancer activity (the European 7th Framework Programme project PANACREAS – www.panacreas.eu), we have recently reported the preparation and biological evaluation of FK866 analogues that retain the (pyridin-3-yl)acrylamide moiety and vary the linker and tail group [15]. In the present work, we have also focused on modifications of the connecting unit and cap group. In addition to the triazolylpyridine and cyanoguanidino-pyridine cores present in inhibitors 5 and 6, the incorporation of thiourea as connecting group has been explored. The substitution of the pyridine moiety by other aromatic ring as cap group was also considered (Fig. 2). A structure-based design was used for the preparation of the new inhibitors. The introduction of a furan moiety in the structure of the new NAMPT inhibitors could increase the polarity of the molecule and minimize retinal toxicity due to a reduced exposure in the retina, as previously reported [16]. Moreover recent publications have demonstrated that biologically relevant furan

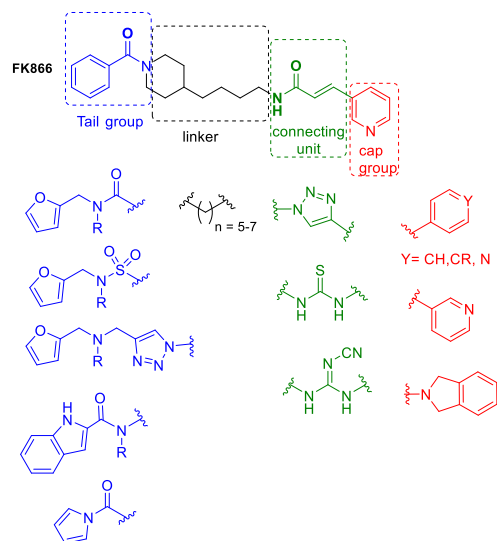


Fig. 2. Structural motifs for the new inhibitors prepared in this work.

containing cargos can be easily and selectively released in *in vivo* models in a novel strategy for target drug delivery [17,18]. As a consequence, furan has been chosen as a tail group for most of the newly prepared compounds.

2. Results and discussion

2.1. Chemistry

Preparation of (pyridin-3-yl)triazole-based inhibitors. This family of compounds (8–12, Scheme 1) is characterized by a 3-triazolylpyridine core connected to the piperidine alkyl chain of FK866 or to a flexible carbon chain. The phenyl group of FK866 was modified with different more hydrophilic heteroaromatic moieties (furan, pyrrole, indole), which could improve the water solubility of the resulting inhibitor. In this set of compounds, incorporation of the pyridine moiety into the inhibitor was carried out by copper-catalyzed alkyne azide cycloaddition (CuAAC) of commercial 3-ethynylpyridine with azide-functionalized derivatives 13–15 and 17. The preparation of the target compounds is depicted in Scheme 1. The S_N2 reaction of commercial 8-

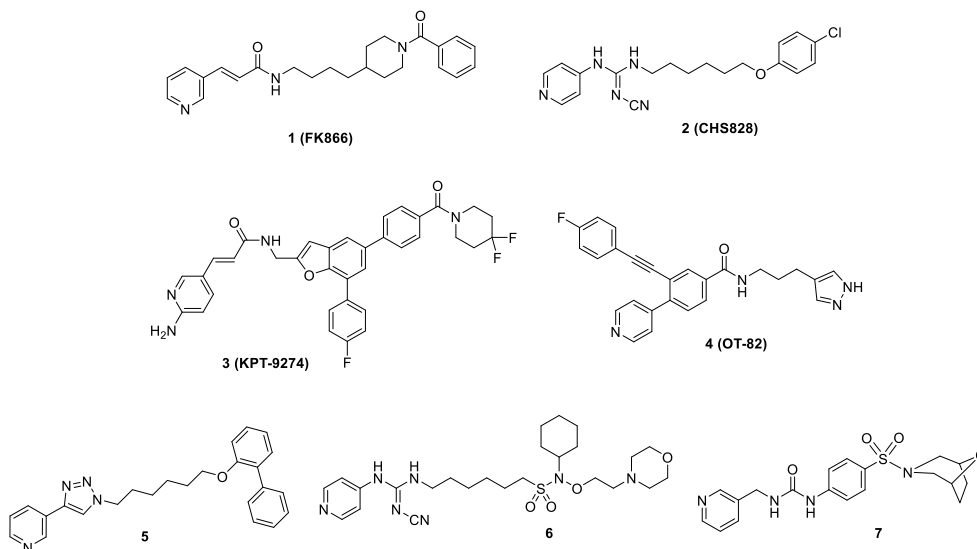
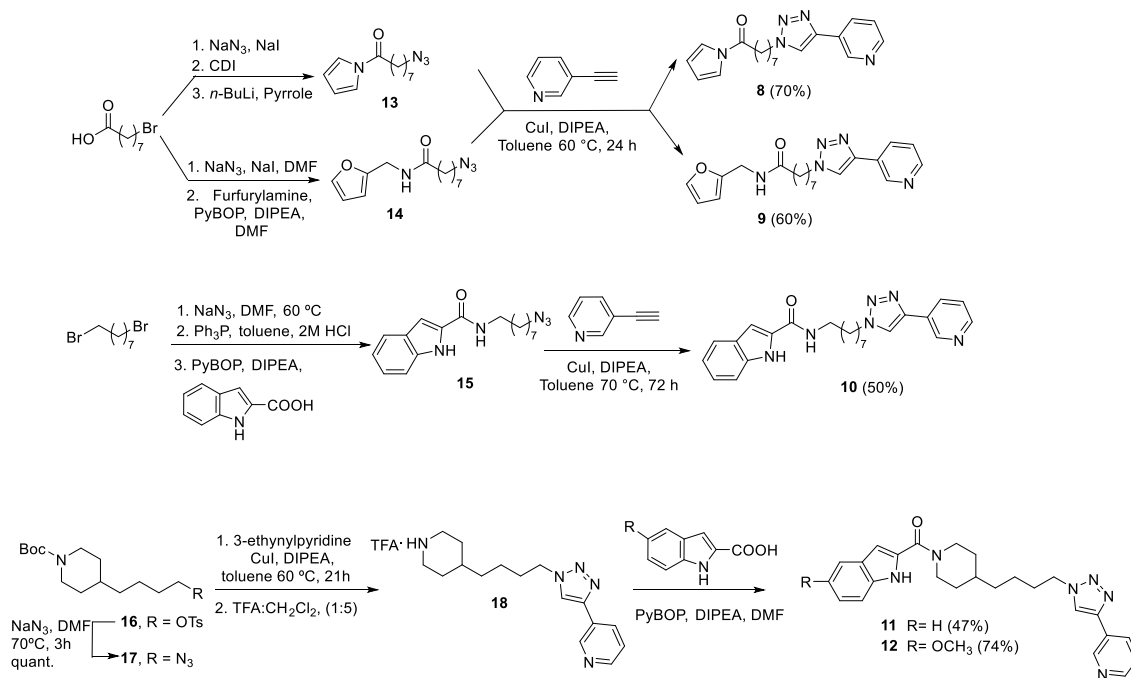


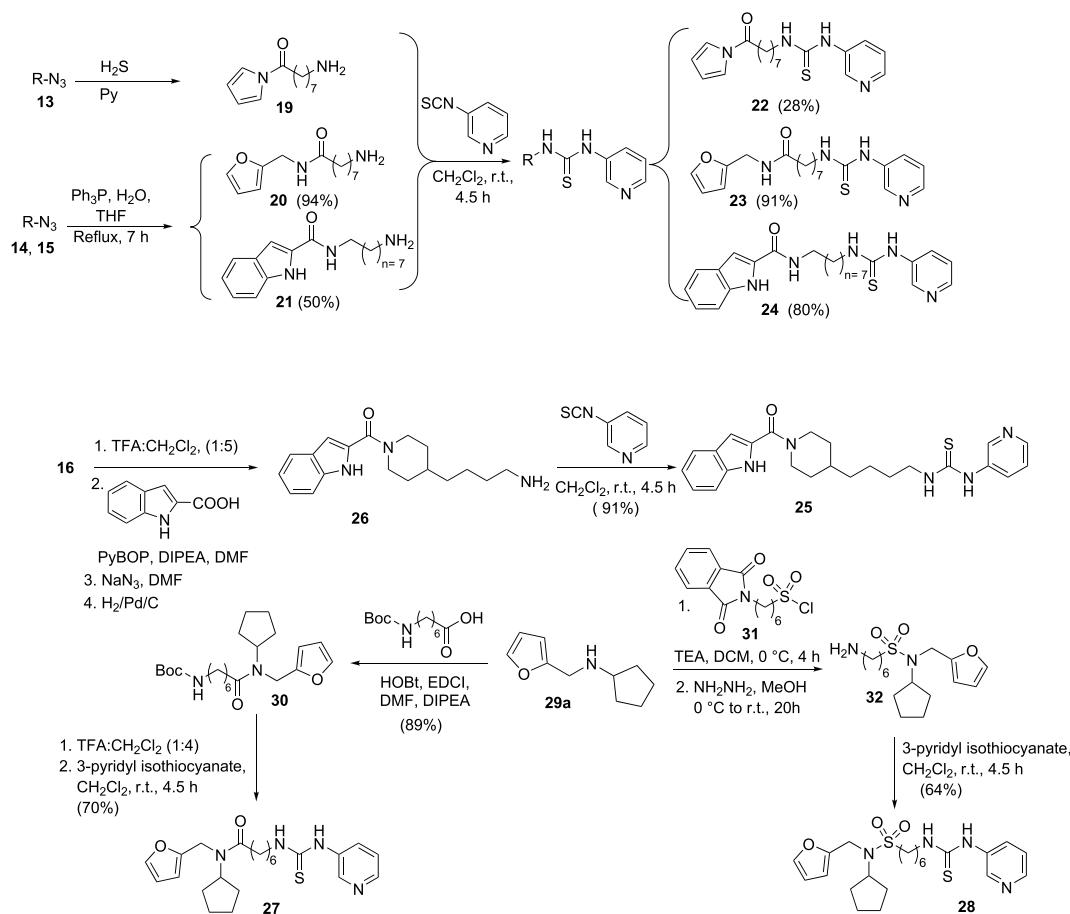
Fig. 1. Representative examples of known NAMPT inhibitors with relevant anticancer activity.



Scheme 1. Synthesis of (pyridin-3-yl)triazole-based inhibitors.

bromo-octanoic acid with NaN_3 , followed by coupling of the resulting intermediate with lithium pyrrolate in the presence of 1,1-carbonyldiimidazole (CDI), gave the azido-acylated pyrrole **13**. On its side,

standard amide coupling of 8-azido-octanoic acid with furfurylamine afforded **14**. CuAAC reaction of azides **13** and **14** with 3-ethynylpyridine in the presence of catalytic amount of CuI and DIPEA in toluene led to



Scheme 2. Synthesis of (pyridin-3-yl)thiourea-based inhibitors.

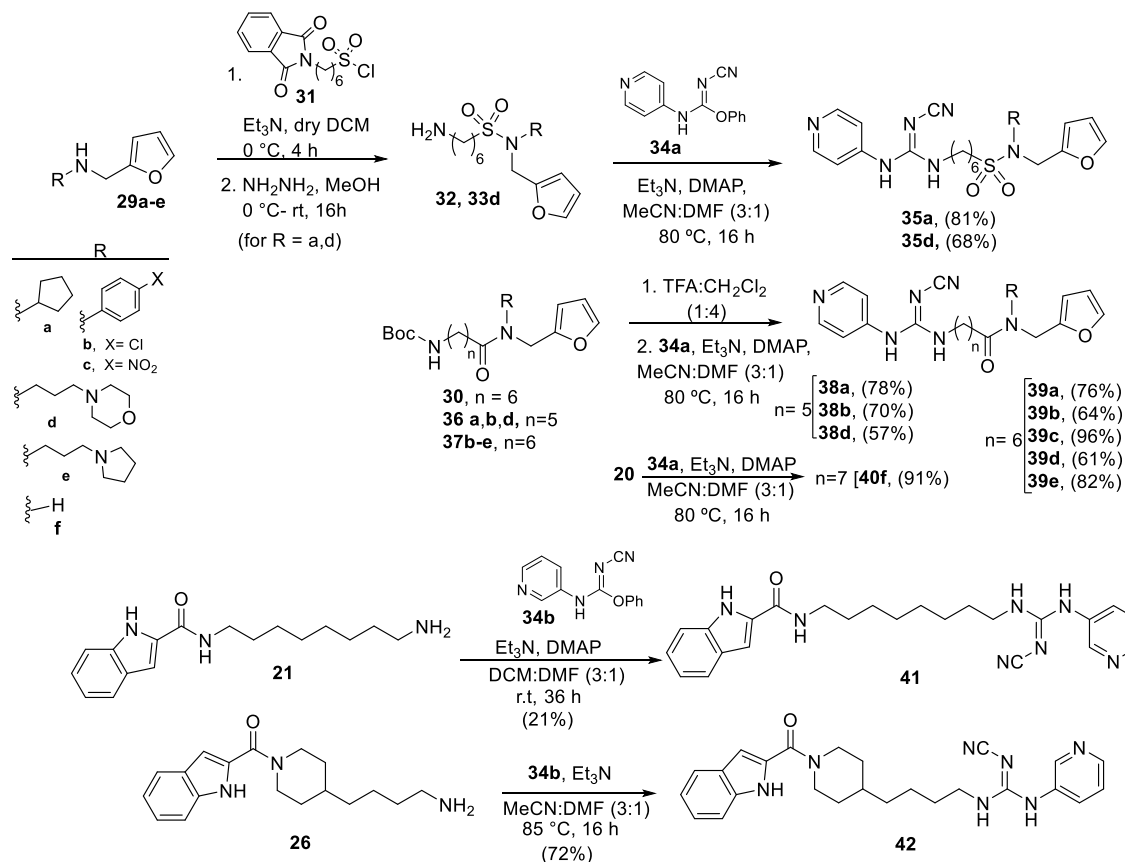
triazoles **8** and **9** in moderate-to-good yield. On the other hand, starting from commercial 1,8-dibromooctane, S_N2 displacement with NaN_3 gave the corresponding diazido derivative. Monoreduction of one of the azido groups was feasible by the Staudinger reaction under biphasic media (toluene-aq. HCl). Standard coupling reaction of the resulting amino derivative with 1*H*-indole-2-carboxylic acid gave derivative **15**. Click reaction of **15** with 3-ethynylpyridine, as described above, gave **10** in 50% yield. The preparation of **11** and **12** was carried out from *tert*-butyl 4-(4-tosyloxybutyl)piperidine-1-carboxylate **16** [19] which was transformed into *N*-Boc-protected azide derivative **17** by displacement with NaN_3 . Subsequent CuAAC click reaction with 3-ethynylpyridine, *N*-deprotection, and standard amide coupling with 1*H*-indole-2-carboxylic acid derivatives gave **11** and **12** in moderate-to good overall yield, respectively (3 steps).

Preparation of (pyridin-3-yl)thiourea-based inhibitors. The (thio)urea group is a well-established functional group in medicinal chemistry because of the ability of establishing stable hydrogen bonds with key elements of proteins and enzymes, enhancing the ligand–receptor interactions [20]. Regarding NAMPT inhibitors it has been reported the crystallographic data of the complex inhibitor-NAMPT enzyme. Thus Zheng et al. [21] studied the crystal structure of a thiourea-derived compound in complex with NAMPT and observed the interaction of Asp219 and Ser245 with the NH of the thiourea moiety through water-mediated hydrogen bonds. We envisioned that the substitution of the acrylamide group by a more powerful hydrogen-bond-donating group could enhance the interaction inhibitor/NAMPT. The preparation of these compounds is described in Scheme 2. Azido derivatives **13**, **14**, and **15** were reduced to the corresponding amino derivatives **19–21** through the Staudinger reaction. Subsequent coupling with commercial 3-pyridyl isothiocyanate gave thiourea analogues **22**, **23** and **24** in moderate-to-good yield. The preparation of **25** requires Boc-deprotection of **16** [16] followed by coupling with

1*H*-indole-2-carboxylic acid, displacement of the tosylate group with NaN_3 and subsequent azido reduction, affording amine **26**. Reaction of **26** with 3-pyridyl isothiocyanate gave compound **25** in excellent yield. The preparation of **27** and **28** followed a similar strategy using *N*-cyclopentylfurfurylamine **29a** as starting furan precursor. Conventional amide coupling of **29a** with *N*-Boc-7-aminoheptanoic acid followed by Boc-deprotection and reaction with 3-pyridyl isothiocyanate furnished **27** in good overall yield. The preparation of the thiourea-based inhibitor **28** involves the reaction of **29a** with (1,3-dioxoisindolin-2-yl)hexanesulfonyl chloride **31** [22] followed by hydrazinolysis and coupling with 3-pyridyl isothiocyanate.

Preparation of (pyridin-3/4-yl)cyanoguanidine based inhibitors. The preparation of this family of inhibitors (Scheme 3) was carried out starting from the amino-functionalized furan precursors **29a–f** (see Supporting Information for synthetic details). Reaction of **29a** and **29d** with sulfonyl chloride **31** followed by hydrazinolysis gave sulfonamides **32** and **33d**. Subsequent coupling with phenyl *N*-cyano-*N'*-(pyridin-4-yl) carbamimidate **34a**, easily prepared [23] from commercial diphenyl cyanocarbonimidate, gave compounds **35a** and **35d**, respectively in moderate-to-good yields. Similarly, deprotection of Boc derivatives **30**, **36a**, **36b**, **36d**, and **37b–e** and subsequent coupling with carbamimidate **34a** furnished derivatives **38a**, **38b**, **38d** and **39a–e** in moderate-to-good yields. Compound **40f** was obtained by reaction of **20** with **34a** under the same standard coupling conditions. Similar reaction conditions applied to indole derivatives **21** and **26** afforded indole-(pyridin-3-yl) cyanoguanidine derivatives **41** and **42**.

As this family of (pyridin-3/4-yl)cyanoguanidine-based inhibitors (compounds **35**, **38–42**) showed excellent results in cytotoxicity assays (see Table 1), two new compounds were additionally prepared incorporating a triazole moiety to link the tunnel binder and the furan tail. Reaction of 1,6-dibromohexane with an excess of sodium azide gave the corresponding diazido derivative, which was further subjected to a



Scheme 3. Synthesis of (pyridin-3/4-yl)cyanoguanidine-based inhibitors (subfamily I).

Table 1

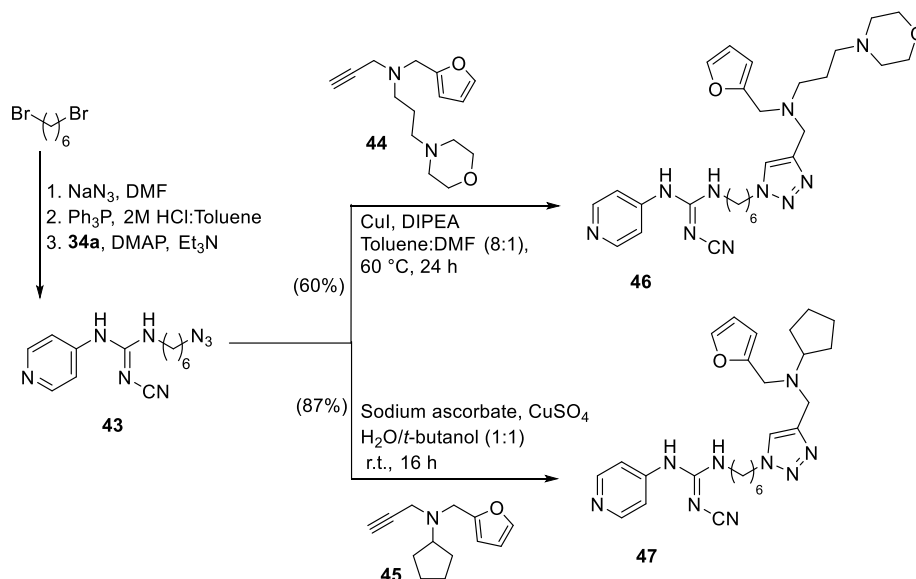
Evaluation of the cytotoxicity and iNAD⁺ depletion on MiaPaCa-2 cells for the new compounds. NAMPT inhibition assays.

Entry	Compound	Viability MiaPaCa-2 cells (IC ₅₀ in nM)	iNAD ⁺ depletion 24h on MiaPaCa-2 cells (IC ₅₀ in nM)	NAMPT inhibition assay (IC ₅₀ in nM)
1	1 (FK866) (pyridin-3-yl)triazoles	2.4 ± 0.51	0.34 ± 0.08	3.27 ± 0.38
2	8	494 ± 143	NA	NA
3	9	>1000	NA	NA
4	10	549 ± 101	NA	NA
5	11	727 ± 187	NA	NA
6	12 (pyridin-3-yl)thioureas	860 ± 191	NA	NA
7	22	854 ± 188.5	NA	NA
8	23	>1000	NA	NA
9	24	605 ± 140.5	NA	NA
10	25	>1000	NA	NA
11	27	153 ± 17.4	NA	NA
12	28 (pyridin-3/4-yl)cyanoguanidines	16.4 ± 2.35	0.43 ± 0.11	69.1 ± 4.43
13	35a	0.005 ± 0.001	0.25 ± 0.08	3.50 ± 0.77
14	35d	2.26 ± 0.37	1.50 ± 0.62	NA
15	38a	3.0 ± 0.94	0.20 ± 0.05	NA
16	38b	6.3 ± 1.74	0.50 ± 0.12	NA
17	38d	16.3 ± 2.64	11.25 ± 0.65	NA
18	39a	0.45 ± 0.085	0.88 ± 0.32	12.45 ± 0.50
19	39b	1.7 ± 0.415	0.17 ± 0.05	NA
20	39c	2.1 ± 0.556	0.14 ± 0.04	NA
21	39d	3.0 ± 0.827	1.43 ± 0.49	NA
22	39e	4.5 ± 0.099	2.00 ± 0.78	NA
23	40f	>1000	NA	NA
24	41	81 ± 14.6	NA	NA
25	42	113 ± 14.4	NA	NA
26	46	25.8 ± 6.7	2.36 ± 0.75	NA
27	47	2.81 ± 0.761	1.48 ± 0.33	4.98 ± 0.46
<i>Non pyridine-based inhibitors</i>				
28	51	>1000	NA	NA
29	52	>1000	NA	NA
30	53	>1000	NA	NA
31	54	>1000	NA	NA
32	55	>1000	NA	NA
33	57	>1000	NA	NA
34	58	176 ± 11.7	4.70 ± 0.27	NA
35	59	738 ± 148	NA	NA
36	60	1000	NA	NA

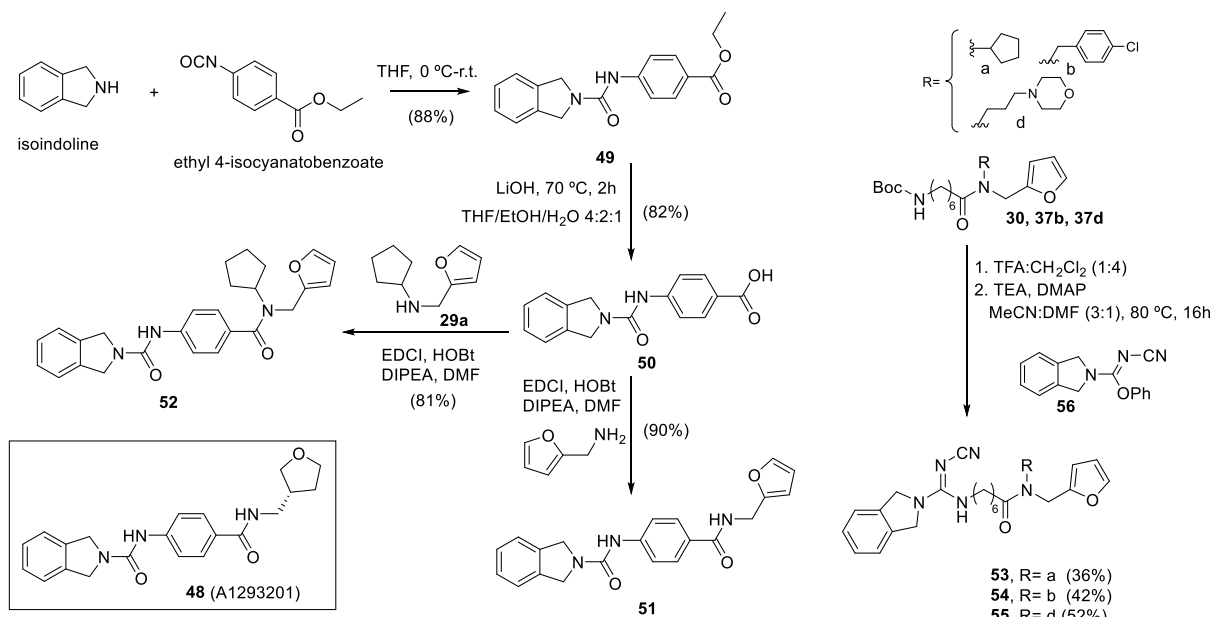
NA = not available. Data are mean ± SD, n ≥ 3.

controlled Staudinger reduction in biphasic media that afforded the corresponding monoamino derivative. Subsequent coupling with **34a** gave azide **43** (Scheme 4) with an acceptable overall yield. CuAAC reactions of azide **43** and the furan-containing fragments **44** and **45** bearing a terminal alkyne yielded **46** and **47** in good yields.

Non pyridine-based inhibitors (non-substrate inhibitors). The pyridine moiety is present in the most potent NAMPT inhibitors reported so far, which could be explained considering that NAM is the substrate of NAMPT. The pyridine ring of FK866 is sandwiched between Tyr18 and Phe193 of the active site, making a π - π stacking interaction between the aromatic rings of two amino acids of the active site, mimicking the position of NAM. Simultaneously, pyridine nitrogen establishes a hydrogen bond with the OH group of Ser275 [24]. However, *in vitro* metabolic stability studies on previously reported pyridine-based NAMPT inhibitors have shown that pyridine nitrogen is prone to microsomal oxidation giving the corresponding *N*-oxide metabolite whose cytotoxicity is reduced with respect to the non-oxidized precursor [10]. This fact could be one of the reasons for the lack of efficacy of the inhibitors *in vivo*. Moreover, it has been recently demonstrated that phosphorylation of the pyridine nitrogen of NAMPT inhibitors is not required for *in vivo* antitumor efficacy [25] as it was previously postulated [26]. This evidence led to explore non pyridine-based structures as possible NAMPT inhibitors [27]. Therefore, in this paper we also report the preparation of some analogues of potent NAMPT inhibitors where the pyridine moiety has been replaced by other aromatic rings less prone to oxidation than pyridine. First, we focused on the preparation of isoindoline-based derivatives inspired by the interesting results previously obtained with NAMPT inhibitor **48** (A1293201) [21]. Thus, the reaction between commercial isoindoline and ethyl 4-isocyanobenzoate gave urea **49** (Scheme 5). Basic hydrolysis of **49** followed by standard amide coupling between the resulting acid **50** and furfurylamine afforded the furyl analogue of **48**, compound **51**. A similar strategy was followed for the preparation of **52**, except that *N*-cyclopentylfurfurylamine **29a** was used in the final coupling. Then, we turned to the substitution of pyridine by the isoindoline moiety in the subfamily I of cyanoguanidine derivatives. For this purpose, we focused on three of the most cytotoxic compounds prepared in this family (**39a**, **39b**, **39d**, Scheme 3, Table 1) and synthesized their isoindoline analogues **53**, **54** and **55**. A similar strategy to the above described in Scheme 3 was followed for the preparation of these compounds, except that phenyl *N*-cyanoisoindoline-2-carbimide **56** (see Supporting Information for synthetic details) was used in the final coupling.



Scheme 4. Synthesis of (pyridin-4-yl)cyanoguanidine-based inhibitors (subfamily II).



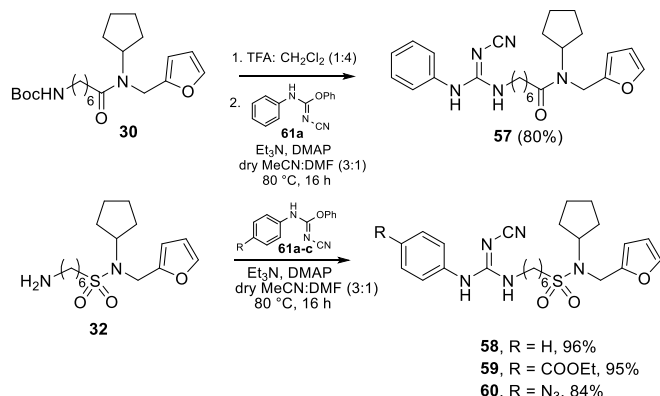
Scheme 5. Synthesis of isoindoline-based inhibitors.

Finally, we decided to replace the pyridin-4-yl moiety by a phenyl moiety in two highly cytotoxic cyanoguanidines, sulfonamide **35a** and its amide analogue **39a** (Scheme 3). For the synthesis of these new non-pyridine analogues **57–60** we followed a similar synthetic strategy than the one already described in Scheme 3, except that (*p*-substituted)phenyl *N*-cyano-*N'*-phenylcarbamimidates **61** instead of the pyridine analogues **34** were used in the synthesis (Scheme 6).

2.2. Biological evaluation

Cytotoxicity on MiaPaCa-2 cells, effect on intracellular NAD⁺ concentration and NAMPT inhibition. The new compounds were tested *in vitro* for their anti-proliferative effects on a cancer cell line (Table 1). Human pancreatic MiaPaca-2 was used as model for cell lines sensitive to NAMPT inhibitors [28].

Triazoles **8–12** were much less cytotoxic than FK866 (Table 1, entries 2–6). FK866 analogues **11** and **12** were approximately 300-fold less cytotoxic than FK866, what indicates that the substitution of the acrylamide group by a triazole and the benzamido group by a more hydrophilic indole substituent was detrimental to biological activity. A similar modification was introduced in **25** (Scheme 2) and **42** (Scheme 3), with the exception that a thiourea and a cyanoguanidine groups were incorporated, respectively, instead of the triazole moiety of **11**.



Scheme 6. Phenyl-based inhibitors prepared in this work.

Cyanoguanidine **42** (Table 1, entry 25) showed a cytotoxic effect 6.4 times greater than triazole **11** while the cytotoxicity of thiourea **25** (Table 1, entry 10) was even lower than that presented by compound **11**.

Other pyridine-3-yl thioureas were also prepared using a more flexible tunnel binder (C6 or C7 alkyl chain) to connect the thiourea and tail groups. One of the members of this family, sulfonamide **28**, showed a high cytotoxicity ($IC_{50} = 16.4$ nM, Table 1, entry 12). The comparison between the cytotoxicity data obtained for **28** and the amide counterpart **27** ($IC_{50} = 153$ nM, Table 1, entry 11) clearly showed the benefit having a sulfonamide group to connect the tail group (a furan moiety in both cases). The sulfonamide function is less prone to hydrolysis under biological conditions than the amide. Moreover, the sulfone can behave as a very good hydrogen bond acceptor for the interaction within the binding site.

The analysis of the cytotoxicity of (pyridin-3/4-yl)cyanoguanidine derivatives (**35a**, **35d**, **38a**, **38b**, **38d**, **39a–39e**, **41** and **42**) afforded several conclusions. Most cyanoguanidines (Table 1, entries 13–22) share a general structure which contains: i) a flexible alkyl C5 or C6 carbon chain as a tunnel binder connecting cyanoguanidine and tail groups through a tertiary amide/sulfonamide function and ii) a furan as a tail group. The cytotoxicity of the members of this first group (except for **41** and **42**) was excellent, with $IC_{50} < 16$ nM. In fact, in some cases, the IC_{50} values were lower than the one obtained with FK866 in this cell line ($IC_{50} = 2.4$ nM). The C5 alkyl chain was always found to lead to slightly higher IC_{50} values (less cytotoxicity) than the C6 alkyl chain in different analogues (entry 15 vs 18, entry 16 vs 19, entry 17 vs 21). In the series of tertiary amides, different *N*-substituents together with the 2-furyl group were used, but no high differences in cytotoxicity were observed, being the compounds with *N*-cyclopentyl group slightly better cytotoxic agents (entry 15 vs entries 16,17; entry 18 vs entries 19–22). As was already observed for the family of pyridine-3-yl thioureas, substituting the amide function in the *N*-cyclopentylamide **39a** with a *N*-cyclopentylsulfonamide led to a remarkable improvement of the cytotoxic activity (entry 18 vs 13), yielding the most potent compound of this study (**35a**, $IC_{50} = 5$ μ M). Another example where the above mentioned bioisosterism led to a compound with improved potency is represented by the non-substrate inhibitor **58** (Table 1, entry 34). Compared to the amide analogue **57** (entry 34 vs 33), the sulfonamide **58** showed an increase in potency of 40-fold. Amide **39e** and sulfonamide **35d** (entries 22 and 14), presented similar cytotoxicity. The NMR spectra of **35d**

showed signals corresponding to a mixture of rotamers, in contrast with the other sulfonamide derivatives where only one set of signals was observed in the ^1H and ^{13}C NMR spectra. Our hypothesis to explain the lower cytotoxicity of **35d** compared to other sulfonamide derivatives is that one of the rotamers could fit better than the other at the active site of NAMPT due to a more favorable binding pose, leading to a decrease in binding efficacy. In addition to amide and sulfonamide connecting groups, the triazole moiety was also explored in some of the compounds. The biological evaluation of **46** and **47** showed a decrease in their cytotoxicity compared to amides **39d** and **39a** or sulfonamides **35d** and **35a**, respectively (entry 26 vs entries 21,14; entry 27 vs entries 18 and 13).

Finally, the cytotoxicity of the series of non-pyridine-based compounds was also analyzed. Replacement of pyridine with an isoindoline group was detrimental to the antitumor activity of the compounds in all cases (entries 28–32 vs. entries 19–21). In addition, compounds **51** and **52**, which bear a 2-furyl moiety instead of the 2-tetrahydrofuryl group of the known analogue **48** (Scheme 5), showed cytotoxicity in the μM range (entries 28 and 29) as in the case of the other isoindoline analogues **53–55**. Replacement of the pyridine-4-yl moiety in the highly cytotoxic sulfonamide **35a** with a phenyl or with 4-substituted-phenyl moieties (compounds **57–60**) was detrimental in terms of cytotoxicity (entry 13 vs entries 34–36). Compound **58** was the most cytotoxic compound in this family of non pyridine-based inhibitors with an $\text{IC}_{50} = 176 \text{ nM}$.

Next, we evaluated intracellular NAD^+ concentration (iNAD^+) in MiaPaCa-2 cells in response to the most cytotoxic compounds, in order to confirm that the observed antitumor effect was associated with NAD^+ depletion, which would be in line with these compounds being NAMPT inhibitors. Consistent with this hypothesis, all of the tested compounds reduced NAD^+ concentration in cells (Table 1). Some of the compounds **28**, **35a**, **38a**, **39b**, **39a**, and **39c** reduced iNAD^+ to similar, or even higher extent compared to FK866. Compound **58**, a nonpyridine-based compound, reduced iNAD^+ when added in the nM range. Compounds **28**, **35a**, **39a** and **47**, which all effectively lowered iNAD^+ levels, were also assayed as NAMPT inhibitors on the recombinant enzyme. All these compounds exerted a strong inhibition of NAMPT activity ($\text{IC}_{50} < 70 \text{ nM}$). Again, compound **35a** showed the highest potency, ($\text{IC}_{50} = 3.5 \text{ nM}$), which was similar to the potency of the reference compound, FK866 ($\text{IC}_{50} = 3.3 \text{ nM}$). Interestingly, the potency of **35a** in terms of inhibition of recombinant NAMPT did not exactly match its cytotoxic activity in MiaPaCa-2 cells, the latter being already clearly detectable in the low μM range. For the other compounds, **28**, **39a**, and **47**, inhibiting NAMPT activity in the nM range, such a discrepancy was not observed. Therefore, these results suggest that the exceptional cytotoxic activity of **35a** may also reflect other mechanisms in addition to NAMPT inhibition in MiaPaCa-2 cells. Indeed, in MDA-MB-231 cells, the IC_{50} s obtained with **35a** for iNAD^+ reduction and for cell toxicity were similar (0.56 ± 0.15 and $0.47 \pm 0.64 \text{ nM}$, respectively). By comparison, in these cells, the FK866 IC_{50} s for iNAD^+ depletion and cell toxicity were 0.54 ± 0.12 and $3.47 \pm 0.412 \text{ nM}$, respectively, being similar values to those obtained in MiaPaCa-2 cells. The time-dependent decrease in NAD^+ and

ATP levels in MiaPaCa-2 cells demonstrated that the high cytotoxic activity observed in the presence of **35a** is not due to a NAD^+ -unrelated intracellular ATP depletion, since NAD^+ decrease preceded the fall in ATP levels (Fig. S47 A). Cell death induced by FK866 analogues could be due to the triggering of apoptotic processes, as confirmed by the detection of PARP cleavage after 48 h of treatment with compound **47** and **35a** (Fig. S47 B).

Molecular Modeling. Docking analysis (Glide) was performed to investigate the potential role of the furan moiety of **35a** in the binding site of NAMPT (Crystal structure, PDB: 2GVJ). The binding pose of **1** (FK866) was mainly stabilized in the active site by a π - π stacking interaction of the pyridine ring with Phe193 and Tyr18' and H-bonding of the carbonyl group with Ser275 (Fig. 3A). On the other hand, the docked structure of compound **35a** (Fig. 3B) showed the π - π stacking interaction of the pyridine ring with Phe193, two hydrogen bonds between the cyanoguanidine moiety and Asp219 and a π - π stacking interaction of the furan tail group with Tyr188. As showed in recent publications, interactions of the tail group of NAMPT inhibitors have been reported to strongly enhance the inhibitory potency and to anchor the molecule to the enzyme [23].

Cytotoxicity on haematological cancer cells

To demonstrate the broad antitumor activity of novel compounds, a selection of the most promising ones was evaluated in cells from various haematological malignancies, including acute myeloid leukemia (AML; ML2 and NB4); acute lymphoblastic leukemia (ALL; Jurkat); Burkitt's lymphoma (BL; Namalwa) and multiple myeloma (MM; RPMI8226). As summarized in Table 2, **35a** showed the highest antitumor activity against acute myeloid leukemia (ML2), with IC_{50} in the picomolar range ($\text{IC}_{50} = 18 \text{ pM}$). Two other compounds **39a** and **47** also presented cytotoxicity in the picomolar range with IC_{50} of 46 and 49 μM , respectively. Overall, these three molecules were the most potent and AML cells were the most sensitive cells to all tested inhibitors. Therefore, **35a**, **39a** and **47** together with FK866 as a positive control were further used to decipher their molecular mechanism of action in blood cancers.

To this end, the effect of the new NAMPT inhibitors, compounds **35a**, **39a** and **47**, on the intracellular NAD^+ content was assessed in several hematopoietic malignant cells [7c,29,30]. In agreement with data obtained on MiaPaCa-2 cells, all tested compounds led to a profound NAD^+ depletion in a time dependent manner (Fig. 4A, B, C). NAD^+ concentrations decreased by half already after 6 h and were completely depleted after 24 h. Moreover, compound **35a** was the most efficient to deplete iNAD^+ in haematological cancer cells, with the lowest iNAD^+ IC_{50} compared to FK866 (Table 3). As NAD^+ cell content plays an important role in ATP synthesis, the impact of these NAMPT inhibitors on intracellular ATP content was next evaluated. As expected, the drop in NAD^+ cell content was followed by that of ATP (Fig. 4D, E, F).

The intracellular content of NAD(P)H/NAD(P)^+ plays a crucial role in oxidative stress and thus, the depletion of NAD^+ upon exposure to NAMPT inhibitors is expected to result in an increased ROS production. To test this issue, mitochondrial (mO_2^-) and cytosolic (cO_2^-) superoxide anions, as well as intracellular hydrogen peroxide (H_2O_2) were

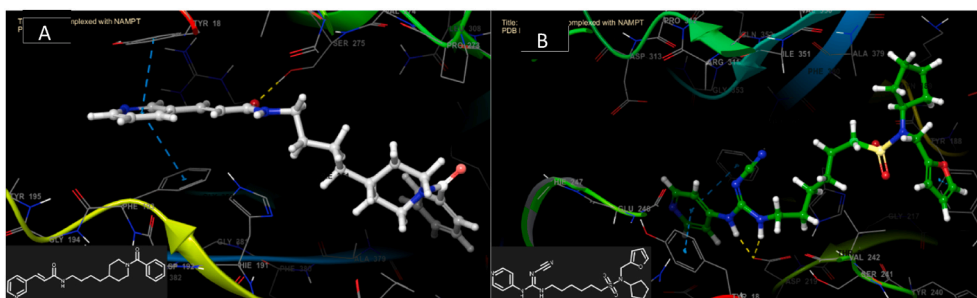


Fig. 3. Compounds **1** (FK866) (A) and **35a** (B) docked in the active site of NAMPT (Crystal structure, PDB: 2GVJ). The cyanoguanidine moiety of compound **35a** clearly forms two hydrogen bonds with Asp219 while the furan group is stabilized by a π - π stacking interaction with Tyr188.

Table 2

Evaluation of the cytotoxicity on MiaPaCa-2 and different haematological cancer cell lines for compounds **28**, **35a**, **38a**, **39a**, **39c**, **47** and **58** depicted as IC₅₀ [nM].

Compound	MiaPaCa-2	ML2	JRKT	NMLW	RPMI8226	NB4
1 (FK866)	2.4 ± 0.51	0.24 ± 0.08	0.73 ± 0.04	0.37 ± 0.09	0.76 ± 0.08	2.0 ± 0.2
28	16.4 ± 2.35	3.1 ± 0.1	NA	4.23 ± 1	20.15 ± 2	NA
35a	0.005 ± 0.001	0.018 ± 0.001	0.15 ± 0.001	0.23 ± 0.08	0.16 ± 0.04	0.4 ± 0.08
38a	3.0 ± 0.94	0.36 ± 0.01	NA	1.77 ± 0.1	1.9 ± 0.1	NA
39a	0.45 ± 0.085	0.046 ± 0.01	0.2 ± 0.01	0.33 ± 0.006	0.27 ± 0.01	0.6 ± 0.03
39c	2.1 ± 0.556	0.32 ± 0.007	NA	1.39 ± 0.5	2.13 ± 0.2	NA
47	2.81 ± 0.761	0.049 ± 0.01	0.5 ± 0.01	0.36 ± 0.04	0.47 ± 0.09	0.7 ± 0.01
58	176 ± 11.7	nd	NA	nd	nd	NA

NA = not available. nd: not detected; ML2: acute myeloid leukemia; JRKT: acute lymphoblastic leukemia; NMLW: Burkitt lymphoma; RPMI8226: multiple myeloma; NB4: acute myeloid leukemia. Data are mean ± SD, n ≥ 3.

monitored in leukemic cells treated with new NAMPT inhibitors (FK866, **35a**, **39a** and **47**) using MitoSOX, DHE, and carboxy-H2DCFDA probes, respectively. The novel compounds caused a tremendous increase in ROS levels production in all treated cell types (Fig. 5A–F).

Excess ROS generation is known to lead to mitochondrial damage. Therefore, we evaluated whether these compounds could affect the mitochondrial membrane potential (MMP). Different hematopoietic malignant cells were exposed to NAMPT inhibitors and a time-dependent analysis of the MMP loss was measured using a fluorescent dye (TMRM) and flow cytometry analysis. As shown in Fig. 6A–C, treatment with the new NAMPT inhibitors induced a potent, time-dependent mitochondrial membrane depolarization at 72 h, but not at earlier time point (24-h; Fig. 6A–C). The timing of MMP loss correlates

with that of cell death (Fig. 6D–F).

To provide evidence that NAD⁺ depletion is the primary cause of cell death in malignant cells treated with the new NAMPT inhibitors, various hematopoietic malignant cells were incubated with inhibitors and with an excess of NAD⁺ precursors (NAM, nicotinic acid [NA]) or NAD⁺ itself. Cell death was monitored as described above. Indeed, supplementation with NAM, NA, or NAD⁺ fully blunted the killing effect of all tested NAMPT inhibitors (Fig. 7A–C), supporting that NAD⁺ depletion was responsible for cell death.

We previously reported that treatment with FK866 leads to the decrease in catalase (CAT), a powerful ROS scavenger enzyme, resulting in ROS accumulation, what ultimately leads to cell death. Therefore, we tested the ability of CAT to prevent the cell death mediated by the new NAMPT inhibitors. As shown in Fig. 8 the extracellular addition of CAT before **35a**, **39a** and **47** fully abrogated their cytotoxic effects, which is in line with our previous studies [31,32].

Altogether, these results indicate that the new NAMPT inhibitors are highly potent and promising antitumor agents. Mechanistically, these data demonstrate that, similarly to FK866, they deplete NAD⁺ cell content, which induces ROS accumulation that damage mitochondria, leading to ATP loss, and ultimately to cell death. NAD⁺ depletion was indeed responsible for cell death.

3. Conclusions

In summary, in this work we have prepared and evaluated several families of furan-containing NAMPT inhibitors. The compounds were designed by combining a furan-tail moiety with different structural motifs that had been successfully used in previously reported NAMPT

Table 3

Evaluation of iNAD⁺ depletion after 24 h of drug treatment on different haematological cancer cell lines for compounds **FK866**, **35a**, and **47** depicted as IC₅₀ [nM]. Data are mean ± SD, n ≥ 3.

Compound	ML2	JRKT	RPMI8226
1 (FK866)	0.11 ± 0.03	0.37 ± 0.003	0.1 ± 0.005
35a	0.05 ± 0.03	0.09 ± 0.009	0.05 ± 0.01
47	0.09 ± 0.01	0.2 ± 0.2	0.06 ± 0.04

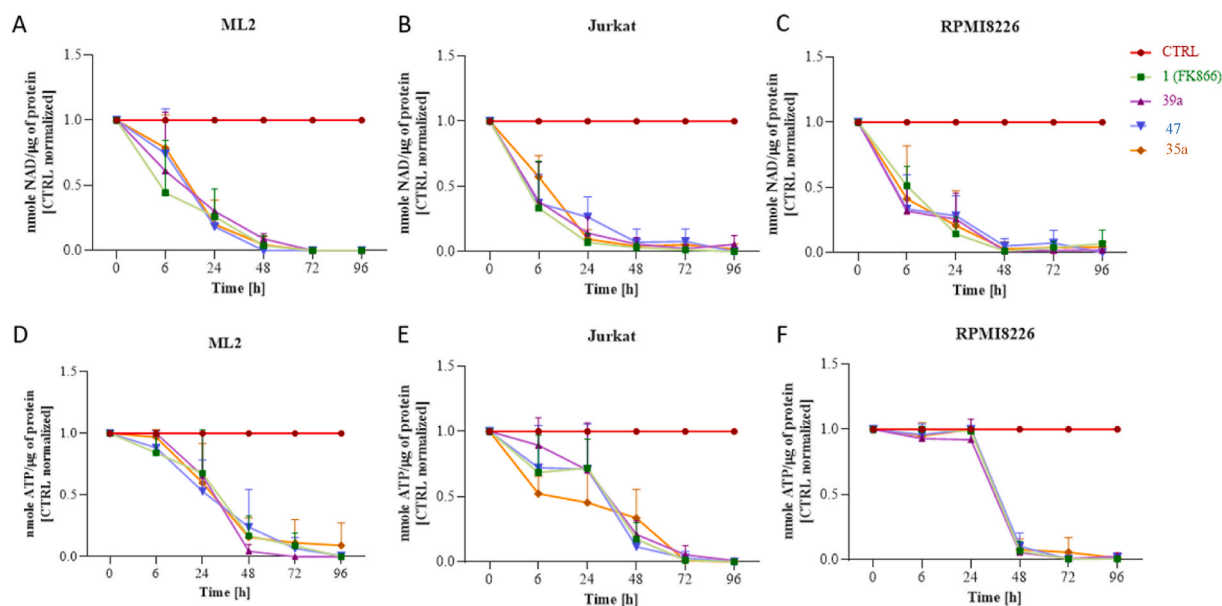


Fig. 4. NAMPT inhibitors induce the depletion of intracellular NAD⁺ and ATP. ML2 (A, D), Jurkat (B, E) and RPMI8226 (C, F) cells were incubated with NAMPT inhibitors (FK866, **35a**, **39a** and **47**) for 96 h. Intracellular NAD⁺ (A, B, C) and ATP (D, E, F) contents were measured every day. Both, NAD⁺ and ATP concentrations were first normalized to the total protein and then to control at each time point. Data are ± SD, n = 4.

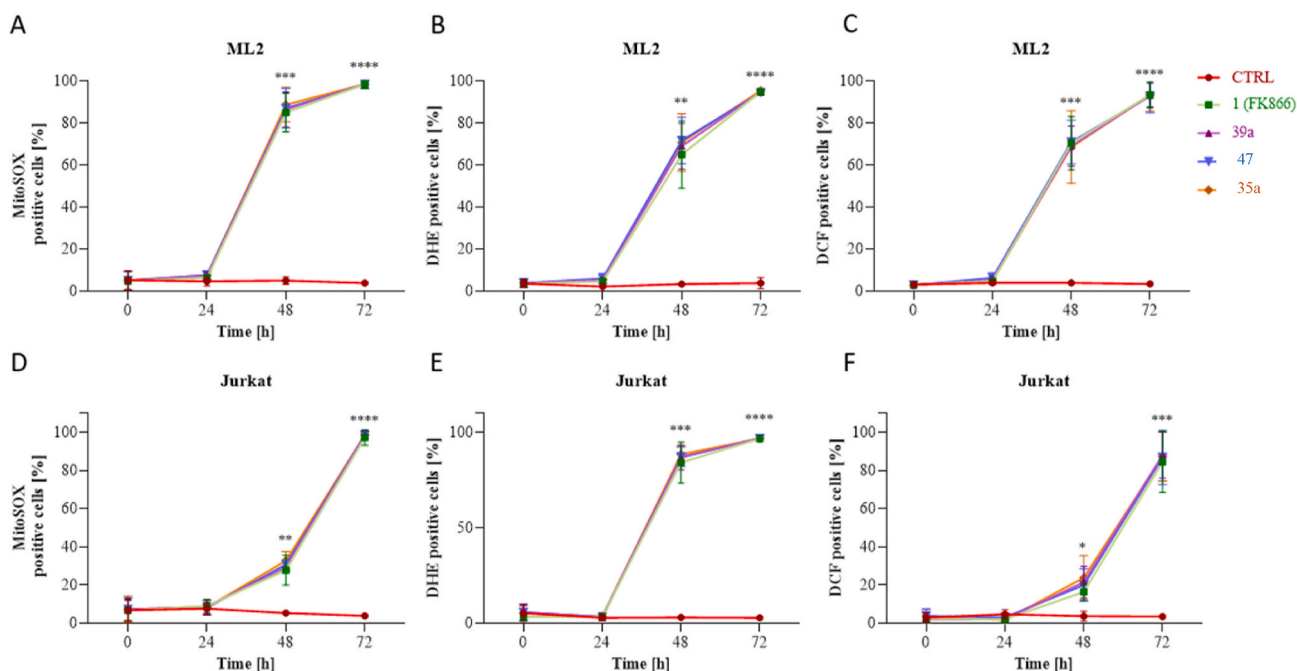


Fig. 5. NAMPT inhibitors induce ROS production upon cell death in malignant cells. ML2 (A, B, C) and Jurkat (D, E, F) cells were treated with compounds (FK866, 35a, 39a and 47) for 72 h. Mitochondrial (A, D), cytosolic (B, E) superoxide anions, and hydrogen peroxide (C, F) were detected with MitoSOX, DHE and H2DCFDA probes, respectively, using flow cytometry. The percentage of positive cells is proportional to the amount of superoxide anions and hydrogen peroxide produced. Data are \pm SD, $n = 3$, ** $P < 0.005$, *** $P < 0.001$, **** $P < 0.0001$.

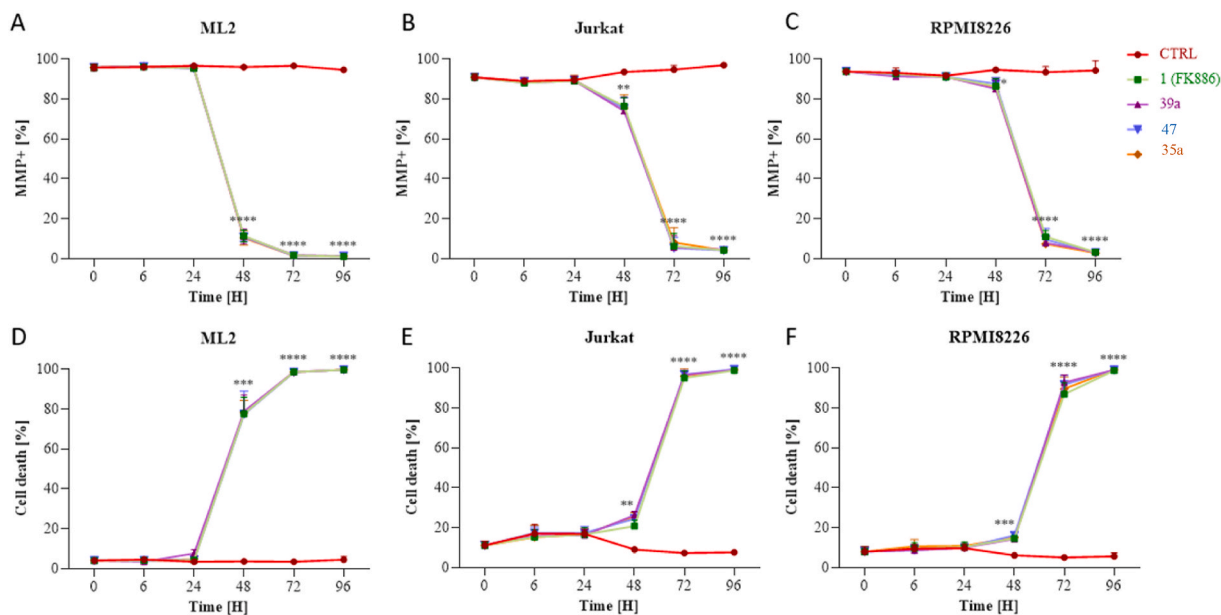


Fig. 6. NAMPT inhibitors induce the loss of MMP and cell death over time. ML2 (A, D), Jurkat (B, E) and RPMI8226 (C, F) cells were incubated with NAMPT inhibitors (FK866, 35a, 39a and 47) for 96 h. MMP (A, B, C) and cell death (D, E, F) were measured every day over a period of 96 h. MMP was measured using TMRM staining, and cell death is depicted here as a total cell death consisting of annexin V (ANXN) and 7AAD stainings. Both were assessed with flow cytometry. Data are \pm SD, $n = 3$. * $P < 0.05$, ** $P < 0.005$, *** $P < 0.001$, **** $P < 0.0001$.

inhibitors. Compound 35a was identified as the most potent NAMPT inhibitor with an $IC_{50} = 3.5$ nM, similar to that of FK866 ($IC_{50} = 3.3$ nM). However, 35a was 500-fold more cytotoxic in the pancreatic cell line MiaPaCa-2 (IC_{50} of 5.0 μ M) than FK866 (IC_{50} of 2.4 nM), indicating that another mechanism in addition to NAMPT inhibition may be responsible for its antitumor effects. This compound was also moderately to slightly more cytotoxic than FK866 on other five different haematological cancer cell lines. Although further research is warranted

and needed to elucidate the mechanism of action of these new inhibitors, 35a can be considered as promising lead compound to develop more potent and efficient NAMPT inhibitors. The furan moiety on these compounds mimics the role of the benzamide group of FK866 while helping to anchor the molecule in the active site of NAMPT. Furthermore, the furan moiety can be used as a handle for bioconjugation strategies making these compounds amenable to linker chemistry for target drug delivery [14,15].

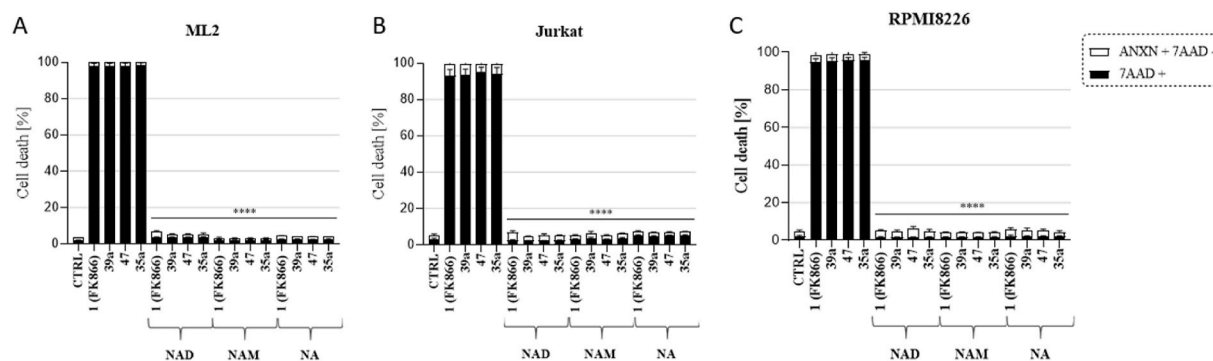


Fig. 7. The addition of NAD, NAM, and NA can reverse the cytotoxic effect of NAMPT inhibitors. ML2 (A), Jurkat (B) and RPMI8226 (C) cells were incubated for 96 h with NAMPT inhibitors (FK866, 35a, 39a and 47) without or with NAD (0.5 mM), NAM (1 mM) or NA (10 μ M). Cell death was assessed with flow cytometry by double staining with annexin V (ANXN) and 7AAD after 96 h of treatment. The percentages of early apoptotic cells (ANXN+ 7AAD-) are shown in white and the percentage of late apoptotic and dead cells (7AAD+) are shown in black. Data are \pm SD, n = 3. ****p < 0.0001 (inhibitors treated vs. NAD, NAM, and NA groups).

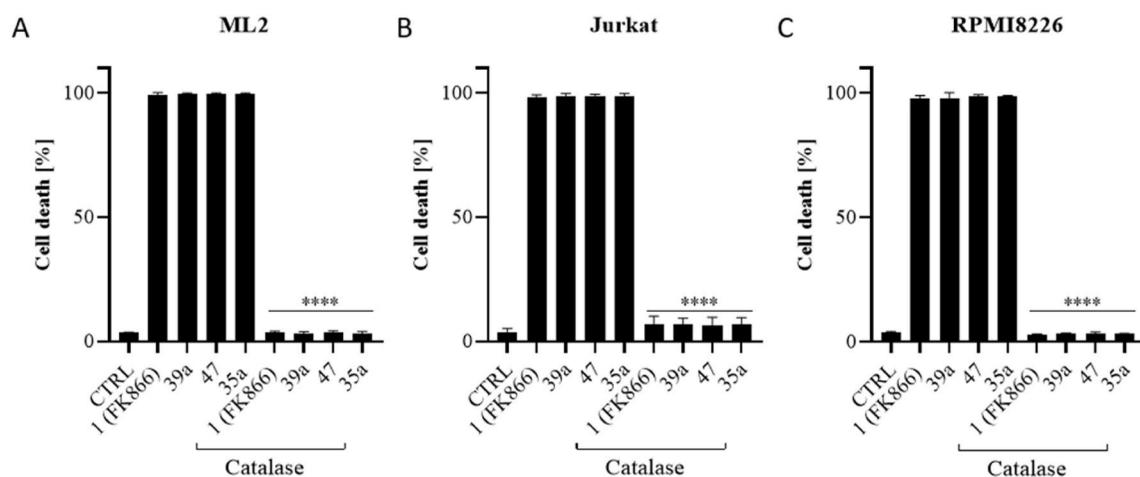


Fig. 8. Supplementation of catalase abrogates the killing effect of NAMPT inhibitors in tested cell lines. Catalase was added 1 h before the inhibitors. The cell death at 96 h was assessed on ML2 (A), Jurkat (B) and RPMI8226 (C). Cell death was determined as in Fig. 5 and is depicted here as total cell death. Data are \pm SD, n = 3. ****p < 0.0001 (inhibitors treated vs. catalase treated groups).

4. Experimental section

4.1. Chemistry

General methods

^1H and ^{13}C NMR spectra were recorded with a Bruker AMX300 spectrometer for solutions in CDCl_3 , $\text{DMSO}-d_6$, acetone- d_6 and CD_3OD . δ are given in ppm and J in Hz. Chemical shifts are calibrated using residual solvent signals. All the assignments were confirmed by 2D spectra (COSY and HSCQ). High resolution mass spectra were recorded on a Q-Exactive spectrometer. TLC was performed on silica gel 60 F_{254} (Merck), with detection by UV light charring with *p*-anisaldehyde, KMnO_4 , ninhydrin, phosphomolybdic acid or with reagent $[(\text{NH}_4)_6\text{MoO}_4, \text{Ce}(\text{SO}_4)_2, \text{H}_2\text{SO}_4, \text{H}_2\text{O}]$. Purification by silica gel chromatography was carried out using either hand-packed glass columns (Silica gel 60 Merck, 40–60 and 63–200 μm) or Puriflash XS520 Plus Interchim system with prepacked cartridges. The purity of representative final compounds was assessed by HPLC and was >95%. The HPLC analysis was performed on a Thermo UltiMate 3000 instrument with Accucore C18 column (2.1 mm \times 150 mm). Mobile phase consisted in solvent A (H_2O , 0.1% TFA) and solvent B (CH_3CN). The samples were eluted with a linear gradient from 70% A and 30% B to 0% A and 100% B, between 5 and 20 min. All chromatograms were registered at 254 nm wavelength.

8-Azido-1-(1H-pyrrol-1-yl)octan-1-one (13). To a suspension of NaN_3 (1.0 g, 16 mmol) and NaI (0.1 g, 0.9 mmol) in DMF (50 mL), 8-

bromooctanoic acid (2.0 g, 9.0 mmol) was added. The reaction mixture was stirred at r.t. for 16 h. Then, the reaction was cooled to 0 $^\circ\text{C}$ and 1 M HCl was added dropwise until the suspension became clear. The reaction mixture was extracted with EtOAc (2 \times 50 mL). The organic layer was washed with brine, dried over NaSO_4 , filtered, and concentrated in vacuo to give 8-azido-octanoic acid [33] that was used in the next step without further purification. A solution of 8-azido-octanoic acid (1.6 g, 8.4 mmol) and 1,1'-carbonyldiimidazole (1.4 g, 8.6 mmol) were dissolved in dry THF (20 mL) and the reaction was stirred under Ar at r.t. for 16 h. Pyrrole (0.7 mL, 9.5 mmol) was taken up in dry THF (5.0 mL) and the solution was cooled to -78°C . *n*-Butyllithium (2.5 M in hexanes; 5.0 mL, 13 mmol) was added and the mixture was stirred at -78°C for 3 h under Ar. Then, the activated compound was added quickly via syringe and the reaction was slowly warmed to r.t. and stirred overnight. A sat. aq. soln. of NH_4Cl was added and the mixture extracted with EtOAc . The organic phases were dried over NaSO_4 , filtered, and concentrated in vacuo. Purification was performed by chromatography column on silica gel (EtOAc :Cyclohexane, 1:15) to yield 13 (800 mg, 40%) as a white solid. ^1H NMR (300 MHz, CDCl_3 , δ ppm) 7.37–7.25 (m, 2H, pyrrole), 6.33–6.24 (m, 2H, pyrrole), 3.26 (t, J = 6.9 Hz, 2H, $\text{CH}_2\text{-N}_3$), 2.82 (t, J = 7.4 Hz, 2H, $\text{CH}_2\text{-C=O}$), 1.84–1.73 (m, 2H, CH_2), 1.67–1.54 (m, 2H, CH_2), 1.43–1.35 (m, 6H, 3 CH_2). ^{13}C NMR (75.4 MHz, CDCl_3 , δ ppm) 170.6 (C=O), 119.1 (2 CH, pyrrole), 113.1 (2 CH, pyrrole), 51.5 ($\text{CH}_2\text{-N}_3$), 34.6 ($\text{CH}_2\text{-C=O}$), 29.1 (CH_2), 29.0 (CH_2), 28.9 (CH_2), 26.6 (CH_2), 24.5 (CH_2). ESI-HRMS m/z calcd for $\text{C}_{12}\text{H}_{18}\text{N}_4\text{O}_2\text{Na}$ [$\text{M}+\text{Na}$] $^+$,

257.1373; found, 257.1373.

8-Azido-N-(furan-2-ylmethyl)octanamide (14). A solution of 8-azido-octanoic acid (1.7 g, 9.0 mmol), furfurylamine (1.2 mL, 13 mmol) and PyBOP (7.9 g, 15 mmol) in DMF (36 mL) was cooled to 0 °C. DIPEA (7.5 mL, 43 mmol) was slowly added at 0 °C, and the reaction mixture was stirred at r.t. for 16 h. The reaction mixture was dried under vacuum and diluted with EtOAc (50 mL) and washed with 1 M HCl (x3) and brine (x3), dried over Na₂SO₄, filtered, and concentrated in vacuo. The crude was purified by chromatography column on silica gel (EtOAc:Cyclohexane 1:2) to yield **14** (1.9 g, 81%) as a white solid. ¹H NMR (300 MHz, CDCl₃, δ ppm) 7.37–7.29 (m, 1H, furan), 6.30 (dd, *J* = 3.1, 1.9 Hz, 1H, furan), 6.20 (d, *J* = 3.2 Hz, 1H, furan), 5.92 (br s, 1H, NH–C=O), 4.41 (d, *J* = 5.3 Hz, 2H, CH₂–NH), 3.23 (t, *J* = 6.9 Hz, 2H, CH₂–N₃), 2.17 (t, *J* = 7.2 Hz, 2H, CH₂–CO), 1.69–1.50 (m, 4H, 2 CH₂), 1.39–1.26 (m, 6H, 3 CH₂). ¹³C NMR (75.4 MHz, CDCl₃, δ ppm) 172.9 (C=O), 151.5 (qC, furan), 142.3 (CH, furan), 110.6 (CH, furan), 107.5 (CH, furan), 51.5 (CH₂–N₃), 36.6 (2C, CH₂–NH, CH₂–C=O), 29.1 (CH₂), 28.9 (CH₂), 28.8 (CH₂), 26.6 (CH₂), 25.6 (CH₂). ESI-HRMS *m/z* calcd. for C₁₃H₂₀N₄O₂Na [M+Na]⁺, 287.1479; found, 287.1478.

N-(8-Azido-octyl)-1H-indole-2-carboxamide (15). NaN₃ (977 mg, 15.0 mmol) was added to a solution of 1,8-dibromooctane (1.0 mL, 5.4 mmol) in DMF (25 mL) and the mixture was stirred at 60 °C for 10 h. Then, water was added (125 mL) and the product was extracted with Et₂O (3 × 20 mL). The organic phase was washed with water (3 × 20 mL), dried, filtered and the solvent was evaporated to afford 1,8-diazido-octane. To a solution of this compound (930 mg, 4.70 mmol) in toluene:HCl 2 M (1:1, 80 mL), Ph₃P (1.24 g, 4.74 mmol) was slowly added, and the mixture was vigorously stirred at r.t. for 16 h. The aqueous phase was separated and washed three times with Et₂O and dried under vacuum to obtain 8-azido-octan-1-amine hydrochloride [34]. A solution of this compound (720 mg, 3.50 mmol), 1H-indole-2-carboxylic acid (842 mg, 5.20 mmol) and PyBOP (3.1 g, 5.9 mmol) in DMF (16 mL) was cooled to 0 °C. DIPEA (2.9 mL, 17 mmol) was slowly added at 0 °C, and the reaction mixture was stirred at r.t. overnight. The reaction mixture was diluted with EtOAc (160 mL) and washed with 1 M HCl (x3) and brine (x3), dried over Na₂SO₄, filtered, and concentrated in vacuo. The crude was purified by chromatography column on silica gel (EtOAc:Toluene 1:9) to yield **15** (860 mg, 80%) as a white solid. ¹H NMR (300 MHz, CDCl₃, δ ppm) 10.00 (s, 1H, NH indole), 7.64 (d, *J* = 8.0 Hz, 1H, indole), 7.45 (t, *J* = 7.0 Hz, 1H, indole), 7.32–7.23 (m, 1H, indole), 7.13 (t, *J* = 7.2 Hz, 1H, indole), 6.85 (d, *J* = 1.4 Hz, 1H, indole), 6.36 (s, 1H, NH–C=O), 3.57–3.45 (m, 2H, CH₂–N₃), 3.24 (t, *J* = 6.9 Hz, 2H, CH₂–NH), 1.77–1.49 (m, 4H, 2 CH₂), 1.46–1.25 (m, 8H, 4 CH₂). ¹³C NMR (75.4 MHz, CDCl₃, δ ppm) 162.0 (C=O), 136.6 (qC, indole), 130.9 (qC, indole), 127.7 (qC, indole), 124.5 (CH, indole), 121.9 (CH, indole), 120.7 (CH, indole), 112.2 (CH, indole), 101.9 (CH, indole), 51.5 (CH₂–N₃), 39.9 (CH₂–NH), 29.9 (CH₂), 29.3 (CH₂), 29.1 (CH₂), 28.9 (CH₂), 27.0 (CH₂), 27.7 (CH₂). ESI-HRMS *m/z* calcd for C₁₇H₂₃N₅O₂Na [M+Na]⁺, 336.1793; found, 336.1795.

8-(4-(Pyridin-3-yl)-1H-1,2,3-triazol-1-yl)-1-(1H-pyrrol-1-yl)octan-1-one (8). To a solution of **13** (50.0 mg, 0.21 mmol) in toluene (3 mL), 3-ethynylpyridine (45.0 mg, 0.43 mmol), DIPEA (0.14 mL, 0.81 mmol) and CuI (8.0 mg, 40 μmol) were added, and the solution was stirred at 60 °C for 24 h. Quadrasil® resin (150 mg) was added and the mixture stirred for 1 h at r.t. Then, it was filtrated through a Celite pad, and the solvent evaporated. The resulting residue was dissolved in EtOAc and a sat. aq. soln. of NaHCO₃ was added. The aq. phase was extracted with EtOAc (x2) and the organic layers were dried over Na₂SO₄, filtered and evaporated. The resulting residue was purified by chromatography column on silica gel (EtOAc:Cyclohexane, 7:1) to obtain **8** (50 mg, 70%) as a white solid. ¹H NMR (300 MHz, CDCl₃, δ ppm) 9.00 (br s, 1H, Py), 8.56 (br s, 1H, Py), 8.25–8.14 (m, 1H, Py), 7.84 (s, 1H, triazole), 7.41–7.32 (m, 1H, Py), 7.31–7.25 (m, 2H, pyrrole), 6.32–6.22 (m, 2H, pyrrole), 4.41 (t, *J* = 7.2 Hz, 2H, CH₂–triazole), 2.80 (t, *J* = 7.3 Hz, 2H, CH₂–C=O), 2.03–1.90 (m, 2H, CH₂), 1.83–1.69 (m, 2H, CH₂), 1.44–1.34 (m, 6H, 3 CH₂). ¹³C NMR (75.4 MHz, CDCl₃, δ ppm) 170.5 (C=O), 149.2

(qC, Py), 147.1 (CH, Py), 144.8 (qC, triazole), 133.1 (CH, Py), 127.0 (CH, Py), 123.9 (2CH, pyrrole), 119.9 (CH, Py), 119.1 (CH, triazole), 113.2 (2CH, pyrrole), 50.6 (CH₂–triazole), 34.5 (CH₂–C=O), 30.3 (CH₂), 28.9 (CH₂), 28.8 (CH₂), 26.4 (CH₂), 24.4 (CH₂). ESI-HRMS *m/z* calcd for C₁₉H₂₄N₅O [M+H]⁺, 338.1975; found, 338.1975.

N-(Furan-2-ylmethyl)-8-(4-(pyridin-3-yl)-1H-1,2,3-triazol-1-yl)octanamide (9). CuAAC reaction of **14** (50.0 mg, 0.21 mmol) and 3-ethynylpyridine (40.0 mg, 0.4 mmol) followed the same procedure as that used to prepare **8**. Chromatography column (MeOH:EtOAc:CH₂Cl₂, 0.4:5:1). Yield: 60%, white solid. ¹H NMR (500 MHz, CDCl₃, δ ppm) 8.99 (s, 1H, Py), 8.57 (d, *J* = 3.6 Hz, 1H, Py), 8.21 (dd, *J* = 6.1, 1.8 Hz, 1H, Py), 7.84 (s, 1H, triazole), 7.41–7.29 (m, 2H, 1H Py, 1H furan), 6.35–6.26 (m, 1H, furan), 6.21 (d, *J* = 2.9 Hz, 1H, furan), 5.79 (s, 1H, NH), 4.47–4.36 (m, 4H, CH₂–NH, CH₂–triazole), 2.24–2.11 (m, 2H, CH₂–C=O), 2.01–1.89 (m, 2H, CH₂), 1.68–1.57 (m, 2H, CH₂), 1.43–1.28 (m, 6H, 3 CH₂). ¹³C NMR (125.7 MHz, CDCl₃, δ ppm) 172.7 (C=O), 151.6 (qC, furan), 149.3 (CH, Py), 147.2 (CH, Py), 144.9 (qC, triazole), 142.3 (CH, furan), 133.2 (CH, Py), 127.0 (qC, Py), 123.9 (CH, Py), 119.9 (CH, triazole), 110.6 (CH, furan), 107.5 (CH, furan), 50.6 (CH₂–NH), 36.6 (CH₂–triazole), 36.5 (CH₂–C=O), 30.3 (CH₂), 28.9 (CH₂), 28.6 (CH₂), 26.3 (CH₂), 25.4 (CH₂). ESI-HRMS *m/z* calcd for C₂₀H₂₆N₅O₂ [M+H]⁺, 368.2076; found, 368.2081.

N-(8-(4-(Pyridin-3-yl)-1H-1,2,3-triazol-1-yl)octyl)-1H-indole-2-carboxamide (10). CuAAC reaction of **15** (50.0 mg, 0.16 mmol) and 3-ethynylpyridine (50.0 mg, 0.48 mmol) in toluene:DMF 3:1 followed the same procedure as that used to prepare **8**. Chromatography column (MeOH:EtOAc:CH₂Cl₂, 1:5:1). Yield: 50%, white solid. ¹H NMR (300 MHz, DMSO-*d*₆, δ ppm) 11.51 (s, 1H, NH indole), 9.05 (d, *J* = 1.5 Hz, 1H, Py), 8.70 (s, 1H, triazole), 8.53 (dd, *J* = 4.8, 1.5 Hz, 1H, Py), 8.45–8.38 (m, 1H, NH–C=O), 8.24–8.16 (m, 1H, Py), 7.62–7.56 (m, 1H, Py), 7.48 (dd, *J* = 8.0, 4.8 Hz, 1H, indole), 7.42 (d, *J* = 8.2 Hz, 1H, indole), 7.20–7.12 (m, 1H, indole), 7.09 (d, *J* = 1.4 Hz, 1H, indole), 7.06–6.98 (m, 1H, indole), 4.40 (t, *J* = 7.1 Hz, 2H, CH₂–triazole), 3.26 (q, *J* = 6.7 Hz, 2H, CH₂–NH), 1.94–1.80 (m, 2H, CH₂), 1.60–1.46 (m, 2H, CH₂), 1.34–1.26 (m, 8H, 4 CH₂). ¹³C NMR (75.4 MHz, DMSO-*d*₆, δ ppm) 160.9 (C=O), 148.7 (CH, Py), 146.3 (CH, Py), 143.4 (qC, triazole), 136.3 (qC, indole), 132.4 (qC, Py), 131.9 (qC, indole), 127.1 (CH, Py), 126.8 (qC, indole), 124.0 (CH, indole), 123.1 (CH, Py), 121.9 (CH, triazole), 121.4 (CH, indole), 119.6 (CH, indole), 112.2 (CH, indole), 102.1 (CH, indole), 49.6 (CH₂–triazole), 39.0 (CH₂–NH), 29.6 (CH₂), 29.2 (CH₂), 28.6 (CH₂), 28.4 (CH₂), 26.4 (CH₂), 25.8 (CH₂). ESI-HRMS *m/z* calcd for C₂₄H₂₉N₆O [M+H]⁺, 417.2392; found, 417.2397.

3-(1-(4-(Piperidin-4-yl)butyl)-1H-1,2,3-triazol-4-yl)pyridine 2,2,2-trifluoroacetate (18). Compound **16** [16] (636 mg, 1.60 mmol) was dissolved in DMF (10 mL), NaN₃ (302 mg, 4.60 mmol) was added. The mixture was stirred at 70 °C for 3 h and then was evaporated under vacuum and the residue dissolved in CH₂Cl₂. The organic layer was washed with water and brine, dried over Na₂SO₄, filtered, and concentrated in vacuo to give **17** as a colourless oil. CuAAC reaction of **17** (192 mg, 0.68 mmol) and 3-ethynylpyridine (175 mg, 1.70 mmol) followed the same procedure as that described for **8**. Chromatography column (CH₂Cl₂:Acetone: 1:0 to 5:1). Yield: 88%, white solid. This compound was dissolved in 20% TFA/CH₂Cl₂ (5 mL) at 0 °C and the mixture was stirred at r.t. for 3.5 h. The solvent was evaporated in vacuo and the solvent was co-evaporated with toluene to yield **18** as a white solid that was used in the next step without further purification.

(1H-Indol-2-yl)(4-(4-(4-(pyridin-3-yl)-1H-1,2,3-triazol-1-yl)butyl)piperidin-1-yl)methanone (11). A solution of **18** (112.0 mg, 0.28 mmol), 1H-Indole-2-carboxylic acid (68.0 mg, 0.42 mmol) and PyBOP (248 mg, 0.48 mmol) in dry DMF (2.5 mL) was cooled to 0 °C. DIPEA (0.24 mL, 1.35 mmol) was slowly added at 0 °C, and the reaction mixture was stirred at r.t. for 16 h. The solvent was evaporated under reduced pressure and the crude was diluted with EtOAc (20 mL) and washed with sat. aq. soln. of NH₄Cl (x3), dried over Na₂SO₄, filtered and concentrated. The residue was purified by chromatography column on silica gel (MeOH:EtOAc, 1:20 → 1:10) to yield **11** (56 mg, 47%) as a white solid.

^1H NMR (300 MHz, DMSO- d_6 , δ ppm) 11.51 (s, 1H, NH indole), 9.11–8.99 (m, 1H, Py), 8.72 (s, 1H, triazole), 8.54 (dd, $J = 4.8, 1.5$ Hz, 1H, Py), 8.21 (dt, $J = 7.9, 1.9$ Hz, 1H, Py), 7.59 (d, $J = 7.9$ Hz, 1H, indole), 7.52–7.44 (m, 1H, Py), 7.40 (d, $J = 7.9$ Hz, 1H, indole), 7.23–7.10 (m, 1H, indole), 7.09–6.98 (m, 1H, indole), 6.75–6.67 (m, 1H, indole), 4.53–4.31 (m, 4H, CH₂-triazole, 2H piperidine), 2.96 (br s, 2H, piperidine), 1.96–1.81 (m, 2H, piperidine), 1.78–1.66 (m, 2H, piperidine), 1.62–1.44 (m, 1H, piperidine), 1.39–1.19 (m, 4H, 2 CH₂), 1.18–1.00 (m, 2H, CH₂). ^{13}C NMR (75.4 MHz, DMSO- d_6 , δ ppm) 161.8, 148.8, 146.3, 143.5, 135.8, 132.3, 130.3, 126.8, 124.0, 123.0, 122.0, 121.2, 119.6, 112.0, 103.4, 49.6, 35.4, 35.3, 32.2, 32.1, 27.7, 22.1. ESI-HRMS m/z calcd for C₂₅H₂₉N₆O [M+H]⁺, 429.2391; found, 429.2397.

(5-Methoxy-1H-indol-2-yl)(4-(4-(pyridin-3-yl)-1H-1,2,3-triazol-1-yl)butyl)piperidin-1-ylmethanone (**12**). Reaction of **18** (112.0 mg, 0.28 mmol) and 5-methoxy-1H-indole-2-carboxylic acid (80.0 mg, 0.42 mmol) was performed according to the same procedure as that used to prepare **11**. Chromatography column (MeOH:EtOAc, 1:20 → 1:10). Yield: 74%, white solid. ^1H NMR (300 MHz, DMSO- d_6 , δ ppm) 11.37 (s, 1H, NH, indole), 9.06 (d, $J = 1.7$ Hz, 1H, Py), 8.72 (s, 1H, triazole), 8.58–8.50 (m, 1H, Py), 8.28–8.15 (m, 1H, Py), 7.55–7.41 (m, 1H, Py), 7.29 (d, $J = 8.9$ Hz, 1H, indole), 7.06 (d, $J = 2.3$ Hz, 1H, indole), 6.82 (dd, $J = 8.9, 2.4$ Hz, 1H, indole), 6.63 (d, $J = 1.6$ Hz, 1H, indole), 4.54–4.29 (m, 4H, CH₂-triazole, 2H piperidine), 3.74 (s, 3H, OCH₃), 2.96 (br s, 2H, piperidine), 1.96–1.81 (m, 2H, piperidine), 1.79–1.64 (m, 2H, piperidine), 1.63–1.44 (m, 1H, piperidine), 1.40–1.20 (m, 4H, CH₂), 1.19–0.98 (m, 2H, CH₂). ^{13}C NMR (75.4 MHz, DMSO- d_6 , δ ppm) 161.8, 153.7, 148.8, 146.3, 143.5, 132.3, 131.1, 130.7, 127.1, 126.8, 124.0, 122.0, 114.0, 112.8, 103.2, 101.9, 55.2, 49.6, 35.2, 35.1, 32.1, 29.7, 22.1. ESI-HRMS m/z calcd for C₂₆H₃₁N₆O₂ [M+H]⁺, 459.2495; found, 459.2503.

1-(8-Oxo-8-(1H-pyrrol-1-yl)octyl)-3-(pyridin-3-yl)thiourea (**22**). To a solution of **13** (0.50 g, 2.1 mmol) in pyridine (15 mL), H₂S was bubbled. After stirring at r.t. overnight the mixture was evaporated under vacuum. The crude product **19** was used directly in the next step without any further purification. ESI-HRMS m/z calcd for C₁₂H₂₁N₂O [M+H]⁺, 209.1647; found, 209.1648. To a solution of **19** (60.0 mg, 0.3 mmol) in dry CH₂Cl₂ (5 mL), 3-pyridyl isothiocyanate (40 μL , 0.4 mmol) was added. After stirring at r.t. for 6 h, the solvent was removed under vacuum and the resulting residue was purified by chromatography column on silica gel (EtOAc:Cyclohexane 4:1) to give **22** (25.0 mg, 28%) as a white solid. ^1H NMR (300 MHz, CDCl₃, δ ppm) 8.54 (d, $J = 2.0$ Hz, 1H, Py), 8.44 (d, $J = 3.9$ Hz, 1H, Py), 8.32 (br s, 1H, NH-Py), 7.85 (d, $J = 7.9$ Hz, 1H, Py), 7.37 (dd, $J = 8.1, 4.8$ Hz, 1H, Py), 7.29 (br s, 2H, pyrrole), 6.44–6.31 (m, 1H, NH-CH₂), 6.31–6.24 (m, 2H, pyrrole), 3.60 (q, $J = 6.4$ Hz, 2H, CH₂-NH), 2.81 (t, $J = 7.3$ Hz, 2H, CH₂-C=O), 1.82–1.68 (m, 2H, CH₂), 1.68–1.52 (m, 2H, CH₂), 1.44–1.30 (m, 6H, 3 CH₂). ^{13}C NMR (75.4 MHz, CDCl₃, δ ppm) 181.3 (C=S), 170.8 (C=O), 147.4 (qC, Py), 146.1 (CH, Py), 134.2 (CH, Py) 132.6 (CH, Py), 124.3 (CH, Py), 119.1 (2CH, pyrrole), 113.2 (2CH, pyrrole), 45.5 (CH₂-NH), 35.5 (CH₂-C=O), 29.8 (CH₂), 29.0 (CH₂), 28.8 (CH₂), 26.6 (CH₂), 24.4 (CH₂). ESI-HRMS m/z calcd for C₁₈H₂₅N₄OS [M+H]⁺, 345.1737; found, 345.1744.

N-(Furan-2-ylmethyl)-8-(3-(pyridin-3-yl)thioureido)octanamide (**23**). To a solution of **14** (100 mg, 0.38 mmol) in THF (1 mL), H₂O (40 μL) and Ph₃P (150 mg, 0.60 mmol) were added. The reaction mixture was stirred on reflux for 7 h. The resulting residue was evaporated under vacuum and purified by chromatography column on silica gel (MeOH: CH₂Cl₂: NH₄OH, 1:10:0.1) to yield **20** (85 mg, 94%) as a white solid. Reaction of **20** (70.0 mg, 0.3 mmol) and 3-pyridyl isothiocyanate (80 μL , 0.8 mmol) was performed according to the same procedure as that used to prepare **22**. Chromatography column (MeOH:EtOAc:CH₂Cl₂, 0.4:5:1). Yield: 91%, white solid. ^1H NMR (300 MHz, CD₃OD, δ ppm) 8.57 (dd, $J = 2.5, 0.6$ Hz, 1H, Py), 8.28 (dd, $J = 4.8, 1.3$ Hz, 1H, Py), 8.10–7.89 (m, 1H, Py), 7.44–7.36 (m, 2H, 1H Py, 1H, furan), 6.33 (dd, $J = 3.2, 1.9$ Hz, 1H, furan), 6.22 (dd, $J = 3.2, 0.7$ Hz, 1H, furan), 4.34 (s, 2H, CH₂-NH), 3.68–3.44 (m, 2H, CH₂-thiourea), 2.21 (t, $J = 7.4$ Hz, 2H, CH₂-C=O), 1.71–1.54 (m, 4H, 2 CH₂), 1.44–1.29 (m, 6H, 3 CH₂). ^{13}C NMR (75.4

MHz, CD₃OD, δ ppm) 183.1 (C=S), 176.1 (C=O), 153.2 (qC, furan), 145.8 (2CH, Py), 143.3 (CH, furan), 138.3 (qC, Py), 133.3 (CH, Py), 124.9 (CH, Py), 111.3 (CH, furan), 108.0 (CH, furan), 45.6 (CH₂-thiourea), 37.1 (CH₂-NH), 36.9 (CH₂-C=O), 30.04 (CH₂), 30.02 (CH₂), 27.8 (CH₂), 26.8 (CH₂), 25.7 (CH₂). ESI-HRMS m/z calcd for C₁₉H₂₇N₄O₂S [M+H]⁺, 375.1845; found, 375.1849.

N-(8-(3-(Pyridin-3-yl)thioureido)octyl)-1H-indole-2-carboxamide (**24**). To a solution of **15** (100 mg, 0.32 mmol) in THF (1 mL), H₂O (30 μL) and Ph₃P (126 mg, 0.50 mmol) were added. The reaction mixture was stirred on reflux for 30 h. The resulting residue was evaporated under vacuum and purified by chromatography column on silica gel (MeOH:CH₂Cl₂:NH₄OH, 1:10:0.1) to yield **21** (45 mg, 50%) as a white solid. Reaction of **21** (37.0 mg, 0.1 mmol) and 3-pyridyl isothiocyanate (36 μL , 0.3 mmol) was performed according to the same procedure as that used to prepare **22**. Chromatography column (MeOH:EtOAc: CH₂Cl₂, 0.4:5:1). Yield: 80%, white solid. ^1H NMR (300 MHz, DMSO- d_6 , δ ppm) 11.52 (s, 1H, NH indole), 9.53 (s, 1H, NH-Py), 8.55 (t, $J = 2.2$ Hz, 1H, Py), 8.43 (t, $J = 5.7$ Hz, 1H, NH-C=O), 8.28 (dd, $J = 4.7, 1.4$ Hz, 1H, Py), 8.03–7.86 (m, 1H, Py), 7.60 (d, $J = 7.9$ Hz, 1H, indole), 7.42 (dd, $J = 8.2, 0.7$ Hz, 1H, indole), 7.33 (dd, $J = 8.2, 4.7$ Hz, 1H, Py), 7.20–7.12 (m, 1H, indole), 7.09 (s, 1H, indole), 7.07–6.98 (m, 1H, indole), 3.51–3.39 (m, 2H, CH₂-thiourea), 3.28 (q, $J = 6.4$ Hz, 2H, CH₂-amide), 1.60–1.49 (m, 4H, 2 CH₂), 1.40–1.26 (m, 8H, 4 CH₂). ^{13}C NMR (75.4 MHz, DMSO- d_6 , δ ppm) 180.9 (C=S), 161.0 (C=O), 144.6 (CH, Py), 144.4 (CH, Py), 136.3 (qC, indole), 131.9 (qC, indole), 131.8 (qC, Py), 130.2 (CH, Py), 127.1 (qC, indole), 123.1 (2CH, Py, indole), 121.4 (CH, indole), 119.6 (CH, indole), 112.2 (CH, indole), 102.1 (CH, indole), 43.9 (CH₂-thiourea), 38.7 (CH₂-amide), 29.3 (CH₂), 28.8 (2(CH₂)), 28.4 (CH₂), 26.5 (CH₂), 26.4 (CH₂). ESI-HRMS m/z calcd for C₂₃H₃₀N₅OS [M+H]⁺, 424.2162; found, 424.2166.

(4-(4-Aminobutyl)piperidin-1-yl)(1H-indol-2-yl)methanone (**26**). Compound **16** [**19**] (483 mg, 1.2 mmol) was dissolved in 20% TFA/CH₂Cl₂ (9 mL) and the mixture was stirred at r.t. for 4.5 h. The mixture was evaporated under vacuum and the crude product (257 mg, 0.60 mmol) was dissolved in DMF (3.5 mL), cooled to 0 °C and 1H-indole-2-carboxylic acid (146 mg, 0.91 mmol), PyBOP (534 mg, 1.00 mmol) and DIPEA (0.51 mL, 2.90 mmol) were slowly added. After stirring at r.t. for 16 h, the reaction mixture was diluted with EtOAc (35 mL) and washed with 1 M HCl (x3) and brine (x3), dried over Na₂SO₄, filtered, and concentrated in vacuo. The crude was purified by chromatography column on silica gel (EtOAc:Toluene, 1:2) to yield the corresponding *N*-acylated intermediate (193 mg, 70%) as a white solid. This compound (170 mg, 0.37 mmol) was dissolved in DMF (2.5 mL), sodium azide (73.0 mg, 1.10 mmol) was added and the mixture was stirred at 120 °C for 32 h. The mixture was evaporated under vacuum and the residue dissolved in CH₂Cl₂. The organic layer was washed with water and brine, dried over Na₂SO₄, filtered, and concentrated in vacuo. The residue thus obtained (113 mg, 0.35 mmol) in MeOH (10 mL), Pd/C 10% (50 mg) was added, and the reaction mixture was stirred under H₂ (1 atm) at r.t. overnight. The mixture was filtered through a Celite pad and concentrated in vacuo. The crude product **26** was used in the next step without further purification.

1-(4-(1-(1H-Indole-2-carbonyl)piperidin-4-yl)butyl)-3-(pyridin-3-yl)thiourea (**25**). Reaction of **26** (22.0 mg, 0.1 mmol) and 3-pyridyl isothiocyanate (18 μL , 0.2 mmol) was performed according to the same procedure as that used to prepare **22**. Chromatography column (MeOH: EtOAc:CH₂Cl₂, 0.5:1 to 1.5:1). Yield: 91%, white solid. ^1H NMR (300 MHz, Acetone- d_6 , δ ppm) 10.63 (s, 1H, NH indole), 8.91 (s, 1H, NH-Py), 8.65–8.53 (m, 1H, Py), 8.31 (dd, $J = 4.7, 1.3$ Hz, 1H, Py), 8.07–7.94 (m, 1H, Py), 7.68–7.58 (m, 1H, indole), 7.57–7.39 (m, 2H, 1H indole, NH-CH₂), 7.31 (dd, $J = 8.1, 4.6$ Hz, 1H, Py), 7.27–7.15 (m, 1H, indole), 7.15–7.00 (m, 1H, indole), 6.80 (d, $J = 1.3$ Hz, 1H, indole), 4.71–4.51 (m, 2H, piperidine), 3.72–3.54 (m, 2H, CH₂-NH), 3.00 (br s, 2H, piperidine), 1.90–1.75 (m, 2H, piperidine), 1.75–1.55 (m, 3H, 1H piperidine, CH₂), 1.52–1.10 (m, 2H piperidine, 2 CH₂). ^{13}C NMR (75.4 MHz, Acetone- d_6 , δ ppm) 181.8, 161.8, 145.3, 136.1, 136.0, 130.4,

127.5, 123.3, 122.9, 121.3, 119.8, 111.8, 111.7, 103.8, 103.7, 44.9, 44.2, 35.9, 32.4, 28.8, 23.6. ESI-HRMS m/z calcd for $C_{24}H_{30}N_5O_5$ $[M+H]^+$, 436.2158; found, 436.2166.

tert-Butyl (7-(cyclopentyl(furan-2-ylmethyl)amino)-7-oxoheptyl)carbamate (30). A solution of **29a** [35] (80.0 mg, 0.48 mmol), 7-((*tert*-Butoxycarbonyl)amino)heptanoic acid [36] (178 mg, 0.73 mmol) and PyBOP (428 mg, 0.82 mmol) in DMF (2.5 mL) was cooled to 0 °C. DIPEA (0.21 mL, 1.21 mmol) was slowly added at 0 °C, and the reaction mixture was stirred at r.t. for 16 h. The reaction mixture was concentrated in vacuo and diluted with EtOAc (20 mL) and washed with 1 M HCl (x3) and brine (x3), dried over Na_2SO_4 and concentrated in vacuo. Chromatography column (EtOAc:Cyclohexane, 1:4 → 1:1) yielded **30** (170 mg, 89%) as a colourless oil. 1H NMR (300 MHz, $CDCl_3$, δ ppm, mixture of rotamers) 7.46–7.10 (m, 2H, furan), 6.39–6.23 (m, 2H, furan), 6.23–6.07 (m, 2H, furan), 4.86–4.63 (m, 1H, CH cyclopentyl rotamer A), 4.58–4.28 (m, 6H, 2 CH_2 -furan, 2 NH), 4.28–4.10 (m, 1H, CH cyclopentyl rotamer B), 3.08 (br s, 4H, 2 CH_2 -NH), 2.50–2.26 (m, 4H, 2 CH_2 -C=O), 1.91–1.21 (m, 46H, 8 CH_2 , 8 CH_2 cyclopentyl, 2C (CH_3)). ^{13}C NMR (75.4 MHz, $CDCl_3$, δ ppm, mixture of rotamers) 173.9, 173.2, 156.2, 152.3, 152.3, 142.1, 141.0, 110.6, 107.6, 107.0, 79.2, 77.6, 77.2, 76.7, 60.5, 58.8, 56.2, 41.9, 38.4, 30.1, 29.8, 29.2, 28.6, 26.7, 25.4, 23.9, 14.3. ESI-HRMS m/z calcd for $C_{22}H_{36}N_2O_4Na$ $[M+Na]^+$, 415.2564; found, 415.2567.

N-Cyclopentyl-N-(furan-2-ylmethyl)-7-(3-(pyridin-3-yl)thioureido)heptanamide (27). Compound **30** (156 mg, 0.40 mmol) was dissolved in 20% TFA/ CH_2Cl_2 (2.5 mL) at 0 °C and the mixture was stirred at r.t. for 3 h. The solvent was evaporated in vacuo and the residue was azeotropically dried with toluene (2 × 5 mL). After drying under high vacuum, the unprotected compound (110 mg, 0.27 mmol) was dissolved in dry CH_2Cl_2 (6 mL) and 3-pyridyl isothiocyanate (75 μ L, 0.7 mmol) was added. After stirring at r.t. for 3 h, the solvent was removed under vacuo and the resulting residue was purified by chromatography column on silica gel (MeOH:EtOAc, 1:9) to give **27** (80.0 mg, 70%) as a white solid. 1H NMR (300 MHz, $CDCl_3$, δ ppm, mixture of rotamers) 8.92–8.72 (m, 2H, Py), 8.55–8.41 (m, 2H, Py), 8.41–8.26 (m, 2H, Py), 8.18–8.00 (m, 2H, Py), 7.41–7.07 (m, 6 h, 2H furan, 2 NH-Py, 2 NH- CH_2), 6.40–6.16 (m, 2H, furan), 6.18–6.02 (m, 2H, furan), 4.69 (quint, $J = 8.3$ Hz, 1H, CH cyclopentyl rotamer A), 4.40 (br d, 4H, 2 CH_2 -furan), 4.29–4.09 (m, 1H, CH cyclopentyl rotamer B), 3.72–3.51 (m, 4H, 2 CH_2 -NH), 2.67–2.31 (m, 4H, 2 CH_2 -C=O), 1.94–1.23 (m, 32H, 8 CH_2 cyclopentyl, 8 CH_2). ^{13}C NMR (75.4 MHz, $CDCl_3$, δ ppm, mixture of rotamers) 181.8, 174.5, 173.9, 152.0, 151.6, 145.8, 145.6, 145.0, 142.3, 141.4, 136.0, 132.2, 123.6, 123.6, 110.6, 107.3, 77.6, 77.2, 76.7, 59.0, 56.5, 45.2, 44.9, 41.8, 38.8, 33.6, 33.3, 30.0, 29.1, 28.3, 27.6, 27.1, 26.8, 24.6, 24.4, 23.9, 23.8. ESI-HRMS m/z calcd for $C_{23}H_{33}N_4O_2S$ $[M+H]^+$, 429.2316; found, 429.2319.

6-Amino-N-cyclopentyl-N-(furan-2-ylmethyl)hexane-1-sulfonamide (32). To a suspension of **29a** (1.1 g, 6.7 mmol) in dry CH_2Cl_2 (38 mL) was added Et_3N (2.6 mL, 19 mmol) under argon at 0 °C and stirred over 3 Å MS. Compound **31** [37] (5.3 g, 16 mmol) in dry CH_2Cl_2 (40 mL) was added over 1 h and the resulting mixture stirred for 3 h at 0 °C. The reaction mixture was quenched with water and extracted with CH_2Cl_2 . The combined organic layers were washed with water, brine, dried over anhydrous Na_2SO_4 and concentrated in vacuo. The crude product was purified by flash chromatography on silica gel (toluene:EtOAc, 20:1 → 12:1) to give the protected sulfonamide (1.8 g, 62%) as a white solid. To a stirred solution of this compound (1.9 g, 4.2 mmol) in dry MeOH (20 mL), was added NH_2NH_2 (1.2 mL, 25 mmol) at 0 °C and stirred for 3 h at 0 °C and at r.t. overnight. The white precipitate was filtered off and washed with MeOH (20 mL). The solvent was evaporated in vacuo and the crude product was dissolved in 2 N HCl (90 mL) and washed with Et_2O (90 mL x 3). The aqueous layer was basified with sat. aq. soln. of NaOH to pH = 8 and extracted with EtOAc (90 mL x 3). The organic layers were collected and dried over anhydrous Na_2SO_4 and concentrated in vacuo to yield **32** as a sticky solid that was carried forward to the next step without purification.

N-Cyclopentyl-N-(furan-2-ylmethyl)-6-(3-(pyridin-3-yl)thioureido)hexane-1-sulfonamide (28). Reaction of **32** (115 mg, 0.35 mmol) and 3-pyridyl isothiocyanate (100 μ L, 0.90 mmol) was performed according to the same procedure as that used to prepare **22**. Chromatography column (EtOAc:Cyclohexane, 9:1). Yield: 64%, white solid. 1H NMR (300 MHz, $CDCl_3$, δ ppm) 8.62–8.51 (m, 1H, Py), 8.50–8.37 (m, 1H, Py), 8.17 (br s, 1H, NH-Py), 7.96–7.76 (m, 1H, Py), 7.42–7.30 (m, 2H, Py, furan), 6.45–6.22 (m, 3H, 2H furan, NH- CH_2), 4.36 (s, 2H, CH_2 -furan), 4.24–4.04 (m, 1H, CH cyclopentyl), 3.60 (q, $J = 6.6$ Hz, 2H, CH_2 -NH), 2.88–2.67 (m, 2H, CH_2SO_2), 1.98–1.47 (m, 12H, 8H cyclopentyl, 2 CH_2), 1.47–1.21 (m, 4H, 2 CH_2). ^{13}C NMR (75.4 MHz, $CDCl_3$, δ ppm) 181.5 (C=S), 151.4 (qC, furan), 147.0 (CH, Py), 145.7 (CH, Py), 142.3 (CH, furan), 134.6 (qC, Py), 132.7 (CH, Py), 124.3 (CH, Py), 110.8 (CH, furan), 109.2 (CH, furan), 59.3 (CH, cyclopentyl), 53.2 (CH_2SO_2), 45.2 (CH_2 -NH), 40.1 (CH_2 -furan), 30.0 (2 CH_2 , cyclopentyl), 28.5 (CH_2), 27.9 (CH_2), 26.3 (CH_2), 23.6 (2 CH_2 , cyclopentyl), 23.3 (CH_2). ESI-HRMS m/z calcd for $C_{22}H_{33}N_4O_3S_2$ $[M+H]^+$, 465.1982; found, 465.1989.

1-(Furan-2-yl)-N-(4-nitrobenzyl)methanamine (29c). A solution of furfuryl amine (0.73 mL, 8.20 mmol) and 4-nitrobenzaldehyde (1.24 g, 8.20 mmol) were stirred in dry CH_2Cl_2 (20.0 mL) over 3 Å MS at r.t. for 24 h. Then the reaction mixture was concentrated in vacuo and the residue was dissolved in MeOH (20 mL). $NaBH_4$ (623 mg, 16.5 mmol) was added in small portion to the mixture at 0 °C. The reaction was warmed to r.t. and stirred for 16 h. The solvent was removed under reduce pressure and the residue was dissolved in water (100 mL) and extracted with EtOAc (3 × 100 mL). The organic phases were extracted with 3% HCl (3 × 100 mL), and the pH of the obtained acidic aqueous solution was raised to pH 10 with sat. aq. soln. of NaOH. The aqueous phase was extracted with EtOAc (3 × 100 mL), and the organic phases were washed with water (100 mL), brine (100 mL), and dried over Na_2SO_4 . The solvent was evaporated in vacuo to give **29c** (1.42 g, 75%) as a red oil. 1H NMR (300 MHz, $CDCl_3$, δ ppm) 8.17 (d, $J = 8.7$ Hz, 2H, Ph), 7.51 (d, $J = 8.8$ Hz, 2H, Ph), 7.42–7.32 (m, 1H, furan), 6.37–6.25 (m, 1H, furan), 6.24–6.12 (m, 1H, furan), 3.89 (s, 2H, CH_2 -Ph), 3.80 (s, 2H, CH_2 -furan), 1.85 (s, 1H, NH). ^{13}C NMR (75.4 MHz, $CDCl_3$, δ ppm) 153.3 (qC, Furan), 147.7 (qC, Ph), 147.3 (qC, Ph), 142.2 (CH, furan), 128.9 (2 CH, Ph), 123.8 (2 CH, Ph), 110.4 (CH, furan), 107.6 (CH, furan), 52.0 (CH_2 -furan), 45.5 (CH_2 -Ph). ESI-HRMS m/z calcd for $C_{12}H_{13}N_2O_3$ $[M+H]^+$, 233.0922; found, 233.0921.

N-(Furan-2-ylmethyl)-3-morpholinopropan-1-amine (29d). Reaction of furfural (3.5 mL, 42 mmol) and 3-morpholinopropan-1-amine (6.1 mL, 42 mmol) as indicated for the synthesis of **29c** afforded **29d** (8.0 g, 86%) as a yellow oil. 1H NMR (300 MHz, $CDCl_3$, δ ppm) 7.34 (dd, $J = 1.8, 0.8$ Hz, 1H, furan), 6.30 (dd, $J = 3.2, 1.8$ Hz, 1H, furan), 6.17 (dd, $J = 3.2, 0.8$ Hz, 1H, furan), 3.77 (s, 2H, CH_2 -furan), 3.73–3.63 (m, 4H, morpholine), 2.67 (t, $J = 6.8$ Hz, 2H, CH_2), 2.48–2.34 (m, 6H, morpholine, CH_2), 2.16 (s, 1H, NH), 1.76–1.62 (m, 2H, CH_2). ^{13}C NMR (75.4 MHz, $CDCl_3$, δ ppm) 153.9 (qC, furan), 141.9 (CH, furan), 110.2 (CH, furan), 107.0 (CH, furan), 67.1 (2C, morpholine), 57.5 (CH_2), 53.9 (2C, morpholine), 47.9 (CH_2), 46.3 (CH_2 -furan), 26.6 (CH_2). ESI-HRMS m/z calcd for $C_{12}H_{21}N_2O_2$ $[M+H]^+$, 225.1596; found, 225.1598.

N-(Furan-2-ylmethyl)-3-(pyrrolidin-1-yl)propan-1-amine (29e). Reaction of furfural (0.34 mL, 4.20 mmol) and 3-(pyrrolidin-1-yl)propan-1-amine (0.53 mL, 4.20 mmol) as indicated for the synthesis of **29c** afforded **29e** (630 mg, 73%) as a colourless oil. 1H NMR (300 MHz, $CDCl_3$, δ ppm) 7.34 (dd, $J = 1.9, 0.9$ Hz, 1H, furan), 6.29 (dd, $J = 3.2, 1.9$ Hz, 1H, furan), 6.18–6.12 (m, 1H, furan), 3.81–3.72 (m, 2H, CH_2 -furan), 2.66 (t, $J = 7.0$ Hz, 2H, CH_2), 2.55–2.43 (m, 6H, CH_2 , 2 CH_2 pyrrolidine), 2.05 (s, 1H, NH), 1.83–1.65 (m, 6H, CH_2 , 2 CH_2 pyrrolidine). ^{13}C NMR (75.4 MHz, $CDCl_3$, δ ppm) 154.1 (qC, furan), 141.8 (CH, furan), 110.1 (CH, furan), 106.8 (CH, furan), 54.8 (CH_2), 54.3 (2C, pyrrolidine), 47.9 (CH_2), 46.3 (CH_2 -furan), 29.3 (CH_2), 23.5 (2C, pyrrolidine). ESI-HRMS m/z calcd for $C_{12}H_{21}N_2O$ $[M+H]^+$, 209.1649; found, 209.1648.

6-Amino-N-(furan-2-ylmethyl)-N-(3-morpholinopropyl)hexane-1-sulfonamide (33d). To a suspension of **29d** (643 mg, 1.95 mmol) in dry

CH₂Cl₂ (12.0 mL) was added Et₃N (0.76 mL, 5.5 mmol) at 0 °C under argon. Compound **31** (643 mg, 1.95 mmol) in dry CH₂Cl₂ (5 mL) was added dropwise over 30 min at 0 °C and the resulting mixture was stirred at r.t. for 16 h. The reaction mixture was quenched with water (45 mL) and extracted with CH₂Cl₂ (50 mL x 3). The combined organic layers were washed with water, brine, dried over anh. Na₂SO₄ and concentrated in vacuo. Chromatography column (MeOH:CH₂Cl₂, 1:20) afforded protected sulfonamide (630 mg, 62%) as a white solid. This compound (610 mg, 1.18 mmol) in dry MeOH (6 mL), was added NH₂NH₂ (0.35 mL, 7.2 mmol) at 0 °C and stirred for 3 h at 0 °C and at r.t. overnight. The white precipitate was filtered off and washed with MeOH (6 mL). The solvent was evaporated in vacuo and the crude product was dissolved in 2 N HCl (30 mL) and washed with diethyl ether. The aqueous layer was basified with sat. aq. soln. of NaOH to pH = 8 and extracted with EtOAc. The combined organic layers were dried over anh. Na₂SO₄ and concentrated in vacuo to yield **33d** as a sticky solid that was carried forward to the next step without purification.

(E)-6-(2-Cyano-3-(pyridin-4-yl)guanidino)-N-cyclopentyl-N-(furan-2-ylmethyl)hexane-1-sulfonamide (**35a**). Compound **34a** [23] (920.0 mg, 3.86 mmol) was dissolved in dry MeCN:DMF (48 mL, 3:1), **32** (1.65 g, 5.02 mmol), Et₃N (1.51 mL, 10.8 mmol) and DMAP (100 mg, 0.81 mmol) were added, and the mixture was heated and stirred at 80 °C under argon for 16 h. The reaction mixture was concentrated in vacuo and the residue was purified by flash chromatography on silica gel (MeOH:EtOAc, 1:12) to yield **35a** (1.48 g, 81%) as a white solid. ¹H NMR (300 MHz, CDCl₃, δ ppm) 8.50–8.33 (m, 2H, Py), 7.41–7.30 (m, 1H, furan), 7.30–7.16 (m, 2H, Py), 6.37–6.22 (m, 2H, furan), 6.10 (t, J = 5.6 Hz, 1H, NH–CH₂), 4.34 (s, 2H, CH₂-furan), 4.11 (quint, J = 8.5 Hz, 1H, CH cyclopentyl), 3.36 (q, J = 6.7 Hz, 2H, CH₂-NH), 2.82–2.67 (m, 2H, CH₂SO₂), 1.94–1.45 (m, 12H, 8H cyclopentyl, 2 CH₂), 1.45–1.23 (m, 4H, 2 CH₂). ¹³C NMR (75.4 MHz, CDCl₃, δ ppm) 157.7 (C=N), 151.3 (qC, furan), 150.5 (2CH, Py), 145.4 (qC, Py), 142.3 (CH, furan), 117.1 (CN), 115.8 (CH, Py), 110.8 (CH, furan), 109.2 (CH, furan), 59.3 (CH, cyclopentyl), 53.1 (CH₂SO₂), 42.5 (CH₂-NH), 40.1 (CH₂-furan), 30.0 (2CH₂, cyclopentyl), 28.9 (CH₂), 27.8 (CH₂), 26.1 (CH₂), 23.6 (2CH₂, cyclopentyl), 23.2 (CH₂). ESI-HRMS *m/z* calcd for C₂₃H₃₃N₆O₃S [M+H]⁺, 473.2328; found, 473.2329.

(E)-6-(2-Cyano-3-(pyridin-4-yl)guanidino)-N-(furan-2-ylmethyl)-N-(3-morpholinopropyl)hexane-1-sulfonamide (**35d**). Reaction of **34a** (73.0 mg, 0.31 mmol) and **33d** (130.0 mg, 0.34 mmol) followed the procedure described for **35a**. Chromatography column (MeOH:EtOAc, 1:6). Yield: 68%, white solid. ¹H NMR (300 MHz, CDCl₃, δ ppm, mixture of rotamers) 8.56–8.33 (m, 2H, Py), 7.62–7.34 (m, 4H, 2H furan, 2 NH-Py), 7.31–7.16 (m, 2H, Py), 6.88 (t, J = 5.7 Hz, 1H, NH–CH₂ rotamer A), 6.41–6.23 (m, 4H, furan), 5.94 (t, J = 5.5 Hz, 1H, NH–CH₂ rotamer B), 4.40 (s, 4H, 2 CH₂-furan), 3.77–3.60 (m, 8H, 4 CH₂ morpholine), 3.43–3.31 (m, 4H, 2 CH₂-NH), 3.24 (t, J = 7.3 Hz, 4H, 2 CH₂-NSO₂), 2.95–2.81 (m, 4H, 2 CH₂SO₂), 2.51–2.28 (m, 12H, 4 CH₂ morpholine, 2 CH₂), 1.82–1.67 (m, 8H, 4 CH₂), 1.67–1.50 (m, 4H, 2 CH₂), 1.50–1.29 (m, 8H, 4 CH₂). ¹³C NMR (75.4 MHz, CDCl₃, δ ppm, mixture of rotamers) 169.5, 157.6, 150.8, 150.1, 150.0, 145.0, 143.0, 143.0, 134.9, 130.4, 128.4, 115.8, 110.8, 110.7, 110.0, 109.9, 67.0, 66.9, 55.7, 55.7, 53.7, 52.2, 52.0, 50.9, 45.4, 45.3, 43.2, 42.4, 40.1, 29.2, 28.9, 28.1, 27.8, 26.5, 26.1, 25.5, 25.4, 23.3. ESI-HRMS *m/z* calcd for C₂₅H₃₈N₇O₄S [M+H]⁺, 532.2693; found, 532.2700.

tert-Butyl (6-(cyclopentyl(furan-2-ylmethyl)amino)-6-oxohexyl)carbamate (**36a**). Reaction of **29a** (80.0 mg, 0.48 mmol) and 6-((tert-butoxycarbonyl)amino)hexanoic acid [32] (168 mg, 0.73 mmol) followed the procedure described for **30**. Chromatography column (EtOAc:Cyclohexane, 1:1). Yield: 90%, yellow oil. ¹H NMR (300 MHz, CDCl₃, δ ppm, mixture of rotamers) 7.40–7.19 (m, 2H, furan), 6.38–6.23 (m, 2H, furan), 6.23–6.05 (m, 2H, furan), 4.88–4.30 (m, 7H, 2 CH₂-furan, CH cyclopentyl rotamer A, 2 NH), 4.29–4.03 (m, 1H, CH cyclopentyl rotamer B), 3.22–2.94 (m, 4H, 2 CH₂-NH), 2.49–2.26 (m, 4H, 2 CH₂-C=O), 1.88–1.17 (m, 46H, 6 CH₂, 8 CH₂ cyclopentyl, 2C(CH₃)₃). ¹³C NMR (75.4 MHz, CDCl₃, δ ppm, mixture of rotamers) 173.1, 156.1,

152.7, 152.3, 142.1, 141.0, 110.6, 107.6, 107.0, 79.2, 58.7, 56.2, 41.9, 40.7, 38.4, 33.8, 33.6, 30.0, 29.2, 28.6, 26.7, 25.1, 23.9. ESI-HRMS *m/z* calcd for C₂₁H₃₄N₂O₄Na [M+Na]⁺, 401.2407; found, 401.2411.

tert-Butyl (6-((4-chlorobenzyl)(furan-2-ylmethyl)amino)-6-oxohexyl)carbamate (**36b**). The same procedure to that described for the synthesis of **36a** but starting from **29b** (80.0 mg, 0.36 mmol). Chromatography column (EtOAc:Cyclohexane, 1:2 → 1:1). Yield: 83%, colorless oil. ¹H NMR (300 MHz, CDCl₃, δ ppm, mixture of rotamers) 7.45–7.20 (m, 6H, 2H furan, 4H Ph), 7.20–7.00 (m, 4H, Ph), 6.38–6.23 (m, 2H, furan), 6.23–6.09 (m, 2H, furan), 4.60–4.29 (m, 10H, 2 NH, 2 CH₂-furan, 2 CH₂-Ph), 3.21–2.99 (m, 4H, 2 CH₂-NH), 2.53 (t, J = 7.6 Hz, 2H, CH₂-C=O rotamer A), 2.32 (t, J = 7.3 Hz, 2H, CH₂-C=O rotamer B) 1.80–1.60 (m, 4H, 2 CH₂), 1.57–1.20 (m, 26H, 2C(CH₃)₃, 4 CH₂). ¹³C NMR (75.4 MHz, CDCl₃, δ ppm, mixture of rotamers) 173.2, 156.2, 151.0, 150.1, 142.9, 142.4, 136.1, 135.4, 133.5, 133.3, 129.8, 129.2, 128.8, 127.8, 110.5, 109.0, 108.4, 79.1, 50.1, 47.6, 43.7, 41.6, 40.7, 33.2, 30.0, 28.6, 26.7, 25.0. ESI-HRMS *m/z* calcd for C₂₃H₃₁ClN₂O₄Na [M+Na]⁺, 457.1860; found, 457.1865.

tert-Butyl (6-((furan-2-ylmethyl)(3-morpholinopropyl)amino)-6-oxohexyl)carbamate (**36d**). The same procedure to that described for the synthesis of **36a** but starting from **29d** (80.0 mg, 0.48 mmol). Chromatography column (MeOH:EtOAc, 1:12 → 1:6). Yield: 80%, yellow oil. ¹H NMR (300 MHz, CDCl₃, δ ppm, mixture of rotamers) 7.40–7.33 (m, 1H, furan rotamer A), 7.34–7.28 (m, 1H, furan rotamer B), 6.35–6.25 (m, 2H, furan), 6.25–6.15 (m, 2H, furan), 4.65–4.47 (m, 4H, CH₂-furan rotamer A, 2 NH), 4.43 (s, 2H, CH₂-furan rotamer B), 3.82–3.62 (m, 8H, morpholine), 3.49–3.24 (m, 4H, 2 CH₂), 3.13–3.05 (m, 4H, 2 CH₂), 2.61–2.21 (m, 16H, 8H morpholine, 4 CH₂), 1.76–1.56 (m, 12H, 6 CH₂), 1.56–1.26 (m, 24H, 2C(CH₃)₃, 2 NH, 2 CH₂). ¹³C NMR (75.4 MHz, CDCl₃, δ ppm, mixture of rotamers) 173.2, 172.9, 156.1, 151.6, 150.6, 142.7, 142.0, 110.6, 110.5, 108.5, 108.1, 79.1, 77.6, 77.2, 76.7, 66.9, 66.4, 56.2, 55.6, 53.7, 53.4, 45.3, 45.1, 44.2, 41.5, 34.4, 33.2, 33.0, 30.0, 29.8, 28.5, 26.7, 25.5, 25.0, 24.9, 24.1. ESI-HRMS *m/z* calcd for C₂₃H₄₀N₃O₅ [M+H]⁺, 438.2959; found, 438.2962.

tert-Butyl (7-((4-chlorobenzyl)(furan-2-ylmethyl)amino)-7-oxoheptyl)carbamate (**37b**). To a solution of **29b** (80.0 mg, 0.36 mmol) and 7-((tert-butoxycarbonyl)amino)heptanoic acid [32] (106 mg, 0.43 mmol) in CH₂Cl₂ (2 mL), DMAP (4.0 mg, 40 μmol) and DCC (112 mg, 0.54 mmol) in CH₂Cl₂ (1 mL) were added at 0 °C. The reaction mixture was stirred overnight at r.t., filtered through Celite, washed with EtOAc (20.0 mL) and concentrated under vacuum, and the residue was purified by chromatography column on silica gel (EtOAc:Cyclohexane, 1:2 → 1:1) to obtain **37b** (130 mg, 80%) as a colourless oil. ¹H NMR (300 MHz, CDCl₃, δ ppm, mixture of rotamers) 7.40–7.20 (m, 6H, 2H furan, 4H Ph), 7.19–6.98 (m, 4H, Ph), 6.36–6.22 (m, 2H, furan), 6.22–6.08 (m, 2H, furan), 4.98–3.99 (m, 10H, 2 NH, 2 CH₂-furan, 2 CH₂-Ph), 3.18–2.96 (m, 4H, 2 CH₂-NH), 2.60–2.22 (m, 4H, 2 CH₂-C=O), 2.00–1.53 (m, 8H, 4 CH₂), 1.53–1.19 (m, 26H, 2C(CH₃)₃, 4 CH₂). ¹³C NMR (75.4 MHz, CDCl₃, δ ppm, mixture of rotamers) 173.7, 173.3, 156.1, 154.2, 151.0, 150.1, 142.8, 142.3, 136.1, 135.4, 133.4, 133.2, 129.7, 129.1, 128.8, 127.8, 110.5, 108.9, 108.3, 79.1, 77.6, 77.2, 76.7, 56.0, 50.0, 49.8, 47.5, 43.7, 41.5, 35.7, 33.2, 33.1, 32.8, 31.0, 30.0, 30.0, 29.1, 29.0, 28.9, 28.5, 26.7, 26.6, 26.4, 25.6, 25.4, 25.2, 25.1, 24.8. ESI-HRMS *m/z* calcd for C₂₄H₃₃ClN₂O₄Na [M+Na]⁺, 471.2016; found, 471.2021.

tert-Butyl (7-((furan-2-ylmethyl)(4-nitrobenzyl)amino)-7-oxoheptyl)carbamate (**37c**). The same procedure to that described for the synthesis of **37b** but starting from **29c** (80.0 mg, 0.35 mmol). Yield: 76%, yellow oil. ¹H NMR (300 MHz, CDCl₃, δ ppm, mixture of rotamers) 8.23–7.94 (m, 4H, Ph), 7.35–7.14 (m, 6H, 2H furan, 4H Ph), 6.29–6.18 (m, 2H, furan), 6.18–6.06 (m, 2H, furan), 4.69–4.22 (m, 10H, 2 NH, 2 CH₂-furan, 2 CH₂-Ph), 3.13–2.88 (m, 4H, 2 CH₂-NH), 2.60–2.15 (m, 4H, 2 CH₂-C=O), 1.93–1.49 (m, 6H, 3 CH₂), 1.49–0.96 (m, 28H, 2C(CH₃)₃, 5 CH₂). ¹³C NMR (75.4 MHz, CDCl₃, δ ppm, mixture of rotamers) 173.4, 173.1, 156.0, 154.1, 150.5, 149.6, 147.5, 147.2, 145.3, 144.5, 142.9, 142.3, 128.6, 127.0, 124.1, 123.7, 110.5, 110.4, 109.2, 108.6, 79.0, 77.5, 77.1, 76.7, 50.3, 49.3, 48.2, 44.4, 41.8, 35.6, 33.7, 33.1, 33.0,

32.7, 30.9, 29.9, 29.0, 28.9, 28.8, 28.4, 26.6, 26.5, 26.3, 25.6, 25.5, 25.3, 25.0, 25.0, 24.9, 24.7. ESI-HRMS m/z calcd for $C_{24}H_{33}N_3O_6Na$ $[M+Na]^+$, 482.2259; found, 482.2262.

tert-Butyl (7-((furan-2-ylmethyl)(3-morpholinopropyl)amino)-7-oxoheptyl)carbamate (37d). The same procedure to that described for the synthesis of **37b** but starting from **29d** (80.0 mg, 0.36 mmol). Chromatography column (MeOH:EtOAc, 1:10 → 1:6). Yield: 67%, colourless oil. 1H NMR (300 MHz, $CDCl_3$, δ ppm, mixture of rotamers) 7.36–7.31 (m, 1H, furan rotamer A), 7.31–7.27 (m, 1H, furan rotamer B), 6.36–6.23 (m, 2H, furan), 6.23–6.10 (m, 2H, furan), 4.68–4.45 (m, 4H, CH_2 -furan rotamer A, 2 NH), 4.40 (s, 2H, CH_2 -furan rotamer B), 3.76–3.54 (m, 8H, 4 CH_2), 3.46–3.22 (m, 4H, 2 CH_2), 3.13–2.92 (m, 4H, 2 CH_2), 2.53–2.12 (m, 16H, morpholine), 1.77–1.54 (m, 8H, 4 CH_2), 1.54–1.21 (m, 30H, 2C(CH_3)₃, 2 NH, 5 CH_2). ^{13}C NMR (75.4 MHz, $CDCl_3$, δ ppm, mixture of rotamers) 173.0, 172.9, 156.1, 151.6, 150.7, 142.6, 141.9, 110.5, 110.4, 108.4, 107.8, 79.0, 77.6, 77.2, 76.7, 67.0, 56.2, 55.5, 53.7, 53.6, 45.2, 45.1, 44.4, 41.4, 33.2, 33.0, 30.0, 29.7, 29.2, 29.1, 28.5, 26.7, 26.6, 25.5, 25.3, 25.1, 24.5.

tert-Butyl (7-((furan-2-ylmethyl)(3-pyrrolidin-1-yl)propyl)amino)-7-oxoheptyl)carbamate (37e). The same procedure to that described for the synthesis of **37b** but starting from **29e** (80 mg, 0.4 mmol). Chromatography column (MeOH:DCM:NH₄OH, 1:20:0.1 → 1:10:0.1). Yield: 44%, colourless oil. 1H NMR (300 MHz, $CDCl_3$, δ ppm, mixture of rotamers) 7.36–7.21 (m, 2H, furan), 6.31–6.20 (m, 2H, furan), 6.20–6.11 (m, 2H, furan), 4.59 (s, 2H, 2 NH), 4.49 (s, 2H, CH_2 -furan rotamer A), 4.39 (s, 2H, CH_2 -furan rotamer B), 3.44–3.22 (m, 4H, 2 CH_2 -NH), 3.09–2.97 (m, 4H, CH_2 -N-C=O), 2.84–2.70 (m, 4H, 2 CH_2 -N), 2.69–2.22 (m, 12H, 4 CH_2 pyrrolidine, 2 CH_2 -C=O), 1.92–1.77 (m, 6H, 2 CH_2 pyrrolidine, CH_2), 1.77–1.65 (m, 4H, 2 CH_2 pyrrolidine), 1.65–1.49 (m, 4H, 2 CH_2), 1.49–1.11 (m, 30H, 2C(CH_3)₃, 6 CH_2). ^{13}C NMR (75.4 MHz, $CDCl_3$, δ ppm, mixture of rotamers) 173.4, 172.9, 156.0, 151.5, 150.3, 142.6, 141.8, 110.4, 110.4, 108.3, 108.2, 78.9, 77.6, 77.2, 76.7, 54.0, 53.8, 53.5, 53.0, 45.4, 44.8, 43.6, 41.4, 33.0, 32.8, 30.1, 29.9, 29.6, 29.3, 29.0, 28.9, 28.4, 27.6, 26.6, 26.5, 25.7, 25.2, 25.0, 23.3. ESI-HRMS m/z calcd for $C_{24}H_{42}N_3O_4$ $[M+H]^+$, 436.3165; found, 436.3170.

(E)-6-(2-Cyano-3-(pyridin-4-yl)guanidino)-N-cyclopentyl-N-(furan-2-ylmethyl)hexanamide (38a). Compound **36a** (144 mg, 0.38 mmol) was dissolved in 20% TFA/ CH_2Cl_2 (0.5 mL TFA, 2 mL CH_2Cl_2) at 0 °C and the mixture was stirred at r.t. for 2.5 h. The solvent was evaporated in vacuo and the residue was azeotropically dried with toluene (2 × 5 mL). Finally, the residue was dried under high vacuum to yield a colourless oil that was used in the next step without further purification. This compound (149.0 mg, 0.38 mmol) was dissolved in dry MeCN:DMF (4 mL, 3:1) and **34a** (82.0 mg, 0.35 mmol), Et₃N (0.23 mL, 1.70 mmol) and DMAP (9.0 mg, 70 μ mol) were added, and the mixture was heated and stirred at 80 °C under argon for 16 h. The reaction mixture was concentrated under vacuum and the residue was purified by chromatography column on silica gel (MeOH:EtOAc: CH_2Cl_2 , 0.8:5:1) to give **38a** (113.0 mg, 78%) as white sticky solid. 1H NMR (300 MHz, $CDCl_3$, δ ppm, mixture of rotamers) 8.50–8.30 (m, 4H, Py), 7.40–7.20 (m, 4H, 2H Py, 2H furan), 6.49 (br s, 2H, 2 NH-Py), 6.39–6.21 (m, 2H, furan), 6.15–6.03 (m, 2H, furan), 4.72–4.53 (m, 1H, CH cyclopentyl rotamer A), 4.38 (s, 4H, 2 CH_2 -furan), 4.28–4.09 (m, 1H, CH cyclopentyl rotamer B), 3.52–3.40 (m, 4H, 2 CH_2 -NH), 2.52–2.31 (m, 4H, 2 CH_2 -C=O), 1.91–1.21 (m, 30H, 6 CH_2 , 8 CH_2 cyclopentyl, 2 NH- CH_2). ^{13}C NMR (75.4 MHz, $CDCl_3$, δ ppm, mixture of rotamers) 173.6, 157.7, 152.1, 151.6, 150.4, 150.2, 145.7, 142.3, 141.4, 117.0, 115.5, 115.3, 110.7, 107.2, 58.9, 56.3, 42.2, 41.6, 38.8, 33.4, 33.1, 30.0, 29.8, 29.1, 28.3, 28.1, 26.0, 25.8, 23.8. ESI-HRMS m/z calcd for $C_{23}H_{31}N_6O_2$ $[M+H]^+$, 423.2497; found, 423.2503.

(E)-N-(4-Chlorobenzyl)-6-(2-cyano-3-(pyridin-4-yl)guanidino)-N-(furan-2-ylmethyl)hexanamide (38b). Same procedure as described for **38a** starting from **36b**. Chromatography column (NH₄OH:MeOH:EtOAc, 0.1:0.5:10). Yield: 70%, colourless sticky solid. 1H NMR (300 MHz, $CDCl_3$, δ ppm, mixture of rotamers) 8.51–8.25 (m, 4H, Py), 7.43–7.18

(m, 10H, 2H furan, 4H Ph, 4H Py), 7.16–6.94 (m, 4H, Ph), 6.51–6.36 (m, 2H, 2 NH-Py), 6.36–6.24 (m, 2H, furan), 6.19–6.10 (m, 2H, furan), 4.55–4.28 (m, 8H, 2 CH_2 -Ph, 2 CH_2 -furan), 3.51–3.41 (m, 4H, 2 CH_2 -NH), 2.58 (t, J = 6.7 Hz, 2H, CH_2 -C=O rotamer A), 2.35 (t, J = 6.7 Hz, 2H, CH_2 -C=O rotamer B), 1.80–1.30 (m, 14H, 6 CH_2 , 2 NH- CH_2). ^{13}C NMR (75.4 MHz, $CDCl_3$, δ ppm, mixture of rotamers) 173.6, 157.7, 150.4, 150.2, 149.6, 145.7, 145.7, 143.0, 142.6, 135.6, 134.9, 133.7, 133.4, 129.3, 128.9, 127.8, 117.1, 115.6, 110.6, 109.1, 108.8, 50.8, 50.1, 47.9, 43.9, 42.2, 41.8, 32.8, 32.7, 28.5, 28.4, 26.2, 26.0, 23.5, 23.4. ESI-HRMS m/z calcd for $C_{25}H_{28}ClN_6O_2$ $[M+H]^+$, 479.1949; found, 479.1957.

(E)-6-(2-Cyano-3-(pyridin-4-yl)guanidino)-N-(furan-2-ylmethyl)-N-(3-morpholinopropyl)hexanamide (38d). Same procedure as described for **38a** starting from **36d**. Chromatography column (MeOH:Acetone: CH_2Cl_2 , 0.4:1:1). Yield: 57%, white sticky solid. 1H NMR (300 MHz, $CDCl_3$, δ ppm, mixture of rotamers) 8.43–8.31 (m, 4H, Py), 7.40–7.18 (m, 6H, 4H Py, 2H furan), 6.62–6.42 (m, 2H, 2 NH-Py), 6.36–6.22 (m, 2H, furan), 6.22–6.10 (m, 2H, furan), 4.49–4.37 (m, 4H, 2 CH_2 -furan), 3.70–3.57 (m, 8H, 4 CH_2 morpholine), 3.48–3.26 (m, 8H, 4 CH_2), 2.61–2.12 (m, 18H, 2 NH, 4 CH_2 morpholine, 4 CH_2), 1.72–1.50 (m, 12H, 6 CH_2), 1.45–1.28 (m, 4H, 2 CH_2). ^{13}C NMR (75.4 MHz, $CDCl_3$, δ ppm, mixture of rotamers) 173.1, 157.7, 150.3, 150.3145.5, 142.7, 142.1, 117.1, 115.4, 110.5, 108.4, 108.1, 66.9, 66.8, 55.0, 55.3, 53.6, 53.5, 45.3, 45.1, 44.5, 42.2, 42.0, 41.7, 32.7, 32.4, 28.5, 28.4, 26.1, 26.0, 25.3, 24.4, 23.6, 23.5. ESI-HRMS m/z calcd for $C_{25}H_{36}N_7O_3$ $[M+H]^+$, 482.2868; found, 482.2874.

(E)-7-(2-Cyano-3-(pyridin-4-yl)guanidino)-N-cyclopentyl-N-(furan-2-ylmethyl)heptanamide (39a). Same procedure as described for **38a** starting from **30**. Chromatography column (MeOH:EtOAc: CH_2Cl_2 , 0.8:5:1). Yield: 76%, white sticky solid. 1H NMR (300 MHz, $CDCl_3$, δ ppm, mixture of rotamers) 8.50–8.30 (m, 4H, Py), 7.40–7.20 (m, 6H, 4H Py, 2H furan), 6.49 (br s, 2H, NH-Py), 6.39–6.21 (m, 2H, furan), 6.15–6.03 (m, 2H, furan), 4.82–4.64 (m, 1H, CH cyclopentyl rotamer A), 4.53–4.30 (m, 4H, 2 CH_2 -furan), 4.26–4.08 (m, 1H, CH cyclopentyl rotamer B), 3.52–3.40 (m, 4H, 2 CH_2 -NH), 2.52–2.31 (m, 4H, 2 CH_2 -C=O), 1.91–1.21 (m, 32H, 8 CH_2 , 8 CH_2 cyclopentyl, 2 NH- CH_2). ^{13}C NMR (75.4 MHz, $CDCl_3$, δ ppm, mixture of rotamers) 174.3, 173.6, 157.7, 152.1, 151.6, 150.4, 150.2, 145.7, 142.3, 141.4, 117.0, 115.5, 115.3, 110.7, 110.7, 107.2, 77.6, 77.2, 76.7, 58.9, 56.3, 42.2, 41.6, 38.8, 33.4, 33.0, 30.0, 29.8, 29.1, 28.3, 26.1, 26.0, 23.8, 23.3. ESI-HRMS m/z calcd for $C_{24}H_{33}N_6O_2$ $[M+H]^+$, 437.2656; found, 437.2660.

(E)-N-(4-Chlorobenzyl)-7-(2-cyano-3-(pyridin-4-yl)guanidino)-N-(furan-2-ylmethyl)heptanamide (39b). Same procedure as described for **38a** starting from **37b**. Chromatography column (MeOH:EtOAc: CH_2Cl_2 , 0.8:5:1). Yield: 64%, white sticky solid. 1H NMR (300 MHz, $CDCl_3$, δ ppm, mixture of rotamers) 8.46–8.30 (m, 4H, Py), 7.42–7.20 (m, 10H, 2H furan, 4H Ph, 4H Py), 7.16–6.99 (m, 4H, Ph), 6.37–6.23 (m, 4H, 2H furan, 2 NH-Py), 6.21–6.09 (m, 2H, furan), 4.58–4.30 (m, 8H, 2 CH_2 -Ph, 2 CH_2 -furan), 3.49–3.35 (m, 4H, 2 CH_2 -NH), 2.57 (t, J = 6.9 Hz, 2H, CH_2 -C=O rotamer A), 2.35 (t, J = 6.9 Hz, 2H, CH_2 -C=O rotamer B), 1.77–1.23 (m, 18H, 8 CH_2 , 2 NH- CH_2). ^{13}C NMR (75.4 MHz, $CDCl_3$, δ ppm, mixture of rotamers) 173.6, 157.5, 150.5, 149.9, 149.7, 145.9, 143.0, 142.5, 135.7, 135.0, 133.4, 129.4, 129.3, 128.9, 127.8, 116.9, 115.6, 110.6, 109.1, 108.7, 77.6, 77.2, 76.7, 50.1, 47.9, 43.9, 42.4, 41.8, 32.9, 28.6, 28.5, 28.3, 28.1, 26.1, 24.3. ESI-HRMS m/z calcd for $C_{26}H_{30}ClN_6O_2$ $[M+H]^+$, 493.2107; found, 493.2113.

(E)-7-(2-Cyano-3-(pyridin-4-yl)guanidino)-N-(furan-2-ylmethyl)-N-(4-nitrobenzyl)heptanamide (39c). Same procedure as described for **38a** starting from **37c**. Chromatography column (MeOH:EtOAc: CH_2Cl_2 , 0.8:5:1). Yield: 96%, yellow sticky solid. 1H NMR (300 MHz, $CDCl_3$, δ ppm, mixture of rotamers) 8.44–8.33 (m, 4H, Py), 8.24–8.04 (m, 4H, Py), 7.40–7.18 (m, 8H, 2H furan, 4H Ph), 6.41–6.23 (m, 4H, 2H furan, 2 NH-Py), 6.23–6.11 (m, 2H, furan), 4.75–4.35 (m, 8H, 2 CH_2 -Ph, 2 CH_2 -furan), 3.45–3.31 (m, 4H, 2 CH_2 -NH), 2.69–2.25 (m, 4H, 2 CH_2 -C=O), 1.82–1.29 (m, 18H, 8 CH_2 , 2 NH- CH_2). ^{13}C NMR (75.4 MHz, $CDCl_3$, δ ppm, mixture of rotamers) 173.9, 173.7, 157.5, 150.1, 149.9, 149.3,

147.7, 147.4, 146.0, 145.0, 143.1, 142.7, 128.5, 127.1, 124.3, 123.9, 116.9, 116.8, 115.7, 110.7, 109.5, 109.1, 77.6, 77.4, 77.2, 76.7, 50.9, 48.5, 44.7, 42.5, 42.2, 33.0, 28.7, 28.5, 28.2, 26.2, 24.5. ESI-HRMS m/z calcd for $C_{26}H_{30}N_7O_4$ $[M+H]^+$, 504.2346; found, 504.2354.

(E)-7-(2-Cyano-3-(pyridin-4-yl)guanidino)-N-(furan-2-ylmethyl)-N-(3-morpholinopropyl)heptanamide (**39d**). Same procedure as described for **38a** starting from **37d**. Chromatography column (MeOH:EtOAc:NH₄OH, 1:10:0.1 → 1:6:0.1). Yield: 61%, white sticky solid. ¹H NMR (300 MHz, CDCl₃, δ ppm, mixture of rotamers) 8.49–8.34 (m, 4H, Py), 7.42–7.22 (m, 6H, 4H Py, 2H furan), 6.36–6.26 (m, 2H, furan), 6.26–6.12 (m, 4H, furan, 2 NH-Py), 4.53 (s, 2H, CH₂-furan rotamer A), 4.45 (s, 2H, CH₂-furan rotamer B), 3.75–3.58 (m, 8H, 4 CH₂ morpholine), 3.52–3.28 (m, 8H, 4 CH₂), 2.53–2.22 (m, 16H, 4 CH₂ morpholine, 4 CH₂), 1.77–1.52 (m, 12H, 6 CH₂), 1.52–1.22 (m, 10H, 2 NH, 4 CH₂). ¹³C NMR (75.4 MHz, CDCl₃, δ ppm, mixture of rotamers) 173.4, 173.4, 157.6, 151.0, 150.6, 150.5, 150.3, 145.4, 142.8, 142.3, 117.0, 115.6, 115.6, 110.6, 110.6, 108.5, 108.2, 77.6, 77.2, 76.7, 67.0, 66.8, 56.1, 55.5, 53.8, 53.6, 50.8, 45.5, 45.2, 44.5, 42.4, 42.3, 41.9, 32.9, 32.6, 28.5, 28.2, 28.0, 26.0, 25.9, 25.5, 24.4, 24.2, 24.0. ESI-HRMS m/z calcd for $C_{26}H_{38}N_7O_3$ $[M+H]^+$, 496.3021; found, 496.3031.

(E)-7-(2-Cyano-3-(pyridin-4-yl)guanidino)-N-(furan-2-ylmethyl)-N-(3-pyrrolidin-1-yl)propyl)heptanamide (**39e**). Same procedure as described for **38a** starting from **37e**. Chromatography column (MeOH:DCM:NH₄OH, 1:10:0.1 → 1:6:0.1). Yield: 82%, white sticky solid. ¹H NMR (300 MHz, CDCl₃, δ ppm, mixture of rotamers) 8.36–8.23 (m, 4H, Py), 7.36–7.24 (m, 6H, 4H Py, 2H furan), 6.50 (br s, 2H, 2 NH-Py), 6.32–6.28 (m, 2H, furan), 6.24–6.20 (m, 2H, furan), 4.54–4.33 (m, 4H, 2 CH₂-furan), 3.51–3.28 (m, 8H, 2 CH₂-NH, 2 CH₂-N-C=O), 3.12–2.59 (m, 12H, 2 CH₂-N, 4 CH₂ pyrrolidine), 2.52–2.24 (m, 4H, 2 CH₂-C=O), 2.04–1.89 (m, 6H, 3 CH₂), 1.89–1.70 (m, 6H, 3 CH₂), 1.69–1.47 (m, 8H, 4 CH₂), 1.42–1.20 (m, 8H, 4 CH₂). ¹³C NMR (75.4 MHz, CDCl₃, δ ppm, mixture of rotamers) 174.3, 173.2, 162.7, 157.2, 150.2, 149.7, 145.8, 142.9, 142.1, 116.9, 114.9, 110.6, 108.7, 77.5, 77.0, 76.6, 54.0, 53.8, 53.1, 52.8, 45.1, 43.2, 42.3, 41.8, 32.7, 31.5, 30.1, 29.7, 29.2, 28.8, 28.2, 26.0, 24.9, 24.4, 23.4, 23.2, 22.7, 14.1. ESI-HRMS m/z calcd for $C_{26}H_{38}N_7O_2$ $[M+H]^+$, 480.3075; found, 480.3081.

(E)-8-(2-Cyano-3-(pyridin-4-yl)guanidino)-N-(furan-2-ylmethyl)octanamide (**40f**). Reaction of **34a** (63.6 mg, 0.27 mmol) and **20** (70.0 mg, 0.3 mmol) followed the procedure described for **35a**. Chromatography column (MeOH:EtOAc, 1:10 → 1:5). Yield: 91%, white solid. ¹H NMR (300 MHz, CD₃OD, δ ppm) 8.43–8.35 (m, 2H, Py), 7.46–7.39 (m, 1H, furan), 7.39–7.31 (m, 2H, Py), 6.33 (dd, $J = 3.1, 1.9$ Hz, 1H, furan), 6.28–6.21 (m, 1H, furan), 4.34 (s, 2H, CH₂-furan), 3.38 (t, $J = 7.2$ Hz, 2H, CH₂-NH-C=N), 2.21 (t, $J = 7.4$ Hz, 2H, CH₂-C=O), 1.70–1.53 (m, 4H, 2 CH₂), 1.43–1.30 (m, 6H, 3 CH₂). ¹³C NMR (75.4 MHz, CD₃OD, δ ppm) 176.0 (C=O), 159.2 (C=N), 153.2 (qC, Py), 150.6 (2CH, Py), 148.4 (qC-furan), 143.3 (CH, furan), 117.8 (C=N), 116.4 (2CH, Py), 111.3 (CH, furan), 108.0 (CH, furan), 43.4 (CH₂-NH-C=N), 37.1 (CH₂-furan), 36.8 (CH₂), 30.2 (CH₂), 30.0 (CH₂), 29.9 (CH₂), 27.6 (CH₂), 26.8 (CH₂). ESI-HRMS m/z calcd for $C_{20}H_{27}N_6O_2$ $[M+H]^+$, 383.2186; found, 383.2190.

(E)-N-(8-(2-Cyano-3-(pyridin-3-yl)guanidino)octyl)-1H-indole-2-carboxamide (**41**). A solution of **21** (48.0 mg, 0.17 mmol), **34b** (44.0 mg, 0.18 mmol) and Et₃N (26.0 μ L, 0.18 mmol) in dry CH₂Cl₂:DMF (3:1, 6.6 mL) was stirred at r.t. for 36 h. Then, the solvent was evaporated under reduced pressure and the residue was purified by chromatography column on silica gel (MeOH:EtOAc, 1:40) to yield **41** (15.0 mg, 21%) as a white solid. ¹H NMR (300 MHz, CD₃OD, δ ppm) 8.51–8.42 (m, 1H, Py), 8.37–8.29 (m, 1H, 1H, Py), 7.83–7.71 (m, 1H, Py), 7.63–7.53 (m, 1H, indole), 7.45–7.38 (m, 1H Py, 1H indole), 7.24–7.16 (m, 1H, indole), 7.09–7.00 (m, 2H, indole), 3.39 (t, $J = 7.1$ Hz, 2H, CH₂-NH-C=N), 1.68–1.55 (m, 4H, CH₂-NH, CH₂), 1.44–1.35 (m, 10H, 5 CH₂). ¹³C NMR (75.4 MHz, CD₃OD, δ ppm) 164.2 (C=O), 160.1 (C=N), 146.8 (CH, Py), 146.1 (CH, Py), 138.3 (qC, Py), 136.3 (qC, indole), 133.7 (CH, indole), 132.4 (qC, indole), 129.1 (qC, indole), 125.5 (CH, indole), 125.4 (CH, indole), 125.0 (CH, Py), 122.7 (CH, indole), 121.1 (CH, indole), 118.7

(CN), 113.0 (CH, Py), 104.2 (CH, indole), 43.2 (CH₂-NH-C=N), 40.6 (CH₂-C=O), 30.6 (CH₂), 30.4 (CH₂), 30.3 (CH₂), 30.2 (CH₂), 28.0 (CH₂), 27.7 (CH₂). ESI-HRMS m/z calcd for $C_{24}H_{30}N_7O$ $[M+H]^+$, 432.2507; found, 432.2506.

(E)-1-(4-(1-(1H-Indole-2-carbonyl)piperidin-4-yl)butyl)-2-cyano-3-(pyridin-3-yl)guanidine (**42**). A solution of compound **26** (35.0 mg, 0.1 mmol), **34b** (26 mg, 0.1 mmol) and Et₃N (16 μ L, 0.1 mmol) in dry MeCN:DMF, 3:1 (4 mL), was stirred at 85 °C for 16 h. The solvent was evaporated under reduced pressure and the residue was purified by chromatography column on silica gel (MeOH:EtOAc:CH₂Cl₂, 1:5:1) to give **42** (34.0 mg, 72%) as a white solid. ¹H NMR (300 MHz, Acetone-*d*₆, δ ppm) 10.62 (s, 1H, NH, indole), 8.68–8.52 (m, 1H, Py), 8.47–8.27 (m, 2H, NH-Py, 1H Py), 7.90–7.73 (m, 1H, Py), 7.69–7.57 (m, 1H, indole), 7.57–7.45 (m, 1H, indole), 7.45–7.31 (m, 1H, Py), 7.31–7.13 (m, 1H, indole), 7.13–6.98 (m, 1H, indole), 6.84–6.76 (m, 1H, indole), 6.77–6.63 (m, 1H, NH-CH₂), 4.70–4.52 (m, 2H, piperidine), 3.49–3.32 (m, 2H, CH₂-NH), 3.01 (br s, 2H, piperidine), 1.93–1.75 (m, 2H, piperidine), 1.72–1.54 (m, 3H, 1H piperidine, CH₂), 1.51–1.08 (m, 6H, 2H piperidine, 2 CH₂). ¹³C NMR (75.4 MHz, Acetone-*d*₆, δ ppm) 161.8, 160.1, 146.8, 146.1, 138.3, 136.0, 132.4, 127.5, 123.2, 121.4, 119.8, 118.7, 111.8, 111.7, 103.8, 103.7, 43.3, 41.7, 35.9, 32.4, 29.7, 23.4. ESI-HRMS m/z calcd for $C_{25}H_{30}N_7O$ $[M+H]^+$, 444.2501; found, 444.2506.

(E)-1-(6-Azidohexyl)-2-cyano-3-(pyridin-4-yl)guanidine (**43**). Reaction of **34a** (762 mg, 3.20 mmol) and 6-azidohexan-1-amine [**38**] (500 mg, 3.52 mmol) as indicated for **35a**. Chromatography column (MeOH:CH₂Cl₂, 1:8). Yield: 79%, white solid. ¹H NMR (300 MHz, CDCl₃, δ ppm) 8.48–8.29 (m, 2H, Py), 7.25–7.15 (m, 2H, Py), 6.24–6.04 (m, 1H, NH-Py), 3.37 (q, $J = 6.8$ Hz, 2H, CH₂-NH), 3.25 (t, $J = 6.7$ Hz, 2H, CH₂-N₃), 1.69–1.49 (m, 4H, 2 CH₂), 1.49–1.29 (m, 4H, 2 CH₂). ¹³C NMR (75.4 MHz, CDCl₃, δ ppm) 157.7 (C=N), 150.3 (2 CH, Py), 145.6 (Cq, Py), 117.1 (CN), 115.9 (2 CH, Py), 51.4 (CH₂-N₃), 42.6 (CH₂-NH), 29.2 (CH₂), 28.8 (CH₂), 26.4 (CH₂), 26.4 (CH₂). ESI-HRMS m/z calcd for $C_{13}H_{19}N_8$ $[M+H]^+$, 287.1729; found, 287.1727.

N-(Furan-2-ylmethyl)-N-(3-morpholinopropyl)prop-2-yn-1-amine (**44**). To a mixture of propargyl bromide (75 μ L, 0.84 mmol) and **29d** (377 mg, 1.68 mmol) in dry DMF (6 mL), anh. K₂CO₃ (349 mg, 2.52 mmol) was added, and the reaction mixture was stirred at r.t. for 24 h. The reaction mixture was quenched with ice cold water and dried in vacuo. The residue was dissolved in EtOAc and washed with water (3x). The combined organic layers were dried over Na₂SO₄, the solvent was evaporated, and the crude product was purified by flash chromatography on silica gel (MeOH:EtOAc, 1:20 → 1:10) to yield **44** (140 mg, 64%) as a colourless oil. ¹H NMR (300 MHz, CDCl₃, δ ppm) 7.36 (dd, $J = 1.9, 0.9$ Hz, 1H, furan), 6.30 (dd, $J = 3.2, 1.9$ Hz, 1H, furan), 6.22 (d, $J = 3.1$ Hz, 1H, furan), 3.76–3.62 (m, 6H, 2 CH₂-O morpholine, CH₂-furan), 3.36 (d, $J = 2.4$ Hz, 2H, CH₂-C≡CH), 2.58 (t, $J = 7.5$ Hz, 2H, CH₂), 2.48–2.30 (m, 6H, 2 CH₂ morpholine, CH₂), 2.21 (t, $J = 2.4$ Hz, 1H, CH≡C), 1.69 (quint, $J = 7.4$ Hz, 2H, CH₂). ¹³C NMR (75.4 MHz, CDCl₃, δ ppm) 152.1 (qC, furan), 142.3 (CH, Furan), 110.2 (CH, Furan), 108.9 (CH, Furan), 78.4 (C≡CH), 73.3 (CH), 67.1 (2 CH₂-O), 56.9 (CH₂), 53.8 (2 CH₂ morpholine), 51.2 (CH₂), 50.2 (CH₂-furan), 41.9 (CH₂-C≡CH), 24.7 (CH₂). ESI-HRMS m/z calcd for $C_{15}H_{23}N_2O_2$ $[M+H]^+$, 263.1753; found, 263.1754.

N-(Furan-2-ylmethyl)-N-(prop-2-yn-1-yl)cyclopentanamine (**45**). Reaction of propargyl bromide (0.55 mL, 5.05 mmol) and **29a** (1.67 g, 10.1 mmol) was performed as indicated for **44**. Chromatography column (Et₂O:Cyclohexane, 1:9). Yield: 99%, yellow oil. ¹H NMR (300 MHz, CDCl₃, δ ppm) δ 7.41–7.32 (m, 1H, furan), 6.33–6.28 (m, 1H, furan), 6.27–6.22 (m, 1H, furan), 3.76 (s, 2H, CH₂-furan), 3.37 (d, $J = 2.4$ Hz, 2H, CH₂-C≡CH), 3.01–2.87 (m, 1H, CH), 2.24–2.17 (m, 1H, CH≡C), 2.04–1.87 (m, 2H, CH₂), 1.82–1.67 (m, 2H, CH₂), 1.67–1.39 (m, 4H, 2 CH₂). ¹³C NMR (75.4 MHz, CDCl₃, δ ppm) 152.1 (qC, furan), 142.3 (CH, Furan), 110.2 (CH, Furan), 109.0 (CH, Furan), 78.7 (C≡CH), 73.2 (CH≡C), 63.3 (CH, cyclopentyl), 48.5 (CH₂-furan), 40.7 (CH₂-C≡CH), 31.5 (2 CH₂), 24.1 (2 CH₂). ESI-HRMS m/z calcd for $C_{13}H_{18}NO$ $[M+H]^+$,

204.1380; found, 204.1383.

(E)-2-Cyano-1-(6-(4-(((furan-2-ylmethyl)(3-morpholinopropyl)amino)methyl)-1H-1,2,3-triazol-1-yl)hexyl)-3-(pyridin-4-yl)guanidine (**46**). To a solution of **43** (48.0 mg, 0.17 mmol) in toluene:DMF (8:1, 4.5 mL), **44** (97.0 mg, 0.37 mmol), DIPEA (0.14 mL, 0.81 mmol) and CuI (6.0 mg, 34 μ mol) were added, and the solution was stirred at 60 °C for 24 h. After evaporation, the resulting residue was dissolved in EtOAc and washed with a sat. aq. soln. of NaHCO₃. The aq. phase was extracted with EtOAc (x2), and the organic phases were collected, dried over Na₂SO₄, filtered, and evaporated. The resulting residue was purified by chromatography column on silica gel (NH₄OH:MeOH:EtOAc, 0.1:1:9) to yield **46** (54.0 mg, 60%) as a white solid. ¹H NMR (300 MHz, CDCl₃, δ ppm) 8.49–8.30 (m, 2H, Py), 7.48 (s, 1H, triazole), 7.34 (d, *J* = 1.9 Hz, 1H, furan), 7.30–7.20 (m, 2H, Py), 6.37–6.23 (m, 2H, furan, NH–CH₂), 6.19 (d, *J* = 3.2 Hz, 1H, furan), 4.32 (t, *J* = 6.9 Hz, 2H, CH₂-triazole), 3.81–3.54 (m, 8H, CH₂-furan, N–CH₂-triazole, 2 CH₂-O morpholine), 3.38 (q, *J* = 6.5 Hz, 2H, CH₂-NH), 2.56–2.24 (m, 8H, 2 CH₂ morpholine, 2 CH₂), 1.95–1.81 (m, 2H, CH₂), 1.80–1.64 (m, 2H, CH₂), 1.64–1.50 (m, 2H, CH₂), 1.46–1.20 (m, 4H, 2 CH₂). ¹³C NMR (75.4 MHz, CDCl₃, δ ppm) 157.5 (C=N), 152.1 (qC, furan), 150.6 (2CH, Py), 145.5 (qC, Py), 142.1 (CH, furan), 122.9 (CH, triazole), 116.9 (qC, triazole), 115.6 (2CH, Py), 110.3 (CH, furan), 109.0 (CH, furan), 66.9 (2 CH₂-O morpholine), 56.9 (CH₂), 53.8 (2 CH₂ morpholine), 51.5 (CH₂), 50.1 (CH₂-triazole), 49.9 (N–CH₂-triazole), 48.8 (CH₂-furan), 42.2 (CH₂-NH), 29.9 (CH₂), 29.0 (CH₂), 25.8 (CH₂), 25.7 (CH₂), 24.2 (CH₂). ESI-HRMS *m/z* calcd for C₂₈H₄₁N₁₀O₂ [M+H]⁺, 549.3405; found, 549.3408.

(E)-2-Cyano-1-(6-(4-(((cyclopentyl(furan-2-ylmethyl)amino)methyl)-1H-1,2,3-triazol-1-yl)hexyl)-3-(pyridin-4-yl)guanidine (**47**). Compounds **43** (118.0 mg, 0.41 mmol) and **45** (134 mg, 0.66 mmol) were suspended in a mixture of H₂O/t-butanol (1:1) (4 mL). Sodium ascorbate (16.3 mg, 82.4 μ mol) and CuSO₄·5H₂O (2.1 mg, 8.2 μ mol) were dissolved in H₂O and added to the mixture. The resulting solution was stirred at r.t. for 16 h. The solvent was evaporated, and the residue was purified by flash chromatography on silica gel (NH₄OH:MeOH:EtOAc, 0.1:1:9 → 0.1:1:5) to yield **47** (175.0 mg, 87%) as a white solid. ¹H NMR (300 MHz, CDCl₃, δ ppm) 8.46–8.34 (m, 2H, Py), 7.49 (s, 1H, triazole), 7.39–7.33 (m, 1H, furan), 7.31–7.23 (m, 2H, Py), 6.37–6.26 (m, 2H, furan, NH–CH₂), 6.22 (d, *J* = 3.2 Hz, 1H, furan), 4.32 (t, *J* = 6.9 Hz, 2H, CH₂-triazole), 3.79 (s, 2H, CH₂-furan), 3.66 (s, 2H, N–CH₂-triazole), 3.39 (q, *J* = 6.7 Hz, 2H, CH₂-NH), 3.02–2.84 (m, 1H, CH cyclopentyl), 1.99–1.79 (m, 4H, 2 CH₂), 1.76–1.39 (m, 8H, 4 CH₂), 1.39–1.22 (m, 4H, 2 CH₂). ¹³C NMR (75.4 MHz, CDCl₃, δ ppm) 157.5 (C=N), 152.2 (qC, furan), 150.6 (2CH, Py), 145.8 (qC, Py), 142.1 (CH, furan), 123.2 (CH, triazole), 117.0 (qC, triazole), 115.5 (2CH, Py), 110.3 (CH, furan), 109.2 (CH, furan), 63.6 (CH, cyclopentyl), 50.0 (CH₂-triazole), 47.8 (N–CH₂-triazole), 46.4 (CH₂-furan), 42.2 (CH₂-NH), 30.6 (2 CH₂), 29.9 (CH₂), 28.9 (CH₂), 25.7 (CH₂), 25.6 (CH₂), 24.3 (2 CH₂). ESI-HRMS *m/z* calcd for C₂₆H₃₆N₉O [M+H]⁺, 490.3036; found, 490.3037.

N-(4-((Furan-2-ylmethyl)carbamoyl)phenyl)isoindoline-2-carboxamide (**51**). Compound **50** [39] (45.0 mg, 0.16 mmol), HOBT (32 mg, 0.24 mmol), furfurylamine (19.0 mg, 0.19 mmol) and DIPEA (110 μ L, 0.64 mmol) were suspended in DMF (0.5 mL) and EDCI (46.0 mg, 0.24 mmol) was added. The mixture was stirred at r.t. overnight to give a solution that was diluted with 5 mL of ice water. The resulting turbid mixture was stirred at 0 °C for 1 h, then filtered and concentrated to yield **51** (52.0 mg, 90%) as an off-white solid. ¹H NMR (300 MHz, DMSO-*d*₆, δ ppm) δ 8.76 (t, *J* = 5.8 Hz, 1H, NH, amide), 8.58 (s, 1H, NH, urea), 7.81 (d, *J* = 8.4 Hz, 2H, H–Ar, phenyl), 7.67 (d, *J* = 8.4 Hz, 2H, H–Ar, phenyl), 7.56 (d, *J* = 1.8 Hz, 1H, furan), 7.44–7.23 (m, 4H, H–Ar, isoindoline), 6.39 (br t, 1H, furan), 6.26 (br d, 1H, furan), 4.79 (s, 4H, CH₂, isoindoline), 4.45 (d, *J* = 5.6 Hz, CH₂-furan). ¹³C NMR (75.4 MHz, DMSO-*d*₆, δ ppm) δ 165.7 (C=O, amide), 153.6 (C=O, urea), 152.7 (qC, furan), 143.3 (C–Ar, isoindoline), 141.9 (CH, furan), 136.7 (qC, Ph), 127.8 (2CH, Ph), 127.3 (Arom. C–H, isoindoline), 127.0 (qC, Ph), 122.7 (2 HC–Ar, isoindoline), 118.2 (2CH, Ph), 110.4 (CH, furan) 106.7 (CH, furan), 51.9 (CH₂, isoindoline), 35.9 (N–CH₂). HRESIMS *m/z* obsd. 384.1313, calc

for C₂₁H₁₉N₃O₃ [M+Na]⁺: 384.1324.

N-(4-(Cyclopentyl(furan-2-ylmethyl)carbamoyl)phenyl)isoindoline-2-carboxamide (**52**). Reaction of **50** and **29a** as indicated for the synthesis of **51**. Yield: 81%, off-white solid. ¹H NMR (300 MHz, DMSO-*d*₆, δ ppm) δ 8.52 (s, 1H, N–H, Urea), 7.65 (d, *J* = 8.2 Hz, 2H, H–Ar, Phenyl), 7.57 (d, *J* = 1.9 Hz, 1H, furan), 7.42–7.26 (m, 6H, H–Ar, Ph, isoindoline), 6.40 (t, *J* = 2.7 Hz, 1H, furan), 6.26 (d, *J* = 3.2 Hz, 1H, furan), 4.79 (s, 4H, CH₂, Isoindoline), 4.52 (s, 2H, CH₂-furan), 4.21 (br s, 1H, CH, Cyclopentyl), 1.80–1.32 (m, 8H, CH₂, Cyclopentyl). ¹³C NMR (75.4 MHz, DMSO-*d*₆, δ ppm) δ 171.4 (C=O, amide), 154.3 (C=O, urea), 152.9 (C–Ar, CH, furan), 142.2 (qC, Ph), 142.0 (CH, furan), 137.2 (C–Ar, isoindoline), 130.6 (qC, Ph), 127.8 (HC–Ar, isoindoline), 127.4 (2CH, Ph), 123.3 (HC–Ar, isoindoline), 119.2 (2CH, Ph), 111.1 (CH, furan), 107.4 (CH, furan), 59.6 (CH, Cyclopentyl), 52.4 (CH₂, Isoindoline), 40.4 (N–CH₂), 29.5 (2C, CH₂, Cyclopentyl), 24.0 (2C, CH₂, Cyclopentyl). HRESIMS *m/z* obsd. 452.1940, calc for C₂₆H₂₇N₃O₃ [M+Na]⁺: 452.1950.

(E)-7-(N'-Cyanoisoindoline-2-carboximidamido)-N-cyclopentyl-N-(furan-2-ylmethyl)heptanamide (**53**). Same procedure as that described for **38a** but starting from **30** (371 mg, 0.95 mmol) and **56** (226.0 mg, 0.86 mmol). Chromatography column (EtOAc:Cyclohexane, 2:1). Yield: 36%, white solid. ¹H NMR (300 MHz, CDCl₃, δ ppm, mixture of rotamers) 7.42–7.17 (m, 10H, 8H isoindoline, 2H furan), 6.29 (br d, 2H, furan), 6.14 (br s, 2H, furan), 5.36 (br s, 1H, NH–CH₂ rotamer A), 5.25 (br s, 1H, NH–CH₂ rotamer B), 4.90 (s, 8H, 4 CH₂ isoindoline), 4.81–4.61 (m, 1H, CH cyclopentyl rotamer A), 4.48–4.33 (m, 4H, 2 CH₂-furan), 4.27–4.11 (m, 1H, CH cyclopentyl rotamer B), 3.62–3.44 (m, 4H, 2 CH₂-NH), 2.49–2.28 (m, 4H, 2 CH₂-C=O), 1.91–1.28 (m, 32H, 8 CH₂ cyclopentyl, 8 CH₂). ¹³C NMR (75.4 MHz, CDCl₃, δ ppm, mixture of rotamers) 173.8, 173.2, 156.0, 152.7, 152.1, 142.1, 141.1, 135.5, 128.0, 122.7, 118.0, 110.6, 107.3, 107.1, 103.3, 77.6, 77.2, 76.7, 58.8, 56.3, 53.7, 43.0, 42.7, 41.9, 38.5, 33.7, 33.5, 30.1, 29.9, 29.1, 28.7, 28.4, 26.4, 26.0, 25.1, 23.9. ESI-HRMS *m/z* calcd for C₂₇H₃₆N₅O₂ [M+H]⁺, 462.2860; found, 462.2864.

(E)-N-(4-Chlorobenzyl)-7-(N'-cyanoisoindoline-2-carboximidamido)-N-(furan-2-ylmethyl)heptanamide (**54**). Same procedure as described for **53** starting from **37b**. Yield: 42%, white solid. ¹H NMR (300 MHz, CDCl₃, δ ppm, mixture of rotamers) 7.40–7.02 (m, 18H, 8H Ph, 8H isoindoline, 2H furan), 6.41–6.25 (m, 2H, furan), 6.25–6.11 (m, 2H, furan), 5.17–5.01 (m, 2H, NH–CH₂), 4.89 (s, 8H, 4 CH₂ isoindoline), 4.58–4.29 (m, 8H, 2 CH₂-Ph, 2 CH₂-furan), 3.66–3.44 (m, 4H, CH₂-NH), 2.55 (t, *J* = 7.3 Hz, 2H, CH₂-C=O rotamer A), 2.35 (t, *J* = 7.3 Hz, 2H, CH₂-C=O rotamer B), 1.83–1.27 (m, 16H, 8 CH₂). ¹³C NMR (75.4 MHz, CDCl₃, δ ppm, mixture of rotamers) 173.4, 156.0, 150.9, 150.0, 142.9, 142.4, 136.1, 135.4, 135.3, 133.6, 133.3, 129.6, 129.2, 128.9, 128.1, 127.9, 122.7, 117.9, 110.5, 108.9, 108.5, 77.6, 77.2, 76.7, 53.7, 50.1, 47.7, 43.8, 43.1, 41.6, 33.0, 30.0, 28.8, 28.6, 26.4, 26.3, 25.0. ESI-HRMS *m/z* calcd for C₂₉H₃₃ClN₅O₂ [M+H]⁺, 518.2314; found, 518.2317.

(E)-7-(N'-Cyanoisoindoline-2-carboximidamido)-N-(furan-2-ylmethyl)-N-(3-morpholinopropyl)heptanamide (**55**). Same procedure as described for **53** starting from **37d**. Chromatography column (NH₄OH:MeOH:EtOAc, 0.1:1:10). Yield: 52%, colourless oil. ¹H NMR (300 MHz, CDCl₃, δ ppm, mixture of rotamers) 7.42–7.22 (m, 10H, 8H isoindoline, 2H furan), 6.36–6.26 (m, 2H, furan), 6.26–6.15 (m, 2H, furan), 5.15–4.99 (m, 2H, 2 NH–CH₂), 4.90 (s, 8H, isoindoline), 4.56 (s, 2H, CH₂-furan rotamer A), 4.45 (s, 2H, CH₂-furan rotamer B), 3.77–3.64 (m, 8H, 4 CH₂ morpholine), 3.62–3.49 (m, 4H, 2 CH₂-NH), 3.44–3.29 (m, 4H, 2 CH₂), 2.54–2.23 (m, 16H, 4 CH₂ morpholine, 4 CH₂), 1.78–1.53 (m, 8H, 4 CH₂), 1.52–1.30 (m, 8H, 4 CH₂). ¹³C NMR (75.4 MHz, CDCl₃, δ ppm, mixture of rotamers) 173.2, 173.0, 156.0, 151.5, 150.7, 142.7, 142.1, 135.4, 128.1, 122.8, 117.8, 110.6, 108.4, 108.1, 77.6, 77.2, 76.7, 67.1, 67.0, 56.3, 55.6, 53.8, 53.7, 50.9, 45.4, 45.2, 44.5, 43.1, 43.0, 41.6, 33.1, 32.9, 30.0, 29.9, 28.7, 26.3, 26.3, 25.6, 25.1, 25.0, 24.5. ESI-HRMS *m/z* calcd for C₂₉H₄₁N₆O₃ [M+H]⁺, 521.3339; found, 521.3235.

(E)-7-(2-Cyano-3-phenylguanidino)-N-cyclopentyl-N-(furan-2-ylmethyl)heptanamide (**57**). Same procedure as described for **38a**

starting from **30** and **61a**. Chromatography column (EtOAc:Cyclohexane, 1:2 → 1:1). Yield 80%, white solid. ^1H NMR (300 MHz, CDCl_3 , δ ppm, mixture of rotamers) 7.60–7.16 (m, 14H, 10H Ph, 2H furan, 2 NH-Ph), 6.29 (br d, 2H, furan), 6.13 (br s, 2H, furan), 5.02 (s, 2H, 2 NH-CH₂), 4.80–4.60 (m, 1H, CH cyclopentyl rotamer A), 4.38 (br d, 4H, 2 CH₂-furan), 4.28–4.06 (m, 1H, CH cyclopentyl rotamer B), 3.33–3.17 (m, 4H, 2 CH₂-NH), 2.47–2.23 (m, 4H, 2 CH₂-C=O), 1.89–1.15 (m, 32H, 8 CH₂ cyclopentyl, 8 CH₂). ^{13}C NMR (75.4 MHz, CDCl_3 , δ ppm, mixture of rotamers) 173.7, 173.0, 158.8, 152.7, 152.2, 142.1, 141.0, 135.6, 130.2, 127.4, 125.5, 118.0, 110.6, 107.5, 107.0, 77.6, 77.2, 76.7, 58.7, 56.2, 41.9, 41.8, 38.4, 33.7, 33.5, 30.0, 29.1, 29.0, 28.7, 26.4, 25.0, 23.9. ESI-HRMS m/z calcd for $\text{C}_{25}\text{H}_{34}\text{N}_5\text{O}_2$ $[\text{M}+\text{H}]^+$, 436.2707; found, 436.2707.

(E)-6-(2-Cyano-3-phenylguanidino)-N-cyclopentyl-N-(furan-2-ylmethyl)hexane-1-sulfonamide (**58**). Same procedure as that described for **35a** starting from **32** and **61a**. Column chromatography EtOAc:Cyclohexane, 1:1 → 2:1. Yield: 96%, white solid. ^1H NMR (300 MHz, CDCl_3 , δ ppm) 7.52–7.16 (m, 7H, 5H Ph, 1H furan, NH-Py), 6.41–6.21 (m, 2H, furan), 4.89 (t, $J = 5.8$ Hz, 1H, NH-CH₂), 4.35 (s, 2H, CH₂-furan), 4.13 (quint, $J = 8.3$ Hz, 1H, CH cyclopentyl), 3.31–3.18 (m, 2H, CH₂-NH), 2.80–2.67 (m, 2H, CH₂SO₂), 1.95–1.41 (m, 12H, 8H cyclopentyl, 2 CH₂), 1.41–1.17 (m, 4H, 2 CH₂). ^{13}C NMR (75.4 MHz, CDCl_3 , δ ppm) 158.9 (C=N), 151.5 (qC, furan), 142.2 (CH, furan), 135.4 (qC, Ph), 130.3 (2CH, Ph), 127.8 (CH, Ph), 125.8 (2CH, Ph), 118.0 (C, Ph), 110.8 (CH, furan), 109.2 (CH, furan), 59.3 (CH, cyclopentyl), 53.3 (CH₂SO₂), 41.8 (CH₂-NH), 40.0 (CH₂-furan), 30.0 (2CH₂, cyclopentyl), 29.1 (CH₂), 27.9 (CH₂), 26.2 (CH₂), 23.6 (2CH₂, cyclopentyl), 23.3 (CH₂). ESI-HRMS m/z calcd for $\text{C}_{24}\text{H}_{33}\text{N}_5\text{O}_3\text{SNa}$ $[\text{M}+\text{Na}]^+$, 494.2196; found, 494.2196.

Ethyl (E)-4-(2-cyano-3-(6-(N-cyclopentyl-N-(furan-2-ylmethyl)sulfonyl)hexyl)guanidino)benzoate (**59**). Same procedure as described for **58** starting from **61b**. Column chromatography EtOAc:Cyclohexane, 1:2 → 1:1. Yield: 95%, pale-yellow solid. ^1H NMR (300 MHz, CDCl_3 , δ ppm) 8.06 (d, $J = 8.6$ Hz, 2H, Ph), 7.88 (s, 1H, NH-Ph), 7.38–7.34 (m, 1H, furan), 7.30 (d, $J = 8.6$ Hz, 2H, Ph), 6.36–6.25 (m, 2H, furan), 5.24 (br s, 1H, NH-CH₂), 4.43–4.30 (m, 4H, CH₂CH₃, CH₂-furan), 4.13 (quint, $J = 8.4$ Hz, 1H, CH cyclopentyl), 3.30 (q, $J = 6.8$ Hz, 2H, CH₂-NH), 2.79–2.70 (m, 2H, CH₂SO₂), 1.92–1.45 (m, 12H, 8H cyclopentyl, 2 CH₂), 1.45–1.20 (m, 7H, CH₃CH₂, 2 CH₂). ^{13}C NMR (75.4 MHz, CDCl_3 , δ ppm) 165.7 (C=O), 158.2 (C=N), 151.4 (qC, furan), 142.2 (CH, furan), 140.2 (qC, Ph) 131.5 (2CH, Ph), 128.5 (qC, Ph), 123.5 (2CH, Ph), 110.8 (CH, furan), 109.2 (CH, furan), 61.4 (CH₂CH₃), 59.3 (CH, cyclopentyl), 53.2 (CH₂SO₂), 42.1 (CH₂-NH), 40.0 (CH₂-furan), 30.0 (2CH₂, cyclopentyl), 29.0 (CH₂), 27.8 (CH₂), 26.2 (CH₂), 23.6 (2CH₂, cyclopentyl), 23.3 (CH₂), 14.4 (CH₃CH₂). ESI-HRMS m/z calcd for $\text{C}_{27}\text{H}_{37}\text{N}_5\text{O}_3\text{SNa}$ $[\text{M}+\text{Na}]^+$, 566.2400; found, 566.2408.

(E)-6-(3-(4-Azidophenyl)-2-cyanoguanidino)-N-cyclopentyl-N-(furan-2-ylmethyl)hexane-1-sulfonamide (**60**). Same procedure as described for **58** starting from **61c**. Chromatography column (EtOAc:Cyclohexane, 1:2 → 1:1). Yield: 84%, light-red solid. ^1H NMR (300 MHz, CDCl_3 , δ ppm) 7.64 (s, 1H, NH-Ph), 7.35 (dd, $J = 1.9, 0.9$ Hz, 1H, furan), 7.23 (d, $J = 8.7$ Hz, 2H, Ph), 7.06 (d, $J = 8.7$ Hz, 2H, Ph) 6.40–6.16 (m, 2H, furan), 4.89 (br s, 1H, NH-CH₂), 4.35 (s, 2H, CH₂-furan), 4.13 (quint, $J = 8.5$ Hz, 1H, CH, cyclopentyl), 3.24 (q, $J = 6.8$ Hz, 2H, CH₂-NH), 2.80–2.69 (m, 2H, CH₂SO₂), 1.95–1.41 (m, 12H, 8H cyclopentyl, CH₂), 1.41–1.08 (m, 6H, 3 CH₂). ^{13}C NMR (75.4 MHz, CDCl_3 , δ ppm) 159.0 (C=N), 151.5 (qC, furan), 142.2 (CH, furan), 139.6 (C≡N), 132.1 (qC, Ph), 127.4 (2CH, Ph), 120.7 (2CH, Ph), 118.0 (qC, Ph), 110.8 (CH, furan), 109.2 (CH, furan), 59.3 (CH, cyclopentyl), 53.2 (CH₂SO₂), 41.9 (CH₂-NH), 40.0 (CH₂-furan), 30.0 (2CH₂, cyclopentyl), 29.8 (CH₂), 29.1 (CH₂), 27.9 (CH₂), 26.2 (CH₂, cyclopentyl), 23.6 (CH₂, cyclopentyl), 23.3 (CH₂). ESI-HRMS m/z calcd for $\text{C}_{24}\text{H}_{32}\text{N}_8\text{O}_3\text{SNa}$ $[\text{M}+\text{Na}]^+$, 535.2209; found, 535.2210.

4.2. Biological evaluation

Cell lines and reagents

MiaPaCa-2 and MDA-MB-231 were purchased from ATCC (LGC Standards S.r.l., Milan, Italy) and maintained in RPMI1640 medium supplemented with 10% FBS, penicillin (50U/mL) and streptomycin (50 $\mu\text{g}/\text{mL}$) (ThermoFisher, Italy). Five hematological cell lines (ML2 – Acute myeloid leukemia, Jurkat – Acute lymphoblastic leukemia, Namalwa – Burkitt lymphoma, RPMI8226 – Multiple Myeloma and NB4 – acute myeloid leukemia M3) were purchased from DSMZ (German Collection of Microorganisms and Cell Cultures) or ATCC. The cell lines were cultured in RPMI medium (Invitrogen AG, 61870-01) supplemented with 10% heat inactivated fetal calf serum (Amimed, 2-01F30-I) and 1% penicillin/streptomycin at 37 °C (Amimed, 4-01F00-H) in a humidified atmosphere of 95% air and 5% CO₂. FK866 was obtained from the NIMH Chemical Synthesis and Drug Supply Program.

Cell viability assay

2×10^3 MiaPaCa-2 or MDA-MB-231 cells were plated in 96 well plates and let adhere overnight. 24 h later cells were treated with the analogues of FK866. Viability was determined 72 h after. The culture plates were fixed with cold 3% trichloroacetic acid at 4 °C for 30 min, washed with cold water and dried overnight. Finally, the plates were stained with 0.4% sulforodamine B (SRB) in 1% acetic acid, washed four times with 1% acetic acid to remove unbound dye, dried overnight and then the stain was extracted with 10 mM Tris Base and the absorbance was read at 560 nm.

Measurement of intracellular NAD⁺ levels

MiaPaCa-2 or MDA-MB-231 cells were plated at a density of 3×10^4 cells/well in 24-well plates. After 24 h, cells were treated (or not) with the different compounds and cultured for further 24 h (in the time course experiments, cells were cultured for further 24 h, 48 h and 72 h). Cells were harvested and lysed in 0.1 ml 0.6 M perchloric acid. Intracellular NAD⁺ levels were determined as previously reported [40] and ATP levels were quantified by a commercially available ATP determination kit (Invitrogen, Carlsbad, CA) following the manufacturer's instruction. Luminescence was measured using a FLUOstar OPTIMA (BMG Labtech, Ortenberg, Germany) and ATP concentrations in the samples were calculated from the ATP standard curve.

Immunoblotting

For protein lysate generation from cultured cells, 2.5×10^5 MiaPaCa-2 cells were plated in 100 mm Petri dishes. After 24 h, cells were treated with compound **47** and **35a** for 48 h. Thereafter, cells were washed and protein lysates were generated in the presence of 50–200 μL lysis buffer (25 mM Tris-phosphate, pH 7.8; 2 mM DTT; 2 mM 1,2-diaminocyclohexane-*N,N,N',N'*-tetraacetic acid; 10% glycerol; 1% Triton X-100). Cell lysates were incubated on ice for 15 min with 10 s vortex shaking every 5 min. Finally, lysates were spun at 10,000 g for 2 min at 4 °C. Supernatants were recovered and either used immediately or stored for subsequent use. Proteins (35 μg) were separated by SDS-PAGE, transferred to a PVDF membrane (Immobilon-P, Millipore S.p. A.), and detected with the following antibodies: PARP (Cell Signaling #9542) and Vinculin (Santa Cruz/sc-5573). Band intensities were quantified by Quantity One SW software (Bio-Rad Laboratories, Inc.) using standard enhanced chemiluminescence.

Determination of NAMPT inhibition

NAMPT inhibition was determined as previously reported [41]. Briefly, 10 ng of recombinant human NAMPT protein (#ab198090, Abcam, Cambridge, UK) were incubated in 40 μL reaction buffer (0.4 mM PRPP, 2 mM ATP, 0.02% BSA, 2 mM DTT, 12 mM MgCl₂ and 50 mM Tris-HCl) in eppendorf tubes, in the presence or absence of the different compounds. After a 5 min incubation at 37 °C, 9.0 μL of NAM (0.2 μM final concentration) were added and the reaction was stopped after 15 min, by heating samples at 95 °C for 1 min. Samples were then cooled to 0 °C and NMN was detected by adding 20 μL of 20% acetophenone and 20 μL KOH (2 M) into each tube. The mixture was vortexed and kept at 0 °C for 3 min; 90 μL of 88% formic acid were then added and the tubes

were incubated at 37 °C for 10 min. Finally, 100 µL of the mixture was transferred into a flat-bottom 96-well plate and the fluorescence (excitation 382 nm, emission 445 nm) was measured using a CLARIOstar®^{Plus} (BMG Labtech).

Flow cytometry analyses

The cytotoxic and cellular effects of **35a**, **39a** and **47** on malignant cell lines were evaluated using a Beckman Coulter Cytomics FC500 flow cytometer (Beckman Coulter International S.A.). The measured parameters included cell death, MMP assessments and ROS production.

Cell death analysis

To assess cell death, cells were stained with ANNEXIN-V (ANXN, eBioscience, BMS306FI/300) and 7-aminoactinomycin D (7AAD, Immunotech, A07704) as described by the manufacturer and analyzed using flow cytometry. Dead cells were identified as 7AAD⁺ and early apoptotic cells as ANXN⁺ 7AAD⁻.

Assessment of mitochondrial membrane potential (MMP)

ML2, Jurkat and RPMI8226 cells were incubated with NAMPT inhibitors for up to 96 h. At each time point, cells were stained with Tetramethylrhodamine, methyl ester (TMRM, ThermoFisher Scientific, T668) according to the manufacturer's protocol. TMRM is a cell-permeant dye that accumulates in the active mitochondria, showing red-orange fluorescence, detected by flow cytometer. The amount of the dye is directly proportional to the amount of live cells with active mitochondria. The graphs depict the percentage of cells losing MMP over time.

Detection of cellular and mitochondrial ROS

Intracellular levels of H₂O₂, mitochondrial and cytosolic superoxide anions were determined in NAMPT inhibitor-treated and control hematological cell lines by flow cytometry. The cell permeant specific fluorescent probes were used, i.e. dihydroethidium (DHE, Marker Gene Technologies, M1241), MitoSOX (Molecular Probes, M36008) and 6-carboxy-2',7'-dichlorodihydrofluorescein diacetate ester (carboxy-H2DCFDA; Molecular Probes, C-400). DHE is oxidized intracellularly to ethidium by superoxide anions giving bright red fluorescence. MitoSOX, is selectively targeted to mitochondria, where it is oxidized by ROS and exhibits red fluorescence. Instead, carboxy-H2DCFDA is hydrolyzed yielding a polar non-fluorescent product (DCFH), which in the presence of hydrogen peroxide is then oxidized to green fluorescent dichlorofluorescein (DCF). Cells were stained separately with 5 µM of TMRM and H2DCFDA dyes and 10 µM of DHE in PBS, incubated in the dark at 37 °C for 15 min. Then, the cell suspension was analyzed using flow cytometry.

Determination of intracellular NAD⁺ and ATP contents

Cells (1 × 10⁶/mL) in log growth phase were seeded in 6-well plate in presence or absence of NAMPT inhibitors. At each time point 800 µL of cells was centrifuged at 900 g (2000 rpm) for 5 min and washed with cold PBS. Then, supernatant was discarded and cells were re-suspended in 300 µL of lysis buffer (NaHCO₃ 20 mM and NA₂CO₃ 100 mM) and kept at -80 °C for at least 4 h before analysis.

Total NAD⁺ content was measured in cell lysates using a biochemical assay described previously [42]. Briefly, cell lysates (20 µL) were plated in a 96-well flat bottom plate. A standard curve was generated using a 1:3 serial dilution in lysis buffer of a β-NAD stock solution. Cycling buffer (160 µL) was added into each well and the plate was incubated for 5 min at 37 °C. After, pre-warmed at 37 °C ethanol (20 µL) was added into each well and the plate was incubated for an additional 5 min at 37 °C. The absorbance was measured in a kinetic mode at 570 nm after 5, 10, 15, 20, and 30 min at 37 °C on a spectrophotometer. The amount of NAD⁺ in each sample was normalized to the protein content for each test sample at each time point.

Total ATP cell content was quantified using the ATP determination Kit (Life Technologies, A22066) according to manufacturer's instructions.

Declaration of competing interest

The authors declare that they have no known competing financial interests or personal relationships that could have appeared to influence the work reported in this paper.

Data availability

Data will be made available on request.

Acknowledgements

This work has received funding from the European Union's Horizon 2020 research and innovation programme under the Marie Skłodowska-Curie grant agreement No671881 (INTEGRATA). This work was also supported by the Ministerio de Ciencia e Innovación (Grant PID2020-116460RB-I00 funded by MCIN/AEI/10.13039/501100011033), the Associazione Italiana per la Ricerca sul Cancro (AIRC; IG#22098, to A. Nencioni) and the Italian Ministry of Health (PE-2016-02362694 and PE-2016-02363073). We also thank CITIUS-Universidad de Sevilla for MS and NMR services. The authors acknowledge Carlos G. Newburn for technical assistance.

Appendix A. Supplementary data

Supplementary data to this article can be found online at <https://doi.org/10.1016/j.ejmech.2023.115170>.

References

- [1] L.E. Navas, A. Carnero, NAD⁺ metabolism, stemness, the immune response, and cancer, *Signal Transduct. Targeted Ther.* 6 (2021) 1–20.
- [2] a) A. Chiarugi, C. Dölle, R. Felici, M. Ziegler, The NAD metabolome—a key determinant of cancer cell biology, *Nat. Rev. Cancer* 12 (2012) 741–752; b) S. Chowdhry, C. Zanca, U. Rajkumar, T. Koga, Y. Diao, R. Raviram, F. Liu, K. Turner, H. Yang, E. Brunk, J. Bi, F. Furnari, V. Bafna, B. Ren, P.S. Mische, NAD metabolic dependency in cancer is shaped by gene amplification and enhancer remodelling, *Nature* (2019) 570–575.
- [3] M.S. Ghanem, F. Monacelli, A. Nencioni, Advances in NAD-lowering agents for cancer treatment, *Nutrients* 13 (2021) 1665.
- [4] Wei, Y.; Xiang, H.; Zhang, W. Review of various NAMPT inhibitors for the treatment of cancer. *Front. Pharmacol.* 13:970553.
- [5] J.A. Khan, X. Tao, L. Tong, Molecular basis for the inhibition of human NMPRTase, a novel target for anticancer agents, *Nat. Struct. Mol. Biol.* 13 (2006) 582–588.
- [6] K. Holen, L.B. Saltz, E. Hollywood, K. Burk, A.R. Hanauke, The pharmacokinetics, toxicities, and biologic effects of FK866, a nicotinamide adenine dinucleotide biosynthesis inhibitor, *Invest. N. Drugs* 16 (2008) 45–51.
- [7] A. von Heideman, A. Berglund, R. Larsson, P. Nygren, Safety and efficacy of NAD depleting cancer drugs: results of a phase I clinical trial of CHS 828 and overview of published data, *Cancer Chemother. Pharmacol.* 65 (2010) 1165–1172.
- [8] T.S. Zabka, J. Singh, P. Dhawan, B.M. Liederer, J. Oeh, M.A. Kauss, Y. Xiao, M. Zak, T. Lin, B. McCray, N. La, T. Nguyen, J. Beyer, C. Farman, H. Uppal, P. S. Dragovich, T. O'Brien, D. Sampath, D.L. Misner, Retinal toxicity, in vivo and in vitro, associated with inhibition of nicotinamide phosphoribosyltransferase, *Toxicol. Sci.* 144 (2015) 163–172 (and references therein).
- [9] a) O.A. Aboud, C.-H. Chen, W. Senapedis, E. Baloglu, C. Argueta, R.H. Weiss, Dual and specific inhibition of NAMPT and PAK4 by KPT-9274 decreases kidney cancer growth, *Mol. Cancer Therapeut.* 15 (2016) 2119–2129; b) N. Li, M.A. Lopez, M. Linares, S. Kumar, S. Oliva, J. Martinez-Lopez, L. Xu, Y. Xu, T. Perini, W. Senapedis, E. Baloglu, M.A. Shammas, Z. Hunter, K. C. Anderson, S.P. Treon, N.C. Munshi, M. Fulciniti, Dual PAK4-NAMPT inhibition impacts growth and survival, and increases sensitivity to DNA-damaging agents in waldenstrom macroglobulinemia, *Clin. Cancer Res.* 25 (2019) 369–377; c) S.R. Mitchell, K. Larkin, N.R. Grieselhuber, T.-H. Lai, M. Cannon, S. Orwick, P. Sharma, Y. Asemelash, P. Zhang, V.M. Goettl, L. Beaver, A. Mims, V.K. Puduvali, J.S. Blachly, A. Lehman, B. Harrington, S. Henderson, J.T. Breitbach, K.E. Williams, S. Dong, E. Baloglu, W. Senapedis, K. Kirschner, D. Sampath, R. Lalapombella, J. C. Byrd, Selective targeting of NAMPT by KPT-9274 in acute myeloid leukemia, *Blood Adv* 3 (2019) 242–255.
- [10] G.B. Mpiilla, Md H. Uddin, M.N. al Al-Hallak, A. Aboukameel, Y. Li, S.H. Kim, R. Beydoun, G. Dyson, E. Baloglu, W.T. Senapedis, Y. Landesman, K.-U. Wagner, N.T. Viola, B.F. El-Rayes, P.A. Philip, R.M. Mohammad, A.S. Azmi, Neuroendocrine tumors to everolimus, *Mol. Cancer Therapeut.* 20 (2021) 1836–1845.
- [11] L. Korotchkina, D. Kazylkin, P.G. Komarov, A. Polinsky, E.L. Andrianova, S. Joshi, M. Gupta, S. Vujcic, E. Kononov, I. Toshkov, Y. Tian, P. Krasnov, M.V. Chernov, J. Veith, M.P. Antoch, S. Middlemiss, K. Somers, R.B. Lock, M.D. Norris, M. J. Henderson, M. Haber, O.B. Chernova, A.V. Gudkov, OT-82, a novel anticancer

- drug candidate that targets the strong dependence of hematological malignancies on NAD biosynthesis, *Leukemia* 34 (2020) 1828–1839.
- [12] C. Travelli, S. Aprile, R. Rahimian, A.A. Grolla, F. Rogati, M. Bertolotti, F. Malagnino, R. di Paola, D. Impellizzeri, R. Fusco, V. Mercalli, A. Massarotti, G. Stortini, S. Terrazzino, E. del Grosso, G. Fakhfouri, M.P. Troiani, M.A. Alisi, G. Grosa, G. Sorba, P.L. Canonico, G. Orsomando, S. Cuzzocrea, A.A. Genazzani, U. Galli, G.C. Tron, Identification of novel triazole-based nicotinamide phosphoribosyltransferase (NAMPT) inhibitors endowed with antiproliferative and anti-inflammatory activity, *J. Med. Chem.* 60 (2017) 1768–1792.
- [13] M.K. Christensen, K.D. Erichsen, U.H. Olesen, J. Tjørnelund, P. Fristrup, A. Thougard, S.J. Nielsen, M. Sehested, P.B. Jensen, E. Loza, I. Kalvinsh, A. Garten, W. Kiess, F. Björklind, Nicotinamide phosphoribosyltransferase inhibitors, design, preparation, and structure–activity relationship, *J. Med. Chem.* 56 (2013) 9071–9088.
- [14] X. Zheng, P. Bauer, T. Baumeister, A.J. Buckmelter, M. Caligiuri, K.H. Clodfelter, B. Han, Y.-C. Ho, N. Kley, J. Lin, D.J. Reynolds, G. Sharma, C.C. Smith, Z. Wang, P. S. Dragovich, A. Oh, W. Wang, M. Zak, J. Gunzner-Toste, G. Zhao, P.-W. Yuen, K. W. Bair, Structure-based identification of ureas as novel nicotinamide phosphoribosyltransferase (NAMPT) inhibitors, *J. Med. Chem.* 56 (2013) 4921–4937.
- [15] J. Bai, S.R. Majjigapu, B. Sordat, S. Poty, P. Vogel, P. Elías-Rodríguez, A.J. Moreno-Vargas, A.T. Carmona, I. Caffa, M. Ghaneme, A. Khalifa, I. Robina, C. Gajate, F. Mollinedo, A. Nahimana, M. Duchosal, A. Nencioni, Identification of new FK866 analogues with potent anticancer activity against pancreatic cancer, *Eur. J. Med. Chem.* 239 (2022), 114504.
- [16] G. Zhao, C.F. Green, Y.-H. Hui, L. Prieto, R. Shepard, S. Dong, T. Wang, B. Tan, X. Gong, L. Kays, R.L. Johnson, W. Wu, S. Bhattachar, M. Del Prado, J.R. Gillig, M. C. Fernandez, K.D. Roth, S. Buchanan, M.-S. Kuo, S. Geeganage, T.P. Burkholder, Discovery of a highly selective NAMPT inhibitor that demonstrates robust efficacy and improved retinal toxicity with nicotinic acid coadministration, *Mol. Cancer Therapeut.* 16 (2017) 2677–2688.
- [17] C.J. Higginson, M.R. Eno, S. Khan, M.D. Cameron, M.G. Finn, Albumin-oxanorbornadiene conjugates formed *ex vivo* for the extended circulation of hydrophilic cargo, *ACS Chem. Biol.* 11 (2016) 2320–2327.
- [18] C.A. Sanhueza, M.M. Baksh, B. Thuma, M.D. Roy, S. Dutta, C. Prévile, B. A. Chrnyk, K. Beaumont, R. Dullea, M. Ammirati, S. Liu, D. Gebhard, J.E. Finley, C.T. Salatto, A. King-Ahmad, I. Stock, K. Atkinson, B. Reidich, W. Lin, R. Kumar, M. Tu, E. Menhaji-Klotz, D.A. Price, S. Liras, M.G. Finn, V. Mascitti, Efficient liver targeting by polyvalent display of a compact ligand for the asialoglycoprotein receptor, *J. Am. Chem. Soc.* 139 (2017) 3528–3536.
- [19] M. Duchosal, N. Aimable, P. Vogel, I. Robina, F. Mollinedo, A. Nencioni, A. “Piperidine Derivatives for Use in the Treatment of Pancreatic Cancer”, 2018. WO 2018/024907 A1, International Application n° PCI/EP2017/069870.
- [20] R. Ronchetti, G. Moroni, A. Carotti, A. Gioiello, E. Camaion, Recent advances in urea- and thiourea-containing compounds: focus on innovative approaches in medicinal chemistry and organic synthesis, *RSC Med. Chem.* 12 (2021) 1046–1064.
- [21] X. Zheng, P. Bauer, T. Baumeister, A.J. Buckmelter, M. Caligiuri, K.H. Clodfelter, B. Han, Y.-C. Ho, N. Kley, J. Lin, D.J. Reynolds, G. Sharma, C.C. Smith, Z. Wang, P. S. Dragovich, A. Oh, W. Wang, M. Zak, J. Gunzner-Toste, G. Zhao, P. Yuen, K. W. Bair, Structure-based identification of ureas as novel Nicotinamidephosphoribosyltransferase (Nampt) inhibitors, *J. Med. Chem.* 56 (2013) 4921–4937.
- [22] Compound 31 Was Prepared Following an Alternative Procedure by N-Chlorosuccinimide-Mediated Oxidation (See Supplementary Material) that Showed to Be More Efficient than the One Previously Described in Reference 13.
- [23] J. O'Brien-Brown, A. Jackson, T.A. Reekie, M.L. Barron, E.L. Werry, P. Schiavini, M. McDonnell, L. Munoz, S. Wilkinson, B. Noll, S. Wang, M. Kassiou, Discovery and pharmacological evaluation of a novel series of adamantyl cyanoguanidines as P2X7 receptor antagonists, *Eur. J. Med. Chem.* 130 (2017) 433–439.
- [24] J.A. Khan, X. Tao, L. Tong, Molecular basis for the inhibition of human NMPRTase, a novel target for anticancer agents, *Nat. Struct. Mol. Biol.* 13 (2006) 582–586, <https://doi.org/10.1038/nsmb1105>.
- [25] J.L. Wilsbacher, M. Cheng, D. Cheng, S.A.J. Trammell, Y. Shi, J. Guo, S.L. Koeniger, P.J. Kovar, Y. He, S. Selvaraju, H.R. Heyman, B.K. Sorensen, R.F. Clark, T. M. Hansen, K.L. Longenecker, D. Raich, A.V. Korepanova, S. Cepa, D.L. Towne, V. C. Abraham, H. Tang, P.L. Richardson, S.M. McLoughlin, I. Badagnani, M.L. Curtin, M.R. Michaelides, D. Maag, F.G. Buchanan, G.G. Chiang, W. Gao, S.H. Rosenberg, C. Brenner, C. Tse, Discovery and characterization of novel nonsubstrate and substrate NAMPT inhibitors, *Mol. Cancer Therapeut.* 16 (2017) 1236–1245.
- [26] A. Oh, Y.-C. Ho, M. Zak, Y. Liu, X. Chen, P.-W. Yuen, X. Zheng, Y. Liu, P. S. Dragovich, W. Wang, Structural and biochemical analyses of the catalysis and potency impact of inhibitor phosphoribosylation by human nicotinamide phosphoribosyltransferase, *ChemBiochem* 15 (2014) 1121–1130.
- [27] U. Galli, G. Colombo, C. Travelli, G.C. Tron, A.A. Genazzani, A.A. Grolla, Recent advances in NAMPT inhibitors: a novel immunotherapeutic strategy, *Front. Pharmacol.* 11 (2020) 656.
- [28] Z. Moore, G. Chakrabarti, X. Luo, A. Ali, Z. Hu, F.J. Fattah, R. Vemireddy, R. J. DeBerardinis, R.A. Brekken, D.A. Boothman, NAMPT inhibition sensitizes pancreatic adenocarcinoma cells to tumor-selective, PAR-independent metabolic catastrophe and cell death induced by β -lapachone, *Cell Death Dis.* 6 (2015) e1599.
- [29] A. Nahimana, A. Attinger, D. Aubry, P. Greaney, C. Ireson, A.V. Thougard, J. Tjørnelund, K.M. Dawson, M. Dupuis, M.A. Duchosal, The NAD biosynthesis inhibitor APO866 has potent antitumor activity against hematologic malignancies, *Blood* 113 (2009) 3276–3286.
- [30] M. Hasmann, I. Schemainda, FK866, a highly specific noncompetitive inhibitor of nicotinamide phosphoribosyltransferase, represents a novel mechanism for induction of tumor cell apoptosis, *Cancer Res.* 63 (2003) 7436–7442.
- [31] V. Ginet, J. Puyal, C. Rummel, D. Aubry, C. Breton, A.J. Cloux, S.R. Majjigapu, B. Sordat, P. Vogel, S. Bruzzone, A. Nencioni, M.A. Duchosal, A. Nahimana, A critical role of autophagy in antileukemia/lymphoma effects of APO866, an inhibitor of NAD biosynthesis, *Autophagy* 10 (2014) 603–617.
- [32] A.J. Cloux, D. Aubry, M. Heulot, C. Widmann, O. ElMokh, F. Piacente, M. Cea, A. Nencioni, A. Bellotti, K. Bouzourene, M. Pellegrin, L. Mazzolai, M.A. Duchosal, N. Aimable, Reactive oxygen/nitrogen species contribute substantially to the antileukemia effect of APO866, a NAD lowering agent, *Oncotarget* 10 (2019) 6723–6738.
- [33] O. David, W.J.N. Meester, H. Bieräugel, H.E. Schoemaker, H. Hiemstra, J.H. Van Maarseveen, Intramolecular staudinger ligation: a powerful ring-closure method to form medium-sized lactams, *Angew. Chem. Int. Ed.* 42 (2003) 4373–4375.
- [34] P.N.H. Trinh, D.J.W. Chong, K. Leach, S.J. Hill, J.D.A. Tyndall, L.T. May, A. J. Vernall, K.J. Gregory, Development of covalent, clickable probes for adenosine A1 and A3 receptors, *J. Med. Chem.* 64 (2021) 8161–8178.
- [35] M. Giroud, J. Ivkovic, M. Martignoni, M. Fleuti, N. Trapp, Inhibition of the cysteine protease human cathepsin L by triazine nitriles: amide \cdots heteroarene π -stacking interactions and chalcogen bonding in the S3 pocket, *ChemMedChem* 12 (2017) 257–270.
- [36] C.M. Jakobsen, S.R. Denmeade, J.T. Isaacs, A. Gady, C.E. Olsen, S.B. Christensen, Design, synthesis, and pharmacological evaluation of thapsigargin analogues for targeting apoptosis to prostatic cancer cells, *J. Med. Chem.* 44 (2001) 4696–4703.
- [37] M.K. Christensen, K.D. Erichsen, U.H. Olesen, J. Tjørnelund, P. Fristrup, A. Thougard, S.J. Nielsen, M. Sehested, P.B. Jensen, E. Loza, I. Kalvinsh, A. Garten, W. Kiess, F. Bjo, Nicotinamide phosphoribosyltransferase inhibitors, design, preparation, and structure – activity relationship, *J. Med. Chem.* 56 (2013) 9071–9088.
- [38] C. Romuald, E. Busseron, F. Coutrot, Very contracted to extended Co-conformations with or without oscillations in two- and three-station [2]Daisy chains, *J. Org. Chem.* 75 (2010) 6516–6531.
- [39] M.L. Curtin, H.R. Heyman, R.F. Clark, B.K. Sorensen, G.A. Doherty, T.M. Hansen, R.R. Frey, K.A. Sarris, A.L. Aguirre, A. Shrestha, N. Tu, K. Woller, M.A. Plushchev, R.F. Sweis, M. Cheng, J.L. Wilsbacher, P.J. Kovar, J. Guo, D. Cheng, K. L. Longenecker, D. Raich, A.V. Korepanova, N.B. Soni, M.A. Algire, P. L. Richardson, V.L. Marin, I. Badagnani, A. Vasudevan, F.G. Buchanan, D. Maag, G. G. Chiang, C. Tse, M.R. Michaelides, SAR and characterization of non-substrate isoindoline urea inhibitors of nicotinamide phosphoribosyltransferase (NAMPT), *Bioorg. Med. Chem. Lett.* 27 (2017) 3317–3325.
- [40] G. Sociali, A. Grozio, I. Caffa, S. Schuster, P. Becherini, P. Damonte, L. Sturla, C. Fresia, M. Passalacqua, F. Mazzola, N. Raffaelli, A. Garten, W. Kiess, M. Cea, A. Nencioni, S. Bruzzone, SIRT6 deacetylase activity regulates NAMPT activity and NAD(P)(H) pools in cancer cells, *Faseb. J.* 33 (2019) 3704–3717.
- [41] R.Y. Zhang, Y. Qin, X.Q. Lv, P. Wang, T.Y. Xu, L. Zhang, C.Y. Miao, A fluorometric assay for high-throughput screening targeting nicotinamide phosphoribosyltransferase, *Anal. Biochem.* 412 (2011) 18–25.
- [42] A. Rongvaux, F. Andris, F. Van Gool, O. Leo, Reconstructing eukaryotic NAD metabolism, *Bioessays* 25 (2003) 683–690.